Axisymmetric Numerical Relativity

Oliver Rinne

Trinity College, Cambridge

A dissertation submitted to the

University of Cambridge

for the degree of

Doctor of Philosophy

13 September 2005

Preface

This thesis is based on research carried out under the supervision of Dr. John M. Stewart at the Department of Applied Mathematics and Theoretical Physics from November 2002.

Chapters 2, 3 and 6 contain work done in collaboration with my supervisor and published in a joint paper [119]. The dynamical shift conditions in chapter 6 are a later addition by myself. The remaining chapters are my own work.

All computer programmes were written by myself unless otherwise stated.

Abstract

This thesis is concerned with formulations of the Einstein equations in axisymmetric spacetimes which are suitable for numerical evolutions. The common basis for our formulations is provided by the (2+1)+1 formalism. General matter sources and rotational degrees of freedom are included.

A first evolution system adopts elliptic gauge conditions arising from maximal slicing and conformal flatness. The numerical implementation is based on the finite-difference approach, using a Multigrid algorithm for the elliptic equations and the method of lines for the hyperbolic evolution equations. Problems with both constrained and free evolution are explained from an analytical as well as a numerical viewpoint.

The second half of the thesis is concerned with a strongly hyperbolic first-order formulation of the axisymmetric Einstein equations. Hyperbolicity is achieved by combining the (2+1)+1 formalism with the Z4 formalism. The system is supplemented with generalized harmonic gauge conditions. A careful study of the behaviour of regular axisymmetric tensor fields enables us to cast the equations in a form that is well-behaved on the axis.

A class of exact solutions of linearized theory are used as a test problem in order to demonstrate the accuracy of our implementation. We derive various outer boundary conditions of dissipative and of differential type based on the Newman-Penrose scalars and the constraint and gauge propagation systems. The stability of these boundary conditions is examined both analytically and numerically.

The code is applied to the evolution of strong Brill waves close to the threshold of black hole formation. As a novel ingredient, a nonzero twist is included. Adaptive mesh refinement is found to be crucial in order to resolve the highly distorted waveforms that occur if harmonic slicing is used.

Acknowledgements

I would like to express my gratitude to Dr. John Stewart, my research supervisor, for his advice and encouragement throughout this project.

I would also like to thank Dr. Nikolaos Nikiforakis of the Laboratory of Computational Dynamics and fellow students Dr. Anita Barnes and Joshua Horwood for helpful discussions, and Dr. Stuart Rankin, the Relativity Group's computer officer, for helping me with my computing problems.

I appreciated the hospitality of the numerical relativity groups at the Max Planck Institute for Gravitational Physics (Albert Einstein Institute), Golm, Germany, and at the University of Southampton.

Financial support from the Gates Cambridge Trust, the Engineering and Physical Sciences Research Council and Trinity College Cambridge is gratefully acknowledged.

My final thanks go to my friends at Cambridge and beyond and, above all, to my parents, for all their sympathy and support.

Contents

1 Introduction **1**

1.1 Numerical relativity 1

1.2 Axisymmetry 2

1.3 Evolution formalisms 4

1.4 Numerical methods and implementation 7

1.5 Gravitational waves and critical collapse 9

1.6 Outline of the thesis 10

1.7 Notation and conventions 11

2 Implications of axisymmetry **13**

2.1 Functions 14

2.2 Vectors and covectors 15

2.3 Symmetric 2-tensors 16

3 The (2+1)+1 formalism **20**

3.1 The Geroch decomposition 21

3.2 The ADM decomposition 26

3.3 Matter evolution equations 32

4 Numerical methods **35**

4.1 The finite difference technique 36

4.1.1 The numerical grid 36
4.1.2 Centred finite difference operators 37
4.1.3 The ghost cell technique 38
4.2 The method of lines 41
4.2.1 Properties of Runge-Kutta and ICN schemes 41
4.2.2 Numerical dissipation 49
4.3 The Multigrid method 51
4.3.1 Relaxation Methods 51
4.3.2 The Multigrid idea 54
4.3.3 Nonlinear Multigrid 58
4.3.4 Extension to systems and multidimensions 60
4.4 Alternative methods 61
4.4.1 Finite volume methods 61
4.4.2 Conjugate gradient methods 63
4.5 Adaptive mesh refinement 65
4.5.1 The grid hierarchy 66
4.5.2 Time-stepping the grid hierarchy 67
4.5.3 Adapting the grid hierarchy 69

5 A mixed hyperbolic-elliptic system 73
5.1 Elliptic gauge conditions 74
5.2 Regularity on axis 76
5.3 Final equations 78
5.4 Alternate evolution schemes 82
5.4.1 A free evolution scheme 82
5.4.2 A constrained evolution scheme 83
5.4.3 A partially constrained evolution scheme 84
5.5 Solvability of the elliptic equations 84

5.5.1 Analytical considerations 85
5.5.2 Numerical considerations 90
5.6 Evolution of the constraints 91
5.7 Evolutions of Brill waves 94
5.7.1 Initial data 94
5.7.2 Boundary conditions 95
5.7.3 Numerical method 97
5.7.4 Weak Brill waves with twist 98
5.7.5 Strong Brill waves 100
5.8 Conclusions 102

6 The Z(2+1)+1 system **107**
6.1 The Z4 extension of the (2+1)+1 formalism 109
6.2 Dynamical gauge conditions 112
6.3 First-order reduction 115
6.4 Hyperbolicity 120
6.4.1 Generalities, well-posedness of the IVP 120
6.4.2 The dynamical shift case 122
6.4.3 The vanishing shift case 127
6.5 Regularity on axis 129
6.5.1 The main regularization procedure 129
6.5.2 Choice of gauge source functions 131
6.5.3 Regularized conservation forms 132
6.5.4 Hyperbolicity and the characteristic transformation . . 134
6.6 Equation checks and code generation 137
6.6.1 Checking the equations with exact solutions 137
6.6.2 Code generation 140

7 A test problem in linearized theory **141**

7.1 The linearized Z(2+1)+1 equations 142

7.2 Transverse-traceless gauge 144

7.3 Teukolsky's quadrupole solution 147

7.3.1 The even-parity solution 147

7.3.2 The odd-parity solution 150

7.4 An even-parity twisting octupole solution 151

7.5 Numerical evolutions 153

7.5.1 Numerical method 154

7.5.2 Snapshots of the evolution 155

7.5.3 Convergence tests 157

7.5.4 Conclusions 159

8 Outer boundary conditions **162**

8.1 Linearized characteristic variables 163

8.2 Dissipative boundary conditions 166

8.2.1 Well-posedness of the IBVP 167

8.2.2 Absorbing boundary conditions 168

8.2.3 Zero-Z boundary conditions 169

8.3 Outgoing-radiation boundary conditions 170

8.3.1 Newman-Penrose scalars and the peeling theorem . . . 170

8.3.2 Construction of the NP tetrad 173

8.3.3 Computation of Ψ_0 175

8.4 Constraint-preserving boundary conditions 177

8.5 Gauge boundary conditions and summary 181

8.6 Fourier-Laplace analysis 185

8.7 Numerical experiments 193

8.7.1 Numerical method 194

8.7.2 Numerical results 195
8.7.3 Conclusions 199

9 Evolutions of nonlinear Brill waves **201**
9.1 Initial data and gauge choices 202
9.2 Convergence test 208
9.3 Apparent horizon finder 213
9.4 Adaptive collapse simulations 220

10 Conclusions and outlook **227**
10.1 Conclusions 227
10.2 Outlook on future work 231

A Perfect fluid **233**
A.1 Conservation form 233
A.2 Matter model 234
A.3 Characteristic decomposition 236
A.4 From conserved to primitive variables 238

B Regularized conservation form **241**
B.1 Fluxes in the r direction 241
B.2 Fluxes in the z direction 245
B.3 Sources 249

List of Figures

3.1 The manifold $\mathcal{N}$ 21
3.2 The ADM setup 27

4.1 Stability regions of the Runge-Kutta methods 45
4.2 Stability regions of the ICN method 46
4.3 The CFL condition 48
4.4 Multigrid cycles 57
4.5 AMR grid hierarchy 67

5.1 Weak Brill waves with twist: central lapse 99
5.2 Weak Brill wave with twist: constraint convergence 100
5.3 Strong Brill waves: central lapse 101
5.4 Strong Brill wave: snapshots of s for $A_s = 4$ 103
5.5 Strong Brill wave: snapshots of s for $A_s = 6$ 104

7.1 Snapshots of s: even quadrupole, vanishing shift 156
7.2 Convergence test: even quadrupole, vanishing shift 158
7.3 Convergence factor, dependence on boundary location 159
7.4 Convergence test: even quadrupole, dynamical shift 160
7.5 Convergence test: even octupole 161
7.6 Dependence of growth of Z^φ on boundary location 161

8.1 Test of boundary conditions: even quadrupole, vanishing shift 196
8.2 Instability of differential boundary conditions 197
8.3 Test of boundary conditions: even quadrupole, dynamical shift 198
8.4 Test of boundary conditions: even octupole 199

9.1 Dynamical vs. vanishing shift 204
9.2 Kretschmann scalar 205
9.3 The need for AMR 208
9.4 Convergence test 211
9.5 Mass conservation 212
9.6 Dependence of ADM mass on boundary location 213
9.7 Test of the apparent horizon finder 218
9.8 Example of the AMR hierarchy 221
9.9 Central lapse and Kretschmann scalar 223
9.10 Z constraints and constraint-damping 224
9.11 Dependence of constraint growth on boundary location 225
9.12 Snapshots of a twisting Brill wave 226

List of Tables

5.1 Hyperbolic-elliptic system: r-parity of the variables 78
5.2 Hyperbolic-elliptic system: z-parity of the variables 96

6.1 Z(2+1)+1 system: r-parity of regularized conserved variables . 132
6.2 Z(2+1)+1 system: r-parity of z-characteristic variables 136

7.1 Z(2+1)+1 system: z-parity of regularized conserved variables . 155

Chapter 1

Introduction

1.1 Numerical relativity

Albert Einstein's 1915 theory of general relativity has radically changed our understanding of space and time. Whereas in previous field theories the spacetime geometry was regarded as being fixed, with the other fields evolving on top of it, the geometry is now part of the field equations themselves and has thus entered the dynamical arena. Spacetime is described as a four-dimensional manifold endowed with a Lorentzian metric, which sets the lengths and angles measured between spacetime events. According to general relativity, the metric is determined by the matter content of spacetime via the field equations, and in turn the motion of the matter is determined by the metric. Thus gravitation becomes a purely geometric concept.

Despite their elegant tensorial form, Einstein's equations turn out to be a complicated set of coupled nonlinear second-order partial differential equations when written out explicitly in terms of the metric. Only under rather restrictive assumptions has one been able to find analytical solutions to these equations, e.g., by imposing symmetries or considering weak perturbations

about a fixed background solution.

One of the most promising routes towards a deeper understanding of the full implications of general relativity appears to be the use of numerical methods to solve the field equations. Since its first steps in the 1960s [75], numerical relativity has sparked many new insights, including the discovery of critical phenomena by Choptuik [40]. With gravitational wave observatories such as LIGO, VIRGO, GEO, and TAMA soon expected to be fully operating, there is today a strong demand for waveform templates from numerical simulations of astrophysical scenarios such as the collision of black holes or neutron stars.

Current research focuses on two main branches, which are increasingly moving towards each other. The general relativistic side of the field is mainly concerned with the geometry of spacetime, studying, for example, vacuum black hole spacetimes, most notably the binary black hole problem. The astrophysical side concentrates on the general relativistic motion of matter, e.g., stellar collapse, and tries to incorporate physically realistic forms of matter, equations of state and interactions. This thesis is almost entirely concerned with the first approach.

For a comprehensive review of numerical relativity, we refer the reader to the review article by Lehner [96].

1.2 Axisymmetry

Most of the early calculations in numerical relativity were concerned with spherically symmetric spacetimes. Because this is effectively a one-dimensional problem, it could be tackled with the modest computational resources available at that time. Powered by the rapid increase in the capacity and speed

of hardware, attention has now almost entirely turned to the case without any symmetries.

The intermediate case, axisymmetry, has not been studied to the same extent. However, axisymmetric situations occur frequently in astrophysics and there are many interesting problems one can study: e.g., the head-on collision of two black holes, rotating stars and accretion disks. In contrast to spherical symmetry (as a consequence of Birkhoff's theorem [20]), axisymmetric spacetimes admit gravitational waves. Evolving axisymmetric spacetimes is less computationally expensive than the case without symmetries because there are only two (rather than three) effective spatial dimensions. Thus many questions in numerical relativity can be investigated much more directly.

The main difficulty with axisymmetric spacetimes is the coordinate singularity on the axis in the coordinate system that is adapted to the symmetry, cylindrical polar coordinates. Many attempts to deal with this proved unsuccessful and numerical evolutions became unstable. There are many ways to address this problem, of which we only outline the two most often used.

The *cartoon method* of Alcubierre et al. [7] uses Cartesian coordinates and thereby avoids the coordinate singularity. In one of the three spatial dimensions, the numerical grid consists only of a few (typically three) grid points, and the axisymmetry is imposed by appropriate boundary conditions in that direction. This method has been used successfully in practice, although its stability properties are somewhat dubious [55]. An interesting variant of the method that avoids the use of a third dimension altogether can be found in [112].

The second approach, which we shall adopt in this thesis, uses cylindrical polar coordinates and imposes appropriate *regularity conditions* on the variables at the axis $r = 0$ so that the equations are well-behaved there.

This is the method used by Nakamura et al. [104] and later by Garfinkle and Duncan [62] and Choptuik et al. [41] for a relatively simple formulation of the axisymmetric Einstein equations. One of the main objectives of this thesis is to develop a systematic regularization procedure for a rather general (and complicated) system such as the one studied in chapter 6. Our regularity conditions are based on the small-r behaviour of various axisymmetric tensor fields derived in chapter 2.

We apply a differential geometric trick in order to reduce the number of variables we need to evolve: the axisymmetry is essentially "divided out" and the Einstein equations are expressed entirely within the three-dimensional manifold formed by the trajectories of the Killing vector generating the symmetry. This was invented in this context by Geroch [65] although the idea resembles the famous Kaluza-Klein reduction [85, 89]. In contrast to previous numerical studies [41, 62], we do not restrict ourselves to the case in which the Killing vector is hypersurface-orthogonal. Thus we are able to evolve rotating spacetimes.

1.3 Evolution formalisms

To make the Einstein equations suitable for numerical treatment, one typically introduces a foliation of spacetime into three-dimensional hypersurfaces. The most frequently used approach is to choose the hypersurfaces to be spacelike, which leads to the *ADM* or *3+1* or *Cauchy formulation* of general relativity [12]. Another possibility is to take the hypersurfaces to be null, which leads to the *characteristic formulation* [28, 120]. A third approach is known as the *conformal Einstein equations* [56], in which one applies the ADM approach to a larger unphysical spacetime which contains the physical

one in a finite region. In this thesis, we will adopt the ADM formulation and combine it with the aforementioned dimensional reduction, resulting in what is known as the *(2+1)+1 formalism* [100]. In this case, the slices of the foliation are two-dimensional.

In the ADM approach, the Einstein equations split into elliptic *constraint equations* within the spacelike hypersurfaces and *hyperbolic evolution equations* governing the time evolution normal to the hypersurfaces. The constraints are conserved by the evolution equations. In addition, certain *gauge variables* appear that can be freely specified and that reflect the general covariance of general relativity – the field equations are invariant under transformations of the spacetime coordinates. These basic properties immediately raise two questions: firstly, how to choose the gauge (i.e., the coordinates) and secondly, how to deal with the constraints during the evolution.

Since one does not normally know in advance what spacetime the initial data one specifies on the initial hypersurface will evolve to, one would not like to specify the gauge *a priori* as a fixed function of spacetime. Rather, one would like to tie it to the dynamics so that it can adapt itself to the solution. A first class of gauge conditions we consider in chapter 5 are based on geometrical considerations: we choose the foliation such that the slices have maximal proper volume and their induced metric is conformally flat. This leads to *elliptic* equations for the gauge variables. The resulting system is similar to the ones considered in [41, 62] but our version is more general in that it includes rotation.

There are two different ways of dealing with the constraints. One can either solve them during the evolution to update some of the variables (*constrained evolution*) or one can evolve all the variables via the evolution equations, leaving the constraints unsolved (*free evolution*). As we shall see, both

approaches have certain advantages and disadvantages.

If one decides to adopt the free evolution approach, one can look for *strongly* (or even *symmetric*) *hyperbolic* formulations of the Einstein equations, in a sense made mathematically precise in section 6.4. This requires certain modifications to the ADM system, for that system is itself only weakly hyperbolic [87]. Hyperbolic formulations of the Einstein equations have been a very active area of research over the past few years and there exist today a plethora of examples (see [116] for a recent review).

Of the many techniques for obtaining hyperbolic systems, a particularly simple and beautiful one is the so-called *Z4 extension* of the field equations developed by Bona et al. [23]. This involves adding a covariant extra term to the Einstein equations such that the enlarged ADM system is automatically hyperbolic (subject to certain provisos). We apply this technique to the (2+1)+1 formalism to obtain a new strongly hyperbolic formulation of the Einstein equations tailored to axisymmetric spacetimes. Of course, we now have to replace our elliptic gauge conditions with hyperbolic ones, and the ones we use are a generalization of *harmonic gauge*, in which the spacetime coordinates obey the wave equation.

In contrast to mixed hyperbolic-elliptic formulations, hyperbolic ones have the advantage that there is a well-developed mathematical machinery for analyzing the well-posedness of the initial boundary value problem. This depends crucially on the boundary conditions that one imposes at the outer boundaries of the (finite) computational domain. Obtaining stable boundary conditions that avoid spurious reflections is another objective of this thesis.

1.4 Numerical methods and implementation

Once one has decided on a particular evolution formalism, the next question is how to solve the system numerically.

The first step is to discretize the spatial domain. The approach that is used most often in numerical relativity and that we shall follow here is the *finite difference technique* [73]. Thereby the domain is covered by a discrete grid and the numerical approximation is represented by its values at the grid points. Differential operators are translated into finite differences by means of Taylor expansions. A different approach is based on an expansion of the numerical solution with respect to a given set of basis functions. This leads to methods such as *finite element, spectral* and *pseudo-spectral methods*. Considerable progress for the vacuum Einstein equations has been obtained with the latter [122, 67]. Finite element methods have been used to construct initial data for black hole and Brill wave spacetimes [11, 82].

As mentioned in the previous section, the ADM formalism generically leads to two different types of PDEs: hyperbolic and elliptic ones. Accordingly, their solution requires two rather different classes of numerical methods.

The framework we use for the hyperbolic equations is the *method of lines*, whereby the PDE is first only discretized in space, leaving the time dependence continuous. A suitable ODE integrator is then used for the time integration. The method of lines combined with straightforward finite differencing works well for smooth solutions such as those of vacuum general relativity considered in this thesis. Once matter is included, e.g., a perfect fluid, one has to deal with discontinuities such as shocks and more sophisticated methods from computational fluid dynamics are needed (see [97] for a comprehensive introduction).

Elliptic equations are generally thought to be expensive to solve numerically because they typically require $O(N^2)$ operations (N being the number of unknowns, i.e., grid points) as opposed to $O(N)$ operations for hyperbolic equations. A class of elliptic methods that achieve a complexity of $O(N)$ as well are *Multigrid methods* [31]. This makes them the ideal method for numerical relativity if elliptic equations need to be solved at each time step of the evolution. However, as we shall see in this thesis, Multigrid is not suitable for the solution of certain indefinite elliptic equations such as one of the constraint equations (the Hamiltonian constraint). *Conjugate gradient methods* [125] provide an alternative but are much more computationally expensive.

Solutions of partial differential equations often exhibit a variety of relevant length scales. For example, certain hyperbolic gauge conditions tend to produce highly distorted slices. As a consequence, steep gradients and peaks appear in the metric variables that propagate through the numerical grid, whereas the solution is completely smooth elsewhere. *Adaptive mesh refinement (AMR)* is a numerical technique that addresses this problem in a computationally efficient way. More resolution is added in regions where and when it is needed, and discarded when it becomes obsolete. We use Berger and Oliger's [19] classic version of the algorithm for hyperbolic partial differential equations.

All algorithms employed in this thesis have been implemented in C++. In order to manipulate the equations to be solved, we make extensive use of the computer algebra language REDUCE [80], from which we also generate C code automatically. Gnuplot and the Data-Vault [110] are used for visualization.

1.5 Gravitational waves and critical collapse

The main application we consider in this thesis is the numerical evolution of gravitational waves. Axisymmetric gravitational waves (with time-symmetric initial data) are known as *Brill waves* [32].

For weak perturbations of flat space, one can construct analytical solutions of the linearized field equations. We use some of these as test problems for our code (chapter 7).

No analytical solutions are known in the nonlinear case and one has to resort to numerical methods. The earliest numerical study of Brill waves we know of is the one by Eppley [48, 49], which uses a similar gauge as the one described in section 5.1 of this thesis. Those early experiments indicated that while weak Brill waves disperse to leave flat space behind, sufficiently strong ones collapse to form a black hole. Abrahams and Evans [1, 2] looked closer at the threshold of black hole formation and found what is known as *critical behaviour* in gravitational collapse.

Critical behaviour was first discovered by Choptuik [40], albeit for a very different system: the massless scalar field in spherical symmetry. Choptuik considered a one-parameter family of asymptotically flat smooth initial data. Let p_* be the critical value of the parameter p separating dispersal of the field and black hole formation. For slightly supercritical evolutions, Choptuik found a *scaling relation* for the mass of the black holes formed,

$$M_{\mathrm{BH}} \propto (p - p_*)^{\gamma}\,, \tag{1.1}$$

where the *critical exponent* γ appeared to be independent of the particular family of initial data chosen. Note the similarity of (1.1) with the scaling relations found in thermodynamic phase transitions. Moreover, the critical solution Z^* appeared to be *universal*, i.e., independent of the initial data,

and *discretely self-similar* with *echoing exponent* Δ:

$$Z^*(x,\tau) = Z^*(x,\tau+\Delta)\,, \qquad x \equiv r/(-t)\,, \qquad \tau \equiv -\ln(-t)\,. \tag{1.2}$$

(Here r is an areal radial coordinate and t is proper time of the central observer such that $t = 0$ coincides with the *accumulation point* [40].) For a review of critical phenomena in gravitational collapse see Gundlach [69].

Abrahams and Evans found the same type of critical behaviour as described above (commonly referred to as *Type II*) in Brill wave collapse and estimated the constants γ and Δ. This is important because it suggests that critical behaviour is a property of general relativity alone rather than of the specific matter model used. It would be important to confirm their calculation, possibly with greater precision and longer run times (only ≈ 4 echos of the critical solution were tracked in [1]), which has not been done yet as far as I can determine. In addition, Abrahams and Evans have only considered the case in which the Killing vector is hypersurface-orthogonal. The formalism presented in this thesis does not rely on that restriction, and it would be interesting to see how a nonzero twist might influence the critical behaviour.

Even if our code is not yet capable of addressing these questions quantitatively, we have come across a variety of problems along the way which appear to be ubiquitous in current research in numerical relativity. This thesis documents our efforts towards a solution of those problems.

1.6 Outline of the thesis

We begin by deriving the regularity conditions that various axisymmetric tensor fields must obey on the axis (chapter 2). This will be used throughout the thesis in order to cast the equations to be solved in a regular form. The evolution formalism that forms the basis of all later developments, the

(2+1)+1 formalism, is derived in chapter 3. The numerical methods we use are described in chapter 4. We then construct in chapter 5 a first evolution system that uses elliptic gauge conditions and (partially) constrained evolution. Some preliminary results on the simulation of Brill waves are presented. To my knowledge, this is the first time twisting Brill waves have been evolved.

The remainder of this thesis is concerned entirely with a strongly hyperbolic formulation of the Einstein equations for axisymmetric spacetimes. This so-called Z(2+1)+1 system is derived in chapter 6. By a careful choice of variables we write the equations in a form that is well-behaved on the axis, which is one of our main results. Exact solutions of linearized theory are constructed in chapter 7 and are used in order to demonstrate the accuracy of our numerical implementation. Chapter 8 is concerned with various ways of imposing boundary conditions at the outer boundaries of the computational domain. Their stability is analyzed both analytically and numerically. AMR evolutions of strong Brill waves close to the critical point are presented in chapter 9, including twist. We conclude and give an outlook on future work in chapter 10.

1.7 Notation and conventions

The Einstein summation convention is used for tensor indices, i.e., repeated indices are summed over. Round (square) brackets enclosing tensor indices denote (anti-)symmetrization, i.e., $T_{(\alpha\beta)} = \frac{1}{2}(T_{\alpha\beta} + T_{\beta\alpha})$ and $T_{[\alpha\beta]} = \frac{1}{2}(T_{\alpha\beta} - T_{\beta\alpha})$. Ordinary (partial) differentiation is denoted by a comma (,). Sometimes the comma is left out if no ambiguity arises, e.g., $f_\alpha \equiv f_{,\alpha}$ for a scalar f.

We use a Lorentzian metric of signature $(-+++)$. Our curvature con-

vention is

$$R_{\alpha\beta\gamma\delta}v^{\delta} = 2\nabla_{[\alpha}\nabla_{\beta]}v^{\gamma}\,. \tag{1.3}$$

Geometric units are chosen, in which Newton's constant G and the speed of light c are equal to 1 so that $\kappa = 8\pi$ in Einstein's equations

$$G_{\alpha\beta} = \kappa T_{\alpha\beta}\,. \tag{1.4}$$

Chapter 2

Implications of axisymmetry

Many problems with axisymmetry arise from the fact that the coordinate system adapted to the symmetry, cylindrical polar coordinates, is singular on the axis of symmetry. As a consequence, axisymmetric tensor fields that are regular on the axis (in a sense made precise below) may take strange forms when expressed in those coordinates. In this chapter, we derive the regularity conditions that various axisymmetric tensor fields must obey on the axis.

We want to use a (t, z, r, φ) chart adapted to the Killing vector $\xi = \partial/\partial\varphi$. We shall assume *elementary flatness*: in a neighbourhood of the axis we can introduce local Cartesian coordinates $x^A = (x, y)$ such that

$$x = r\cos\varphi, \quad y = r\sin\varphi \quad \Longleftrightarrow \quad r = \sqrt{x^2 + y^2}, \quad \varphi = \arctan\frac{y}{x}\,. \tag{2.1}$$

Note that the Cartesian chart is regular on the axis $r = 0$, while the polar chart is not. With respect to Cartesian coordinates, the Killing vector is

$$\xi = -y\frac{\partial}{\partial x} + x\frac{\partial}{\partial y}\,. \tag{2.2}$$

This representation is valid everywhere, while $\xi = \partial/\partial\varphi$ is valid only for $r > 0$.

We say that a tensor field T is *regular on axis* if its Cartesian components have a Taylor expansion with respect to x and y about $x^A = 0$ convergent in some neighbourhood of $r = 0$. (Throughout this chapter we are ignoring t and z dependencies, which are implicit in all calculations.) It is *axisymmetric* if its Lie derivative with respect to the Killing vector vanishes,

$$\mathcal{L}_\xi T = 0\,. \tag{2.3}$$

2.1 Functions

Let us start with an axisymmetric function f that is regular on axis. Axisymmetry implies that

$$k \equiv \mathcal{L}_\xi f = -y f_{,x} + x f_{,y} = 0, \tag{2.4}$$

which is valid everywhere. In particular, we may differentiate (2.4) an arbitrary number of times with respect to x and y and require all the derivatives to vanish on axis:

$$\begin{aligned}
0 = k_{,x} = x f_{,xy} - y f_{,xx} + f_{,y} \quad &\Rightarrow \quad f_{,y} \doteq 0\,, \\
0 = k_{,y} = -y f_{,xy} - f_{,x} + x f_{,yy} \quad &\Rightarrow \quad f_{,x} \doteq 0\,, \\
0 = k_{,xx} = 2 f_{,xy} - y f_{,xxx} + x f_{,xxy} \quad &\Rightarrow \quad f_{,xy} \doteq 0\,, \\
0 = k_{,xy} = x f_{,xyy} - y f_{,xxy} - f_{,xx} + f_{,yy} \quad &\Rightarrow \quad f_{,xx} \doteq f_{,yy} \equiv f_2\,, \\
0 = k_{,yy} = -y f_{,xyy} - 2 f_{,xy} + x f_{,yyy} & \\
&\vdots
\end{aligned} \tag{2.5}$$

where $\doteq$ denotes equality on axis. We find that the Taylor expansion of f in a neighbourhood of the axis has the form

$$f = \sum_{n=0}^{\infty} \frac{f_{2n}}{(2n)!} (x^2 + y^2)^n\,, \tag{2.6}$$

i.e., f is an even function of r:

$$f = f(t, z, r^2)\,. \tag{2.7}$$

2.2 Vectors and covectors

Next consider a vector field u^α. For $a = (t, z)$, $\mathcal{L}_\xi u^a = 0$ implies $\partial u^a/\partial\varphi = 0$. This reduces to the scalar field case and we may deduce $u^a = u^a(r^2)$. For u^x and u^y we have

$$\frac{\partial u^x}{\partial\varphi} + u^y = 0, \quad \frac{\partial u^y}{\partial\varphi} - u^x = 0. \tag{2.8}$$

The general solution for $r > 0$ is

$$u^x = \widehat{a}(r)\cos\varphi - \widehat{b}(r)\sin\varphi, \quad u^y = \widehat{a}(r)\sin\varphi + \widehat{b}(r)\cos\varphi. \tag{2.9}$$

However in the Cartesian chart, (2.8) takes the form

$$-yu^x{}_{,x} + xu^x{}_{,y} + u^y = 0, \quad -yu^y{}_{,x} + xu^y{}_{,y} - u^x = 0. \tag{2.10}$$

Setting $x^A = 0$ we see that $u^A = 0$ on axis. We may thus write $\widehat{a} = ra$, $\widehat{b} = rb$ so that (2.9) becomes

$$u^x = xa - yb, \quad u^y = ya + xb. \tag{2.11}$$

We now regard a and b as unknown functions of x and y to be determined by substituting (2.11) into (2.10), differentiating the latter an arbitrary number of times, and then solving the recurrence relations for the Taylor coefficients of a and b. Again we find that a and b are even functions of r. Finally, the polar components of u are obtained from (2.11) as

$$u^r = \frac{\partial r}{\partial x^A}u^A = ra(r^2)\,, \quad u^\varphi = \frac{\partial\varphi}{\partial x^A}u^A = b(r^2)\,. \tag{2.12}$$

Thus in the (t, z, r, φ) chart an axisymmetric vector field which is regular on axis must take the form

$$u^\alpha = (A, B, rC, D), \tag{2.13}$$

where A, B, C and D are functions of t, z and r^2.

Next consider an axisymmetric covector field ω_α which is regular on axis. For $a = (t, z)$, $\mathcal{L}_\xi \omega_a = 0$ implies $\partial\omega_a/\partial\varphi = 0$. This reduces to the scalar field case and we may deduce $\omega_a = \omega_a(r^2)$. For the other indices we find

$$-y\omega_{x,x} + x\omega_{x,y} + \omega_y = 0, \quad -y\omega_{y,x} + x\omega_{y,y} - \omega_x = 0, \tag{2.14}$$

which is equivalent to (2.10), interchanging u^A and ω_A. We therefore deduce the analogue of (2.11) and hence, in polar coordinates,

$$\omega_\alpha = (A, B, rC, r^2D), \tag{2.15}$$

where A, B, C and D are functions of t, z and r^2.

2.3 Symmetric 2-tensors

Finally we consider a symmetric valence 2 tensor field $M_{\alpha\beta}$ which is both axisymmetric and regular on axis. For $(a, b) = (t, z)$ we have $\mathcal{L}_\xi M_{ab} = 0$ and so $M_{ab} = M_{ab}(r^2)$. The mixed (aA) components obey the Killing equations

$$-yM_{ax,x} + xM_{ax,y} + M_{ay} = 0, \quad -yM_{ay,x} + xM_{ay,y} - M_{ax} = 0. \tag{2.16}$$

This is essentially the same as (2.14) and we may deduce $M_{ar} = rA_a(r^2)$ and $M_{a\varphi} = r^2B_a(r^2)$. The remaining Killing equations are

$$-yM_{xx,x} + xM_{xx,y} + 2M_{xy} = 0, \quad -yM_{yy,x} + xM_{yy,y} - 2M_{xy} = 0,$$

$$-yM_{xy,x} + xM_{xy,y} + M_{yy} - M_{xx} = 0\,. \tag{2.17}$$

If we introduce new variables $u = \frac{1}{2}(M_{xx} + M_{yy})$, $v = \frac{1}{2}(M_{xx} - M_{yy})$ and $w = M_{xy}$ then

$$-yu_{,x} + xu_{,y} = 0 \tag{2.18}$$

which implies $u = u(r^2)$. The remaining equations are

$$-yv_{,x} + xv_{,y} + 2w = 0, \quad -yw_{,x} + xw_{,y} - 2v = 0. \tag{2.19}$$

For $r > 0$ these can be written as

$$v_{,\varphi} + 2w = 0, \quad w_{,\varphi} - 2w = 0, \tag{2.20}$$

so that

$$v = \widehat{a}(r)\cos 2\varphi - \widehat{b}(r)\sin 2\varphi, \quad w = \widehat{a}(r)\sin 2\varphi + \widehat{b}(r)\cos 2\varphi, \tag{2.21}$$

where $\widehat{a}$ and $\widehat{b}$ are arbitrary functions of r. But (2.19) and its first derivatives imply that v, w and their first derivatives vanish on axis so that we may set $\widehat{a} = r^2 a$ and $\widehat{b} = r^2 b$ to obtain

$$v = (x^2 - y^2)a - 2xyb, \quad w = 2xya + (x^2 - y^2)b. \tag{2.22}$$

Substituting (2.22) into (2.19) gives

$$\begin{aligned} x^3 a_{,y} - x^2 y(a_{,x} + 2b_{,y}) - xy^2(a_{,y} - 2b_{,x}) + y^3 a_{,x} &= 0, \\ x^3 b_{,y} + x^2 y(-b_{,x} + 2a_{,y}) + xy^2(-2a_{,x} - b_{,y}) + y^3 b_{,x} &= 0. \end{aligned} \tag{2.23}$$

Differentiating these many times and proceeding as in the scalar and vector cases, we conclude that a and b are functions of r^2. Thus

$$M_{xx} = u + (x^2 - y^2)a - 2xyb, \quad M_{yy} = u - (x^2 - y^2)a + 2xyb,$$

$$M_{xy} = 2xya + (x^2 - y^2)b\,. \tag{2.24}$$

Re-expressing these as polar components we obtain

$$M_{rr} = u + r^2 a, \quad M_{r\varphi} = r^3 b, \quad M_{\varphi\varphi} = r^2(u - r^2 a). \tag{2.25}$$

Finally combining all of the results we have

$$M_{\alpha\beta} = \begin{pmatrix} A & B & rD & r^2F \\ B & C & rE & r^2G \\ rD & rE & H + r^2J & r^3K \\ r^2F & r^2G & r^3K & r^2\,(H - r^2J) \end{pmatrix}, \tag{2.26}$$

where $A, B, \ldots, K$ are functions of t, z and r^2.

One should remark that one could relax our definition of regularity on axis. If we only required functions to be C^0, vectors and covectors to be C^1 and 2-tensors to be C^2 in a neighbourhood of the axis, the above analysis would still go through and we would arrive at the same regularity conditions. However, the coefficients $A, B, \ldots$ in (2.13), (2.15) and (2.26) would then only be continuous and not necessarily even functions of r. For numerical purposes of course, it is not unduly restrictive to assume analyticity if the solutions are smooth.

Summarizing, we have derived the regularity conditions that axisymmetric functions (2.7), vectors (2.13), covectors (2.15) and symmetric 2-tensors (2.26) must obey in order to be regular on the axis of symmetry. Note in particular the subtle relation between the (rr) and $(\varphi\varphi)$ components in (2.26). If a numerical evolution scheme fails to preserve precisely the indicated r-dependencies then the fields become irregular on axis and instability is inevitable. In chapters 5 and 6, we will use the regularity conditions in

order to cast reductions of Einstein's equations into forms that are free of any divergencies on the axis.

Chapter 3

The (2+1)+1 formalism

Quite generally, the existence of a symmetry can be used to reduce the dimensionality of the problem under consideration. This should be exploited whenever possible in order not only to simplify the problem mathematically but also to save computational resources when attempting a numerical solution.

We shall see how in the case of axisymmetry, the Einstein equations can be reduced from four-dimensional spacetime $\mathcal{M}$ to a three-dimensional Lorentzian manifold $\mathcal{N}$ (section 3.1). This was first performed for vacuum spacetimes by Geroch [65], although the original idea goes back to the famous papers by Kaluza [85] and Klein [89]. We extend the reduction to include general matter sources.

The three-dimensional Lorentzian manifold $\mathcal{N}$ then undergoes an ADM-like decomposition (cf. [12] for the standard $3+1$ version), i.e., it is foliated into level surfaces of a time function (section 3.2). The Einstein equations split into elliptic constraint equations to be solved within the hypersurfaces and hyperbolic evolution equations governing the evolution normal to the hypersurfaces, making the problem suitable for numerical simulations. This

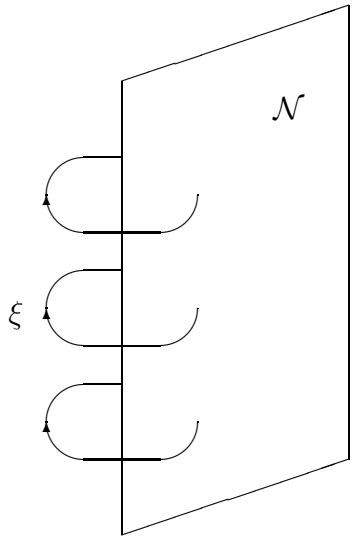

Figure 3.1: The manifold $\mathcal{N}$

procedure was first applied in this context by Maeda et al. [100] and is commonly referred to as the *(2+1)+1 formalism*.

We use energy-momentum and number conservation to derive evolution equations for the matter variables in this formalism (section 3.3). No particular matter model is chosen at this stage.

We mainly follow the notation of Maeda et al. [100] with some clearly stated changes. In the following, Greek indices range over t, r, z, φ, lower-case Latin indices over t, r, z, and upper-case Latin indices over r, z.

3.1 The Geroch decomposition

Spacetime is assumed to be a four-dimensional manifold $(\mathcal{M}, g_{\alpha\beta})$ with signature $(- + ++)$ and a preferred polar coordinate chart (t, r, z, φ). Axisymmetry means that there is an everywhere spacelike Killing vector field

$\xi = \partial/\partial\varphi$ with closed orbits. Let $\mathcal{N}$ be the collection of the orbits of ξ. We assume that $\mathcal{N}$ is a differentiable 3-manifold and that there is a smooth mapping from $\mathcal{M}$ into $\mathcal{N}$ mapping a point in $\mathcal{M}$ to the orbit passing through it.

Geroch [65] has shown that there is a one-to-one correspondence between tensor fields $M'^{\alpha\ldots}{}_{\beta\ldots}$ in $\mathcal{N}$ and tensor fields $M^{\alpha\ldots}{}_{\beta\ldots}$ in $\mathcal{M}$ that are both orthogonal to the Killing vector,

$$M^{\alpha\ldots}{}_{\beta\ldots}\xi^\beta = M^{\alpha\ldots}{}_{\beta\ldots}\xi_\alpha = \ldots = 0\,, \tag{3.1}$$

and axisymmetric,

$$\mathcal{L}_\xi M^{\alpha\ldots}{}_{\beta\ldots} = 0\,. \tag{3.2}$$

As a shorthand, tensors satisfying these conditions are said to be *in* $\mathcal{N}$.

Some basic tensor fields in $\mathcal{N}$ are the norm of the Killing vector

$$\lambda^2 = g_{\alpha\beta}\xi^\alpha\xi^\beta > 0\,, \tag{3.3}$$

the (Lorentzian) metric in $\mathcal{N}$,

$$h_{\alpha\beta} = g_{\alpha\beta} - \lambda^{-2}\xi_\alpha\xi_\beta\,, \tag{3.4}$$

the Levi-Civita tensor

$$\epsilon_{\alpha\beta\gamma} = \lambda^{-1}\epsilon_{\alpha\beta\gamma\delta}\xi^\delta\,, \tag{3.5}$$

and the *twist vector*

$$\omega_\alpha = \epsilon_{\alpha\beta\gamma\delta}\xi^\beta\nabla^\gamma\xi^\delta\,, \tag{3.6}$$

which encodes the rotational degrees of freedom. Here ∇ is the covariant derivative of $g_{\alpha\beta}$. The covariant derivative D associated with $h_{\alpha\beta}$ is obtained by projecting ∇ into $\mathcal{N}$,

$$D_\alpha v^\beta = h_\alpha{}^\mu h_\nu{}^\beta \nabla_\mu \left(h_\rho{}^\nu v^\rho\right)\,. \tag{3.7}$$

The Riemann tensor of $h_{\alpha\beta}$ is denoted by ${}^{(3)}R_{\alpha\beta\gamma\delta}$.

We wish to reduce Einstein's theory in $\mathcal{M}$ to a set of equations that only involve tensor fields in $\mathcal{N}$. Starting with the Ricci identity in $\mathcal{N}$,

$$D_{[\alpha}D_{\beta]}v_{\gamma} = \tfrac{1}{2}{}^{(3)}R_{\alpha\beta\gamma\delta}v^{\delta}\,, \tag{3.8}$$

we evaluate the left-hand-side using the definition of D (3.7) to find

$${}^{(3)}R_{\alpha\beta\gamma\delta} = h_{[\alpha}{}^{\mu}h_{\beta]}{}^{\nu}h_{[\gamma}{}^{\rho}h_{\delta]}{}^{\sigma}\left[{}^{(4)}R_{\mu\nu\rho\sigma} + 2\lambda^{-2}\left(Q_{\mu\nu}Q_{\rho\sigma} + Q_{\mu\rho}Q_{\nu\sigma}\right)\right]\,, \tag{3.9}$$

where the four-dimensional Ricci identity has been used to produce the Riemann tensor ${}^{(4)}R_{\alpha\beta\gamma\delta}$ of $\mathcal{M}$. The quantity $Q_{\alpha\beta} \equiv \nabla_{\alpha}\xi_{\beta} = \nabla_{[\alpha}\xi_{\beta]}$ can be expressed as

$$Q_{\alpha\beta} = \tfrac{1}{2}\lambda^{-2}\epsilon_{\alpha\beta\gamma\delta}\xi^{\gamma}\omega^{\delta} - 2\lambda^{-1}\xi_{[\alpha}\lambda_{\beta]}\,. \tag{3.10}$$

Contracting (3.9) with $h^{\beta\delta}$ and using (3.10) we obtain

$${}^{(3)}R_{\alpha\gamma} = \perp {}^{(4)}R_{\alpha\gamma} + \lambda^{-1}D_{\alpha}D_{\gamma}\lambda + \tfrac{1}{2}\lambda^{-4}\left(\omega_{\alpha}\omega_{\gamma} - h_{\alpha\gamma}\omega^{\tau}\omega_{\tau}\right)\,. \tag{3.11}$$

Here and in the following, the symbol $\perp$ means projection of the free indices with h, and an index ξ denotes contraction with ξ.

Some more equations are needed in order to reflect all the Einstein equations of the original manifold $\mathcal{M}$. Taking the curl and divergence of (3.6), we obtain, respectively,

$$D_{[\alpha}\omega_{\beta]} = \lambda\epsilon_{\alpha\beta\gamma} \perp {}^{(4)}R^{\gamma}{}_{\xi} \tag{3.12}$$

and

$$D_{\alpha}\omega^{\alpha} = 3\lambda^{-1}\lambda_{,\alpha}\omega^{\alpha}\,, \tag{3.13}$$

where we have used (3.10) and a standard identity for Killing vectors,

$$\nabla_{\alpha}\nabla_{\beta}\xi_{\gamma} = {}^{(4)}R_{\delta\alpha\beta\gamma}\xi^{\delta}\,. \tag{3.14}$$

Finally, applying $D^2 = D^\alpha D_\alpha$ to (3.3), we obtain

$$D^2\lambda = -\frac{1}{2}\lambda^{-3}\omega_\alpha\omega^\alpha - \lambda^{-1}{}^{(4)}R_{\xi\xi}\,. \tag{3.15}$$

Next, we include an energy-momentum tensor $T_{\alpha\beta}$, which is decomposed into

$$\begin{aligned} \tau &\equiv \lambda^{-2}\xi^\mu\xi^\nu T_{\mu\nu}\,, \\ \tau_\alpha &\equiv \lambda^{-2}h_\alpha{}^\mu\xi^\nu T_{\mu\nu}\,, \\ \tau_{\alpha\beta} &\equiv h_\alpha{}^\mu h_\beta{}^\nu T_{\mu\nu}\,. \end{aligned} \tag{3.16}$$

(The powers of λ included in the above definitions differ from the ones in [100]. Our choice guarantees that τ and τ_α have the correct small-r behaviour of scalars (2.7) and covectors (2.15). Note that $\lambda = O(r)$ near the axis.) It follows from axisymmetry

$$\mathcal{L}_\xi T_{\alpha\beta} = 0 \tag{3.17}$$

that the fields τ, τ_α and $\tau_{\alpha\beta}$ are in $\mathcal{N}$. The Einstein equations

$${}^{(4)}R_{\alpha\beta} = \kappa\left(T_{\alpha\beta} - \tfrac{1}{2}Tg_{\alpha\beta}\right) \tag{3.18}$$

can be used to express the projections of the Ricci tensor in terms of those of the energy-momentum tensor,

$$\begin{aligned} \perp {}^{(4)}R_{\alpha\beta} &= \kappa\left[\tau_{\alpha\beta} - \tfrac{1}{2}h_{\alpha\beta}\left(\tau + \tau_\gamma{}^\gamma\right)\right]\,, \\ \perp {}^{(4)}R_{\alpha\xi} &= \kappa\lambda^2\tau_\alpha\,, \\ {}^{(4)}R_{\xi\xi} &= \tfrac{1}{2}\kappa\lambda^2\left(\tau - \tau_\gamma{}^\gamma\right)\,. \end{aligned} \tag{3.19}$$

Inserting (3.19) into (3.11–3.13) and (3.15), we arrive at the Geroch-

Einstein equations

$$\begin{aligned} {}^{(3)}R_{ab} &= \kappa\left[\tau_{ab} - \tfrac{1}{2}h_{ab}\left(\tau + \tau_c{}^c\right)\right] + \tfrac{1}{2}\lambda^{-4}\left(\omega_a\omega_b - h_{ab}\omega^c\omega_c\right) \\ &\quad +\lambda^{-1}\lambda_{|ab}\,, \qquad (3.20) \\ \omega_{[a|b]} &= -\kappa\lambda^3\epsilon_{abc}\tau^c\,, \qquad (3.21) \\ (\lambda^3\omega^c)_{|c} &= 0\,, \qquad (3.22) \\ \lambda_{|a}{}^a &= -\tfrac{1}{2}\lambda^{-3}\omega_c\omega^c - \tfrac{1}{2}\kappa\lambda\left(\tau - \tau_c{}^c\right)\,. \qquad (3.23) \end{aligned}$$

Here $|$ stands for the covariant derivative D. All terms in (3.20–3.23) are in $\mathcal{N}$, which justifies the use of lower-case Latin indices ranging over t, r and z only.

Geroch [65] has also shown how the original four-dimensional manifold $(\mathcal{M}, g_{\alpha\beta})$ can be recovered from the three-dimensional manifold $(\mathcal{N}, h_{ab})$ and the fields ω_α and λ. To begin with, choose an arbitrary four-dimensional manifold $\mathcal{M}$ along with a nowhere-vanishing vector field $\xi = \partial/\partial\varphi$ on $\mathcal{M}$. Consider the following skew 2-form in $\mathcal{N}$:

$$F_{ab} \equiv -\tfrac{1}{2}\lambda^{-3}\epsilon_{abc}\omega^c\,. \qquad (3.24)$$

By equation (3.22), it is curl-free:

$$\epsilon^{abc}D_aF_{bc} = 0\,. \qquad (3.25)$$

If we pull it back to $\mathcal{M}$, we obtain a curl-free 2-form $F_{\alpha\beta}$ because the pull-back commutes with differentiation. By Frobenius' theorem there exists a covector field η_β such that

$$\partial_{[\alpha}\eta_{\beta]} = F_{\alpha\beta}\,. \qquad (3.26)$$

There is a gauge freedom

$$\eta_\alpha \to \eta_\alpha + \partial_\alpha\sigma \qquad (3.27)$$

for an arbitrary function σ. We exploit the φ-dependence of σ to set

$$\eta_\alpha \xi^\alpha = 1\,. \tag{3.28}$$

Next we define

$$g_{\alpha\beta} = h_{\alpha\beta} + \lambda^2 \eta_\alpha \eta_\beta \tag{3.29}$$

so that $\xi_\alpha = g_{\alpha\beta}\xi^\beta = \lambda^2 \eta_\alpha$ and hence

$$g_{\alpha\beta} = h_{\alpha\beta} + \lambda^{-2} \xi_\alpha \xi_\beta\,, \tag{3.30}$$

as desired. It can be verified from (3.10) that

$$\nabla_{(\alpha}\xi_{\beta)} = 0\,, \tag{3.31}$$

i.e., that ξ is a Killing vector of $g_{\alpha\beta}$. It is not clear how to implement this procedure numerically, and indeed there is no need to do so. All physically interesting quantities in $\mathcal{M}$ have their counterparts in $\mathcal{N}$ and so we choose to work entirely within $\mathcal{N}$. For instance, it suffices to know the variables in $\mathcal{N}$ in order to form the Newman-Penrose scalar Ψ_4 containing the gravitational wave information (see section 8.3 for an explicit derivation of Ψ_0; the Ψ_4 calculation is similar).

3.2 The ADM decomposition

Following the standard ADM [12] procedure, a time function t is introduced and the three-dimensional manifold $\mathcal{N}$ is foliated into two-dimensional spacelike hypersurfaces $\Sigma(t)$ of constant t. The future-directed unit timelike normal to the hypersurfaces is

$$n_a = -\alpha\, \partial_a t \tag{3.32}$$

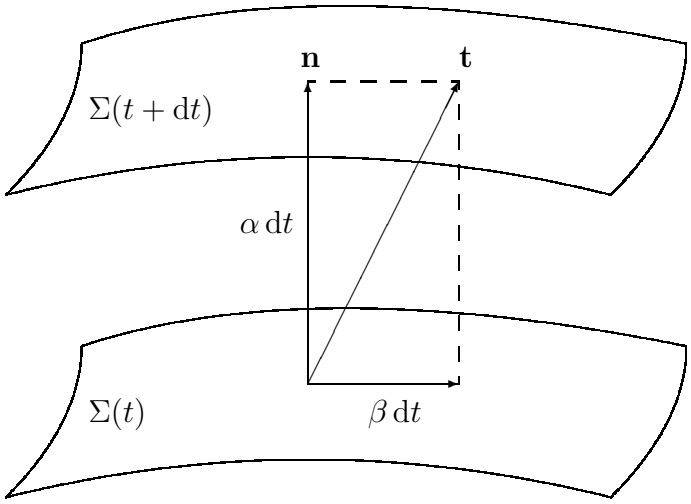

Figure 3.2: The ADM setup

normalized such that $n_a n^a = -1$. Here α is the *lapse function*, which describes the amount of proper time elapsing when passing from one hypersurface $\Sigma(t)$ to a nearby one $\Sigma(t + \mathrm{d}t)$. The direction of time is not unique, however: the spatial coordinate origin in $\Sigma(t+\mathrm{d}t)$ can be shifted with respect to the origin in $\Sigma(t)$ by an arbitrary *shift vector* β^a (figure 3.2),

$$t^a = \alpha n^a + \beta^a. \tag{3.33}$$

The induced 2-metric on the hypersurfaces Σ is

$$H_{ab} = h_{ab} + n_a n_b\,, \tag{3.34}$$

satisfying $H_{ab}n^b = 0$, i.e., it is indeed a tensor in Σ and can thus be written as H_{AB}, where capital Latin indices A, B run over r and z. With those definitions, the line element of $\mathcal{N}$ takes the form

$$\mathrm{d}s^2 = -\alpha^2 \mathrm{d}t^2 + H_{AB}\left(\mathrm{d}x^A + \beta^A \mathrm{d}t\right)\left(\mathrm{d}x^B + \beta^B \mathrm{d}t\right)\,. \tag{3.35}$$

How the hypersurfaces $\Sigma(t)$ are imbedded in $\mathcal{N}$ is described by the *second fundamental form* or *extrinsic curvature*

$$\chi_{ab} = -H_a{}^c H_b{}^d n_{(c|d)} = -\tfrac{1}{2}\mathcal{L}_n H_{ab}\,, \tag{3.36}$$

which because of (3.33) is essentially the time-derivative of the 2-metric.

The Riemann tensor ${}^{(2)}R_{ABCD}$ in $\Sigma(t)$ is related to the one in $\mathcal{N}$ by the well-known *Gauss-Codazzi equations*

$$\perp {}^{(3)}R_{ABCD} = {}^{(2)}R_{ABCD} + \chi_{AC}\chi_{BD} - \chi_{AD}\chi_{BC}\,, \tag{3.37}$$

$$\perp {}^{(3)}R_{ABCn} = \chi_{AC\|B} - \chi_{BC\|A}\,, \tag{3.38}$$

where $\perp$ means projection of the free indices with H, and an index n stands for contraction with n. The symbol $\|$ denotes the covariant derivative d of H_{ab},

$$\mathrm{d}_a v^b = H_a{}^c H_d{}^b D_c \left(H_e{}^d v^e\right)\,. \tag{3.39}$$

The derivation of (3.37) and (3.38) is completely analogous to the reduction of ${}^{(4)}R$ to ${}^{(3)}R$ presented in the previous section. The projections of the three-dimensional Einstein tensor

$${}^{(3)}G_{ab} = {}^{(3)}R_{ab} - \tfrac{1}{2}{}^{(3)}R h_{ab} \tag{3.40}$$

are found to be

$${}^{(3)}G_{nn} = 2{}^{(3)}R_{nn} + {}^{(3)}R = \tfrac{1}{2}\left({}^{(2)}R + (\chi_A{}^A)^2 - \chi_{AB}\chi^{AB}\right)\,, \tag{3.41}$$

$$\perp {}^{(3)}G^{An} = \perp {}^{(3)}R^{An} = \mathrm{d}_B\left(-\chi^{AB} + H^{AB}\chi_C{}^C\right)\,. \tag{3.42}$$

The above two equations form so-called *constraint equations* on the hypersurfaces $\Sigma(t)$ because they do not involve any time derivatives. (3.41) is called the *Hamiltonian* or *energy constraint*, and (3.42) are the *momentum constraints*. Let us also calculate the time derivative of the extrinsic curvature.

Using the Ricci identity,

$$\mathcal{L}_N \chi_{AB} = \alpha \perp {}^{(3)}R_{AnBn} - \alpha \chi_{AC} \chi_B{}^C - \alpha_{\|AB} \,, \tag{3.43}$$

and decomposing the Riemann tensor using the Gauss-Codazzi equations (3.37–3.38),

$$\begin{aligned} \mathcal{L}_n \chi_{AB} &= - \perp {}^{(3)}R_{AB} + \left({}^{(2)}R_{AB} + \chi_C{}^C \chi_{AB} \right) - 2 \chi_{AC} \chi_B{}^C \\ &\quad - \alpha^{-1} \alpha_{\|AB} \,. \end{aligned} \tag{3.44}$$

Equations (3.36) and (3.44) form a set of *evolution equations* for the 2-metric and extrinsic curvature.

We are now ready to insert the results of our $2+1$ decomposition into the Geroch-Einstein equations (3.20-3.23). The trace of the extrinsic curvature is abbreviated as $\chi = \chi_A{}^A$. Further variables defined in each $\Sigma(t)$ are the alternating symbol

$$\epsilon_{AB} = n^c \epsilon_{cAB} \,, \tag{3.45}$$

the $(\varphi\varphi)$-component of the extrinsic curvature,

$$K_\varphi{}^\varphi = -\lambda^{-1} n^a \lambda_a \,, \tag{3.46}$$

and the projections of the twist vector,

$$E^A = \lambda^{-3} \epsilon^{Ab} \omega_b \,, \tag{3.47}$$

$$B^\varphi = \lambda^{-3} n_a \omega^a \,. \tag{3.48}$$

(Again, the last two definitions differ from those in [100] by factors of λ. This ensures that E^A has the correct small-r behaviour of a vector (2.13). Our B^φ is $O(r)$ on the axis, which is easier to enforce numerically than the $O(r^2)$ behaviour of B_φ in [100]). The various projections of the energy-momentum

tensor are

$$\begin{aligned} J^{\varphi} &= -n_a \tau^a \,, \\ S^A &= H_a{}^A \tau^a \,, \\ \rho_H &= n^a n^b \tau_{ab} \,, \\ J_A &= -H_A{}^a n^b \tau_{ab} \,, \\ S_{AB} &= H_A{}^a H_B{}^b \tau_{ab} \,, \end{aligned} \tag{3.49}$$

and, of course, τ defined in (3.16).

The constraint equations. Inserting the Geroch result (3.20) for ${}^{(3)}R_{ab}$ into the constraint equations (3.41, 3.42), we obtain

$$\begin{aligned} \mathcal{C} \equiv\ & \tfrac{1}{2}(\chi^2 - \chi_{AB}\chi^{AB} + {}^{(2)}R) - \lambda^{-1}\lambda_{\|A}{}^A + \chi K_{\varphi}{}^{\varphi} \\ & -\tfrac{1}{4}\lambda^2 \left(E_A E^A + B^{\varphi 2}\right) - \kappa\rho_H = 0 \,, \end{aligned} \tag{3.50}$$

$$\begin{aligned} \mathcal{C}_A \equiv\ & \chi_A{}^B{}_{||B} - (\chi + K_{\varphi}{}^{\varphi})_{,A} + \lambda^{-1}\lambda^B \chi_{AB} - \lambda^{-1}\lambda_A K_{\varphi}{}^{\varphi} \\ & -\tfrac{1}{2}\lambda^2 B^{\varphi}\epsilon_{AB}E^B - \kappa J_A = 0 \,. \end{aligned} \tag{3.51}$$

The Geroch equation (3.21) forms an additional constraint equation, which we call the *Geroch constraint*:

$$\mathcal{C}_{\varphi} \equiv \tfrac{1}{2}E^A{}_{||A} + \tfrac{3}{2}\lambda^{-1}\lambda_A E^A - \kappa J^{\varphi} = 0 \,. \tag{3.52}$$

Hence there are four constraint equations, as in the standard $3+1$ ADM decomposition.

The evolution equations. These are expressed in terms of the Lie derivative along the normal lines, which by (3.33) is

$$\mathcal{L}_n = \alpha^{-1}\partial_t - \mathcal{L}_{\beta} \,. \tag{3.53}$$

Definitions (3.36) and (3.46) form evolution equations for the 2-metric and the norm of the Killing vector,

$$\mathcal{L}_n H_{AB} = -2\,\chi_{AB}\,, \tag{3.54}$$

$$\mathcal{L}_n \lambda = -\lambda K_\varphi{}^\varphi\,. \tag{3.55}$$

In the evolution equation for the extrinsic curvature (3.44), we substitute (3.20) for ${}^{(3)}R_{ab}$ to obtain

$$\begin{aligned}\mathcal{L}_n \chi_{AB} = {}& {}^{(2)}R_{AB} - \lambda^{-1}\lambda_{A||B} - \alpha^{-1}\alpha_{A||B} \\ & +(\chi + K_\varphi{}^\varphi)\chi_{AB} - 2\chi_A{}^C\chi_{CB} \\ & -\tfrac{1}{2}\lambda^2\left[\epsilon_{AC}\epsilon_{BD}E^C E^D - H_{AB}\left(E_C E^C - B^{\varphi 2}\right)\right] \\ & -\kappa\left[S_{AB} + \tfrac{1}{2}H_{AB}\left(\rho_H - S_C{}^C - \tau\right)\right]\,.\end{aligned} \tag{3.56}$$

The Geroch equation (3.23) can be rewritten as

$$\begin{aligned}\mathcal{L}_n K_\varphi{}^\varphi = {}& -\lambda^{-1}\lambda^A{}_{||A} - (\alpha\lambda)^{-1}\lambda_A\alpha^A + K_\varphi{}^\varphi\left(\chi + K_\varphi{}^\varphi\right) \\ & -\tfrac{1}{2}\lambda^2\left(E_A E^A - B^{\varphi 2}\right) - \tfrac{1}{2}\kappa\left(\rho_H - S_A{}^A + \tau\right)\,.\end{aligned} \tag{3.57}$$

Finally using (3.22) together with (3.23), we obtain the following evoluton equations for the twist variables,

$$\begin{aligned}\mathcal{L}_n E^A = {}& \epsilon^{AB}B^\varphi{}_{,B} + (\chi + 3K_\varphi{}^\varphi)E^A \\ & +\epsilon^{AB}(\alpha^{-1}\alpha_B + 3\lambda^{-1}\lambda_B)B^\varphi - 2\kappa S^A\,,\end{aligned} \tag{3.58}$$

$$\mathcal{L}_n B^\varphi = \epsilon^{AB}E_{A||B} + \chi B^\varphi + \alpha^{-1}\epsilon^{AB}E_A\alpha_B\,. \tag{3.59}$$

Equations (3.52) and (3.58–3.59) are remarkably similar to the axisymmetric Maxwell equations for an $\mathbf{E}$ field in the (r, z) plane and a $\mathbf{B}$ field in the φ direction, which justifies the notation:

$$\nabla\cdot\mathbf{E} = \rho\,, \tag{3.60}$$

$$\partial_t\mathbf{E} = \nabla\times\mathbf{B} + \mathbf{j}\,, \tag{3.61}$$

$$\partial_t\mathbf{B} = -\nabla\times\mathbf{E}\,. \tag{3.62}$$

This is not surprising, of course, as the original Kaluza-Klein theory [85, 89] was designed to incorporate electrodynamics into four-dimensional general relativity by assuming an additional compactified spacelike dimension.

3.3 Matter evolution equations

Evolution equations for the matter variables can be obtained from energy-momentum conservation

$$\nabla_\alpha T^{\alpha\beta} = 0\,. \tag{3.63}$$

In our case, the energy-momentum tensor $T^{\alpha\beta}$ is also axisymmetric,

$$\mathcal{L}_\xi T^{\alpha\beta} = 0\,. \tag{3.64}$$

First we decompose $T^{\alpha\beta}$ with respect to the Killing vector ξ^α (Geroch decomposition),

$$T^{\alpha\beta} = \lambda^{-2}\xi^\alpha\xi^\beta\tau + 2\tau^{(\alpha}\xi^{\beta)} + \tau^{\alpha\beta}\,, \tag{3.65}$$

where τ, τ^α and $\tau^{\alpha\beta}$ were defined in (3.16). Contracting (3.63) with ξ_β, we obtain the following conservation law in $\mathcal{N}$,

$$D_a(\lambda^3\tau^a) = 0\,, \tag{3.66}$$

and projecting (3.63) with $h_\beta{}^b$ yields

$$D_a(\lambda\tau^{ab}) = \lambda^{-1}\lambda^b\tau - \lambda^{-1}\epsilon^{bcd}\tau_c\omega_d\,. \tag{3.67}$$

Next we decompose τ^{ab} further with respect to the unit timelike normal n_a (ADM decomposition),

$$\tau^{ab} = \rho_H n^a n^b + 2J^{(a}n^{b)} + S^{ab}\,, \tag{3.68}$$

where ρ_H, J^a and S^{ab} were defined in (3.49). Contracting (3.67) with n_b, we obtain an evolution equation for ρ_H,

$$\begin{aligned}\mathcal{L}_n\rho_H &= -J^A{}_{||A} - J^A(2\alpha^{-1}\alpha_A + \lambda^{-1}\lambda_A) + \chi\rho_H + \chi_{AB}S^{AB} \\ &\quad + K_\varphi{}^\varphi(\tau + \rho_H) + \lambda^2 E^A S_A\,, \end{aligned} \tag{3.69}$$

and projecting (3.67) with $H_b{}^B$ yields an evolution equation for J^A,

$$\begin{aligned}\mathcal{L}_n J_A &= -S_{AB}{}^{||B} + J_A(\chi + K_\varphi{}^\varphi) - S_{AB}(\alpha^{-1}\alpha^B + \lambda^{-1}\lambda^B) \\ &\quad -\alpha^{-1}\alpha_A\rho_H + \lambda^{-1}\lambda_A\tau + \lambda^2(E_A J^\varphi + \epsilon_{AB}S^B B^\varphi)\,. \end{aligned} \tag{3.70}$$

Equation (3.66) can be rewritten as an evolution equation for J^φ (also defined in (3.16)),

$$\mathcal{L}_n J^\varphi = -S^A{}_{||A} - S^A(\alpha^{-1}\alpha_A + 3\lambda^{-1}\lambda_A) + J^\varphi(\chi + 3K_\varphi{}^\varphi)\,. \tag{3.71}$$

We recognize in the above the general relativistic version of the Euler equations: (3.69) expresses energy conservation, (3.70) linear momentum conservation and (3.71) angular momentum conservation.

In some situations (e.g., for a perfect fluid) there may be a conserved particle number density N^α satisfying

$$\nabla_\alpha N^\alpha = 0 \tag{3.72}$$

and which is also axisymmetric,

$$\mathcal{L}_\xi N^\alpha = 0\,. \tag{3.73}$$

Again, we can obtain an evolution equation from (3.72) by performing the same dimensional reductions as above. First we decompose N^α with respect to the Killing vector ξ^α (Geroch decomposition)

$$N^\alpha = \lambda^{-1}\xi^\alpha\nu + \nu^\alpha\,, \tag{3.74}$$

where we have defined

$$\nu \equiv \xi_\alpha N^\alpha \tag{3.75}$$

and

$$\nu^\alpha \equiv h^\alpha{}_\beta N^\beta \,. \tag{3.76}$$

It follows from axisymmetry (3.73) that ν and ν^α are in $\mathcal{N}$. Particle number conservation (3.72) can be expressed in $\mathcal{N}$ as

$$D_a(\lambda\nu^a) = 0 \,. \tag{3.77}$$

Next we decompose ν^α with respect to the unit timelike normal n_a (ADM decomposition),

$$\nu^a = n^a\sigma + \Sigma^a \,, \tag{3.78}$$

where we have defined

$$\sigma \equiv -n_a\nu^a \tag{3.79}$$

and

$$\Sigma^a \equiv H^a{}_b\nu^b \,. \tag{3.80}$$

From (3.77) we obtain an evolution equation for σ,

$$\mathcal{L}_n\sigma = -\Sigma^A{}_{||A} - \Sigma^A(\alpha^{-1}\alpha_A + \lambda^{-1}\lambda_A) + \sigma(\chi + K_\varphi{}^\varphi) \,. \tag{3.81}$$

So far we have not chosen any specific matter model. In appendix A, a perfect fluid is discussed. For the main part of this thesis, however, we will focus on vacuum spacetimes.

Chapter 4

Numerical methods

We have seen in the previous chapter that the Einstein equations split into hyperbolic evolution equations and elliptic constraint equations when an ADM (or "space + time") decomposition is applied. In this chapter we describe the numerical methods we use to solve these two classes of PDEs.

The basis for all the methods is the finite difference technique, which is briefly described in section 4.1, along with the ghost cell technique for implementing boundary conditions.

The basic framework we adopt for solving the hyperbolic evolution equations is the method of lines (section 4.2). We explain the properties of explicit Runge-Kutta and iterative Crank-Nicholson schemes and briefly comment on the use of numerical dissipation.

We then turn to elliptic equations and describe the Multigrid method (section 4.3), starting from linear scalar equations in one dimension and extending the algorithm to nonlinear problems, systems of equations and multidimensions.

Some alternative methods for hyperbolic and elliptic PDEs and their applicability to our problem are discussed in section 4.4.

Finally, we describe the adaptive mesh refinement technique for hyperbolic PDEs in section 4.5, pointing out some of the changes we have made to the algorithm.

4.1 The finite difference technique

4.1.1 The numerical grid

The spatial domain we evolve is a finite rectangular region in the (r, z) plane,

$$\Omega = [0, r_{\max}] \times [0, z_{\max}] \,. \tag{4.1}$$

We restrict ourselves to the upper half of the (r, z) plane ($z \geqslant 0$) because we will impose reflection symmetry about $z = 0$ for all the numerical evolutions carried out in this thesis. (This is not an essential restriction and one could equally well work with a general domain that extends into the lower half of the (r, z) plane.)

The numerical domain is covered by an equidistant *grid* with grid points (r_i, z_j), where

$$r_i = (i - \tfrac{1}{2})h \,, \qquad 1 \leqslant i \leqslant N_r \,, \tag{4.2}$$

$$z_j = (j - \tfrac{1}{2})h \,, \qquad 1 \leqslant j \leqslant N_z \,. \tag{4.3}$$

Here N_r and N_z are the number of grid points in the r and z direction and the grid spacing h is the same in both dimensions,

$$h = \frac{r_{\max}}{N_r} = \frac{z_{\max}}{N_z} \,. \tag{4.4}$$

In all applications, we choose $r_{\max} = z_{\max}$ and hence $N_r = N_z \equiv N$. The Multigrid method (section 4.3) further requires that N be of the form $N =$

$k \times 2^{l-1}$, where l is the number of Multigrid levels and k is the size of the coarsest grid.

Note that the first grid point in the r direction is at $r = h/2$, not at $r = 0$. Thereby we avoid dividing by zero in terms formally containing factors of r^{-1}. The grid points (r_i, z_j) can also be viewed as the centres of the *cells*

$$C_{ij} = [(i-1)h, ih] \times [(j-1)h, jh]\,, \tag{4.5}$$

which cover the entire spatial domain Ω. For this reason, we call the type of grid we use a *cell-centred* one. Using such a grid has certain additional advantages if matter is included, for example in the form of a perfect fluid. This is usually evolved using the *finite volume* technique (e.g., [97]), where the solution is represented by the cell averages in the cells C_{ij}.

4.1.2 Centred finite difference operators

The vacuum equations, however, are discretized using the *finite difference* technique. Thereby continuum functions $u(r, z)$ are represented by their values u_{ij} at the grid points (r_i, z_j). Differential operators are translated into finite difference operators acting on the discrete grid function. These can be derived by means of Taylor expansions: as an example, consider

$$\begin{aligned} u_{i+1,j} &= u_{ij} + h(u_{,r})_{ij} + O(h^2)\,, \\ u_{i-1,j} &= u_{ij} - h(u_{,r})_{ij} + O(h^2)\,, \\ \Rightarrow (u_{,r})_{ij} &= \tfrac{1}{2h}(u_{i+1,j} - u_{i-1,j}) + O(h^2)\,. \end{aligned} \tag{4.6}$$

All the finite-difference operators we use are centred and second-order accurate in the grid spacing, as in the above example. The first-order derivatives

are represented by

$$u_{,r} \rightarrow \tfrac{1}{2h}(u_{i+1,j} - u_{i-1,j})\,, \tag{4.7}$$

$$u_{,z} \rightarrow \tfrac{1}{2h}(u_{i,j+1} - u_{i,j-1})\,, \tag{4.8}$$

$$(r^{-1}u)_{,r} \rightarrow \tfrac{1}{2h}(r_{i+1}^{-1}u_{i+1,j} - r_{i-1}^{-1}u_{i-1,j})\,. \tag{4.9}$$

The second-order finite differences needed for the hyperbolic-elliptic system (chapter 5) are

$$u_{,rr} \rightarrow \tfrac{1}{h^2}(u_{i+1,j} - 2u_{ij} + u_{i-1,j})\,, \tag{4.10}$$

$$u_{,zz} \rightarrow \tfrac{1}{h^2}(u_{i,j+1} - 2u_{ij} + u_{i,j-1})\,, \tag{4.11}$$

$$u_{,rz} \rightarrow \tfrac{1}{4h^2}(u_{i+1,j+1} - u_{i+1,j-1} - u_{i-1,j+1} + u_{i-1,j-1})\,, \tag{4.12}$$

$$(r^{-1}u_{,r})_{,r} \rightarrow \tfrac{1}{4h^2}\left[r_{i+1}^{-1}(u_{i+2,j} - u_{ij}) - r_{i-1}^{-1}(u_{ij} - u_{i-2,j})\right]\,. \tag{4.13}$$

4.1.3 The ghost cell technique

Boundary conditions are implemented using the *ghost cell* technique. Ghost cells are unphysical cells just outside the numerical domain. We add two layers of ghost cells at each boundary, at

$$\begin{aligned} r_0 &= -\tfrac{h}{2}\,, & r_{N_r+1} &= r_{\max} + \tfrac{h}{2}\,, \\ r_{-1} &= -\tfrac{3h}{2}\,, & r_{N_r+2} &= r_{\max} + \tfrac{3h}{2}\,, \end{aligned} \tag{4.14}$$

and similarly in the z direction. The ghost cells are filled with values according to the boundary conditions that one would like to impose. The same finite difference operators can then be applied at all interior points, without having to modify them close to the boundaries. Two layers of ghost cells are required because the stencils we use have a width of up to 5 grid points (the second-order derivative (4.13) and the fourth-order dissipation operator (4.64) have width 5).

In order to implement a *Neumann* condition

$$u_{,r}|_{r=0} = 0\,, \tag{4.15}$$

we note that

$$\begin{aligned} u_{,r}(0,z_j) &= \tfrac{1}{h}(u_{1j} - u_{0j}) + O(h^2) \\ &= \tfrac{1}{3h}(u_{2j} - u_{-1,j}) + O(h^2)\,, \end{aligned} \tag{4.16}$$

so that we choose the values of the ghost cells to be

$$u_{0j} = u_{1j}\,, \qquad u_{-1,j} = u_{2j}\,. \tag{4.17}$$

For a *Dirichlet* condition

$$u|_{r=0} = 0 \tag{4.18}$$

we note that

$$\begin{aligned} u(0,z_j) &= \tfrac{1}{2}(u_{1j} + u_{0j}) + O(h^2) \\ &= \tfrac{1}{2}(u_{2j} + u_{-1,j}) + O(h^2)\,, \end{aligned} \tag{4.19}$$

so that we need

$$u_{0j} = -u_{1j}\,, \qquad u_{-1,j} = -u_{2j}\,. \tag{4.20}$$

For *linear extrapolation* at $r = r_{\max}$, we set

$$u_{N_r+1,j} = 2u_{N_rj} - u_{N_r-1,j}\,, \qquad u_{N_r+2,j} = 2u_{N_r+1,j} - u_{N_rj}\,. \tag{4.21}$$

The *differential* boundary conditions used in this thesis (the "$1/R$ fall-off" condition (5.82) and the differential boundary conditions for the incoming modes in chapter 8) can be written in the general form

$$u_{,r} + f_{,z} + s = 0 \tag{4.22}$$

where f and s may depend on u. (This is sometimes called a *Robin* condition.) To implement (4.22) at the outer r boundary, we use the discretization

$$\begin{aligned} \tfrac{1}{h}(u_{N_r+1,j} - u_{N_rj}) + \tfrac{1}{2h}(f_{N_r,j+1} - f_{N_r,j-1}) + s_{N_rj} &= 0\,, \\ \tfrac{1}{2h}(u_{N_r+2,j} - u_{N_rj}) + \tfrac{1}{2h}(f_{N_r,j+1} - f_{N_r,j-1}) + s_{N_rj} &= 0 \end{aligned} \tag{4.23}$$

(except at $j = 1$ and $j = N_z$, where the z-derivatives are replaced with

$$\tfrac{1}{h}(f_{N_r2} - f_{N_r1})\,, \qquad \tfrac{1}{h}(f_{N_rN_z} - f_{N_r,N_z-1})\,, \tag{4.24}$$

respectively). Hence the ghosts are filled with

$$\begin{aligned} u_{N_r+1,j} &= u_{N_rj} - \tfrac{1}{2}(f_{N_r,j+1} - f_{N_r,j-1}) - hs_{N_rj}\,, \\ u_{N_r+2,j} &= u_{N_rj} - (f_{N_r,j+1} - f_{N_r,j-1}) - 2hs_{N_rj}\,. \end{aligned} \tag{4.25}$$

This discretization is only first-order accurate because a one-sided derivative is used in the r direction. We have also tried a second-order accurate discretization

$$\begin{aligned} \tfrac{1}{2h}(u_{N_r+1,j} - u_{N_r-1,j}) + \tfrac{1}{2h}(f_{N_r,j+1} - f_{N_r,j-1}) + s_{N_rj} &= 0\,, \\ \tfrac{1}{4h}(u_{N_r+2,j} - u_{N_r-2,j}) + \tfrac{1}{2h}(f_{N_r,j+1} - f_{N_r,j-1}) + s_{N_rj} &= 0\,, \end{aligned} \tag{4.26}$$

but this turned out to be less stable in some cases (section 8.7).

The implementation of the boundary conditions at $z = 0$ and $z = z_{\max}$ follows by symmetry.

We fill the ghost cells at each step of the time integration scheme discussed in the following section. This is crucial for the on-axis boundary conditions – if these are not enforced at all stages of the algorithm, instabilities quickly develop.

4.2 The method of lines

The basic framework we adopt in order to integrate the hyperbolic evolution equations forward in time is the *method of lines (MOL)* [123]. The basic idea is to finite-difference the spatial derivatives of the PDE as described in the previous section, leaving the time derivatives continuous. This leads to a coupled set of ODEs for the time dependence of the variables $\mathbf{u} = (u_{ij})$ at the spatial grid points,

$$\partial_t \mathbf{u} = \mathbf{f}(t, \mathbf{u}) \tag{4.27}$$

(in our case, there is no explicit time-dependence on the right-hand-side but we include it here for generality). A suitable ODE integrator is then used to integrate these ODEs forward in time.

4.2.1 Properties of Runge-Kutta and ICN schemes

The ODE integrators we consider here belong to the class of *explicit Runge-Kutta schemes*. Given the unknowns $\mathbf{u}^n$ at time t^n, these compute an approximation $\mathbf{u}^{n+1}$ at time $t^{n+1} = t^n + \Delta t$ in s stages as follows:

$$\begin{aligned}
\mathbf{k}_1 &= \mathbf{f}(t^n, \mathbf{u}^n)\,, && (4.28)\\
\mathbf{k}_2 &= \mathbf{f}(t^n + c_2\Delta t, \mathbf{u}^n + a_{21}\Delta t\mathbf{k}_1)\,, && (4.29)\\
\mathbf{k}_3 &= \mathbf{f}(t^n + c_3\Delta t, \mathbf{u}^n + a_{31}\Delta t\mathbf{k}_1 + a_{32}\Delta t\mathbf{k}_2)\,, && (4.30)\\
&\vdots \\
\mathbf{k}_s &= \mathbf{f}(t^n + c_s h, \mathbf{u}^n + a_{s1}\Delta t\mathbf{k}_1 + a_{s2}\Delta t\mathbf{k}_2 + \ldots \\
&\qquad\qquad + a_{s,s-1}\Delta t\mathbf{k}_{s-1})\,, && (4.31)\\
\mathbf{u}^{n+1} &= \mathbf{u}^n + \Delta t(b_1\mathbf{k}_1 + \ldots + b_s\mathbf{k}_s)\,. && (4.32)
\end{aligned}$$

Obviously a particular scheme is uniquely defined by the coefficients a_{ij}, b_i and c_i, which are conveniently written as a tableau

$$\begin{array}{c|ccccc} 0 & & & & & \\ c_2 & a_{21} & & & & \\ c_3 & a_{31} & a_{32} & & & \\ \vdots & \vdots & \vdots & \ddots & & \\ c_s & a_{s1} & a_{s2} & \cdots & a_{s,s-1} & \\ \hline & b_1 & b_2 & \cdots & b_{s-1} & b_s \end{array} \tag{4.33}$$

The method is said to be pth order if

$$\|u^{n+1} - u^n\| = O(\Delta t^{p+1}) \tag{4.34}$$

for sufficiently smooth $\mathbf{f}$.

The simplest Runge-Kutta method is the *Euler method*

$$\mathbf{u}^{n+1} = \mathbf{u}^n + \Delta t\, \mathbf{f}(t^n, \mathbf{u}^n)\,, \tag{4.35}$$

which is first-order and is represented by the tableau

$$\begin{array}{c|c} 0 & \\ \hline & 1 \end{array} \tag{4.36}$$

Two second-order Runge-Kutta methods are given by the tableaux

$$\begin{array}{c|cc} 0 & & \\ 1 & 1 & \\ \hline & \frac{1}{2} & \frac{1}{2} \end{array} \qquad \begin{array}{c|cc} 0 & & \\ \frac{1}{2} & \frac{1}{2} & \\ \hline & 0 & 1 \end{array} \tag{4.37}$$

The first is known as the *trapezoidal rule*, the second as the *midpoint rule*. Two examples of third-order methods are

$$\begin{array}{c|ccc} 0 & & & \\ \frac{1}{3} & \frac{1}{3} & & \\ \frac{2}{3} & 0 & \frac{2}{3} & \\ \hline & \frac{1}{4} & 0 & \frac{1}{4} \end{array} \qquad \begin{array}{c|ccc} 0 & & & \\ 1 & 1 & & \\ \frac{1}{2} & \frac{1}{4} & \frac{1}{4} & \\ \hline & \frac{1}{6} & \frac{1}{6} & \frac{2}{3} \end{array} \tag{4.38}$$

The first is *Heun's (third order) method*, the second can be found in Shu and Osher [127]. Of the many known fourth-order Runge-Kutta methods we only state the most popular one:

$$\begin{array}{c|cccc} 0 & & & & \\ \frac{1}{2} & \frac{1}{2} & & & \\ \frac{1}{2} & 0 & \frac{1}{2} & & \\ 1 & 0 & 0 & 1 & \\ \hline & \frac{1}{6} & \frac{1}{3} & \frac{1}{3} & \frac{1}{6} \end{array} \tag{4.39}$$

For orders $p > 4$, it is no longer possible to construct a pth order method with $s = p$ stages. For a survey of higher-order Runge-Kutta methods, see for example Butcher [36].

A method that has become very popular in numerical relativity is the *iterative Crank-Nicholson (ICN) method* [133] given by

$$\begin{aligned} \mathbf{k}_1 &= \mathbf{f}(t^n, \mathbf{u}^n)\,, && (4.40)\\ \mathbf{k}_2 &= \mathbf{f}(t^n + \tfrac{1}{2}\Delta t, \mathbf{u}^n + \tfrac{1}{2}\Delta t \mathbf{k}_1)\,, && (4.41)\\ \mathbf{k}_3 &= \mathbf{f}(t^n + \tfrac{1}{2}\Delta t, \mathbf{u}^n + \tfrac{1}{2}\Delta t \mathbf{k}_2)\,, && (4.42)\\ &\vdots \\ \mathbf{k}_s &= \mathbf{f}(t^n + \tfrac{1}{2}\Delta t, \mathbf{u}^n + \tfrac{1}{2}\Delta t \mathbf{k}_{s-1})\,, && (4.43)\\ \mathbf{u}^{n+1} &= \mathbf{u}^n + \Delta t \mathbf{k}_s\,. && (4.44) \end{aligned}$$

In the limit $s \to \infty$ this yields the well-known implicit *Crank-Nicholson method*

$$\frac{\mathbf{u}^{n+1} - \mathbf{u}^n}{\Delta t} = \mathbf{f}\left(\frac{\mathbf{u}^n + \mathbf{u}^{n+1}}{2}\right)\,. \tag{4.45}$$

The iterative version (4.40–4.44) can also be viewed [55] as an explicit Runge-

Kutta scheme with tableau

$$\begin{array}{c|ccccc} 0 & & & & & \\ \frac{1}{2} & \frac{1}{2} & & & & \\ \frac{1}{2} & 0 & \frac{1}{2} & & & \\ \vdots & \vdots & \vdots & \ddots & & \\ \frac{1}{2} & 0 & 0 & \cdots & \frac{1}{2} & \\ \hline & 0 & 0 & \cdots & 0 & 1 \end{array} \tag{4.46}$$

The ICN method is always second-order accurate regardless of the number of steps s.

To analyze the stability of the above ODE integrators, one applies them to the model equation

$$\partial_t \mathbf{u} = \lambda \mathbf{u}\,, \qquad \lambda \in \mathbb{C}\,. \tag{4.47}$$

From the form of the general Runge-Kutta scheme (4.28–4.32) it is clear that

$$\mathbf{u}^{n+1} = P(\lambda \Delta t)\mathbf{u}^n \tag{4.48}$$

for a certain complex polynomial P of degree s, the *stability function* of the method. Since $\|\mathbf{u}^{n+1}\| = |P(\lambda\Delta t)|\,\|\mathbf{u}^n\|$, the numerical approximation will remain bounded if and only if

$$|P(\lambda \Delta t)| \leqslant 1\,. \tag{4.49}$$

The set

$$S \equiv \{z \in \mathbb{C} : |P(z)| \leqslant 1\} \tag{4.50}$$

is called the *stability region* of the method. The Runge-Kutta schemes presented above have the stability function

$$P_{\mathrm{RK}[s]}(z) = \sum_{n=0}^{s} \frac{z^n}{n!} \tag{4.51}$$

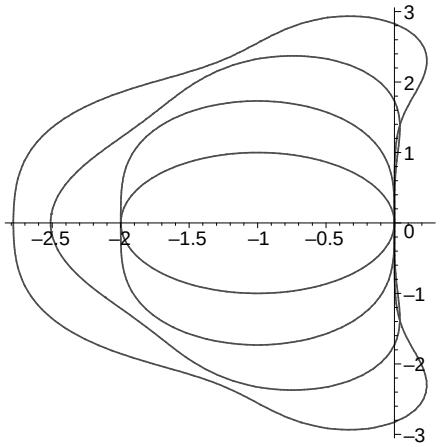

Figure 4.1: Stability regions of the Runge-Kutta methods with $s = 1, 2, 3, 4$ stages (from inward to outward)

(the result is the same for all schemes of a given order $s \leqslant 4$ [36]). The stability function of the ICN method is found to be

$$P_{\mathrm{ICN}[s]}(z) = 1 + z \sum_{n=0}^{s-1} \left(\frac{z}{2}\right)^n . \tag{4.52}$$

Graphs of the stability regions are shown in figures 4.1 and 4.2.

As an example of the method of lines, let us consider the scalar advection equation in one spatial dimension,

$$\partial_t u + c\partial_x u = 0 \,, \tag{4.53}$$

where the speed $c \in \mathbb{R}$ is a constant. Discretizing this in space using second-order centred finite differences, we obtain the system of ODEs

$$\partial_t u_j = -\tfrac{c}{2h}(u_{j+1} - u_{j-1}) \,. \tag{4.54}$$

Suppose we represent the numerical approximation as a superposition of Fourier modes (assuming periodic boundary conditions)

$$u_j = \hat{u}(i\xi)\mathrm{e}^{i\omega x_j} \,, \tag{4.55}$$

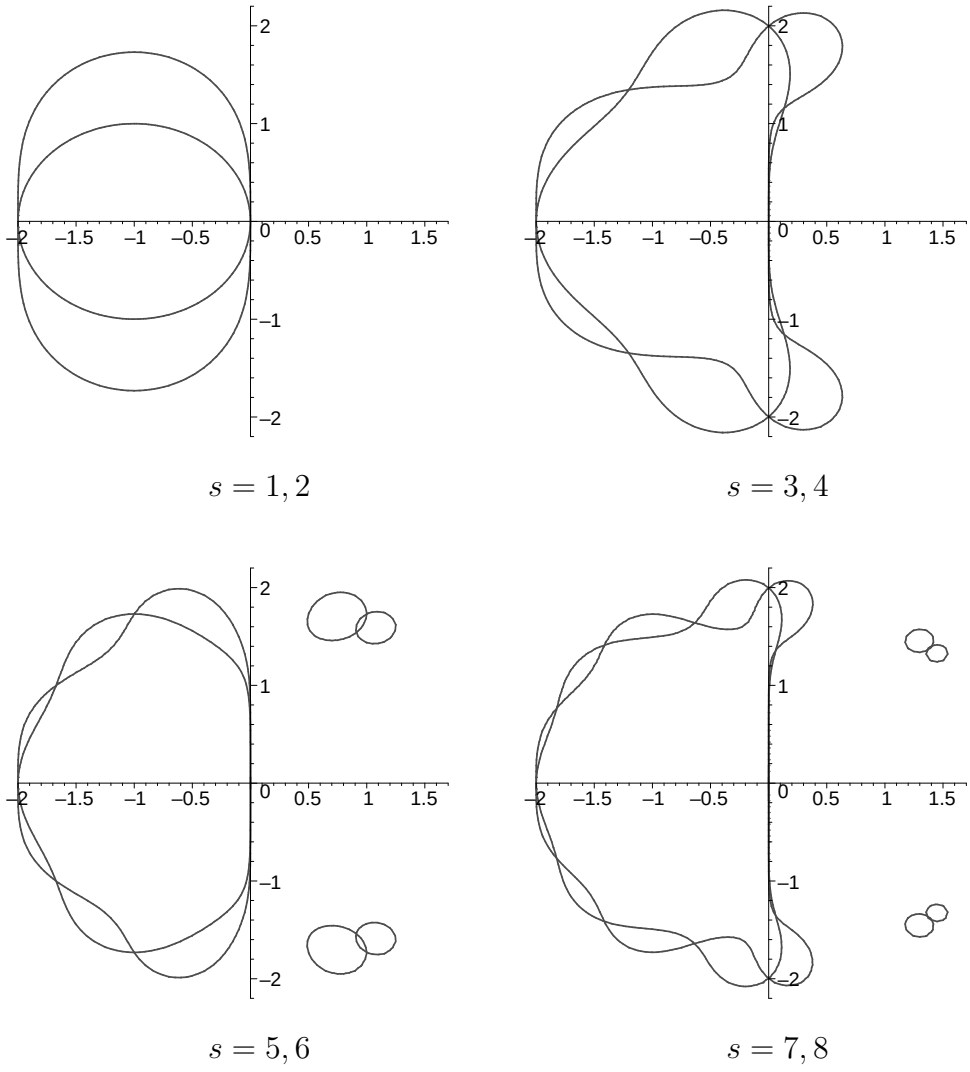

Figure 4.2: Stability regions of the ICN method for iteration numbers $1 \leqslant s \leqslant 8$

where we set $\xi \equiv \omega h$. Inserting this into (4.54) yields

$$\partial_t \hat{u}(i\xi) = -i\tfrac{c}{h} \sin\xi \, \hat{u}(i\xi)\,. \tag{4.56}$$

Hence the eigenvalues of the system (4.54) lie in the interval $[-ih^{-1}c, ih^{-1}c]$ on the imaginary axis.

A method for integrating (4.54) will be stable iff this interval lies within the stability region of that method. Setting $z = iq$ with $q \in \mathbb{R}$ we find for the Runge-Kutta methods

$$|P_{\mathrm{RK}[1]}(iq)|^2 - 1 = q^2\,, \tag{4.57}$$

$$|P_{\mathrm{RK}[2]}(iq)|^2 - 1 = \tfrac{1}{4}q^4\,, \tag{4.58}$$

$$|P_{\mathrm{RK}[3]}(iq)|^2 - 1 = \tfrac{1}{36}q^4(q^2-3)\,, \tag{4.59}$$

$$|P_{\mathrm{RK}[4]}(iq)|^2 - 1 = \tfrac{1}{576}q^6(q^2-8)\,. \tag{4.60}$$

Hence the stability regions of the first- and second-order schemes only touch the imaginary axis in the origin. For the third-order schemes, the boundary of the stability region intersects the imaginary axis at $z = \pm\sqrt{3}\,i$, and for the fourth-order schemes at $z = \pm 2\sqrt{2}\,i$. We conclude that the first- and second-order Runge-Kutta methods are unstable for the advection equation discretized as in (4.54). This result is well-known in the first-order case, which is identical with the *FTCS (forward-time central-space) method*. Setting $\lambda = \pm ih^{-1}c$ for the extremal eigenvalues in (4.49) and thus $z = \lambda\Delta t = \pm ih^{-1}c\Delta t$, we conclude that the third-order methods are stable iff

$$\left|\frac{\Delta t}{h}\, c\right| \leqslant \sqrt{3}\,, \tag{4.61}$$

and the fourth-order methods are stable iff

$$\left|\frac{\Delta t}{h}\, c\right| \leqslant 2\sqrt{2}\,. \tag{4.62}$$

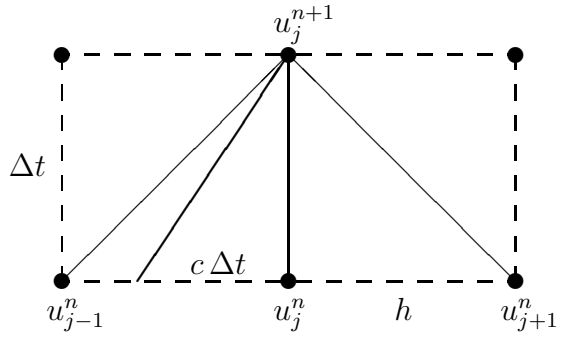

Figure 4.3: The CFL condition. The thick solid lines mark the boundary of the physical past domain of dependence of u_j^{n+1} for the case $c > 0$, the thin solid lines the numerical domain of dependence.

The restriction on the time step Δt as expressed in equations (4.61–4.62) is known as the *Courant-Friedrichs-Lewy (CFL) condition*, and the quotient $\Delta t/h$ is called the *CFL* or *Courant number*. A simple interpretation of the CFL condition is that the time step must be chosen small enough such that the numerical domain of dependence (as given by the stencil $[x_{j-1}, x_j, x_{j+1}]$) contains the physical domain of dependence (figure 4.3).

A similar analysis for the ICN method shows that the method is always unstable for $s = 1, 2, 5, 6, 9, 10, \ldots$ and stable for $s = 3, 4, 7, 8, 11, 12, \ldots$ provided that

$$\left| \frac{\Delta t}{h}\, c \right| \leqslant 2\,. \tag{4.63}$$

Since neither the order of accuracy nor the size of the interval on the imaginary axis contained in the stability region increase as s is increased, the optimal choice for s is $s = 3$. This was pointed out by Teukolsky [133] and confirmed with the method used here by Frauendiener [55]. Since the Runge-Kutta method with the same number of steps ($s = 3$) is third-order while the ICN method is only second-order, Runge-Kutta is always superior to ICN.

For the numerical experiments presented in this thesis, we have chosen

the third-order Runge-Kutta scheme of Shu (4.38b). (Unlike the other third-order method (4.38a) this is *total variation diminishing (TVD)* [127], a property that plays an important role in avoiding spurious oscillations around shocks if a perfect fluid is evolved with the same time integrator.) We found that the fourth-order method (4.39) (although not TVD) has similar stability properties to (4.38a) for our system of equations. We decided not to use the fourth-order method because it is slightly more expensive[1], and it does not improve the overall accuracy because the spatial accuracy of the finite differencing is only 2.

4.2.2 Numerical dissipation

For the scalar advection equation with periodic boundary conditions, we found that the system of ODEs (4.27) solved in the MOL framework had purely imaginary eigenvalues. For more complicated (systems of) PDEs and in particular for non-periodic boundary conditions, this may no longer be the case. There may exist solutions that grow like $\exp(at/h)$ with $a > 0$. These are not present in the continuum problem but are a mere consequence of the spatial finite differencing.

In many cases, these spurious modes can be eliminated by adding *Kreiss-Oliger dissipation* [73, 94] to the right-hand-side of (4.27). An example of a dissipation operator is

$$(D_4 u)_j = -\tfrac{1}{16} h^{-1} (u_{j-2} - 4u_{j-1} + 6u_j - 4u_{j+1} + u_{j+2}) \,. \tag{4.64}$$

This operator has a Taylor expansion

$$(D_4 u)_j = -\tfrac{1}{16} h^3 (u'''')_j + O(h^5) \,. \tag{4.65}$$

[1]However, the fourth-order method has a larger stability region and thus permits a larger time step.

Because our finite-differencing is second-order accurate, the order of accuracy is not changed when adding $D_4\mathbf{u}$ to the right-hand-side,

$$\partial_t \mathbf{u} = \mathbf{f}(t, \mathbf{u}) + \epsilon_D D_4 \mathbf{u} \,. \tag{4.66}$$

Inserting a Fourier mode (4.55) into (4.64) gives us

$$D_4 \hat{u}(i\xi) = -h^{-1} \sin^4 \tfrac{\xi}{2}\, \hat{u}(i\xi) \,. \tag{4.67}$$

We see that adding dissipation will decrease the amplification factor of high-frequency modes (ξ close to π). The same argument as above for the advection equation shows that

$$\left| \frac{\Delta t}{h} \epsilon_D \right| \lesssim 1 \tag{4.68}$$

is needed for stability (the precise bound depending on the ODE integrator). In practice we mostly use $0.1 \lesssim \epsilon_D \lesssim 0.5$.

Our numerical experiments indicate that a small amount of artificial dissipation is essential in order to avoid high-frequency instabilities that occur at very late times during the evolutions, particularly close to the boundaries. For a theoretical justification for a simple model problem see Oliger [107, p 255].

We apply the fourth-order operator (4.64) both in the r and the z direction and add it to the right-hand-side of the discretized evolution equations at all interior grid points. In order to eliminate (or at least postpone) instabilities sometimes caused by outer boundary conditions of the differential type (4.22), we have tried replacing (4.64) with the second-order operator

$$(D_2 u)_j = \tfrac{1}{4} h^{-1} (u_{j+1} - 2u_j + u_{j-1}) = \tfrac{1}{4} h (u'')_j + O(h^3) \,. \tag{4.69}$$

This is only applied at the outermost layer of grid points. Since our discretization (4.23) of the differential boundary conditions is only first-order accurate, the leading-order accuracy is again unaffected.

4.3 The Multigrid method

Solving elliptic equations is generally thought to be expensive because typically $O(N^2)$ operations are required, where N is the number of grid points. In contrast, hyperbolic equations only require $O(N)$ operations per time step. However, the Multigrid method developed by Brandt [30] gets away with $O(N)$ operations and is thus competitive. This section serves as an introduction to this method. We begin by describing basic relaxation methods for elliptic differential equations and how the Multigrid idea can accelerate those methods significantly. We then generalize from linear to non-linear problems, systems of equations and two-dimensional problems. The first half of this section is mainly based on the book by Briggs et al. [31], which gives an excellent introduction to Multigrid methods. Further details can be found in Wesseling [141] and Hackbusch [74].

4.3.1 Relaxation Methods

Consider the simple one-dimensional model problem

$$\begin{aligned} -u''(x) &= f(x)\,, \qquad 0 < x < 1\,, \\ u(0) = u(1) &= 0\,. \end{aligned} \tag{4.70}$$

The domain $\Omega = [0,1]$ is discretized[2] by introducing the grid points $x_j = jh$, $0 \leqslant j \leqslant N$, where $h = 1/N$ is the constant width of the cells. The original differential equation (4.70) is replaced by a system of difference equations

$$\begin{aligned} h^{-2}(-u_{j-1} + 2u_j - u_{j+1}) &= f(x_j)\,, \qquad 1 \leqslant j \leqslant N-1\,, \\ u_0 = u_N &= 0\,, \end{aligned} \tag{4.71}$$

[2]This discretization is vertex-centred rather then cell-centred. We return to cell-centred discretizations in section 4.3.4.

where $u_j \equiv u(x_j)$. In matrix form, this system of linear equations is written as

$$A\mathbf{u} = \mathbf{f} \tag{4.72}$$

where

$$A = \frac{1}{h^2}\begin{bmatrix} 2 & -1 & & & \\ -1 & 2 & -1 & & \\ & \ddots & \ddots & \ddots & \\ & & -1 & 2 & -1 \\ & & & -1 & 2 \end{bmatrix} \tag{4.73}$$

One of the simplest schemes to solve (4.71) iteratively is the *Jacobi* method. It is obtained by solving the jth equation of (4.71) for u_j, using the current approximation for u_{j-1} and u_{j+1}:

$$v_j^{m+1} = \tfrac{1}{2}(v_{j-1}^m + v_{j+1}^m + h^2 f_j)\,, \qquad 1 \leqslant j \leqslant N-1\,, \tag{4.74}$$

where $\mathbf{v}^m$ denotes the mth step approximation to the unknown $\mathbf{u}$. The *Gauss-Seidel* method differs from the Jacobi method in that the components of the new approximation are used as soon as they are available, i.e., we successively replace

$$v_j \leftarrow \tfrac{1}{2}(v_{j-1} + v_{j+1} + h^2 f_j)\,, \qquad 1 \leqslant j \leqslant N-1\,, \tag{4.75}$$

in ascending order. Alternatively, one can sweep through the grid points in descending order, or one can first update the even components of $\mathbf{v}$ and then the odd components. The latter variant is known as *red-black* Gauss-Seidel.

Now consider a general matrix $A = D - L - U$ where D denotes the diagonal and $-L$ and $-U$ the strictly lower and upper triangular parts of A. The Jacobi method can be written as

$$\mathbf{v}^{m+1} = R_J \mathbf{v}^m + D^{-1}\mathbf{f} \tag{4.76}$$

where the *iteration matrix* R_J is given by

$$R_J = D^{-1}(L+U)\,. \tag{4.77}$$

Similarly, the Gauss-Seidel method takes the form

$$\mathbf{v}^{m+1} = R_G\mathbf{v}^m + (D-L)^{-1}\mathbf{f} \tag{4.78}$$

where

$$R_G = (D-L)^{-1}U\,. \tag{4.79}$$

The convergence properties of the above relaxations depend crucially on the size of the largest eigenvalue of the iteration matrix R, which is known as the *spectral radius*

$$\rho(R) = \max|\lambda(R)|\,. \tag{4.80}$$

The iteration converges if and only if $\rho(R) < 1$. This is satisfied if the original matrix $A = (a_{ij})$ is *diagonal dominant*, i.e.

$$\sum_{1\leqslant j\leqslant N-1,\, j\neq i} |a_{ij}| \leqslant |a_{ii}|\,, \qquad 1\leqslant i\leqslant N-1\,. \tag{4.81}$$

This condition imposes quite a severe restriction on realistic problems, as we shall see in section 5.5.2.

To analyze the convergence properties in more detail, it is useful to look at the characteristic structure of the iteration matrix R. We illustrate this for the Jacobi method applied to the model problem (4.71). The eigenvalues of R_J are found to be

$$\lambda_k(R_J) = 1 - 2\sin^2\frac{k\pi}{2N}\,, \qquad 1\leqslant k\leqslant N-1\,, \tag{4.82}$$

and the eigenvectors $\mathbf{w}_k$ are given by

$$w_{k,j} = \sin\frac{jk\pi}{2N}\,, \qquad 1\leqslant k\leqslant N-1\,, \quad 0\leqslant j\leqslant N\,. \tag{4.83}$$

We see that the eigenvectors are simply Fourier modes. Let $\mathbf{e} = \mathbf{u} - \mathbf{v}$ denote the *error* of the approximation $\mathbf{v}$. Suppose we choose the initial error to be one of the Fourier modes, $\mathbf{e}^0 = \mathbf{w}_k$. Then the error after m steps of the iteration is $\mathbf{e}^m = R_J^m \mathbf{e}^0 = \lambda_k^m(R_J)\mathbf{w}_k$. After m iterations, the kth mode of the initial error has been reduced by a factor of $\lambda_k^m(R_J)$. From (4.82), we see that high-frequency or oscillatory modes of the error are damped much more effectively than low-frequency or smooth modes. This so-called *smoothing property* is generic for all classical relaxation schemes. These schemes are very effective in reducing the oscillatory components of the error but the smooth components persist.

4.3.2 The Multigrid idea

The idea of Multigrid is based on a simple observation: a smooth mode on a fine grid appears more oscillatory on a coarser grid. This suggests that when the relaxation on a fine grid begins to stall, we transfer the error to a coarser grid, e.g. with twice the step size of the fine grid, where it can be damped much more effectively. Then the error is transferred back to the fine grid and we relax again. This idea will be made precise below.

The equation we use to reduce the error on the coarser grid is the *residual equation*

$$A\mathbf{e} = \mathbf{r}\,, \tag{4.84}$$

which follows from (4.72) if we define the error to be $\mathbf{e} = \mathbf{u} - \mathbf{v}$ and the *residual* to be $\mathbf{r} = \mathbf{f} - A\mathbf{v}$.

Let $\mathbf{v}^h$ denote the approximation on the fine grid Ω^h with step size h and $\mathbf{v}^{2h}$ the approximation on the coarse grid Ω^{2h} with step size $2h$. Suppose we have a *restriction operator* I_h^{2h} which transfers vectors from Ω^h to Ω^{2h} and a *prolongation operator* I_{2h}^h which transfers vectors from Ω^{2h} to Ω^h. Then we

can define the following algorithm [31, chapter 3]:

Two-Grid Correction Scheme

- Relax ν_1 times on $A^h\mathbf{u}^h = \mathbf{f}^h$ on Ω^h with initial guess $\mathbf{v}^h$.
- Compute the fine-grid residual $\mathbf{r}^h = \mathbf{f}^h - A^h\mathbf{v}^h$ and restrict it to the coarser grid by $\mathbf{r}^{2h} = I_h^{2h}\mathbf{r}^h$.
- Relax on $A^{2h}\mathbf{e}^{2h} = \mathbf{r}^{2h}$ on Ω^{2h}.
- Prolong the coarse-grid error to the fine grid by $\mathbf{e}^h = I_{2h}^h\mathbf{e}^{2h}$ and correct the fine-grid approximation by $\mathbf{v}^h \leftarrow \mathbf{v}^h + \mathbf{e}^h$.
- Relax ν_2 times on $A^h\mathbf{u}^h = \mathbf{f}^h$ on Ω^h with initial guess $\mathbf{v}^h$.

Intergrid transfer. There are many ways to choose the intergrid transfer operators I_{2h}^h and I_h^{2h}. The simplest (and very effective) choice for the prolongation operator is linear interpolation,

$$\begin{aligned} v_{2j}^h &= v_j^{2h}\,, \\ v_{2j+1}^h &= \tfrac{1}{2}(v_j^{2h} + v_{j+1}^{2h})\,, \qquad 0 \leqslant j \leqslant \tfrac{N}{2} - 1\,. \end{aligned} \tag{4.85}$$

A systematic way of defining the restriction operator is given by

$$I_{2h}^h = c\,(I_h^{2h})^T\,, \qquad c \in \mathbb{R}\,, \tag{4.86}$$

with $c = 1$ for one-dimensional problems (for arbitrary dimension, c is determined by the requirement that restriction should preserve constant vectors). For the prolongation operator (4.85), this leads to

$$v_j^{2h} = \tfrac{1}{4}(v_{2j-1}^h + 2v_{2j}^h + v_{2j+1}^h)\,, \qquad 1 \leqslant j \leqslant \tfrac{N}{2} - 1\,, \tag{4.87}$$

which is known as *full weighting*. The coarse-grid operator may then be defined by the *Galerkin condition*

$$A^{2h} = I_h^{2h} A^h I_{2h}^h \,, \tag{4.88}$$

which arises from a minimization principle [31, chapter 10]. For the model problem at hand, it turns out that the coarse-grid matrix A^{2h} defined in this way is just the fine-grid matrix A^h with h replaced by $2h$, which makes it easy to implement. For more complicated problems, this will not be the case and the Galerkin condition is no longer useful in practice. Instead, we will *choose* the coarse grid operator A^{2h} to have the same form as the fine-grid operator A^h. The choice of intergrid transfer operators is restricted by a simple criterion, given by Hackbusch [74]: to obtain a mesh-size independent rate of convergence of Multigrid, it is sufficient that

$$m_r + m_p \geqslant 2m \,, \tag{4.89}$$

where m_r is the interpolation order for restriction, m_p is the interpolation order for prolongation, and $2m$ is the order of the differential equation to be solved. Hence for second-order differential equations, it is sufficient to choose $m_p = 1$ (piecewise-constant interpolation) and $m_r = 2$ (linear interpolation), which is indeed what we have found perfectly satisfactory.

Multigrid cycles. Looking at the two-grid correction scheme again, we see that the coarse-grid problem is not much different from the fine-grid problem. Therefore, we can apply the two-grid correction scheme to the residual equation on Ω^{2h}, i.e. we relax there and move to Ω^{4h} for the correction step. We can repeat this process recursively:

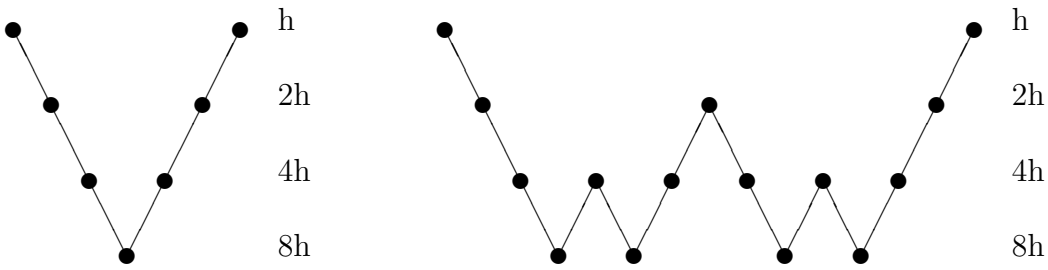

Figure 4.4: Schedule of grids for a (a) V-cycle and (b) W-cycle on four levels

μ-Cycle Scheme $\mathbf{v}^h \leftarrow M\mu^h(\mathbf{v}^h, \mathbf{f}^h)$

1. Relax ν_1 times on $A^h\mathbf{u}^h = \mathbf{f}^h$ with a given initial guess v^h.

2. If Ω^h is the coarsest grid, then go to step 4. Else

$$\begin{aligned} \mathbf{f}^{2h} &\leftarrow I_h^{2h}(\mathbf{f}^h - A^h\mathbf{v}^h)\,, \\ \mathbf{v}^{2h} &\leftarrow \mathbf{0} \quad \text{(initial guess)}, \\ \mathbf{v}^{2h} &\leftarrow M\mu^{2h}(\mathbf{v}^{2h}, \mathbf{f}^{2h}) \quad \mu \,\text{times}. \end{aligned}$$

3. Correct $\mathbf{v}^h \leftarrow \mathbf{v}^h + I_{2h}^h\mathbf{v}^{2h}$.

4. Relax ν_2 times on $A^h\mathbf{u}^h = \mathbf{f}^h$ with initial guess $\mathbf{v}^h$.

For $\mu = 1$ we obtain the *V-cycle* scheme, for $\mu = 2$ the *W-cycle* scheme. The choice of the names becomes obvious from figure 4.4, which shows the order in which the grids are visited. For the elliptic equations considered in this thesis, we found that W-cycles were more efficient than V-cycles in driving the residual below a given threshold.

4.3.3 Nonlinear Multigrid

Nonlinear PDEs lead to nonlinear finite difference discretizations of the form

$$A(\mathbf{u}) = \mathbf{f}\,, \qquad \mathbf{u}, \mathbf{f} \in \mathbb{R}^N\,. \tag{4.90}$$

As before, we define the error of an approximation $\mathbf{v}$ to be $\mathbf{e} = \mathbf{u} - \mathbf{v}$ and the residual to be $\mathbf{r} = \mathbf{f} - A(\mathbf{v})$. By subtracting (4.90) from the definition of the residual, we obtain

$$A(\mathbf{u}) - A(\mathbf{v}) = \mathbf{r}\,. \tag{4.91}$$

The crucial difference between linear and nonlinear problems is that if the operator A is nonlinear, we *cannot* conclude that $A(\mathbf{u}) - A(\mathbf{v}) = A(\mathbf{u} - \mathbf{v}) = A(\mathbf{e})$. We no longer have the simple linear residual equation (4.84) but have to use (4.91) instead.

One way to solve (4.91) is to replace $\mathbf{u} = \mathbf{v} + \mathbf{e}$ and to Taylor-expand about $\mathbf{v}$. Keeping only the linear term, we arrive at the *linear* system

$$J(\mathbf{v})\,\mathbf{e} = \mathbf{r}\,, \tag{4.92}$$

where $J_{ij} = \partial A(\mathbf{v})_i / \partial v_j$ is the $N \times N$ Jabobian matrix. Iteration of this step leads to the well-known *Newton-Raphson method*. To solve the linear equation (4.92), we could use the linear Multigrid methods presented above, and this combination is usually called *Newton-Multigrid*.

However, Multigrid can treat the nonlinearity directly! Let us write down the residual equation (4.91) on the coarse grid Ω^{2h},

$$A^{2h}(\mathbf{u}^{2h}) = A^{2h}(\mathbf{v}^{2h}) + \mathbf{r}^{2h}\,. \tag{4.93}$$

Suppose we have some approximation $\mathbf{v}^h$ on Ω^h. We can restrict that approximation to Ω^{2h},

$$\mathbf{v}^{2h} = I_h^{2h}\mathbf{v}^h\,, \tag{4.94}$$

and similarly restrict the residual,

$$\mathbf{r}^{2h} = I_h^{2h}\mathbf{r}^h = I_h^{2h}(\mathbf{f}^h - A^h(\mathbf{v}^h))\,. \tag{4.95}$$

Then the right-hand-side of (4.93) is known, and we can relax that equation with respect to $\mathbf{u}^{2h}$ to obtain a new approximation on Ω^{2h}. This leads to the following algorithm [31, chapter 6]:

Full Approximation Scheme (FAS)

- Restrict the current approximation and its fine-grid residual to the coarse grid: $\mathbf{r}^{2h} = I_h^{2h}(\mathbf{f}^h - A^h(\mathbf{v}^h))$ and $\mathbf{v}^{2h} = I_h^{2h}\mathbf{v}^h$.
- Relax on the coarse-grid problem $A^{2h}(\mathbf{u}^{2h}) = A^{2h}(\mathbf{v}^{2h}) + \mathbf{r}^{2h}$.
- Compute the coarse-grid approximation to the error: $\mathbf{e}^{2h} = \mathbf{u}^{2h} - \mathbf{v}^{2h}$.
- Prolong the error approximation to the fine grid and correct the current fine-grid approximation: $\mathbf{v}^h \leftarrow \mathbf{v}^h + I_{2h}^h\mathbf{e}^{2h}$.

This is called *full approximation scheme* because apart from the vector that is iterated in the relaxation steps, it requires the additional storage of the current approximation coming from the finer grid. The extension of the above two-grid scheme to the Multigrid μ-cycles is obvious.

The same relaxation schemes as in the linear case can be applied: e.g. for the Gauss-Seidel relaxation, one solves the equation $A(\mathbf{u}) = \mathbf{f}$ for u_j at grid point j. However, since the underlying PDE is nonlinear, the Gauss-Seidel step may require solving a nonlinear equation instead of a linear one as in (4.75). This can be done with Newton's method, as discussed above in the case of Newton-Multigrid. Note, however, that we only need to solve a single nonlinear equation now instead of an $N \times N$ system as in (4.92)!

4.3.4 Extension to systems and multidimensions

Systems of PDEs. It is straightforward to generalize the above algorithms to systems of equations. The vector of unknowns now has the form $\mathbf{u} = (\mathbf{u}^1, \mathbf{u}^2, \ldots, \mathbf{u}^k)^T$ where k is the number of equations and each subvector $\mathbf{u}^i \in \mathbb{R}^N$. For prolongation and restriction, one simply treats the subvectors separately.

For non-static relaxations such as Gauss-Seidel (as opposed to Jacobi), the order in which the unknowns are updated matters. One possibility is to update all the unknowns $u_j^1, u_j^2, \ldots, u_j^k$ simultaneously at each grid point j. Another possibility is to first update u_j^1 over the entire grid, then u_j^2, and so forth. We found that the first method is more efficient for the elliptic equations occurring in our problem.

Multidimensional problems. The extension to two (or more) dimensions is straightforward, too. The vector of unknowns is now $\mathbf{u} = (u_{ij})$, $1 \leqslant i \leqslant N_r$, $1 \leqslant j \leqslant N_z$ for a grid with N_r points in the r direction and N_z points in the z direction. We consider a cell-centred grid here as described in section 4.1. The restriction and prolongation operators are now based on *two-dimensional* interpolation. We use piecewise-constant interpolation for prolongation,

$$\begin{aligned} u^h_{2i-1,2j} = u^h_{2i,2j-1} = u^h_{2i-1,2j-1} = u^h_{2i,2j} = u^{2h}_{ij}\,, \\ 1 \leqslant i \leqslant \tfrac{N_r}{2}\,, \quad 1 \leqslant j \leqslant \tfrac{N_z}{2}\,, \end{aligned} \tag{4.96}$$

and (triangular) linear interpolation for restriction,

$$\begin{aligned} u^{2h}_{ij} \;=\; & \tfrac{1}{16}\big(u^h_{2i,2j-2} + u^h_{2i+1,2j-2} + 2u^h_{2i-1,2j-1} + 3u^h_{2i,2j-1} \\ & + u^h_{2i+1,2j-1} + u^h_{2i-2,2j} + 3u^h_{2i-1,2j} + 2u^h_{2i,2j} \\ & + u^h_{2i-2,2j+1} + u^h_{2i-1,2j+1}\big)\,, \\ & 1 \leqslant i \leqslant \tfrac{N_r}{2}\,, \quad 1 \leqslant j \leqslant \tfrac{N_z}{2}\,. \end{aligned} \tag{4.97}$$

Again, there is an ambiguity in the order of update in the relaxation step for the Gauss-Seidel method. The *lexicographical* Gauss-Seidel method first sweeps through the index i (in ascending order) in an outer iteration and then through j in an inner iteration. The *red-black* Gauss-Seidel method colours the grid points in chessboard manner and first sweeps through all red points (in lexicographical order), then through all black points. We have found the red-black version to be more efficient for most problems.

4.4 Alternative methods

In this section we discuss some alternative methods – finite volume methods for hyperbolic equations and conjugate gradient methods for elliptic equations.

4.4.1 Finite volume methods

Centred finite-differencing in conjunction with the method of lines works well if the solution one tries to approximate is smooth. This is the case for the vacuum gravitational waves considered in this thesis. Once matter is included, however, discontinuous solutions have to be taken into account. For example, the formation of *shocks* is a common phenomenon in fluid dynamics. In [15] it was shown for the coupled Euler-Einstein equations in plane-symmetric Gowdy spacetimes that discontinuities can also show up in the first- and second-order derivatives of the metric.

The method presented in the previous sections is unsuitable for discontinuous solutions because it produces large oscillations around the discontinuities, known as the *Gibbs phenomenon*. A huge variety of methods that are capable of dealing with discontinuities have been developed in computational

fluid dynamics [95, 97, 134]. These methods are typically based on a formulation of the underlying hyperbolic PDEs as *conservation laws* (possibly with sources)

$$\partial_t \mathbf{u} + \partial_A \mathbf{f}^A(\mathbf{u}) = \mathbf{S}(\mathbf{u}) \,, \tag{4.98}$$

and they adopt the finite volume approach. Most methods consist of three stages: starting from the cell averages, the numerical solution is first *reconstructed* at the cell interfaces. A *numerical flux* is then computed from the reconstructed values. Finally, the numerical solution is integrated forward in time.

Since the Z(2+1)+1 system discussed in chapter 6 is written precisely in the form (4.98), one might try to apply finite volume methods to that system as well. Our experiments indicated that this is not feasible for the following reasons.

Consider first the reconstruction procedure. We found that reconstructions which adapt themselves to discontinuities, such as the *weighted essentially non-oscillatory (WENO)* reconstruction [126] and the *slope-limited* reconstruction [134], led to instabilities unless an extremely high resolution was used.

Consider next the numerical flux. Many numerical fluxes used in high-resolution shock capturing methods are based on the solution of the Riemann problem and require that one can compute the characteristic variables from the conserved variables and *vice versa*. It turns out that this cannot be done in a regular way close to the axis for our system (section 6.5.4). Therefore we have to resort to numerical fluxes that do not require any knowledge of the characteristic structure. Possible candidates include the basic Lax-Friedrichs flux and the FORCE flux used in the SLIC and FLIC methods of Toro [134]. Unfortunately, these fluxes are very viscous and led to a severe damping of

the waves in our experiments. The recent higher-order MUSTA flux of Toro and Titarev [136, 135] might be a promising alternative.

We have decided to stick with centred finite-differencing combined with the method of lines as described in the previous sections because it can be applied to second-order as well as first-order (in space) PDEs, it does not include any artificial viscosity, and it appears to be very stable.

However, our long-term goal is to include a perfect fluid, and then we will have to use finite-volume methods at least for the matter equations. Such methods have been successfully applied to general relativistic hydrodynamics (see [54] for a comprehensive review), including a study of perfect fluid critical collapse in Friedmann-Robertson-Walker spacetimes [78, 77].

4.4.2 Conjugate gradient methods

The convergence of the Multigrid method depends crucially on the underlying relaxation. If the diagonal dominance condition (4.81) is strongly violated so that the relaxation diverges then Multigrid will also diverge.

A different class of linear relaxation methods that do not suffer from this problem are based on the *conjugate gradient (CG) method* (see [125] for an elementary introduction). This can be interpreted as a function minimization algorithm applied to the norm of the residual,

$$r(\mathbf{v}) \equiv \|\mathbf{f} - A\mathbf{v}\|_2 \tag{4.99}$$

in the notation of section 4.3. The advantage of these methods as compared with direct matrix solvers is that the matrix A is only ever referred to in the form $A\mathbf{v}$. Since A is sparse for finite difference discretizations, this matrix-vector product can be implemented very efficiently.

While the original conjugate gradient method only converges for symmet-

ric positive definite matrices A, the *bi-conjugate gradient method* in principle converges for any non-singular A. An improved version of that algorithm is the bi-conjugate gradient stabilized (BiCGStab) method of van der Vorst [137]. The convergence of CG methods depends crucially on the use of the so-called *preconditioner*, a matrix B that approximates A and is easy to invert. One then applies the conjugate gradient method to $B^{-1}A$, which is closer to the unit matrix than A and exhibits a much faster convergence. A preconditioner that is straightforward to implement and that worked well in our experiments is the SSOR preconditioner (e.g., [130]).

Still, the complexity of CG methods is greater than that of Multigrid: at least $O(N \ln N)$ operations are required, as compared with $O(N)$ operations for Multigrid. In principle, one can also use CG as a relaxation *within* Multigrid but this is not very efficient because CG methods do not share the smoothing property of the classical relaxation schemes (section 4.3.1). In addition, CG methods are not capable of dealing with nonlinear problems directly. Hence an outer Newton-Raphson iteration has to be applied, which multiplies the workload.

If Multigrid converges, it is always more advisable to use it rather than CG methods. We have successfully implemented the BiCGStab algorithm for the Hamiltonian constraint (5.24) in situations when Multigrid fails for that equation (e.g., in strong Brill wave evolutions). However, as explained later in section 5.5.1, the Hamiltonian constraint might have multiple solutions in those situations. Preliminary results indicate that the CG method sometimes appears to converge to a "wrong solution", i.e., one that is not compatible with the remaining equations (see also the remarks in section 5.8).

4.5 Adaptive mesh refinement

So far we have only considered grids that are uniform across the whole computational domain. The solution of hyperbolic partial differential equations on such a grid can be very inefficient if the solution contains a wide range of relevant length scales. To resolve the small-scale features, a high resolution is needed, whereas a much lower resolution would be sufficient in smooth regions. Since the computational workload scales (roughly) linearly with the number of grid points, having a single grid with a uniformly high resolution is impractical. One way out would be to use a non-uniform grid. The main disadvantage of this is that because of the CFL condition (section 4.2), the whole grid needs to be evolved with a time step restricted by the smallest grid spacing. This is avoided by the *adaptive mesh refinement (AMR)* technique, whereby the computational domain is covered by a dynamical hierarchy of uniform grids of increasing resolution, each advanced with its own time step. During a numerical simulation, refined grids are added in regions where and when they are needed, and discarded when they become obsolete.

AMR was invented in 1984 by Berger and Oliger [19]. It was first applied to numerical relativity by Choptuik [40] to study the critical collapse of a massless scalar field in spherical symmetry. Further one-dimensional applications include the same problem in double-null coordinates by Hamadé and Stewart [76] and perfect fluid collapse in Friedmann-Robertson-Walker universes by Hawke and Stewart [78]. Two-dimensional examples include studies of inhomogeneous cosmologies by Hern [81] and scalar field critical collapse by Choptuik et al. [42]. Three-dimensional AMR has been used in single and binary black hole simulations, see e.g. Pretorius [111] for a promising recent attempt.

In this work, we mainly use Berger and Oliger's classic algorithm (applied

to two spatial dimensions), with certain simplifications and modifications described below. The implementation is based on a code originally written by Stewart and Hern (see [81] for a detailed description). Changes have been made mainly to the boundary treatment (section 4.5.2), regridding procedure and refinement criteria (section 4.5.3). One of the outstanding features of the AMR part of the code is that it is to a large extent independent of the other parts such as the time integrator, the initial data solver, and the actual implementation of the equations being solved.

We have only implemented AMR for hyperbolic systems of partial differential equations. The extension to mixed hyperbolic-elliptic systems and the combination of AMR with the Multigrid method for elliptic equations (section 4.3) is rather complicated, although some progress has been made (see [113] for an implementation with numerical relativity in mind).

4.5.1 The grid hierarchy

The building blocks of the AMR algorithm are the uniform *grids* described in section 4.1.1. We use cell-centred grids rather than vertex-centred ones (this is not an essential restriction – it only affects the details of the interpolation between grids). The grids are arranged in a hierarchy in the following way: the hierarchy consists of $l_{\max}$ *levels*. Each level contains grids of the same resolution. Level 1 only contains a single grid, the *base grid*, the next coarsest level is 2 and so on until level $l_{\max}$, which contains the finest grids in the hierarchy.

The grid spacings of two consecutive levels are related by $h_l/h_{l+1} = \rho$, where $\rho \geqslant 2$ is an integer. We choose $\rho = 2$ in our applications.

Each *child grid* on level $l + 1$ is entirely contained within its *parent grid* on level l, a property called *proper nesting*. Unlike in Berger and Oliger's

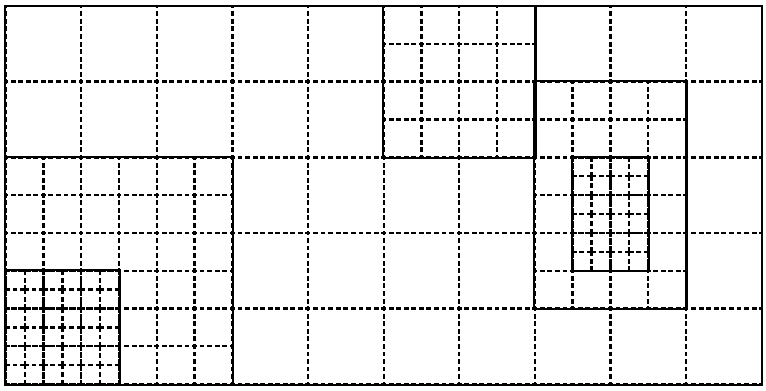

Figure 4.5: Example of an AMR grid hierarchy with 3 levels. The grid functions are defined at the cell centres. Realistic grids contain much more cells.

original work [19], we require that grids on a given level do not overlap. Furthermore, we require that all grids be aligned with the boundaries of the computational domain (Berger and Oliger allowed for rotated grids). Figure 4.5 shows an example of a typical AMR hierarchy.

4.5.2 Time-stepping the grid hierarchy

The grids are advanced in time by the following recursive procedure: first all grids on level l are advanced one time step to time $t + \Delta t_l$, then all grids on level $l + 1$ are advanced to the same time. To be consistent with the CFL condition (4.61–4.63), the time step on level $l + 1$ has to be refined by the same ratio as the grid spacing: $\Delta t_l / \Delta t_{l+1} = \rho$. This means that ρ time steps have to be taken on level $l + 1$ until it has caught up with level l.

Boundary data has to provided before a time step can be carried out. We distinguish between *external* boundaries, which coincide with the boundaries of the computational domain, and *internal* ones, which lie in the interior of the computational domain. External boundaries of a given grid are dealt with outside of the AMR algorithm – the boundary conditions to be enforced there

depend on the problem being solved. To provide data at internal boundaries, we exploit the fact that when a grid is to be advanced in time, its parent grid has already been advanced. Interpolation in time and space is used to interpolate the data from the parent grid to the ghost cells of the child grid (see section 4.1.3 for the ghost cell technique). This requires storage of data from both the current and the previous time step on the parent grid. The interpolation scheme we use is trilinear interpolation. We have not experienced any problems with high-frequency noise at the grid boundaries as reported by some authors. The same fourth-order Kreiss-Oliger dissipation operator (4.64) is applied at all interior grid points, with no modifications necessary close to the boundaries.

Once a child grid on level $l + 1$ has reached the same time as its parent grid on level l, the data on the child grid is *injected* into the parent grid. For cell-centred grids, this involves some sort of interpolation because the cell centres of the parent grid do not coincide with cell centres of the child grid (we use bilinear interpolation). By this update step, the most accurate solution available at a given point is propagated to all grids in the hierarchy.

When implementing systems of hyperbolic conservation laws using the finite volume method, one has to ensure that the scheme is conservative across the grid boundaries. This implies that certain modifications have to be made to the fluxes at the boundaries [18], a technique known as *refluxing*. We have not implemented this because we are using the finite difference rather than the finite volume method, and the "conserved" quantities have no physical significance in our problem (cf. section 6.3).

4.5.3 Adapting the grid hierarchy

The most powerful feature of the AMR algorithm is its ability to automatically adapt the grid hierarchy in order to maintain an appropriate resolution of the data at all times. The process of adding, removing or extending grids is called *regridding*. On each level, regridding takes place every T_r time steps, where T_r is a user-defined integer (we choose $T_r = 4$). We need to address two questions: firstly, how to decide where on a given grid refinement is needed and secondly, how to rearrange the grid hierarchy.

At the start of the regridding phase, grid cells that fail to meet a certain accuracy criterion are *flagged*. A common criterion is based on an estimate of the local truncation error via *Richardson extrapolation*. In the original Berger and Oliger algorithm, this is implemented in the following way. Two copies of the grid under investigation are made, the first one, G^h, being an identical copy, the second one, G^{2h}, a version coarsened by a factor of 2. Two time steps of size Δt are taken on G^h and a single step of size $2\Delta t$ on G^{2h}. Let us write the resulting approximation on G^h as

$$\mathbf{u}^h = \mathbf{u}_0 + \mathbf{e}^h \tag{4.100}$$

and the one on G^{2h} as

$$\mathbf{u}^{2h} = \mathbf{u}_0 + \mathbf{e}^{2h}\,, \tag{4.101}$$

where $\mathbf{u}_0$ denotes the (generally unknown) exact solution. For second-order accurate finite differencing, the error should behave like $\sim h^2$ so that the errors on the two grids are related by

$$\mathbf{e}^{2h} \approx 4\mathbf{e}^h\,. \tag{4.102}$$

Subtracting (4.100) from (4.101) and using (4.102), we obtain an estimate for the error on G^h:

$$\mathbf{e}^h \approx \tfrac{1}{3}(\mathbf{u}^{2h} - \mathbf{u}^h)\,. \tag{4.103}$$

A grid cell is flagged if the absolute value (or some norm, in the case of systems) of the estimated error there is bigger than a user-defined threshold.

We can simplify Berger and Oliger's implementation by recalling that at the time when a child level and its parent level are in synchrony, just before the child→parent update step, the information required for computing the error estimate is readily available. All we need to do is interpolate the data from the parent grid to a copy of the child grid and form the difference (4.103).[3] Because the error is $O(h^2)$, it is important that one uses more than second-order accurate interpolation here (we choose biquadratic interpolation). This simplified scheme has been called a *self-shadow hierarchy* [113] because it is no longer necessary to create a separate "shadow", i.e., a copy of a grid that is merely advanced for truncation error estimation. The only level where this procedure does not work is the coarsest one, for this does not have a parent. We therefore require that the coarsest level always be fully refined. The resolution on level 2 should then be chosen to match the desired coarsest resolution; level 1 is merely used for error estimation (the overhead that this causes is small because the number of grid points on level 1 is only a fourth of that on level 2).

Error estimation via Richardson extrapolation is by no means the only possible refinement criterion. For instance, an indication of how well a function is resolved can be obtained by evaluating its (suitably normalized) second spatial derivative [99, 60]. We have experimented with similar criteria but did not find them appropriate for the wavelike solutions considered in this thesis. Alternatively, one could use certain physically motivated quantities as

[3]Strictly speaking, the fine grid solution might have been modified by injections from even finer grids in the meantime. The correction to the estimate (4.103) is of order $(h/\rho)^2$, i.e., it is suppressed by a factor of ρ^2.

refinement indicators, e.g., the distortion of a spacelike slice or the residuals of the constraints. More details on this will follow in section 9.4 when we discuss our particular application.

Suppose now we have obtained an array of error flags. Next, the flagged regions are enlarged by so-called *buffer zones*. These ensure that high-error features of the solution do not propagate out of the refined regions before the next regridding step is performed. The width of the buffer regions required depends on the choice of T_r and the Courant number λ: signals that propagate at speed c can travel at most $c\lambda T_r$ grid spacings in T_r time steps. Because $\lambda \lesssim 1$ is needed for stability and $c \leqslant 1$ (the speed of light), a safe choice is a buffer width of T_r cells.[4] Also, regions of the grid on level l that are covered by *grandchildren* (i.e., level $l+2$ grids) are flagged. This ensures that (the union of) the newly created child grids contain the grandchild grids. The modified array of flags is then passed to a *clustering* algorithm, which creates a set of rectangular child grids containing the flagged points. The algorithm we use is based on techniques common in computer vision and pattern recognition and is described in detail in Berger and Rigoutsos [17]. The user can specify a target value for the approximate *filling factor* F, the ratio of flagged cells to the total number of cells in a child grid. A high value for this will produce many small child grids, a low value few large ones. Both extremes are computationally unefficient; a good compromise appears to be $F \approx 0.7$. The clustering algorithm had to be modified slightly in order to ensure that each existing grandchild grid is contained within a single newly created child grid, so that proper nesting is maintained.

After clustering, the child grids are filled with data interpolated from

[4] Depending on the width of the stencil used for intergrid interpolation, a slightly larger buffer zone may be required.

their parent (we use bilinear interpolation for this). If there are existing grids on level $l+1$ that overlap with the newly created grids, their data is used instead before they are destroyed.

When it is time to regrid level l, we carry out the above operations first on the finest level $l_{\max}$, then on level $l_{\max}-1$ and so on until level l itself. This is Berger and Oliger's original "top-down" approach; a different "down-top" approach is used by Hern [81].

Chapter 5

A mixed hyperbolic-elliptic system

In this chapter we present a first evolution scheme based on the (2+1)+1 formalism. Apart from hyperbolic evolution equations, it contains elliptic equations that need to be solved at each time step, which distinguishes it from the completely hyperbolic Z(2+1)+1 system considered in the following chapters. This chapter is mainly based on an earlier essay [118].

We begin by explaining our gauge conditions (section 5.1), which are motivated by geometric considerations and by simplifying the system as much as possible. They lead to elliptic equations for the lapse function and the shift vector. We then turn to the issue of regularity on axis and explain how the regularity conditions of chapter 2 can be enforced by an appropriate choice of variables (section 5.2). The final equations to be solved are written out in terms of these variables in section 5.3. Three alternate evolution schemes are then discussed that differ in the way the constraint equations are treated, ranging from a fully constrained scheme to a free evolution scheme (section 5.4). The elliptic equations occurring in the different schemes are

investigated further with regard to uniqueness of solutions and numerical solvability with Multigrid methods (section 5.5). The constraint evolution system is derived in section 5.6 and its well-posedness is analyzed for the three evolution schemes. Numerical evolutions of generalized Brill waves, including twist, are presented in section 5.7. Evidence for the existence of a critical point separating dispersal and black hole formation is given, and the present limitations of the code are indicated.

5.1 Elliptic gauge conditions

To complete our evolution formalism, we have to come up with a prescription for the gauge variables, which specify the coordinate system. We would like to tie them to the evolution so that they can adapt themselves, for instance when a spacetime singularity is approached.

Consider first the prescription for the lapse function, also called the *slicing condition*. The one we choose here is *maximal slicing*. Its name arises from the fact that it maximizes the proper volume of the individual spacelike slices [144]. This suggests that when a high-curvature region of spacetime is approached, the slices try to avoid that region and "pile up" in front of it. In this way, a large part of spacetime can be explored without hitting a potential singularity. Maximal slicings have been constructed analytically for Schwarzschild spacetime [50] but the singularity avoiding property has also been shown to hold in more general situations [46].

For maximal slices, the trace of the second fundamental form of the *three*-dimensional (i.e., including the dimension of the Killing vector) $t = \text{const.}$ surfaces vanishes. In $(2+1)+1$ language, this translates into

$$\chi + K_{\varphi}{}^{\varphi} = 0\,. \tag{5.1}$$

As we want this condition to hold at all times, we also require its Lie derivative along the normal lines to vanish. $\mathcal{L}_n\chi = \mathcal{L}_n(H^{AB}\chi_{AB})$ can be computed using the evolutions equations (3.54) and (3.56), and $\mathcal{L}_n K_\varphi{}^\varphi$ is given by (3.57). Together we obtain

$$\begin{aligned}\mathcal{L}_n\left(\chi + K_\varphi{}^\varphi\right) &= -\alpha^{-1}\alpha_{\|A}{}^A + {}^{(2)}R + \left(\chi + K_\varphi{}^\varphi\right)^2 - \lambda^{-1}\alpha^{-1}\lambda_{,A}\alpha^{,A} \\ &\quad -2\lambda^{-1}\lambda_{\|A}{}^A - \tfrac{1}{2}\lambda^2 B^{\varphi 2} + \tfrac{1}{2}\kappa\left(\tau + S_A{}^A - 3\rho_H\right) . \quad (5.2)\end{aligned}$$

If we now impose (5.1) and subtract twice the Hamiltonian constraint (3.50) from the right-hand-side, we end up with the following elliptic equation for α:

$$\begin{aligned}\mathcal{S} &\equiv \alpha_{\|A}{}^A - \alpha\big[\chi^{AB}\chi_{AB} + K_\varphi{}^{\varphi 2} - \lambda^{-1}\alpha^{-1}\lambda_{,A}\alpha^{,A} + \tfrac{1}{2}\lambda^2 E_A E^A \\ &\quad + \tfrac{1}{2}\kappa\left(\rho_H + \tau + S_A{}^A\right)\big] = 0 . \quad (5.3)\end{aligned}$$

Next we deal with the shift vector. We exploit the fact that every two-dimensional Riemannian manifold is conformally flat. Hence we can choose coordinates such that at all times

$$H_{rr} = H_{zz} \equiv \sqrt{H} , \qquad H_{rz} = 0 . \quad (5.4)$$

This conformal flatness condition thus simplifies the system by reducing the number of variables to be evolved: H_{AB} now has only 1 instead of 3 degrees of freedom. This gauge is also known as *Wilson gauge* [142] in the literature.

Imposing (5.4) on the time derivative of H_{AB} (3.54) now implies that

$$\beta_- \equiv \beta^r{}_{,r} - \beta^z{}_{,z} = \alpha(\chi_r{}^r - \chi_z{}^z) , \quad (5.5)$$

$$\beta_+ \equiv \beta^r{}_{,z} + \beta^z{}_{,r} = 2\alpha\chi_r{}^z . \quad (5.6)$$

By forming the combinations ∂_r (5.5) $+\partial_z$ (5.6) and $-\partial_z$ (5.5) $+\partial_r$ (5.6), we arrive at the following Poisson equations for the components of the shift

vector:

$$\mathcal{S}_r \equiv \beta^r{}_{,rr} + \beta^r{}_{,zz} - [2\alpha\chi_r{}^z]_{,z} - [\alpha(\chi_r{}^r - \chi_z{}^z)]_{,r} = 0\,, \tag{5.7}$$

$$\mathcal{S}_z \equiv \beta^z{}_{,rr} + \beta^z{}_{,zz} - [2\alpha\chi_r{}^z]_{,r} + [\alpha(\chi_r{}^r - \chi_z{}^z)]_{,z} = 0\,. \tag{5.8}$$

An alternate way of solving for the shift vector using the momentum constraints will be explained in section 5.4.

5.2 Regularity on axis

As emphasized in chapter 2, great care must be taken to enforce the regularity conditions for axisymmetric tensor fields during a numerical evolution because otherwise certain terms in the evolution equations become singular on the axis.

Let us first deal with the regularity condition (2.26) applied to the spacetime metric $g_{\alpha\beta}$. It implies that

$$\frac{g_{\varphi\varphi}}{r^2 g_{rr}} = \frac{\lambda^2}{r^2\sqrt{H}} = 1 + O(r^2)\,. \tag{5.9}$$

If we evolved $\sqrt{H}$ and λ independently, this subtle relation would soon be violated during the evolution due to numerical errors. Instead, we replace $\sqrt{H}$ and λ with new variables ψ and s defined by

$$\sqrt{H} = \psi^4 \mathrm{e}^{2rs}\,, \qquad \lambda = r\psi^2\,, \tag{5.10}$$

where $s = O(r)$ and $\psi = O(1)$ on the axis. Indeed, this guarantees that

$$\frac{\lambda^2}{r^2\sqrt{H}} = \mathrm{e}^{-2rs} \approx 1 - 2rs = 1 + O(r^2) \tag{5.11}$$

for small r. Equation (5.10) is the choice of variables made in Garfinkle and Duncan [62]. Another possibility (satisfying (5.11) with s replaced by $-s$) is

$$\sqrt{H} = \psi^4\,, \qquad \lambda = r\psi^2 \mathrm{e}^{rs}\,, \tag{5.12}$$

which are the variables of Choptuik et al. [41]. We have also considered replacing ψ^4 in the above with $\exp 2\psi$, which has the advantage that no logarithmic derivatives $\psi^{-1}\psi_{,A}$ appear in the final equations and thus many nonlinearities drop out. All the various choices have been implemented and it was found that strong Brill wave evolutions were slightly more stable for (5.10) than for the other possibilities. We therefore adopt that choice in the following.

The corresponding regularity condition for the extrinsic curvature implies that

$$K_\varphi{}^\varphi = r^{-2}K_{\varphi\varphi} + O(r^2) = \chi_{rr} + O(r^2) = \chi_r{}^r + O(r^2)\,. \tag{5.13}$$

Hence $K_\varphi{}^\varphi - \chi_r{}^r$ is $O(r^2)$ on axis, while each single term is $O(1)$. This will not hold numerically if we evolve $K_\varphi{}^\varphi$ and $\chi_r{}^r$ separately and so we introduce a new variable Y defined by[1]

$$Y \equiv r^{-1}(K_\varphi{}^\varphi - \chi_r{}^r)\,, \tag{5.14}$$

where $Y = O(r)$ near the axis. Because of the maximal slicing condition $\chi + K_\varphi{}^\varphi = 0$, the extrinsic curvature has only two more independent components, which in agreement with [62] are taken to be

$$U \equiv \chi_r{}^r - \chi_z{}^z\,, \qquad X \equiv \chi_r{}^z = \chi_z{}^r\,. \tag{5.15}$$

Similarly, the regularity condition for the energy-momentum tensor implies that $\tau - S_r{}^r$ is $O(r^2)$ on axis and so we redefine τ by

$$\tilde{\tau} \equiv r^{-1}(\tau - S_r{}^r)\,. \tag{5.16}$$

The set of variables we evolve is summarized in table 5.1, which also states their small-r behaviour. This determines the boundary conditions we impose

[1]This definition is the same as in [41]. The variable W in [62] is $W = -Y$.

$$\alpha, \underline{\beta^r}, \beta^z, \psi, \underline{s}, \underline{Y}, U, \underline{X}, \underline{B^\varphi}, \underline{E^r}, E^z,$$
$$\rho_H, \sigma, J_\varphi, \underline{J_r}, J_z, \underline{\tilde{\tau}}, \underline{S^r}, S^z, \underline{\Sigma^r}, \Sigma^z, {S_r}^r, \underline{{S_r}^z}, {S_z}^z.$$

Table 5.1: Variables of the hyperbolic-elliptic system and their small-r behaviour. Underlined variables are $O(r)$, the remaining variables are $O(1)$ on the axis.

on the axis: for a variable $\underline{u}$ that is $O(r)$ on the axis, a Dirichlet condition

$$\underline{u}|_{r=0} = 0 \tag{5.17}$$

is needed, and for a variable u that is $O(1)$ on axis, we enforce a Neumann condition

$$\partial_r u|_{r=0} = 0\,. \tag{5.18}$$

Now we also see why our definitions of the twist variables (3.47–3.48) differ from those in Maeda et al. [100] by factors of λ (which is $O(r)$ on the axis): if we had adopted their definition then the variables B^φ and E^r would have been $O(r^2)$ on the axis, which is difficult to enforce numerically because we can easily impose a Dirichlet condition or a Neumann condition, but not both at the same time.

5.3 Final equations

We are now ready to write out the equations to be solved in our gauge and variables.

The gauge conditions

The slicing condition (5.3) is

$$\begin{aligned}\hat{\mathcal{S}} \;\equiv\; & \alpha_{,rr} + r^{-1}\alpha_{,r} + \alpha_{,zz} + 2\psi^{-1}(\psi_{,r}\alpha_{,r} + \psi_{,z}\alpha_{,z}) \\ & -\alpha\psi^4 \mathrm{e}^{2rs}\big[\tfrac{2}{3}(U - \tfrac{1}{2}rY)^2 + \tfrac{1}{2}r^2Y^2 + 2X^2 \\ & \quad + \tfrac{1}{2}r^2\psi^8\mathrm{e}^{2rs}(E^{r\,2} + E^{z\,2}) \\ & \quad + \tfrac{1}{2}\kappa(\rho_H + r\tilde{\tau} + 2S_r{}^r + S_z{}^z)\big] = 0\,.\end{aligned} \tag{5.19}$$

Equations (5.5–5.6) imply that U and X are given in terms of the shift by

$$U \;=\; -\alpha^{-1}\beta_-\,, \tag{5.20}$$

$$X \;=\; \tfrac{1}{2}\alpha^{-1}\beta_+\,. \tag{5.21}$$

The elliptic shift conditions (5.7–5.8) read

$$\hat{\mathcal{S}}_r \;\equiv\; \beta^r{}_{,rr} + \beta^r{}_{,zz} - (\alpha X)_{,z} + (\alpha U)_{,r} = 0\,, \tag{5.22}$$

$$\hat{\mathcal{S}}_z \;\equiv\; \beta^z{}_{,rr} + \beta^z{}_{,zz} - 2(\alpha X)_{,r} - (\alpha U)_{,z} = 0\,. \tag{5.23}$$

The constraint equations

The Hamiltonian constraint (3.50) becomes

$$\begin{aligned}\hat{\mathcal{C}} \;\equiv\; & \psi_{,rr} + r^{-1}\psi_{,r} + \psi_{,zz} + \tfrac{1}{4}\psi(rs_{,rr} + 2s_{,r} + rs_{,zz}) \\ & +\psi^5\mathrm{e}^{2rs}\big[\tfrac{1}{3}(U - \tfrac{1}{2}rY)^2 + \tfrac{1}{4}r^2Y^2 + X^2 + \tfrac{1}{4}\kappa\rho_H\big] \\ & +\tfrac{1}{16}r^2\psi^9\mathrm{e}^{2rs}\big[B^{\varphi\,2} + \psi^4\mathrm{e}^{2rs}(E^{r\,2} + E^{z\,2})\big] = 0\,.\end{aligned} \tag{5.24}$$

The momentum constraints (3.51) are

$$\begin{aligned}\hat{\mathcal{C}}_r &\equiv -\tfrac{1}{3}U_{,r} + X_{,z} - \tfrac{1}{3}rY_{,r} - 2\psi^{-1}\psi_{,r}(rY+U) + 6\psi^{-1}\psi_{,z}X \\ &\quad -(rs_{,r}+s)U + 2rs_{,z}X - \tfrac{4}{3}Y - \tfrac{1}{2}r^2\psi^8 \mathrm{e}^{2rs}B^\varphi E^z \qquad (5.25)\\ &\quad -\kappa J_r = 0\,, \\ \hat{\mathcal{C}}_z &\equiv \tfrac{2}{3}U_{,z} + X_{,r} - \tfrac{1}{3}rY_{,z} + 6\psi^{-1}\psi_{,r}X + 2\psi^{-1}\psi_{,z}(2U - rY) \\ &\quad +(2rs_{,r} + 2s + r^{-1})X + rs_{,z}U + \tfrac{1}{2}r^2\psi^8\mathrm{e}^{2rs}B^\varphi E^r \qquad (5.26)\\ &\quad -\kappa J_z = 0\,.\end{aligned}$$

The Geroch constraint (3.52) is

$$\begin{aligned}\hat{\mathcal{C}}_\varphi &\equiv E^r{}_{,r} + E^z{}_{,z} + E^r(10\psi^{-1}\psi_{,r} + 2rs_{,r} + 2s + 3r^{-1}) \\ &\quad +E^z(10\psi^{-1}\psi_{,z} + 2rs_{,z}) - 2\kappa J^\varphi = 0\,. \qquad (5.27)\end{aligned}$$

The evolution equations

Equations (3.54–3.55) imply the following evolution equations for ψ and s:

$$\partial_t\psi = \beta^r\psi_{,r} + \beta^z\psi_{,z} + \psi\big[\tfrac{1}{2}r^{-1}\beta^r + \tfrac{1}{6}(U - 2rY)\big]\,, \qquad (5.28)$$

$$\partial_t s = \beta^r s_{,r} + \beta^z s_{,z} + \alpha Y + (r^{-1}\beta^r)_{,r} + r^{-1}\beta^r s\,. \qquad (5.29)$$

The evolution equations for the extrinsic curvature (3.56–3.57) become

$$\begin{aligned}\partial_t Y &= \beta^r Y_{,r} + \beta^z Y_{,z} + r^{-1}\beta^r Y - r^{-1}X(\beta^z{}_{,r} - \beta^r{}_{,z}) \\ &\quad +\psi^{-4}\mathrm{e}^{-2rs}\big[(r^{-1}\alpha_{,r})_{,r} - r^{-1}\alpha_{,r}(rs_{,r} + s + 4\psi^{-1}\psi_{,r}) \\ &\qquad +\alpha_{,z}s_{,z}\big] \\ &\quad +\alpha\psi^{-4}\mathrm{e}^{-2rs}\big[2\psi^{-1}(r^{-1}\psi_{,r})_{,r} + s_{,rr} + s_{,zz} + (r^{-1}s)_{,r} \qquad (5.30)\\ &\qquad -2r^{-1}\psi^{-1}\psi_{,r}(rs_{,r} + s + 3\psi^{-1}\psi_{,r}) \\ &\qquad +2\psi^{-1}\psi_{,z}s_{,z}\big] \\ &\quad -r\alpha\psi^4\big[B^{\varphi 2} + \psi^4\mathrm{e}^{2rs}(E^{r2} + E^{z2})\big] - \kappa\alpha\tilde{\tau}\,, \qquad (5.31)\end{aligned}$$

$$
\begin{aligned}
\partial_t U &= \beta^r U_{,r} + \beta^z U_{,z} + 2X(\beta^r{}_{,z} - \beta^z{}_{,r}) \\
&\quad + \psi^{-4}\mathrm{e}^{-2rs}\big[2\alpha_{,z}(2\psi^{-1}\psi_{,z} + rs_{,z}) - 2\alpha_{,r}(2\psi^{-1}\psi_{,r} + rs_{,r} + s) \\
&\qquad + \alpha_{,rr} + \alpha_{,zz}\big] \\
&\quad - 2\alpha\psi^{-4}\mathrm{e}^{-2rs}\big[-\psi^{-1}\psi_{,rr} + \psi^{-1}\psi_{,zz} + s_{,r} + r^{-1}s \\
&\qquad + \psi^{-1}\psi_{,r}(3\psi^{-1}\psi_{,r} + 2rs_{,r} + 2s) \\
&\qquad - \psi^{-1}\psi_{,z}(3\psi^{-1}\psi_{,z} + 2rs_{,z})\big] \\
&\quad - \tfrac{1}{2}r^2\alpha\psi^8\mathrm{e}^{2rs}(E^{r2} - E^{z2}) + \kappa\alpha(S_r{}^r - S_z{}^z)\,, \\
\partial_t X &= \beta^r X_{,r} + \beta^z X_{,z} + \tfrac{1}{2}U(\beta^z{}_{,r} - \beta^r{}_{,z}) \\
&\quad + \psi^{-4}\mathrm{e}^{-2rs}\big[-\alpha_{,rz} + \alpha_{,r}(rs_{,z} + 2\psi^{-1}\psi_{,z}) \\
&\qquad + \alpha_{,z}(rs_{,r} + s + 2\psi^{-1}\psi_{,r})\big] \\
&\quad + \alpha\psi^{-4}\mathrm{e}^{-2rs}\big[-2\psi_{-1}\psi_{,rz} + \psi^{-1}\psi_{,r}(3\psi^{-1}\psi_{,z} + 2rs_{,z}) \\
&\qquad + 2\psi^{-1}\psi_{,z}rs_{,z} + s_{,z}\big] \\
&\quad + \tfrac{1}{2}r^2\alpha\psi^8\mathrm{e}^{2rs}E^rE^z - \kappa\alpha S_r{}^z\,.
\end{aligned}
\tag{5.32, 5.33}
$$

The evolution equations for the twist variables (3.58–3.59) are

$$
\begin{aligned}
\partial_t E^r &= \beta^r E^r{}_{,r} + \beta^z E^r{}_{,z} \\
&\quad + \psi^{-4}\mathrm{e}^{-2rs}\big[\alpha_{,z}B^\varphi + \alpha B^\varphi{}_{,z} + 6\alpha\psi^{-1}\psi_{,z}B^\varphi\big] \qquad (5.34) \\
&\quad + E^r\big[\tfrac{2}{3}\alpha(2rY - U) - \beta^r{}_{,r}\big] - E^z\beta^r{}_{,z} - 2\kappa\alpha S^r\,, \\
\partial_t E^z &= \beta^r E^z{}_{,r} + \beta^z E^z{}_{,z} \\
&\quad - \psi^{-4}\mathrm{e}^{-2rs}\big[\alpha_{,r}B^\varphi + \alpha B^\varphi{}_{,r} + 3\alpha B^\varphi(2\psi^{-1}\psi_{,1} + r^{-1})\big] \qquad (5.35) \\
&\quad - E^r\beta^z{}_{,r} + E^z\big[\tfrac{1}{3}\alpha(4rY - 5U) - \beta^r{}_{,r}\big] - 2\kappa\alpha S^z\,, \\
\partial_t B^\varphi &= \beta^r B^\varphi{}_{,r} + \beta^z B^\varphi{}_{,z} + \tfrac{1}{3}\alpha B^\varphi(U - 2rY) \\
&\quad + 2\alpha E^r(2\psi^{-1}\psi_{,z} + rs_{,z}) - 2\alpha E^z(2\psi^{-1}\psi_{,r} + rs_{,r} + s) \qquad (5.36) \\
&\quad + \alpha_{,z}E^r - \alpha_{,r}E^z + \alpha(E^r{}_{,z} - E^z{}_{,r})\,.
\end{aligned}
$$

We focus on vacuum spacetimes in this chapter and so we do not include

the matter evolution equations here (see appendix A for a discussion of a perfect fluid).

The above equations have been derived with the help of a programme written in the computer algebra language REDUCE [80]. Note that they are all regular on axis provided that the variables have the correct small-r behaviour (table 5.1).

5.4 Alternate evolution schemes

In this section we explain in more detail how the various variables are evolved. The variables s, Y, E^r, E^z and B^φ are always evolved using the evolution equations (5.29, 5.30, 5.34, 5.35, 5.36). For the remaining variables, there are several possibilities, and we discuss three alternate evolution schemes here.

5.4.1 A free evolution scheme

In the first scheme, one solves the elliptic gauge conditions (5.19, 5.22–5.23) for the gauge variables α, β^r and β^z and evolves the variables ψ, U and X using their evolution equations (5.28, 5.32, 5.33).

This scheme uses the maximum number of evolution equations to update the variables. None of the constraints are solved during the evolution, which is why this scheme is called a *free evolution scheme*.

This is essentially the scheme of Garfinkle and Duncan [62] (although their scheme does not include the twist variables) with the exception that they use the Hamiltonian constraint (5.24) to solve for ψ.

5.4.2 A constrained evolution scheme

In the second scheme, one eliminates the variables U and X completely using the relations (5.20–5.21). The slicing condition (5.19) then takes the form

$$\begin{aligned}\hat{\mathcal{S}}^{(\mathrm{C})} \equiv\ & \alpha_{,rr} + r^{-1}\alpha_{,r} + \alpha_{,zz} + 2\psi^{-1}(\psi_{,r}\alpha_{,r} + \psi_{,z}\alpha_{,z}) \\ & -\psi^4 \mathrm{e}^{2rs}\big[\tfrac{2}{3}(\alpha^{-1}\beta_-^2 + \alpha r^2 Y^2 + rY\beta_-) + \tfrac{1}{2}\alpha^{-1}\beta_+^2 \\ & \quad +\tfrac{1}{2}\alpha r^2\psi^8 \mathrm{e}^{2rs}(E^{r\,2} + E^{z\,2}) \\ & \quad +\tfrac{1}{2}\kappa\alpha(\rho_H + r\tilde{\tau} + 2S_r{}^r + S_z{}^z)\big] = 0\,. \end{aligned} \tag{5.37}$$

To solve for the shift vector, we use the momentum constraints (5.25–5.26), which can be written as

$$\begin{aligned}\hat{\mathcal{C}}_r^{(\mathrm{C})} =\ & \tfrac{2}{3}\beta^r{}_{,rr} + \beta^r{}_{,zz} + \tfrac{1}{3}\beta^z{}_{,rz} + \beta_+(6\psi^{-1}\psi_{,z} + 2rs_{,z} - \alpha^{-1}\alpha_{,z}) \\ & +\tfrac{2}{3}\beta_-(6\psi^{-1}\psi_{,r} + 3rs_{,r} + 3s - \alpha^{-1}\alpha_{,r}) - \tfrac{8}{3}\alpha Y \\ & -\tfrac{2}{3}\alpha r(6\psi^{-1}\psi_{,r}Y + Y_{,r}) - \alpha r^2\psi^8 \mathrm{e}^{2rs}B^\varphi E^z - 2\kappa\alpha J_r = 0\,, \end{aligned} \tag{5.38}$$

$$\begin{aligned}\hat{\mathcal{C}}_z^{(\mathrm{C})} =\ & \beta^z{}_{,rr} + \tfrac{4}{3}\beta^z{}_{,zz} - \tfrac{1}{3}\beta^r{}_{,rz} - 2\beta_-(4\psi^{-1}\psi_{,z} + rs_{,z} - \tfrac{2}{3}\alpha^{-1}\alpha_{,z}) \\ & +\beta_+(6\psi^{-1}\psi_{,r} + 2rs_{,r} + 2s + r^{-1} - \alpha^{-1}\alpha_{,r}) \\ & -\tfrac{2}{3}\alpha r(6\psi^{-1}\psi_{,z}Y + Y_{,z}) + \alpha r^2\psi^8 \mathrm{e}^{2rs}B^\varphi E^r - 2\kappa\alpha J_z = 0\,. \end{aligned} \tag{5.39}$$

The Hamiltonian constraint (5.24) becomes

$$\begin{aligned}\hat{\mathcal{C}}^{(\mathrm{C})} =\ & \psi_{,rr} + r^{-1}\psi_{,r} + \psi_{,zz} + \tfrac{1}{4}\psi(rs_{,rr} + 2s_{,r} + rs_{,zz}) \\ & +\psi^5 \mathrm{e}^{2rs}\big[\tfrac{1}{3}(\alpha^{-2}\beta_-^2 + r^2Y^2 + rY\alpha^{-1}\beta_-) + \tfrac{1}{4}\alpha^{-2}\beta_+^2 \\ & \quad +\tfrac{1}{4}\kappa\rho_H\big] \\ & +\tfrac{1}{16}r^2\psi^9 \mathrm{e}^{2rs}\big[B^{\varphi\,2} + \psi^4 \mathrm{e}^{2rs}(E^{r\,2} + E^{z\,2})\big] = 0\,. \end{aligned} \tag{5.40}$$

Equations (5.37–5.40) form a system of coupled elliptic equations that is solved for the variables α, β^r, β^z and ψ.

This scheme uses the maximum number of elliptic equations. All the constraints are enforced during the evolution except for the Geroch constraint (5.27). Hence we call this scheme a *constrained evolution scheme*.

This is essentially the scheme of Choptuik et al. [41] (although their scheme does not include the twist variables).

5.4.3 A partially constrained evolution scheme

Finally, we propose a new scheme that can be viewed as a compromise between the two previous ones. Here the variables U and X are first evolved to the next time level using the evolution equations (5.32–5.33). The slicing condition (5.19) is then solved for α as in the free evolution scheme. To solve for the shift, however, we use the momentum constraints (5.38–5.39). After solving for the lapse and shift, the variables U and X are immediately overwritten by (5.20–5.21). Then the slicing condition and the momentum constraints are again solved for the lapse and shift, and the procedure is iterated until convergence. In this way, we enforce both the momentum constraints and the gauge conditions. However, we do not solve the Hamiltonian constraint but evolve ψ using its evolution equation (5.28).

This is the scheme we will use for the numerical evolutions in section (5.7). We will explain its advantages over the other schemes in the following sections.

5.5 Solvability of the elliptic equations

All the evolution systems presented in the previous section involve (to varying extent) the solution of elliptic equations. The question arises whether these equations are well-posed, i.e., whether a unique solution exists. We would

also like to know which numerical methods can by used to solve the equations, in particular whether the Multigrid method (section 4.3) will work.

5.5.1 Analytical considerations

The elliptic equations we encounter are of the general type

$$Lu \equiv a^{AB}\partial_A\partial_B u + b^A\partial_A u + H(u, x^A) = f\,, \tag{5.41}$$

where the coefficients a^{AB}, b^A and the right-hand-side f depend on the coordinates x^A only and $H(u, x^A)$ may be a nonlinear function. We assume that all of these are smooth. The boundary consists of a part where we impose a Neumann condition $\partial_\perp u = 0$ (on the axis $r = 0$) and a part where we impose a Dirichlet condition $u = 0$ (the outer boundaries)[2].

Proving existence and uniqueness of solutions of (5.41) can be decidedly nontrivial. However, it is relatively easy to obtain a necessary condition for the solution (should it exist) to be unique. Suppose we are given a solution u_0 and we consider a small perturbation $u = u_0 + \delta u$. For u to be a solution as well, δu must satisfy the linearized equation

$$a^{AB}\partial_A\partial_B\delta u + b^A\partial_A\delta u + c\delta u = \tilde{f}\,, \tag{5.42}$$

where

$$c \equiv \left.\frac{\partial H}{\partial u}\right|_{u=u_0}. \tag{5.43}$$

For the solution of (5.41) to be unique, the solution of (5.42) must also be unique (*linearization stability*). One can prove using the maximum principle [114, 66] that equation (5.42) has a unique solution satisfying the mixed Dirichlet-Neumann boundary conditions if the following conditions hold:

[2]Strictly speaking, $u = 0$ may only be imposed at infinity but the following analysis requires a bounded domain. We choose it to be sufficiently large such that the Dirichlet boundary conditions are a good approximation.

1. the operator L is *elliptic*, i.e.,

$$a^{AB}\xi_A\xi_B > 0 \quad \forall \xi \in \mathbb{R}^2 \setminus 0\,, \tag{5.44}$$

2.

$$c \leqslant 0\,. \tag{5.45}$$

Let us check whether these conditions are satisfied for the elliptic equations we would like to solve.

The slicing condition. Consider first the slicing condition in the form (5.19) as used in the free evolution scheme (section 5.4.1) and in the partially constrained scheme (section 5.4.3). Its principal part is the Laplace operator, $a^{AB} = \delta^{AB}$, which clearly satisfies (5.44). The equation is already linear with the coefficient c in (5.42) given by

$$\begin{aligned} c \;=\; & -\psi^4 \mathrm{e}^{2rs}\big[\tfrac{2}{3}(U - \tfrac{1}{2}rY)^2 + \tfrac{1}{2}r^2Y^2 + 2X^2 \\ & + \tfrac{1}{2}r^2\psi^8\mathrm{e}^{2rs}(E^{r\,2} + E^{z\,2}) \qquad (5.46) \\ & + \tfrac{1}{2}\kappa(\rho_H + r\tilde{\tau} + 2S_r{}^r + S_z{}^z)\big]\,. \qquad (5.47) \end{aligned}$$

At least in vacuum, we have $c < 0$ (note that $\psi > 0$). Hence a solution of the slicing condition (should it exist) is unique.

Suppose now that we use the constrained evolution scheme (section 5.4.2) so that the slicing condition has the form (5.37). That equation has a non-linear source term $H(\alpha, x^A)$ as in (5.41), and we find

$$\begin{aligned} \frac{\partial H}{\partial \alpha} \;=\; & -\psi^4 \mathrm{e}^{2rs}\big[-\alpha^{-2}(\tfrac{2}{3}\beta_-^2 + \tfrac{1}{2}\beta_+^2) \\ & + r^2Y^2 + \tfrac{1}{2}r^2\psi^8\mathrm{e}^{2rs}(E^{r\,2} + E^{z\,2}) \qquad (5.48) \\ & + \tfrac{1}{2}\kappa(\rho_H + r\tilde{\tau} + 2S_r{}^r + S_z{}^z)\big]\,. \qquad (5.49) \end{aligned}$$

Now the first line inside the square bracket has the wrong sign and so $\partial H/\partial\alpha$ can be non-negative. Hence we cannot prove uniqueness for the linearized equation, and solutions to the nonlinear slicing condition (5.37) could *potentially* be non-unique as well.

The shift conditions. The shift conditions (5.22–5.23) are simple Poisson equations ($a^{AB} = \delta^{AB}$, $b^A = H = 0$ in (5.41)) and therefore have a unique solution.

The momentum constraints. The momentum constraints (5.38–5.39) are linear, $H = 0$. The only condition that is not immediately obvious is the ellipticity of the differential operator, for now we have a coupled system

$$L_{AB}(\partial_r, \partial_z)\beta^B = f_A\,. \tag{5.50}$$

The principal symbol is given by

$$L_{AB}(x,y) = \begin{pmatrix} \frac{2}{3}x^2 + y^2 & \frac{1}{3}xy \\ -\frac{1}{3}xy & x^2 + \frac{4}{3}y^2 \end{pmatrix}. \tag{5.51}$$

Its determinant is

$$\det L(x,y) = \tfrac{2}{3}(x^4 + 3x^2y^2 + 2y^4) > 0 \quad \forall\,(x,y) \in \mathbb{R}^2 \setminus (0,0)\,. \tag{5.52}$$

We have shown that the system is elliptic and hence the momentum constraints have a unique solution.

The Hamiltonian constraint. Finally we turn to the Hamiltonian constraint (5.24) or (5.40). This has the form (5.41) with

$$\begin{aligned} \frac{\partial H}{\partial \psi} &= \tfrac{1}{4}(rs_{,rr} + 2s_{,r} + rs_{,zz}) \\ &\quad + 5\psi^4 \mathrm{e}^{2rs}\left[\tfrac{1}{3}(U - \tfrac{1}{2}rY)^2 + \tfrac{1}{4}r^2Y^2 + \tfrac{1}{4}\kappa\rho_H\right] \\ &\quad + \tfrac{1}{16}r^2\psi^8\mathrm{e}^{2rs}\left[9B^{\varphi 2} + 13\psi^4\mathrm{e}^{2rs}(E^{r\,2} + E^{z\,2})\right]. \end{aligned} \tag{5.53}$$

All the terms in the square brackets are positive, and the terms in the first line are oscillatory. Hence condition (5.45) is *not* satisfied everywhere. We conclude that quite possibly the Hamiltonian constraint (5.24) does not have a unique solution in general.

A few more remarks are about the Hamiltonian constraint are in order. This equation is essentially the *Yamabe equation*

$$\Delta\psi + K^2\psi^p = 0\,, \tag{5.54}$$

where $p = 5$, K^2 is the square of the extrinsic curvature (which we assume to be a smooth function), and we disregard the twist and matter here. If we set $u \equiv \psi - 1$ and $f(u) \equiv K^2(1+u)^p$, equation (5.54) can be written as

$$-\Delta u = f(u)\,, \tag{5.55}$$

and we consider the boundary conditions

$$u|_{\partial\Omega} = 0\,. \tag{5.56}$$

By a theorem in Evans [52, sec. 8.5.2] based on the Mountain Pass Theorem, the boundary value problem (5.55–5.56) has at least one weak solution $u \neq 0$ provided that

$$1 < p < \frac{n+2}{n-2}\,, \tag{5.57}$$

where n is the spatial dimension. In our case ($n = 2$), p is not restricted from above and we deduce that a solution to the Hamiltonian constraint does exist. (Note that in $n = 3$ dimensions, $p = 5$ is the critical case and the theorem is not applicable.)

However, nothing is being said about the uniqueness of the solution. In fact, our argument above indicates that the Hamiltonian constraint might not be linearization stable. We can improve on this by applying York's [144]

conformal rescaling procedure: let us redefine the extrinsic curvature K by setting

$$K = \psi^{-q}\tilde{K}\,. \tag{5.58}$$

Then (5.54) reads (with $p = 5$)

$$\Delta\psi + \tilde{K}^2\psi^{5-2q} = 0\,, \tag{5.59}$$

the linearization of which is

$$\Delta\delta\psi + (5-2q)\tilde{K}^2\delta\psi^{4-2q} = f\,. \tag{5.60}$$

If we choose $q \geqslant 5/2$ then our analysis above shows that the modified Hamiltonian constraint (5.59) is linearization stable. York applies this trick only at the initial time in order to set up a well-posed elliptic problem for the initial data. However, we want to solve the Hamiltonian constraint at each time step, which means that we have to evolve $\tilde{K}$ instead of K. We have implemented this but unfortunately the numerical evolutions quickly became unstable. A somewhat heuristic explanation for this might lie in the fact that a rescaling of the extrinsic curvature is also applied in the *BSSN system* [16], which is known to be much more stable than the standard ADM system.[3] It turns out that our choice of extrinsic curvature K corresponds precisely to the BSSN variables, whereas the rescaled $\tilde{K}$ corresponds to the ADM variables, with $q = 4$.

Summary. We have indicated that the Hamiltonian constraint and the version of the slicing condition that is used in the constrained evolution scheme might not have a unique solution in general. In contrast, all the

[3]On the other hand, some formulations such as NOR [103] appear to be stable without conformal rescalings.

elliptic equations of the free evolution scheme and the partially constrained scheme are well-posed.

5.5.2 Numerical considerations

There is a close connection between the above analytical results and the numerical solvability of the elliptic equations under discussion using the Multigrid method. The Newton-Gauss-Seidel relaxation employed in that method effectively linearizes the elliptic equation so that it suffices to deal with a linear model problem here. For simplicity, we consider the *Helmholtz equation*

$$u_{,rr} + u_{,zz} + cu = f\,. \tag{5.61}$$

This equation is discretized as

$$\tfrac{1}{h^2}(u_{i+1,j} + u_{i-1,j} + u_{i,j+1} + u_{i,j-1} - 4u_{ij}) + c_{ij}u_{ij} = f_{ij}\,. \tag{5.62}$$

As explained in section 4.3, the Gauss-Seidel relaxation converges if the matrix on the left-hand-side of (5.62) is diagonal dominant. The (absolute values of the) off-diagonal terms in (5.62) add up to $4h^{-2}$ and the diagonal term is $-4h^{-2} + c_{ij}$. Hence the matrix is diagonal dominant if and only if $c_{ij} \leqslant 0$, which is again condition (5.45). (If first-order derivatives are included in (5.61) or if the principal part is not the Laplace operator, this condition may not be sufficient to guarantee diagonal dominance.)

In practice, the relaxation still converges if $c > 0$ and c is sufficiently small. For larger and larger positive c, however, the relaxation first stalls and ultimately diverges. The failure of Multigrid for such indefinite Helmholtz equations has been reported many times in the literature (e.g., [29]). Cures of the problem usually involve some kind of conjugate gradient or other Krylov

subspace iterations, which are very slow as compared with standard Multigrid (e.g., [47]; see also section 4.4.2).

We conclude that the Multigrid method is suitable for solving all the equations that occur in the free evolution scheme and the partially constrained scheme but that it might fail for the Hamiltonian constraint and the slicing condition used in the constrained scheme. This is indeed what we have observed when trying to evolve strong Brill waves (section 5.7) with the constrained scheme. Similar observations have been reported by Choptuik et al. [41] and Barnes [14]. The former try to avoid the problem by evolving the conformal factor ψ using its evolution equation (5.28) instead of solving the Hamiltonian constraint for it. However, they find that their Multigrid solver still fails for strong Brill waves. A likely explanation for this is the argument given above for the slicing condition.

5.6 Evolution of the constraints

We have seen how in the (2+1)+1 formalism (as in all ADM-like formalisms), the Einstein equations split into elliptic constraint equations and hyperbolic evolution equations. Analytically, the constraints are preserved by the evolution equations. However, if in a numerical evolution the constraints are only solved initially, they might get violated during the evolution due to numerical errors. Catastrophic growth of the constraints in free evolution schemes is a very common plague in numerical relativity and to-date one of the major limitations to the runtime of simulations.

In this section, we take a closer look at the evolution of the constraints and assess the schemes presented in section 5.4 with regard to their stability against constraint violations.

Suppose first we adopt the free evolution scheme (section 5.4.1). The constraints (5.24–5.27) are found to obey the following evolution equations:

$$\partial_t \hat{\mathcal{C}} \simeq -\beta^r \partial_r \hat{\mathcal{C}} - \beta^z \partial_z \hat{\mathcal{C}} - \tfrac{1}{4}\alpha\psi(\partial_r \hat{\mathcal{C}}_r + \partial_z \hat{\mathcal{C}}_z)\,, \tag{5.63}$$

$$\partial_t \hat{\mathcal{C}}_r \simeq -\beta^r \partial_r \hat{\mathcal{C}}_r - \beta^z \partial_z \hat{\mathcal{C}}_r + 4\alpha\psi^{-5}\mathrm{e}^{-2rs}(\partial_r \hat{\mathcal{C}} + \tfrac{1}{4}\alpha^{-1}\psi\,\partial_r \hat{\mathcal{S}})\,, \tag{5.64}$$

$$\partial_t \hat{\mathcal{C}}_z \simeq -\beta^r \partial_r \hat{\mathcal{C}}_z - \beta^z \partial_z \hat{\mathcal{C}}_z - 4\alpha\psi^{-5}\mathrm{e}^{-2rs}\partial_z \hat{\mathcal{C}}\,, \tag{5.65}$$

$$\partial_t \hat{\mathcal{C}}_\varphi \simeq -\beta^r \partial_r \hat{\mathcal{C}}_\varphi - \beta^z \partial_z \hat{\mathcal{C}}_\varphi\,. \tag{5.66}$$

Here $\hat{\mathcal{S}}$ is the slicing condition (5.19), and $\simeq$ denotes equality to principal parts. The terms we have left out are all linear and homogeneous in the constraints and the gauge conditions, so that the constraints are indeed conserved (equations (5.63–5.66) are satisfied if all the constraints and gauge conditions vanish at all times).

We enforce the slicing condition during the numerical evolution, i.e., we may set $\hat{S} = 0$ in (5.64). Then the constraint evolution system can be written in closed form as

$$\partial_t \mathbf{c} = A^A \partial_A \mathbf{c} + B\mathbf{c}\,, \tag{5.67}$$

where $\mathbf{c} = (\hat{\mathcal{C}}, \hat{\mathcal{C}}_r, \hat{\mathcal{C}}_z, \hat{\mathcal{C}}_\varphi)^T$ and the matrices A^A are given by

$$A^r = \begin{pmatrix} -\beta^r & -\frac{1}{4}\alpha\psi & 0 & 0 \\ 4\alpha\psi^{-5}\mathrm{e}^{-2rs} & -\beta^r & 0 & 0 \\ 0 & 0 & -\beta^r & 0 \\ 0 & 0 & 0 & -\beta^r \end{pmatrix}, \tag{5.68}$$

$$A^z = \begin{pmatrix} -\beta^z & 0 & -\frac{1}{4}\alpha\psi & 0 \\ 0 & -\beta^z & 0 & 0 \\ -4\alpha\psi^{-5}\mathrm{e}^{-2rs} & 0 & -\beta^z & 0 \\ 0 & 0 & 0 & -\beta^z \end{pmatrix}. \tag{5.69}$$

The matrix A^r has complex eigenvalues $-\beta^r \pm i\alpha\psi^{-2}\mathrm{e}^{-rs}$ whereas A^z has real eigenvalues $-\beta^z \pm \alpha\psi^{-2}\mathrm{e}^{-rs}$. This means that A^r is not real diagonalizable, and so the system is not hyperbolic (see section 6.4 for a precise definition of hyperbolicity and its implications). Hence the initial value problem (IVP) for the constraint evolution system is ill-posed, and small violations of the constraints may grow without bound.

The reason for the lack of hyperbolicity lies in the slicing condition (5.3). Recall that when we derived it, we added a multiple of the Hamiltonian constraint. If we undo this and replace

$$\hat{\mathcal{S}} \to \hat{\mathcal{S}}' \equiv \hat{\mathcal{S}} + 8\alpha\psi^{-1}\hat{\mathcal{C}} \tag{5.70}$$

then the evolution equation for the r-momentum constraint (5.64) becomes

$$\partial_t \hat{\mathcal{C}}_r \simeq -\beta^r \partial_r \hat{\mathcal{C}}_r - \beta^z \partial_z \hat{\mathcal{C}}_r - 4\alpha\psi^{-5}\mathrm{e}^{-2rs}(\partial_r \hat{\mathcal{C}} - \tfrac{1}{4}\alpha^{-1}\psi\, \partial_r \hat{\mathcal{S}}')\,. \tag{5.71}$$

Hence

$$A^r = \begin{pmatrix} -\beta^r & -\frac{1}{4}\alpha\psi & 0 & 0 \\ -4\alpha\psi^{-5}\mathrm{e}^{-2rs} & -\beta^r & 0 & 0 \\ 0 & 0 & -\beta^r & 0 \\ 0 & 0 & 0 & -\beta^r \end{pmatrix}, \tag{5.72}$$

which has real eigenvalues $-\beta^r \pm \alpha\psi^{-2}\mathrm{e}^{-rs}$ and so the system is hyperbolic and the IVP is well-posed. However, the modified slicing condition (5.70) can easily become indefinite, depending on the sign of $\hat{\mathcal{C}}$. Indeed, the Multigrid method turns out to fail for the modified slicing condition even for relatively weak perturbations of flat space.

Fortunately there is a way out: suppose we enforce the momentum constraints by using either the constrained scheme (section 5.4.2) or the partially constrained scheme (section 5.4.3). Then the offending equation (5.64) is discarded and the remaining system is clearly hyperbolic.

We have thus given a strong argument for solving the momentum constraints if a maximal slicing condition is used that is manipulated by adding a multiple of the Hamiltonian constraint. Together with the results of section 5.5, we conclude that the partially constrained scheme 5.4.3 is the only one of the schemes presented in section 5.4 that may be suitable for the numerical evolution of strong gravitational waves.

One should remark that hyperbolicity of the constraint evolution system is not sufficient to rule out growth of the constraints. Depending on the matrix B in (5.67), there could well be exponentially growing solutions. One could try to adjust B by adding suitable multiples of the constraints to the main evolution equations, as done, for example, in [143]. We have not investigated this possibility because the constraints appear to be bounded in our numerical evolutions (section 5.7).

5.7 Numerical evolutions of generalized Brill waves

In this section we present some numerical results on the evolution of time-symmetric axisymmetric gravitational waves in vacuum, also known as *Brill waves* [32]. As a new ingredient, we include a nonzero twist.

5.7.1 Initial data

The initial time $t = 0$ is chosen to be a moment of time symmetry, i.e., under the coordinate transformation $t \to t' \equiv -t$ the metric transforms as

$$g'_{\alpha\beta}(t) = g_{\alpha\beta}(-t)\,. \tag{5.73}$$

This implies that the spatial metric is an even function of t and so the extrinsic curvature (the time derivative of the spatial metric) vanishes at $t = 0$:

$$Y = U = X = 0\,. \tag{5.74}$$

From definition (3.6) we infer that the spatial components of the twist vector are odd functions of time and the time component is even. Now definition (3.47) implies that

$$E^r = E^z = 0 \tag{5.75}$$

at $t = 0$. The initial data for the variables s and B^φ is taken to be

$$s = A_s\, r\, \mathrm{e}^{-r^2-z^2}\,, \qquad B^\varphi = A_B\, r\, z\, \mathrm{e}^{-r^2-z^2} \tag{5.76}$$

with constant amplitudes A_s and A_B. The Hamiltonian constraint (5.24) is then solved for the conformal factor ψ. For this initial data the momentum constraints (5.25–5.26) and the Geroch constraint (5.27) are automatically satisfied, and the unique solution of the gauge conditions (5.19, 5.22–5.23) is

$$\alpha = 1\,, \qquad \beta^r = \beta^z = 0\,. \tag{5.77}$$

In Brill's original work [32] and in all subsequent studies we know of, the twist was assumed to vanish. However, we would like to stress that a nonzero B^φ is consistent with time symmetry so that the term *generalized Brill waves* is justified for the problem considered here.

5.7.2 Boundary conditions

On the axis $r = 0$, we enforce the appropriate Dirichlet or Neumann conditions as stated in table 5.1. Since our initial data is reflection-symmetric about the $z = 0$ plane and the evolution equations preserve that symmetry,

$$\alpha, \beta^r, \underline{\beta^z}, \psi, s, Y, U, \underline{X}, \underline{B^\varphi}, E^r, \underline{E^z},$$
$$\rho_H, \sigma, J^\varphi, J_r, \underline{J_z}, \tilde{\tau}, S^r, \underline{S^z}, \Sigma^r, \underline{\Sigma^z}, S_r{}^r, \underline{S_r{}^z}, S_z{}^z.$$

Table 5.2: z-parity of the variables of the hyperbolic-elliptic system if reflection symmetry is assumed. Underlined variables are odd functions of z, the remaining ones are even.

we can save computational time by only evolving the upper half of the (r, z) plane. Reflection symmetry means that under the coordinate transformation $z \to z' \equiv -z$ the metric transforms as

$$g'_{\alpha\beta}(z) = g_{\alpha\beta}(-z)\,. \tag{5.78}$$

This implies that the variables we evolve are either odd or even functions of z. For an odd variable $\underline{u}$, we impose a Dirichlet condition

$$\underline{u}|_{z=0} = 0\,, \tag{5.79}$$

and for an even variable u, a Neumann condition

$$\partial_z u|_{z=0} = 0 \tag{5.80}$$

is needed. The z-parity of all the variables we evolve is summarized in table 5.2.

Throughout this thesis we focus on asymptotically flat spacetimes. We therefore assume a fall-off of all the variables like

$$u = u_\infty + \frac{c}{R} \tag{5.81}$$

for large $R \equiv \sqrt{r^2 + z^2}$, where u_∞ is the flat-space value of the variable u and c is independent of R. This implies that

$$0 = \partial_R[R(u - u_\infty)] = u - u_\infty + r u_{,r} + z u_{,z}\,. \tag{5.82}$$

We use this as a boundary condition at $r = r_{\max}$ and $z = z_{\max}$ for the elliptic equations, i.e., for the variables α, β^r, β^z and initially ψ.

The remaining variables are evolved by hyperbolic evolution equations, and for them we impose an *outgoing wave* or *Sommerfeld condition*

$$u = u_\infty + \frac{f(t-R)}{R}\,, \tag{5.83}$$

which we rewrite as

$$0 = (\partial_R + \partial_t)[R(u-u_\infty)] = u - u_\infty + r u_{,r} + z u_{,z} + R u_{,t}\,. \tag{5.84}$$

These boundary conditions appear to work well in practice, although they are a rather crude choice which is not fully justified theoretically. We refer the reader to chapter 8, where outer boundary conditions are discussed at length for a completely hyperbolic formulation of Einstein's equations.

5.7.3 Numerical method

The equations are discretized using second-order accurate centred finite differencing (section 4.1) on a single uniform cell-centred grid. Unlike Garfinkle and Duncan [62], we do not compactify the spatial coordinates, for fear that we might fail to resolve the waves as they travel out to infinity.

For the time integration, we use the method of lines with the third-order Runge-Kutta scheme (4.38b). The second-order Runge-Kutta schemes (4.37) and the three-step iterative Crank-Nicholson method (4.40–4.44) were also tried but were found to be substantially less stable in strong Brill wave evolutions. In particular, the simulations with those schemes suffered from an unbounded growth of the constraint residuals. The fourth-order Runge-Kutta scheme (4.39) gave results comparable to the third-order one but is computationally more expensive. The Courant number is taken to be $\Delta t/h = 0.5$ in all the evolutions presented here.

Fourth-order Kreiss-Oliger dissipation (4.64) with amplitude $\epsilon_D = 0.5$ is added to the right-hand-side of the evolution equations. We found that without dissipation, a high-frequency instability occurred at very late times, in particular close to the boundaries.

The boundary conditions are implemented via the method of ghost cells as explained in section 4.1.3.

We adopt the partially constrained evolution scheme (section 5.4.3), for the reasons discussed in the previous two sections. The elliptic equations are solved using the Multigrid method (section 4.3) with red-black Gauss-Seidel relaxation. The FAS version of the method is used (although the equations are linear and so linear Multigrid would work just as well). Typically five W-cycles are needed to drive the residual well below the discretization error.

5.7.4 Weak Brill waves with twist

We first consider Brill waves with an amplitude $A_s = 1$, which is well in the subcritical régime. To study the influence of the twist, we perform simulations with three different amplitudes $A_B = 0, 2, 4$. The resolution is taken to be 128 points in both the r and the z direction and the outer boundaries are placed at $r_{\max} = z_{\max} = 10$.

Figure 5.1 shows the lapse function at the origin $r = z = 0$ as a function of time. When a high-curvature region of spacetime is approached, we expect the lapse function to collapse because the (maximal) slices try to avoid that region and pile up. Because the minimum of the lapse is always found to lie in the origin, the value of the lapse there serves as a good "curvature indicator".

We see that the lapse performs a few damped oscillations and eventually returns to its flat-space value. The amplitude of the extrema is found to

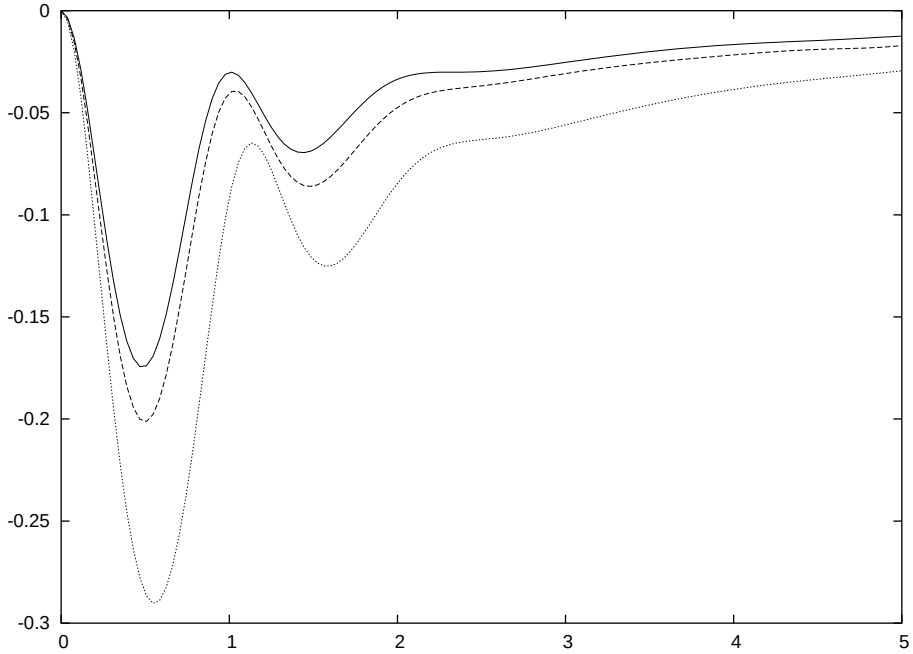

Figure 5.1: $\ln \alpha_0$ (logarithm of the lapse function at the origin) as a function of time for a Brill wave with amplitude $A_s = 1$ and three different amplitudes of the twist: $A_B = 0$ (solid line), 2 (dashed line) and 4 (dotted line)

increase with increasing A_B, while the extrema occur almost at the same times.

To check the accuracy of our code, we perform a convergence test: figure 5.2 shows the L^2 norm[4] of the constraint residuals as a function of time for two different resolutions (here the amplitude of B^φ is taken to be $A_B = 2$). Because the finite-differencing we use is second-order accurate, the residual of the constraints should decrease by a factor of four as the resolution is doubled. The numerical results indicate that we do not quite achieve second-order convergence (the decrease lies between a factor of 2 and 3). This is probably due to reflections caused by the imperfect outer boundary conditions, which do not appear to converge away with increasing resolution.

[4]see equation (7.108) for a definition of the discrete L^2 norm

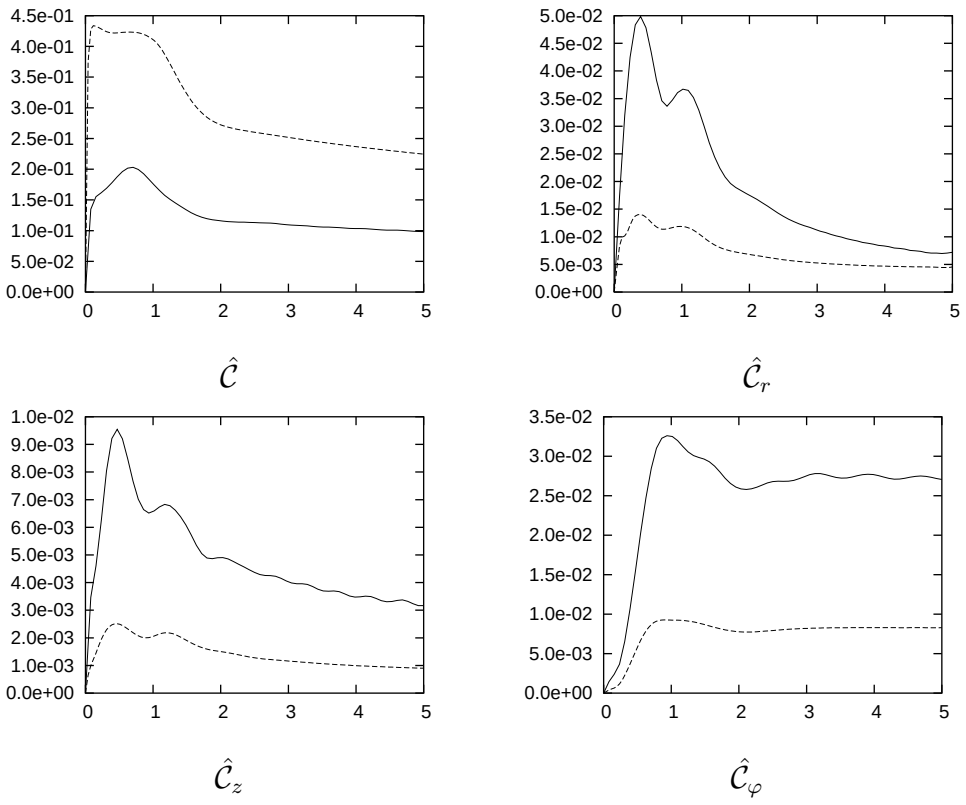

Figure 5.2: L^2 norm of the constraint residuals as a function of time for a Brill wave with amplitudes $A_s = 1$ and $A_B = 2$ and two different resolutions: 64 points (solid lines) and 128 points (dashed lines)

5.7.5 Strong Brill waves

Next we turn to strong Brill waves with amplitudes $A_s \gtrsim 4$. Thanks to the modified evolution scheme we use (section 5.4.3), we are able to evolve much stronger Brill waves than with the constrained scheme (section 5.4.2) used by both Choptuik et al. [41] and Barnes [14]. The constrained scheme failed for amplitudes $A_s \gtrsim 3$ due to a breakdown of the Multigrid solver, as explained in section 5.5.2. We also found that the free evolution scheme (section 5.4.1) suffered from an unbounded growth of the constraints particularly for strong

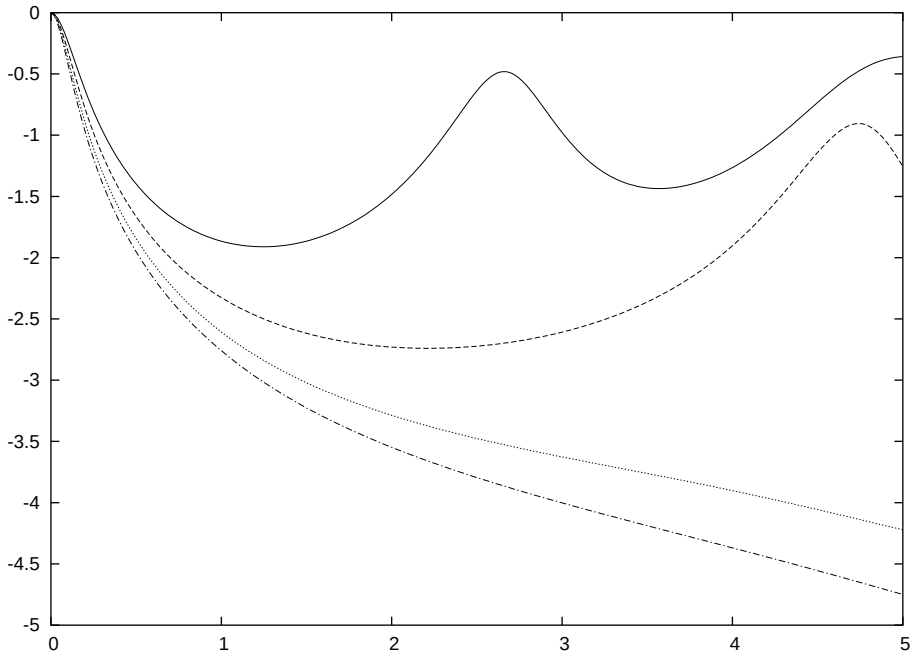

Figure 5.3: $\ln \alpha_0$ (logarithm of the lapse function at the origin) as a function of time for non-twisting Brill waves with amplitudes $A_s = 4$ (solid line), 5 (dashed line), 6 (dotted line) and 7 (dot-dashed line)

Brill wave evolutions, as predicted in section 5.6.

Figure 5.3 shows again the lapse function at the origin as a function of time for four different values of the amplitude A_s. In order to compare our results with those of Garfinkle and Duncan [62], we choose the twist to vanish here. As A_s is increased, the oscillations of the lapse become larger and larger and their frequency decreases. For $A_s \geqslant 6$, the lapse function continues to collapse and the formation of a black hole is expected. The interval

$$5 < A_s^* < 6 \tag{5.85}$$

for the critical amplitude is in agreement with [62].

To get some idea of what happens at the "phase transition", we show a few snapshots of the variable s for a slightly subcritical evolution ($A_s = 4$,

figure 5.4) and a slightly supercritical one ($A_s = 6$, figure 5.5). While we see an outgoing wave form in the subcritical evolution, the marginally supercritical solution contracts rather than disperses. The $A_s = 6$ run crashed at $t \approx 6$ because the resolution was insufficient to resolve the small and highly dynamical features close to the origin.

Critical collapse thus poses a major computational problem: more and more resolution is needed close to the origin as one approaches the critical point. At the same time, the solution is very smooth further away from the origin, so it would be a waste of computational resources to have a high resolution across the entire grid. This is a classic case for adaptive mesh refinement (AMR) (section 4.5): we would like to add resolution only in regions where and when it is needed. We have not implemented AMR for mixed hyperbolic-elliptic systems yet but will use it in chapter 9 for the completely hyperbolic system derived in the following chapter.

5.8 Conclusions

This is a good place to draw some preliminary conclusions before we move on to the second part of the thesis.

In this chapter, we considered a mixed hyperbolic-elliptic system that involved solving elliptic gauge conditions as well as (some or all) constraint equations. Two major problems with such systems were indicated, which we expect to be fairly generic in many formulations of the Einstein equations used in numerical relativity.

Firstly, it is not always clear whether the elliptic equations one tries to solve have unique solutions. In particular, the Hamiltonian constraint in the form used here is problematic. Suppose that one attempts to solve

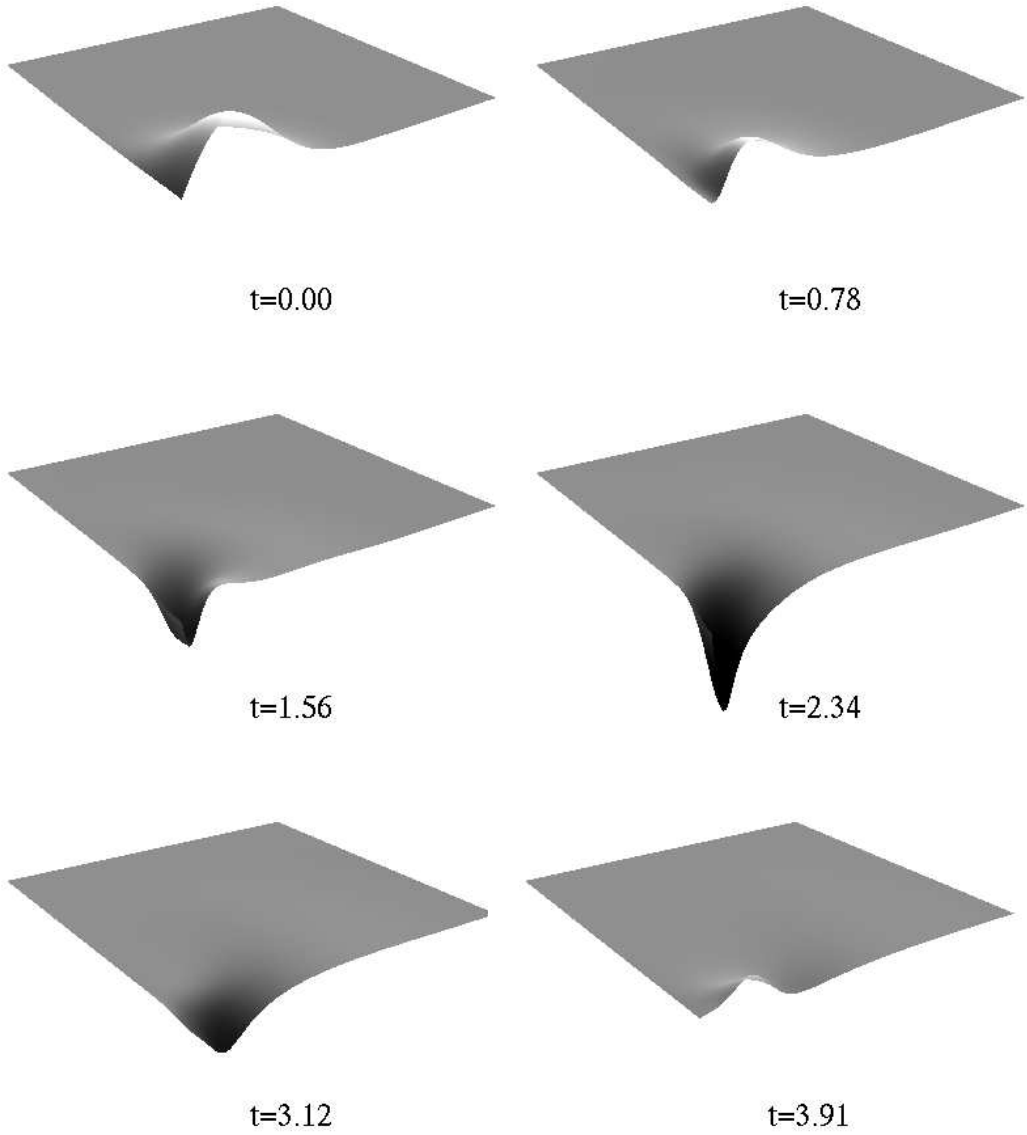

Figure 5.4: Snapshots of the variable s for a subcritical Brill wave with amplitude $A_s = 4$. The resolution is 128 points in each dimension and the outer boundaries are placed at $r_{\max} = z_{\max} = 5$. In all plots of this thesis, the axis $r = 0$ is the bottom left boundary.

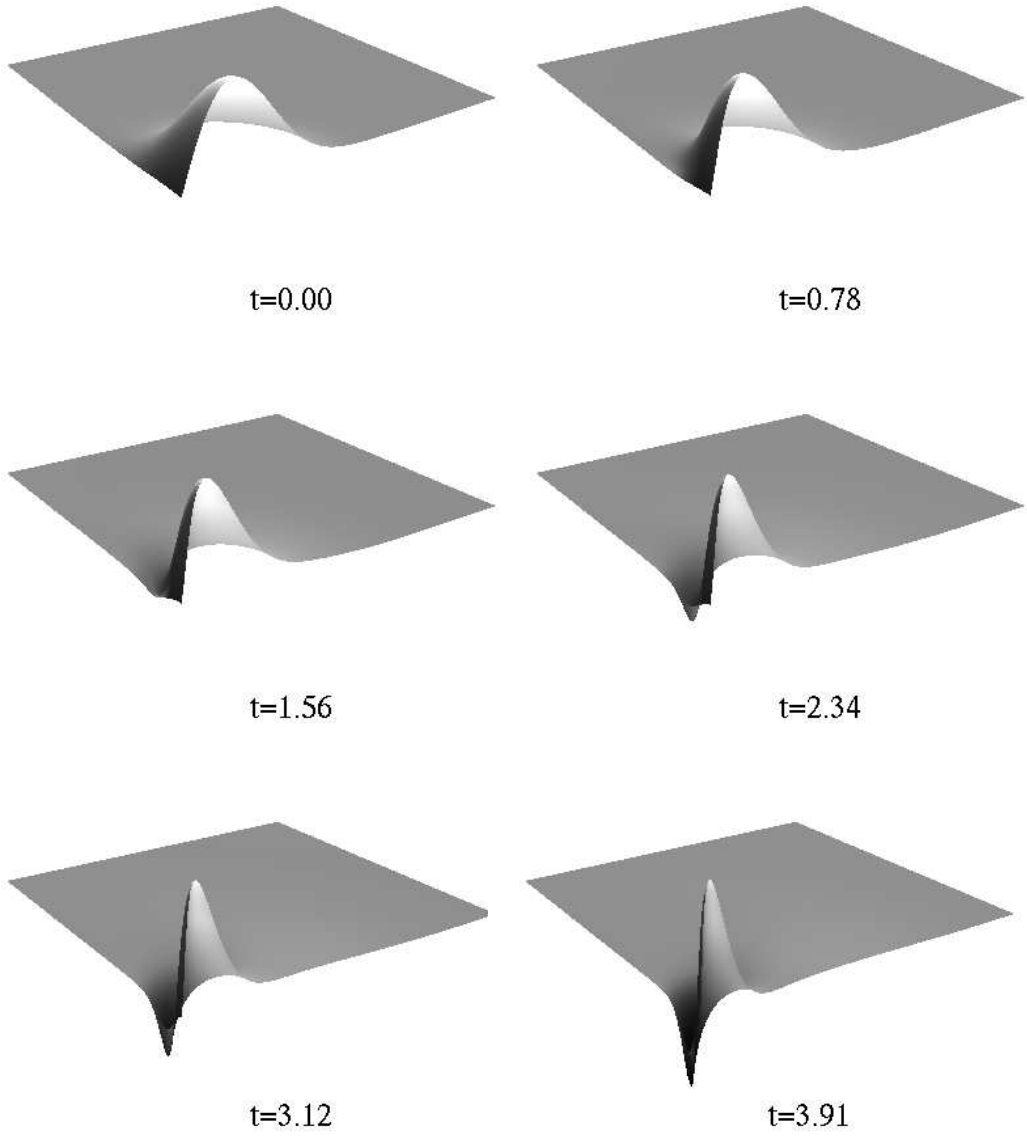

Figure 5.5: Snapshots of the variable s for a supercritical Brill wave with amplitude $A_s = 6$. Same parameters as in figure 5.4.

this constraint during the evolution. Even if the numerical solver finds a solution, that solution could be non-unique. It could be a solution that is not compatible with the evolution equation (5.28) that the conformal factor must also obey. Therefore it is not sufficient to enforce the Hamiltonian constraint alone – one must also check the residual of the evolution equation. Because the Multigrid method we use is unsuitable for the Hamiltonian constraint, we decided to evolve the conformal factor freely and monitor the constraint residual instead.

Secondly, we saw that if one uses free evolution (none of the constraints are solved), the constraint evolution system can become ill-posed if the maximal slicing condition is simplified by adding a multiple of the Hamiltonian constraint, as usually done in the literature. To cure this problem, we proposed a modified evolution scheme which solves the momentum constraints but not the Hamiltonian constraint and which has a well-posed constraint evolution system.

With our modified evolution system we were able to evolve both weak and strong Brill waves. We included a nonzero twist, which to our knowledge is the first time this has been done. The existence of a critical amplitude that separates dispersal of the waves from black hole formation was indicated. At present, we cannot study the critical behaviour more closely because we run out of resolution to resolve the features that occur near the origin on smaller and smaller scales. Adaptive mesh refinement would be needed to tackle this problem in a computationally efficient way.

We decided not to continue to work on this formulation for the time being for a variety of reasons: well-posedness of the initial boundary value problem is difficult to prove for mixed hyperbolic-elliptic systems, it is not clear what the characteristics of the system are because part of the dynamics

resides in the variables that are solved for using elliptic equations, and the outer boundary conditions are ill-understood. All these questions will be addressed in the second part of this thesis for a strongly hyperbolic reduction of Einstein's equations in axisymmetric spacetimes.

Chapter 6

The Z(2+1)+1 system

Whereas in chapter 5 we considered a mixed hyperbolic-elliptic system, we construct in this chapter a completely hyperbolic formulation of the Einstein equations for axisymmetric spacetimes. In contrast to elliptic systems, hyperbolic systems of equations have the property that information propagates with finite speed along the characteristics. This makes them amenable to mathematical analysis more easily than mixed hyperbolic-elliptic systems in which because of the elliptic sector the solution at a given point depends on the solution in the entire spatial domain. In particular, one can use the characteristic structure to set up boundary conditions at the outer boundary of the computational domain. For certain types of hyperbolic systems and boundary conditions, theorems exist that guarantee the well-posedness of the initial boundary value problem (IBVP). By well-posedness we broadly mean that a unique solution exists at least for some finite time and that it depends continuously on the initial and boundary data.

There are many ways of obtaining hyperbolic formulations of the Einstein equations. Most approaches are based on the ADM decomposition outlined in section 3.2. Unfortunately, without further modifications the ADM system is

only weakly hyperbolic and thus does not have a well-posed IBVP (e.g., [87]). Strongly hyperbolic systems can be obtained by adding certain multiples of the constraints to the evolution equations. Among the variety of such systems are the ones of Frittelli and Reula [59] and Kidder, Scheel and Teukolsky [87]. Whereas those authors assume an arbitrary but fixed gauge, dynamical gauge conditions were incorporated later (e.g., Lindblom and Scheel [98]). A particularly simple and beautiful way of producing the required constraint additions "automatically" is a covariant extension of the Einstein equations first introduced by Bona et al. [23] called the *Z4 system*. That formulation has the additional advantage of a simpler constraint structure, as we shall see in the following.

This chapter is mainly based on Rinne & Stewart [119]. We apply the Z4 extension to the (2+1)+1 formalism presented in chapter 3 (section 6.1). The evolution system is completed by dynamical gauge conditions that generalize harmonic gauge (section 6.2). We cast the system in first-order form (section 6.3) and analyze its hyperbolicity (section 6.4). The characteristic variables and speeds are worked out explicitly. Particular emphasis is placed on the treatment of the coordinate singularity on the axis (section 6.5). By a judicious choice of new dependent variables we can write our first-order strongly hyperbolic system in a form where each and every term is manifestly regular on axis. Some exact solutions are used to check the equations using a programme written in the computer algebra language REDUCE (section 6.6). This programme was also used to generate functions written in C for the numerical evolution.

6.1 The Z4 extension of the (2+1)+1 formalism

Bona et al. [23] suggested adding a covariant term $\nabla_{(\alpha}Z_{\beta)}$ to the Einstein equations,

$$R_{\alpha\beta} + 2\nabla_{(\alpha}Z_{\beta)} = \kappa\left(T_{\alpha\beta} - \tfrac{1}{2}Tg_{\alpha\beta}\right) . \tag{6.1}$$

Clearly this reduces to the Einstein equations if and only if $Z_\alpha = 0$.[1] For the extended equations to be axisymmetric, Z_α has to share the axisymmetry,

$$\mathcal{L}_\xi Z_\alpha = 0 . \tag{6.2}$$

We would now like to apply the (2+1)+1 formalism directly to (6.1) rather than to the original Einstein equations. To do this, it is convenient to rewrite (6.1) as Einstein's equations

$$G_{\alpha\beta} = \kappa\widetilde{T}_{\alpha\beta} \tag{6.3}$$

with a modified energy-momentum tensor

$$\widetilde{T}_{\alpha\beta} = T_{\alpha\beta} - \tfrac{2}{\kappa}\left(\nabla_{(\alpha}Z_{\beta)} - \tfrac{1}{2}g_{\alpha\beta}\nabla_\gamma Z^\gamma\right) . \tag{6.4}$$

We then compute the (2+1)+1 matter variables corresponding to (6.4) and insert them into the (2+1)+1 equations (3.50–3.59).

First, we decompose Z_α with respect to the Killing vector ξ^α (Geroch decomposition),

$$Z_\alpha = \hat{Z}_\alpha + \xi_\alpha Z^\varphi , \tag{6.5}$$

where we have defined

$$\hat{Z}_\alpha \equiv h_\alpha{}^\beta Z_\beta \tag{6.6}$$

[1] Strictly speaking, it is sufficient if Z_α is Killing, but from a numerical point of view that is a very special case.

and

$$Z^{\varphi} \equiv \lambda^{-2}\xi^{\alpha}Z_{\alpha}\,. \tag{6.7}$$

The projections of

$$X_{\alpha\beta} \equiv \nabla_{(\alpha}Z_{\beta)} \tag{6.8}$$

are found to be

$$\begin{aligned} X_{\xi\xi} &= \lambda\lambda_a\hat{Z}^a\,, && (6.9)\\ X_{\xi a} &= \tfrac{1}{2}\epsilon_{abc}\hat{Z}^b\omega^c + \tfrac{1}{2}\lambda^2 Z^{\varphi}{}_{,a}\,, && (6.10)\\ X_{ab} &= D_{(a}\hat{Z}_{b)}\,. && (6.11) \end{aligned}$$

Using this, we can easily compute the modified matter variables (3.16) corresponding to (6.4),

$$\begin{aligned} \tilde{\tau} &= \tau - \kappa^{-1}(\lambda^{-1}\lambda_a Z^a - D_a Z^a) && (6.12)\\ \tilde{\tau}_a &= \tau_a - \kappa^{-1}(\lambda^{-3}\epsilon_{abc}Z^b\omega^c + Z^{\varphi}{}_{,a}) && (6.13)\\ \tilde{\tau}_{ab} &= \tau_{ab} - \kappa^{-1}\left[2D_{(a}Z_{b)} - (\lambda^{-1}\lambda_c Z^c + D_c Z^c)h_{ab}\right]\,. && (6.14) \end{aligned}$$

Here and in the following, we leave out the hat in $\hat{Z}_a$ (there should be no ambiguity because it carries a Latin index).

Next, we decompose Z_a with respect to the timelike normal n_a (ADM decomposition),

$$Z_a = \hat{\hat{Z}}_a + n_a\theta\,, \tag{6.15}$$

where we have defined

$$\theta \equiv -n^a Z_a \tag{6.16}$$

and

$$\hat{\hat{Z}}_a \equiv H_a{}^b Z_b\,. \tag{6.17}$$

The projections of

$$X_{ab} \equiv D_{(a}Z_{b)} \tag{6.18}$$

are found to be

$$X_{nn} = -\alpha^{-1}\alpha_A\hat{\hat{Z}}^A - \mathcal{L}_n\theta\,, \tag{6.19}$$

$$X_{nA} = \tfrac{1}{2}\mathcal{L}_n\hat{\hat{Z}}_A + \chi_{AB}\hat{\hat{Z}}^B + \tfrac{1}{2}\alpha^{-1}\alpha_A\theta - \tfrac{1}{2}\theta_A\,, \tag{6.20}$$

$$X_{AB} = d_{(A}\hat{\hat{Z}}_{B)} - \chi_{AB}\theta\,. \tag{6.21}$$

Further identities we need are

$$\lambda_a Z^a = \lambda_A\hat{\hat{Z}}^A - \lambda K_\varphi{}^\varphi\theta\,, \tag{6.22}$$

$$n^a\epsilon_{abc}Z^b\omega^c = \lambda^3 E^A\hat{\hat{Z}}_A\,, \tag{6.23}$$

$$H^a{}_A\epsilon_{abc}Z^b\omega^c = \lambda^3 B^\varphi\epsilon_{AB}\hat{\hat{Z}}^B - \lambda^3 E_A\theta\,, \tag{6.24}$$

where the definitions of $K_\varphi{}^\varphi$ (3.46), E^A (3.47) and B^φ (3.48) have been used. The modified (2+1)+1 matter variables (3.49) are then computed as

$$\widetilde{\tau} = \tau + \kappa^{-1}\left[\mathcal{L}_n\theta + Z^A{}_{||A} + (A_A - L_A)Z^A + (K_\varphi{}^\varphi - \chi)\theta\right]\,, \tag{6.25}$$

$$\widetilde{S}_A = S_A + \kappa^{-1}\left[-Z^\varphi{}_{,A} + B^\varphi\epsilon_{AB}Z^B + E_A\theta\right]\,, \tag{6.26}$$

$$\widetilde{J}^\varphi = J^\varphi + \kappa^{-1}\left[\mathcal{L}_n Z^\varphi + E^A Z_A\right]\,, \tag{6.27}$$

$$\widetilde{S}_{AB} = S_{AB} + \kappa^{-1}\big[-2Z_{(A||B)} + 2\chi_{AB}\theta + H_{AB}\left\{\mathcal{L}_n\theta + Z^C{}_{||C} + (A_C + L_C)Z^C - (\chi + K_\varphi{}^\varphi)\theta\right\}\big]\,, \tag{6.28}$$

$$\widetilde{J}_A = J_A + \kappa^{-1}\left[\mathcal{L}_n Z_A - \theta_{,A} + 2\chi_{AB}Z^B + A_A\theta\right]\,, \tag{6.29}$$

$$\widetilde{\rho}_H = \rho_H + \kappa^{-1}\left[\mathcal{L}_n\theta - Z^A{}_{||A} + (A_A - L_A)Z^A + (\chi + K_\varphi{}^\varphi)\theta\right] \tag{6.30}$$

where we again leave out the double hat in $\hat{\hat{Z}}_A$.

Inserting the modified matter variables into the (2+1)+1 equations, we arrive at what we call the *Z(2+1)+1 equations*. The constraints (3.50–3.52) are turned into evolution equations for the Z vector,

$$\mathcal{L}_n\theta = \mathcal{C} + (\lambda^{-1}\lambda_A - \alpha^{-1}\alpha_A)Z^A + Z^A{}_{||A} - (\chi + K_\varphi{}^\varphi)\theta\,, \tag{6.31}$$

$$\mathcal{L}_n Z_A = \mathcal{C}_A - 2\chi_{AB}Z^B - \alpha^{-1}\alpha_A\theta + \theta_{,A}\,, \tag{6.32}$$

$$\mathcal{L}_n Z^\varphi = \mathcal{C}_\varphi - E^A Z_A\,. \tag{6.33}$$

We see from (6.31–6.33) that if the Z vector vanishes at all times, then $\mathcal{C}, \mathcal{C}_A$ and $\mathcal{C}_\varphi$ also vanish at all times. In this sense, the original constraints $\mathcal{C} = \mathcal{C}_A = \mathcal{C}_\varphi = 0$, which involve derivatives of the metric and extrinsic curvature, are replaced with the purely *algebraic* constraints $\theta = Z_A = Z^\varphi = 0$.

The evolution equations are modified in the following way:

$$\mathcal{L}_n \chi_{AB} = \ldots + 2Z_{(A||B)} - 2\chi_{AB}\theta \,, \tag{6.34}$$

$$\mathcal{L}_n K_\varphi{}^\varphi = \ldots + 2L_A Z^A - 2K_\varphi{}^\varphi \theta \,, \tag{6.35}$$

$$\mathcal{L}_n E^A = \ldots + 2Z^{\varphi,A} - 2E^A\theta - 2B^\varphi \epsilon^{AB} Z_B \,, \tag{6.36}$$

where $\ldots$ denote the right-hand-sides of (3.56), (3.57) and (3.58), respectively. The remaining evolution equations are unchanged. Thus terms homogeneous in the constraints are added to the evolution equations, a feature common to many hyperbolic reductions of the Einstein equations. Here it occurs in a completely natural way – there is no need to add the constraints "by hand".

6.2 Dynamical gauge conditions

To complete our evolution formalism, we need to prescribe the gauge variables α and β^A. Since we are aiming for a completely hyperbolic system, we would like to impose a hyperbolic gauge condition as well. The prototype of such a condition is *harmonic gauge*, which can be derived as follows. The principal part of the Einstein equations can be written as [44, 53]

$$-g^{\gamma\delta} g_{\alpha\beta,\gamma\delta} + 2\Gamma_{(\alpha,\beta)} \simeq 0 \,, \tag{6.37}$$

where we have defined

$$\Gamma_\alpha \equiv \Gamma_{\alpha\gamma}{}^\gamma \equiv g_{\alpha\delta} g^{\beta\gamma} \Gamma^\delta{}_{\beta\gamma} \tag{6.38}$$

and $\simeq$ denotes equality to principal parts. If we now adopt the harmonic gauge condition

$$g^{\gamma\delta}x^{\alpha}{}_{;\gamma\delta} = -\Gamma^{\alpha} = 0\,, \tag{6.39}$$

where the coordinates x^{α} are to be treated as scalar fields, the Einstein equations reduce to a wave equation for the metric,

$$g^{\gamma\delta}g_{\alpha\beta,\gamma\delta} \simeq 0\,. \tag{6.40}$$

This system of PDEs is clearly *symmetric hyperbolic* (section 6.4), a property used by Bruhat [34] in the first well-posedness theorem for the initial-value problem of the Einstein equations.

The principal part of the Z4-Einstein equations (6.1) takes the form

$$-g^{\gamma\delta}g_{\alpha\beta,\gamma\delta} + 2\Gamma_{(\alpha,\beta)} + 4Z_{(\alpha,\beta)} \simeq 0\,. \tag{6.41}$$

In order to retain (6.40), we have to replace (6.39) with

$$g^{\gamma\delta}x^{\alpha}{}_{;\gamma\delta} = -\Gamma^{\alpha} = 2Z^{\alpha}\,. \tag{6.42}$$

This condition can be translated into (2+1)+1 language by going through the Geroch and ADM decompositions as in chapter 3. We arrive at the following evolution equations for the lapse and shift:

$$\begin{aligned} \eth_t\alpha &= -\alpha^2(\chi + K_{\varphi}{}^{\varphi} - 2\theta)\,, & (6.43)\\ \eth_t\beta^A &= -\alpha^2(\partial^A \ln(\alpha\lambda\sqrt{H}) + \partial_B H^{AB} - 2Z^A)\,, & (6.44) \end{aligned}$$

where here and in the following we set

$$\eth_t \equiv \partial_t - \beta^B\partial_B\,. \tag{6.45}$$

Bona et al. [24, 27] have generalized (the 3+1 analogue of) these conditions by inserting some free constant parameters f, m, μ, d and a,

$$\begin{aligned} \partial_t \alpha &= -\alpha^2 \left[f(\chi + K_\varphi{}^\varphi - m\theta) \right] , \qquad (6.46) \\ \partial_t \beta^A &= -\alpha^2 \Big[2\mu \left(\partial^A \ln(\lambda\sqrt{H}) + \tfrac{1}{2} \partial_B H^{AB} - Z^A \right) \\ &\qquad -d\partial^A \ln(\lambda\sqrt{H}) + a\partial^A \ln\alpha \Big] . \qquad (6.47) \end{aligned}$$

Clearly, we recover the original harmonic gauge conditions (6.43–6.44) if we set $f = \mu = d = a = 1$ and $m = 2$.

For even more generality, one could add to the right-hand-side of (6.42) an arbitrary *gauge source function* G^μ, which may depend on the coordinates and the metric but not on its derivatives, so that the principal parts of the Einstein equations are unaffected. Such a modification corresponds to adding

$$\begin{aligned} \partial_t \alpha &= \ldots - \alpha^2 G^0 , \\ \partial_t \beta^A &= \ldots - \alpha^2 G^A \qquad (6.48) \end{aligned}$$

in (6.46–6.47), where

$$\begin{aligned} G^0 &= G^0(x^A, H_{AB}, \lambda, \alpha, \beta^A) , \\ G^A &= G^A(x^A, H_{AB}, \lambda, \alpha, \beta^A) . \qquad (6.49) \end{aligned}$$

Such gauge source functions were first introduced by Friedrich [57] and have recently been applied to numerical relativity [61, 112]. Here we argue that they are particularly important in the context of axisymmetry: notice that the r-component of the right-hand-side of (6.47) is singular on the axis because $\lambda = O(r)$ there and so $\partial^r \ln\lambda = O(r^{-1})$. One might hope that by choosing the gauge source function G^r appropriately, one might be able to cancel the offending term. We will see in section 6.5 that this is indeed possible.

As an alternative to (6.47), one could choose the shift vector to vanish,

$$\beta^A = 0\,, \tag{6.50}$$

and this is the choice we made in [119]. More generally, one could set β^A to some arbitrary but fixed functions.

In both cases, we apply the harmonic slicing condition (6.46). Harmonic slicing has been shown to have similar singularity avoidance properties as maximal slicing [26]. It has been successfully used in stable evolutions of black hole spacetimes [9]. Claims have been made [4] that for $f \neq 1$ in (6.46), coordinate pathologies might arise. Another reason for choosing $f = 1$ is the symmetric hyperbolicity of the system in the zero-shift case (section 6.4).

6.3 First-order reduction

The Z(2+1)+1 equations (6.31–6.36, 3.54–3.55, 3.59), supplemented with the dynamical gauge conditions (6.46–6.47), form a system of pure evolution equations. They contain only first-order time derivatives but up to second-order spatial derivatives. Whilst methods for analyzing the hyperbolicity of such second-order systems have recently been developed (e.g., [103, 71, 72]), the most straightforward way is to perform a reduction to a set of evolution equations that are first-order in space and time.

To eliminate the second-order spatial derivatives, we introduce new variables for the first-order spatial derivatives of the metric and gauge:

$$D_{ABC} \equiv \tfrac{1}{2}\partial_A H_{BC}\,, \tag{6.51}$$

$$L_A \equiv \lambda^{-1}\partial_A \lambda\,, \tag{6.52}$$

$$A_A \equiv \alpha^{-1}\partial_A \alpha\,, \tag{6.53}$$

$$B_A{}^B \equiv \alpha^{-1}\partial_A \beta^B\,. \tag{6.54}$$

Evolution equations for these can be obtained from (3.54–3.55) and (6.46–6.47) by commuting space and time derivatives[2],

$$\partial_t D_{ABC} = \tfrac{1}{2}(\partial_t H_{AB})_{,C} \quad \text{etc.} \tag{6.55}$$

and noting that $\mathcal{L}_n = \alpha^{-1}(\partial_t - \mathcal{L}_\beta)$. Indices are raised and lowered with the 2-metric H_{AB} (formally, for D_{ABC} and $B_A{}^B$ are not tensors). The two independent traces of D_{ABC} are denoted by

$$D^{\mathrm{I}}{}_A \equiv D_{AB}{}^B\,, \qquad D^{\mathrm{II}}{}_A \equiv D^B{}_{BA}\,.$$

A crucial step for obtaining a hyperbolic system is the reduction of the Ricci tensor. We use the De Donder–Fock decomposition [44, 53]

$$\begin{aligned} {}^{(2)}R_{AB} \;=\; & -D^C{}_{AB,C} + 2D^{\mathrm{II}}{}_{(A,B)} - D^{\mathrm{I}}{}_{(A,B)} \\ & -2D_{CAB}D^{\mathrm{II}\,C} - \Gamma_{CAB}(2D^{\mathrm{II}\,C} - D^{\mathrm{I}\,C}) \\ & +4D_{CDA}D^{CD}{}_B - \Gamma_{ACD}\Gamma_B{}^{CD}\,, \end{aligned} \tag{6.56}$$

where of course the Christoffel symbols are given by

$$\Gamma_{ABC} = D_{CAB} + D_{BCA} - D_{ABC}. \tag{6.57}$$

A different possibility would be the standard Ricci decomposition

$${}^{(2)}R_{AB} = \Gamma^C{}_{AB,C} - \Gamma^C{}_{CB,A} + \Gamma^D{}_{DC}\Gamma^C{}_{AB} - \Gamma^C{}_{DA}\Gamma^D{}_{CB} \tag{6.58}$$

or linear combinations of the two [24], but only the choice (6.56) leads to a symmetric hyperbolic system for $f = 1$ (section 6.4).

It is now straightforward to write the Z(2+1)+1 equations in *conservation form* with sources,

$$\mathbf{u}_{,t} + \left[-\beta^D \mathbf{u} + \alpha \mathcal{F}^D(\mathbf{u})\right]_{,D} = \alpha \mathcal{S}(\mathbf{u})\,. \tag{6.59}$$

[2]There is an ordering ambiguity for the second-order spatial derivatives on the right-hand-side of the evolution equations for the first-order variables. We always use the ordering that produces an advection term along the shift, equation (6.59).

Here, $\mathbf{u}$ is the vector of *conserved variables*,

$$\begin{aligned}\mathbf{u} &= (H_{AB}, \lambda, \alpha, \beta^A, D_{ABC}, L_A, A_A, B_A{}^B, \chi_{AB}, K_\varphi{}^\varphi, E^A, B^\varphi, \\ &\quad \theta, Z_A, Z^\varphi)^T . \end{aligned} \tag{6.60}$$

(These variables do *not* have any physical interpretation as conserved quantities such as mass, angular momentum etc.) $\mathcal{F}^D(\mathbf{u})$ are *flux vectors*, whose components are given by

$$\mathcal{F}^D{}_{H_{AB}} = 0 , \tag{6.61}$$

$$\mathcal{F}^D{}_{\lambda} = 0 , \tag{6.62}$$

$$\mathcal{F}^D{}_{\alpha} = 0 , \tag{6.63}$$

$$\mathcal{F}^D{}_{\beta^A} = 0 , \tag{6.64}$$

$$\mathcal{F}^D{}_{D_{ABC}} = \delta_A{}^D(\chi_{BC} - 2B_{(BC)}) , \tag{6.65}$$

$$\mathcal{F}^D{}_{L_A} = \delta_A{}^D K_\varphi{}^\varphi , \tag{6.66}$$

$$\mathcal{F}^D{}_{A_A} = \delta_A{}^D f(\chi + K_\varphi{}^\varphi - m\theta) , \tag{6.67}$$

$$\begin{aligned}\mathcal{F}^D{}_{B_A{}^B} &= \tfrac{1}{2}\delta_A{}^D \left[2\mu(L^B + D^{\mathrm{I}\,B} - D^{\mathrm{II}\,B} - Z^B) - d(L^B + D^{\mathrm{I}\,B})\right. \\ &\qquad \left. + aA^B\right] ,\end{aligned} \tag{6.68}$$

$$\mathcal{F}^D{}_{\chi_{AB}} = D^D{}_{AB} - \delta_{(A}{}^D \left(2D^{\mathrm{II}}{}_{B)} + 2Z_{B)} - D^{\mathrm{I}}{}_{B)} - L_{B)} - A_{B)}\right) \tag{6.69}$$

$$\mathcal{F}^D{}_{K_\varphi{}^\varphi} = L^D , \tag{6.70}$$

$$\mathcal{F}^D{}_{E^A} = -2H^{AD}Z^\varphi - \epsilon^{AD}B^\varphi , \tag{6.71}$$

$$\mathcal{F}^D{}_{B^\varphi} = -\epsilon^{AD}E_A , \tag{6.72}$$

$$\mathcal{F}^D{}_{\theta} = D^{\mathrm{I}\,D} - D^{\mathrm{II}\,D} + L^D - Z^D , \tag{6.73}$$

$$\mathcal{F}^D{}_{Z_A} = -\chi_A{}^D + \delta_A^D(\chi + K_\varphi{}^\varphi - \theta) , \tag{6.74}$$

$$\mathcal{F}^D{}_{Z^\varphi} = -\tfrac{1}{2}E^D . \tag{6.75}$$

We have separated the common advection term along the shift vector in

(6.59) from the fluxes. Because this is a diagonal term, it does not affect the eigenvectors presented below in section 6.4 (it merely shifts the eigenvalues).

$\mathcal{S}(\mathbf{u})$ is a *source term* containing no derivatives, apart from those of the gauge source functions G^0 and G^A, but because of (6.49) those can be written as first-order variables without derivatives. The sources are given by

$$\begin{aligned}
\mathcal{S}_{H_{AB}} &= -2\chi_{AB} + 4B_{(AB)} - 2B_D{}^D H_{AB}\,, && (6.76)\\
\mathcal{S}_{\lambda} &= -\lambda K_\varphi{}^\varphi - 2B_D{}^D\lambda\,, && (6.77)\\
\mathcal{S}_{\alpha} &= -\alpha\left[f(\chi + K_\varphi{}^\varphi - m\theta) + G^0\right] - 2B_D{}^D\alpha\,, && (6.78)\\
\mathcal{S}_{\beta^A} &= -\alpha\left[2\mu(L^A + D^{\mathrm{I}\,A} - D^{\mathrm{II}\,A} - Z^A) - d(L^A + D^{\mathrm{I}\,A})\right.\\
&\qquad \left. + aA^A + G^A\right] - 2B_D{}^D\beta^A\,, && (6.79)\\
\mathcal{S}_{D_{ABC}} &= 2B_A{}^D D_{DBC} - 2B_D{}^D D_{ABC}\,, && (6.80)\\
\mathcal{S}_{L_A} &= 2B_A{}^B A_B - 2B_D{}^D L_A\,, && (6.81)\\
\mathcal{S}_{A_A} &= 2B_A{}^B L_B - G^0{}_{,A} - A_A G^0 - 2B_D{}^D A_A\,, && (6.82)\\
\mathcal{S}_{B_A{}^B} &= 2B_A{}^C B_C{}^B - 2B_D{}^D B_A{}^B + f(\chi + K_\varphi{}^\varphi - m\theta)B_A{}^B\\
&\quad -\tfrac{1}{2}A_A\left[2\mu(L^B + D^{\mathrm{I}\,B} - D^{\mathrm{II}\,B} - Z^B)\right.\\
&\qquad \left. -d(L^B + D^{\mathrm{I}\,B}) + aA^B + 2G^B\right] - \tfrac{1}{2}G^B{}_{,A}\,, && (6.83)\\
\mathcal{S}_{\chi_{AB}} &= A_{(A}\left(-2D^{\mathrm{II}}{}_{B)}D^{\mathrm{I}}{}_{B)} + L_{B)} - 2Z_{B)}\right)\\
&\quad -L_A L_B + D_{CAB}(A^C - 2D^{\mathrm{II}\,C})\\
&\quad -\Gamma_{CAB}(2Z^C + 2D^{\mathrm{II}\,C} - D^{\mathrm{I}\,C} - L^C - A^C)\\
&\quad +4D_{CDA}D^{CD}{}_B - \Gamma_{ACD}\Gamma_B{}^{CD} - 2B_D{}^D\chi_{AB} && (6.84)\\
&\quad +2(2B_{(A}{}^C - \chi_{(A}{}^C)\chi_{B)C} + \chi_{AB}(\chi + K_\varphi{}^\varphi - 2\theta)\\
&\quad -\tfrac{1}{2}\lambda^2\left[\epsilon_{AC}\epsilon_{BD}E^C E^D - H_{AB}(E_C E^C - B^{\varphi 2})\right]\\
&\quad -\kappa\left[S_{AB} + \tfrac{1}{2}H_{AB}(\rho_H - S_C{}^C - \tau)\right]\,,\\
\mathcal{S}_{K_\varphi{}^\varphi} &= L_A(2Z^A - L^A - D^{\mathrm{I}\,A}) + K_\varphi{}^\varphi(\chi + K_\varphi{}^\varphi - 2\theta)
\end{aligned}$$

$$
\begin{aligned}
& -2B_D{}^D K_\varphi{}^\varphi - \tfrac{1}{2}\lambda^2(E_A E^A + B^{\varphi 2}) && (6.85)\\
& -\tfrac{1}{2}\kappa(\rho_H - S_C{}^C + \tau)\,, \\
\mathcal{S}_{E^A} &= (4D^{\mathrm{II}\,A} - 2A^A)Z^\varphi + (\chi + 3K_\varphi{}^\varphi - 2\theta)E^A \\
& -2B_B{}^A E^B - 2B_D{}^D E^A && (6.86)\\
& +\epsilon^{AB}B^\varphi(3L_B - 2Z_B + D^{\mathrm{I}}{}_B) - 2\kappa S^A\,, \\
\mathcal{S}_{B^\varphi} &= \chi B^\varphi + \epsilon^{AB}E_A D^{\mathrm{I}}{}_B - 2B_D{}^D B^\varphi\,, && (6.87)\\
\mathcal{S}_\theta &= A_A(D^{\mathrm{I}\,A} - D^{\mathrm{II}\,A} + L^A - 2Z^A) \\
& +(L_A + D^{\mathrm{I}}{}_A)(Z^A - L^A) - \tfrac{1}{2}D^{\mathrm{I}}{}_A D^{\mathrm{I}\,A} \\
& +D_{ABC}D^{ABC} - \tfrac{1}{2}\Gamma_{ABC}\Gamma^{ABC} - 2B_D{}^D\theta && (6.88)\\
& +\tfrac{1}{2}(\chi^2 - \chi_{AB}\chi^{AB}) + \chi K_\varphi{}^\varphi - (\chi + K_\varphi{}^\varphi)\theta \\
& -\tfrac{1}{4}\lambda^2(E_A E^A + B^{\varphi 2}) - \kappa\rho_H\,, \\
\mathcal{S}_{Z_A} &= 2B_A{}^B Z_B - 2B_D{}^D Z_A + A_A(\chi + K_\varphi{}^\varphi - 2\theta) \\
& -L_A K_\varphi{}^\varphi + \chi_{AB}(D^{\mathrm{I}\,B} + L^B - 2Z^B - A^B) && (6.89)\\
& -\Gamma_{CAB}\chi^{BC} - \tfrac{1}{2}\lambda^2 B^\varphi \epsilon_{AB}E^B - \kappa J_A\,, \\
\mathcal{S}_{Z^\varphi} &= \tfrac{1}{2}E^A(D^{\mathrm{I}}{}_A + 3L_A - 2Z_A - A_A) - 2B_D{}^D Z^\varphi - \kappa J^\varphi\,. && (6.90)
\end{aligned}
$$

Note that H_{AB}, λ, α and β^A have vanishing fluxes and thus trivially propagate along the normal lines. The twist variables E^A, B^φ and Z^φ form a decoupled subsystem on the level of principal parts (i.e., fluxes). In linearized theory, it completely decouples because the twist variables enter the source terms of the remaining equations only quadratically.

6.4 Hyperbolicity

6.4.1 Generalities, well-posedness of the IVP

To investigate the hyperbolicity of the Z(2+1)+1 system, we pick a unit covector μ_A and define an orthogonal covector

$$\pi_A \equiv \epsilon_{AB}\mu^B \,, \tag{6.91}$$

so that

$$\mu_A\mu^A = \pi_A\pi^A = 1 \,, \qquad \mu_A\pi^A = 0 \,.$$

Thus (μ^A, π^A) form an orthonormal basis for the tangent space of the slice $\Sigma(t)$. Projection along μ and π is denoted as[3]

$$V^\perp \equiv V^A\mu_A \,, \qquad V^\parallel \equiv V^A\pi_A \,. \tag{6.92}$$

Consider the Jacobian matrix of the flux in the μ-direction,

$$J \equiv \frac{\partial \mathcal{F}^\perp}{\partial \mathbf{u}} \,. \tag{6.93}$$

A vector $\mathbf{r}$ is a *right eigenvector* of J with *eigenvalue* or *characteristic speed* λ if

$$J\mathbf{r} = \lambda\mathbf{r} \,. \tag{6.94}$$

A vector $\mathbf{l}$ is a *left eigenvector* if

$$J^T\mathbf{l} = \lambda\mathbf{l} \,. \tag{6.95}$$

Note that J^T has the same eigenvalues as J. The *characteristic variable* l corresponding to a left eigenvector $\mathbf{l}$ is defined to be $l = \mathbf{l}^T\mathbf{u}$.

[3]Here we use the opposite notation to [119] because later (chapter 8), μ will be the normal ($\perp$) to the boundary and π will be parallel ($\parallel$) to it.

The system is said to be *weakly hyperbolic* if all the eigenvalues are real, independently of the direction μ. It is *strongly hyperbolic* if in addition there exist complete sets of left and right eigenvectors (i.e., they span the space), independently of μ. Finally, it is *symmetric hyperbolic* if J is symmetrizable (i.e., there exists a symmetric positive-definite matrix H such that HJ is symmetric) with a symmetrizer H that is independent of μ. Clearly, symmetric hyperbolicity implies strong hyperbolicity, which in turn implies weak hyperbolicity, but not the other way around.

The significance of *strongly* hyperbolic systems as opposed to weakly hyperbolic ones is that at least for the case that the fluxes and sources are linear and homogeneous in the unknowns $\mathbf{u}$, they admit a well-posed Cauchy or initial value problem (IVP) in the following sense [73, 129]: for every initial data $\mathbf{f} \in C^\infty(x^A)$, $\mathbf{u}(0, x^A) = f(x^A)$, there exists a unique solution $\mathbf{u}(t, x^A) \in C^\infty(t, x^A)$ such that

$$\|\mathbf{u}(t, \cdot)\| \leqslant K \mathrm{e}^{\alpha t} \|\mathbf{f}(\cdot)\| \,, \tag{6.96}$$

where the constants K and α are independent of f, and we are using L^2 norms[4]. For nonlinear systems such as the one being considered in this chapter, one can only hope for the estimate (6.96) to hold for a finite time. This is because in the nonlinear case, characteristics might cross to form shocks (as is well-known in hydrodynamics) so that a regular solution exists only for a finite time, or the nonlinear source terms might lead to an even more severe blow-up.

The significance of *symmetric* hyperbolicity is that it implies the existence

[4]Technically, one requires the additional condition that the matrix of eigenvectors and its inverse are uniformly bounded.

of a positive-definite *energy* (which has no physical meaning in general),

$$\mathcal{E}(t) = \int_{\Sigma(t)} \mathbf{u}^T H \mathbf{u} \, \mathrm{d}^2x > 0 \,, \tag{6.97}$$

where H is the symmetrizer of the system. Suppose now that the slices $\Sigma(t)$ have a timelike boundary $\partial\Sigma$. Consider a simple linear constant-coefficient problem

$$\mathbf{u}_{,t} = A^A \partial_A \mathbf{u} \,. \tag{6.98}$$

Using the fact that the matrices HA^A are symmetric, and Gauss' theorem, we have

$$\begin{aligned} \partial_t \mathcal{E}(t) &= \int_{\Sigma(t)} 2\mathbf{u}^T H A^A \mathbf{u}_{,A} \, \mathrm{d}^2x = \int_{\Sigma(t)} \partial_A (\mathbf{u}^T H A^A \mathbf{u}) \, \mathrm{d}^2x \\ &= \int_{\partial\Sigma(t)} \mathbf{u}^T H A^\perp \mathbf{u} \, \mathrm{d}x \,, \end{aligned} \tag{6.99}$$

where $A^\perp = A^A \mu_A$ denotes the contraction of A with the normal μ to the boundary. If the boundary conditions are chosen such that the last integral in (6.99) is always non-positive, it follows that $0 \leqslant \mathcal{E}(t) \leqslant \mathcal{E}(0)$ for all $t \geq 0$. Such energy estimates are the key ingredient of well-posedness proofs for the initial boundary value problem [115, 124].

6.4.2 The dynamical shift case

We first deal with the general case in which the dynamical shift condition (6.47) is included.

The system is found to be strongly hyperbolic provided that $f > 0$, $\mu > 0$ and $d > 0$. The parameters m and a are generally unconstrained. However, the following degenerate cases require more care:

- $\underline{f = 1}$: $m = 2$ is needed for strong hyperbolicity.
- $\underline{d = 1}$: Here we must also set $\mu = 1$ and $a = 1$.

- $\underline{d = f}$: $a = 1$ is required.

For $\mu \in \{1, f, d\}$ without any further degeneracies, the remaining parameters need not be adapted.

The characteristic speeds λ and their multiplicities are

$$\begin{aligned} \lambda_0 &= 0 && (7) \\ \lambda_1^{\pm} &= \pm 1 && (2 \times 6) \\ \lambda_f^{\pm} &= \pm\sqrt{f} && (2 \times 1) \\ \lambda_\mu^{\pm} &= \pm\sqrt{\mu} && (2 \times 1) \\ \lambda_d^{\pm} &= \pm\sqrt{d} && (2 \times 1) \end{aligned} \tag{6.100}$$

Note that because of the advection term and the factor of α in the fluxes in (6.59), the actual characteristic speeds are $-\beta^{\perp} + \alpha\lambda$. For $f \leqslant 1$, $\mu \leqslant 1$ and $d \leqslant 1$, the characteristic speeds are all causal. If the equality holds, they are all "physical" (i.e., either zero or equal to the speed of light).

The characteristic variables are given by

Normal modes ($\lambda = 0$):

$$l_{0,1} = D_{\parallel\perp\perp}\,, \tag{6.101}$$

$$l_{0,2} = D_{\parallel\parallel\perp}\,, \tag{6.102}$$

$$l_{0,3} = D_{\parallel\parallel\parallel}\,, \tag{6.103}$$

$$l_{0,4} = L_{\parallel} - D_{\parallel\parallel\parallel}\,, \tag{6.104}$$

$$l_{0,5} = A_{\parallel}\,, \tag{6.105}$$

$$l_{0,6} = B_{\parallel\perp}\,, \tag{6.106}$$

$$l_{0,7} = B_{\parallel\parallel}\,, \tag{6.107}$$

along with the zeroth-order variables H_{AB}, λ, α, $\beta^{\perp}$ and $\beta^{\parallel}$.

Light cone modes ($\lambda = \pm 1$):

$$
\begin{aligned}
l^{\pm}_{1,1} &= K_{\varphi}{}^{\varphi} - \chi_{\|\|\|} + 2B_{\|\|\|} \pm (L_{\perp} - D_{\perp\|\|\|}) \,, && (6.108)\\
l^{\pm}_{1,2} &= E^{\|} \mp B^{\varphi} \,, && (6.109)\\
l^{\pm}_{1,3} &= \theta - 2B_{\|\|\|} \pm (D_{\perp\|\|\|} + L_{\perp} - D_{\|\|\|\perp} - Z_{\perp}) \,, && (6.110)\\
l^{\pm}_{1,4} &= K_{\varphi}{}^{\varphi} + \chi_{\|\|\|} - \theta \pm (D_{\|\|\|\perp} + Z_{\perp}) \,, && (6.111)\\
l^{\pm}_{1,5} &= \chi_{\perp\|} \pm \tfrac{1}{2}(A_{\|} + D_{\|\perp\perp} - D_{\|\|\|\|} + L_{\|} - 2Z_{\|}) \,, && (6.112)\\
l^{\pm}_{1,6} &= E^{\perp} \mp 2Z^{\varphi} \,. && (6.113)
\end{aligned}
$$

Lapse cone modes ($\lambda = \pm\sqrt{f}$):

$$
\begin{aligned}
l^{\pm}_{f} &= A_{\perp} - f c_1 (D_{\perp\|\|\|} + L_{\perp} - D_{\|\|\|\perp} - Z_{\perp}) \\
&\quad \pm \sqrt{f}\left[\chi_{\perp\perp} + \chi_{\|\|\|} + K_{\varphi}{}^{\varphi} - (f c_1 + 2)\,\theta + 2c_1 B_{\|\|\|}\right] \,, && (6.114)
\end{aligned}
$$

where we have set

$$
c_1 \equiv \frac{m-2}{f-1} \,. \qquad (6.115)
$$

For $(f = 1\,, m = 2)$, the undefined expression c_1 is to be replaced with an arbitrary fixed constant (e.g., 0 for simplicity).

Transverse shift cone modes ($\lambda = \pm\sqrt{\mu}$):

$$
\begin{aligned}
l^{\pm}_{\mu} &= a A_{\|} + 2\mu(L_{\|} + D_{\|\perp\perp} - D_{\perp\perp\|} - Z_{\|}) \\
&\quad - d(D_{\|\perp\perp} + D_{\|\|\|\|} + L_{\|}) \pm 2\sqrt{\mu}(B_{\perp\|} + B_{\|\perp}) \,. && (6.116)
\end{aligned}
$$

Longitudinal shift cone modes ($\lambda = \pm\sqrt{d}$):

$$\begin{aligned} l_d^{\pm} &= (fc_2+1)\,(\chi_{\perp\perp}+\chi_{\parallel\parallel}+K_\varphi{}^\varphi) \\ &\quad +(fc_2c_3+2c_4)(2B_{\parallel\parallel}-\theta)-fmc_2\theta-2(B_{\perp\perp}+B_{\parallel\parallel}) \\ &\quad \pm\sqrt{d}\,\big[D_{\perp\perp\perp}+D_{\perp\parallel\parallel}+L_\perp+c_2A_\perp \\ &\qquad -(fc_2c_3+2c_4)(L_\perp+D_{\perp\parallel\parallel}-D_{\parallel\parallel\perp}-Z_\perp)\big]\,, \end{aligned} \tag{6.117}$$

where we have set

$$c_2 \equiv \frac{a-1}{f-d}\,, \qquad c_3 \equiv \frac{m-2}{d-1}\,, \qquad c_4 \equiv \frac{\mu-1}{d-1}\,. \tag{6.118}$$

As stated above, if $f = d$ then we must have $a = 1$, and c_2 is to be replaced with an arbitrary constant. If $d = 1$, we also need $m = 2$ and $\mu = 1$, and both c_3 and c_4 are to be replaced with arbitrary constants.

The inverse transformation from characteristic to conserved variables is given by

$$\begin{aligned} D_{\perp\perp\perp} &= \tfrac{1}{2}(fc_1c_5+2c_4)(l^+_{1,3}-l^-_{1,3})-\tfrac{1}{2}(l^+_{1,3}-l^-_{1,3}+l^+_{1,4}-l^-_{1,4}) \\ &\quad -\tfrac{1}{2}c_2(l^+_f+l^-_f)+\tfrac{1}{2\sqrt{d}}(l^+_d-l^-_d)\,, && (6.119) \\ D_{\perp\perp\parallel} &= \tfrac{a-\mu}{2\mu}l_{0,5}+\tfrac{\mu-d}{2\mu}(l_{0,1}+2l_{0,3}+l_{0,4})+\tfrac{1}{2}(l^+_{1,5}-l^-_{1,5}) \\ &\quad -\tfrac{1}{4\mu}(l^+_\mu+l^-_\mu)\,, && (6.120) \\ D_{\perp\parallel\parallel} &= \tfrac{1}{4}(-l^+_{1,1}+l^-_{1,1}+l^+_{1,3}-l^-_{1,3}+l^+_{1,4}-l^-_{1,4})\,, && (6.121) \\ D_{\parallel\perp\perp} &= l_{0,1}\,, && (6.122) \\ D_{\parallel\parallel\perp} &= l_{0,2}\,, && (6.123) \\ D_{\parallel\parallel\parallel} &= l_{0,3}\,, && (6.124) \\ L_\perp &= \tfrac{1}{4}(l^+_{1,1}-l^-_{1,1}+l^+_{1,3}-l^-_{1,3}+l^+_{1,4}-l^-_{1,4})\,, && (6.125) \\ L_\parallel &= l_{0,3}+l_{0,4}\,, && (6.126) \\ A_\perp &= \tfrac{1}{2}\left(l^+_f+l^-_f\right)+\tfrac{1}{2}fc_1(l^+_{1,3}-l^-_{1,3})\,, && (6.127) \end{aligned}$$

$$A_{\|} = l_{0,5}\,, \tag{6.128}$$

$$B_{\perp\perp} = -\tfrac{1}{4}(l_d^+ + l_d^-) + \tfrac{1}{4\sqrt{f}}(fc_2+1)(l_f^+ - l_f^-) + (m-1)l_{0,7}$$
$$-\tfrac{1}{4}\left[fc_1(c_5-1) + 2(c_4-1)\right](l_{1,3}^+ + l_{1,3}^-)\,, \tag{6.129}$$

$$B_{\perp\|} = \tfrac{1}{4\sqrt{\mu}}(l_\mu^+ - l_\mu^-) - l_{0,6}\,, \tag{6.130}$$

$$B_{\|\perp} = l_{0,6}\,, \tag{6.131}$$

$$B_{\|\|} = l_{0,7}\,, \tag{6.132}$$

$$\chi_{\perp\perp} = \tfrac{1}{2}(fc_1+2)(l_{1,3}^+ + l_{1,3}^-) + \tfrac{1}{2\sqrt{f}}\left(l_f^+ - l_f^-\right)$$
$$-\tfrac{1}{2}(l_{1,3}^+ + l_{1,3}^- + l_{1,4}^+ + l_{1,4}^-) + 2(m-1)l_{0,7}\,, \tag{6.133}$$

$$\chi_{\perp\|} = \tfrac{1}{2}(l_{1,5}^+ + l_{1,5}^-)\,, \tag{6.134}$$

$$\chi_{\|\|} = \tfrac{1}{4}(-l_{1,1}^+ - l_{1,1}^- + l_{1,3}^+ + l_{1,3}^- + l_{1,4}^+ + l_{1,4}^-) + 2l_{0,7}\,, \tag{6.135}$$

$$K_\varphi{}^\varphi = \tfrac{1}{4}(l_{1,1}^+ + l_{1,1}^- + l_{1,3}^+ + l_{1,3}^- + l_{1,4}^+ + l_{1,4}^-)\,, \tag{6.136}$$

$$E^\perp = \tfrac{1}{2}(l_{1,6}^+ + l_{1,6}^-)\,, \tag{6.137}$$

$$E^\| = \tfrac{1}{2}(l_{1,2}^+ + l_{1,2}^-)\,, \tag{6.138}$$

$$B^\varphi = -\tfrac{1}{2}(l_{1,2}^+ - l_{1,2}^-)\,, \tag{6.139}$$

$$\theta = \tfrac{1}{2}(l_{1,3}^+ + l_{1,3}^-) + 2l_{0,7}\,, \tag{6.140}$$

$$Z_\perp = \tfrac{1}{2}(l_{1,4}^+ - l_{1,4}^-) - l_{0,2}\,, \tag{6.141}$$

$$Z_\| = \tfrac{1}{2}(l_{0,1} + l_{0,4} + l_{0,5}) - \tfrac{1}{2}(l_{1,5}^+ - l_{1,5}^-)\,, \tag{6.142}$$

$$Z^\varphi = -\tfrac{1}{4}(l_{1,6}^+ - l_{1,6}^-)\,, \tag{6.143}$$

where in addition we have defined

$$c_5 \equiv \frac{a-1}{d-1}\,. \tag{6.144}$$

Unfortunately, the system with a dynamical shift is never symmetric hyperbolic, not even for harmonic gauge ($f = d = \mu = a = 1$, $m = 2$). This is because the antisymmetric part of B_{AB} does not enter the fluxes (only the symmetric part appears in the flux of D_{ABC}, equation (6.65)). How-

ever, $B_{[AB]}$ itself has a nonzero flux (6.68). Hence a direction-independent symmetrizer does not exist.

6.4.3 The vanishing shift case

Next, we deal with the choice $\beta^A = 0$ for the shift vector. This is the case we considered in [119][5]. The following analysis would be unchanged if we chose β^A to be some nonzero fixed vector (except that the eigenvalues would be shifted by $\lambda \to \lambda - \alpha^{-1}\beta^A$).

The system is found to be strongly hyperbolic for all $f > 0$. The parameter m is unconstrained, expect for $f = 1$, in which case we need $m = 2$ in order to maintain strong hyperbolicity (and hence we recover harmonic slicing (6.43)) .

The characteristic speeds and multiplicities are

$$\begin{aligned} \lambda_0 &= 0 \qquad (7) \\ \lambda_1^{\pm} &= \pm 1 \qquad (2 \times 6) \\ \lambda_f^{\pm} &= \pm\sqrt{f} \quad (2 \times 1) \end{aligned} \tag{6.145}$$

The characteristic variables can readily be obtained from the dynamical shift case with the following modifications:

- Replace the normal modes $l_{0,6}$ and $l_{0,7}$ with

$$\begin{aligned} l_{0,6} &= fm(D_{\perp\parallel\parallel} + L_\perp - D_{\parallel\parallel\perp} - Z_\perp) \\ &\quad -f(D_{\perp\perp\perp} + D_{\perp\parallel\parallel} + L_\perp) + A_\perp \,, \qquad (6.146) \\ l_{0,7} &= fm(D_{\parallel\perp\perp} + L_\parallel - D_{\perp\perp\parallel} - Z_\parallel) \\ &\quad -f(D_{\parallel\perp\perp} + D_{\parallel\parallel\parallel} + L_\parallel) + A_\parallel \,. \qquad (6.147) \end{aligned}$$

[5]The definitions of the characteristic variables in [119] differ from those presented here in the ordering and by linear combinations.

Here we see very clearly how even though two normal modes ($B_{\parallel\perp}$ and $B_{\parallel\parallel}$) are lost, the system manages to remain strongly hyperbolic because two new normal modes appear.

- Set $B_{\parallel\parallel} = 0$ in $l^{\pm}_{1,1}$ and $l^{\pm}_{f}$.
- Clearly, there are no transverse and longitudinal shift modes in this case.

The inverse transformation is obtained from the dynamical shift case by making the following changes:

- Replace the expressions for $D_{\perp\perp\perp}$ and $D_{\perp\perp\parallel}$ with

$$\begin{aligned} D_{\perp\perp\perp} &= -\tfrac{1}{f} l_{0,6} + \tfrac{1}{2}(f c_1 + 2)(l^{+}_{1,3} - l^{-}_{1,3}) \\ &\quad -\tfrac{1}{2}(l^{+}_{1,3} - l^{-}_{1,3} + l^{+}_{1,4} - l^{-}_{1,4}) + \tfrac{1}{2f}\left(l^{+}_{f} + l^{-}_{f}\right) , \quad (6.148) \\ D_{\perp\perp\parallel} &= -\tfrac{1}{fm} l_{0,7} + \tfrac{(m-2)}{2m}(l_{0,1} + 2l_{0,3} + l_{0,4}) \\ &\quad -\tfrac{(fm-2)}{2fm} l_{0,2} + \tfrac{1}{2}(l^{+}_{1,5} - l^{-}_{1,5}) . \quad (6.149) \end{aligned}$$

- Discard the equations for $B_{\perp\perp}$, $B_{\perp\parallel}$, $B_{\parallel\parallel}$ and $B_{\parallel\parallel}$.
- Set $l_{0,7} = 0$ in the expressions for $\chi_{\perp\perp}$, $\chi_{\parallel\parallel}$, $K_{\varphi}{}^{\varphi}$ and θ.

The case ($f = 1$, $m = 2$) corresponding to harmonic slicing is special in that it is the only choice of parameters for which the system is symmetric hyperbolic. An explicit expression for a positive definite energy is

$$\begin{aligned}\mathcal{E} &= \chi_{AB}\chi^{AB} + \lambda_{CAB}\lambda^{CAB} \\ &\quad +(K_\varphi{}^\varphi + \chi - 2\theta)^2 + A_A A^A \\ &\quad +V_A V^A \\ &\quad +K_\varphi{}^{\varphi 2} + L_A L^A \\ &\quad +E_A E^A + B^{\varphi 2} + 4Z^{\varphi 2}\,,\end{aligned} \tag{6.150}$$

where

$$\begin{aligned}V_A &\equiv A_A + D^{\mathrm{I}}{}_A + L_A - 2D^{\mathrm{II}}{}_A - 2Z_A\,, \\ \lambda^C{}_{AB} &\equiv D^C{}_{AB} + \delta_{(A}{}^C V_{B)}\,.\end{aligned} \tag{6.151}$$

When computing the principal part of $\partial_t \mathcal{E}$, the terms in each individual line of (6.150) combine to form a total divergence as in (6.99).

6.5 Regularity on axis

The Z(2+1)+1 equations presented so far in section 6.3 turn out to be singular on the axis $r = 0$ and are thus unsuitable for numerical simulations. For instance, the term $L_r = \lambda^{-1}\lambda_{,r}$ appearing several times in the fluxes and sources is $O(r^{-1})$ for small r because $\lambda = O(r)$. We will see in this section how the regularity conditions for axisymmetric tensor fields (chapter 2) can be used to write the equations in a manifestly regular form.

6.5.1 The main regularization procedure

Let us first deal with one of the regularity conditions for 2-tensors $M_{\alpha\beta}$, which follows from (2.26),

$$\frac{M_{\varphi\varphi}}{r^2 M_{rr}} = 1 + O(r^2) \tag{6.152}$$

near the axis. For the metric $g_{\alpha\beta}$ this implies

$$\frac{\lambda^2}{r^2 H_{rr}} = \frac{g_{\varphi\varphi}}{r^2 g_{rr}} = 1 + O(r^2)\,. \tag{6.153}$$

We enforce this condition by replacing λ with a new variable s defined by

$$\lambda = r\mathrm{e}^{rs}\sqrt{H_{rr}}\,, \tag{6.154}$$

where $s = O(r)$ near the axis. Also, the logarithmic derivatives L_A of λ (6.52) are replaced by the ordinary partial derivatives s_A of s. To satisfy the corresponding regularity condition for the extrinsic curvature, we introduce a new variable Y via

$$K_\varphi{}^\varphi = \frac{\chi_{rr}}{H_{rr}} + rY \tag{6.155}$$

(note that $K_{\varphi\varphi} = \lambda^2 K_\varphi{}^\varphi$) with $Y = O(r)$ on axis. Similary for the energy-momentum tensor, we set

$$\tau = \frac{S_{rr}}{H_{rr}} + r\tilde{\tau}\,, \tag{6.156}$$

where $\tilde{\tau} = O(r)$ on axis. We remark that the definitions of the variables s, Y and $\tilde{\tau}$ can be viewed as generalizations of those in section 5.2.

The second step of the regularization procedure is concerned with the first r-derivatives of those variables u that are $O(r)$ on the axis. Consider the combination

$$(r^{-1}u)_{,r} = r^{-1}u_r - r^{-2}u\,. \tag{6.157}$$

While each term on the right-hand-side is singular on the axis, the left-hand-side shows that their difference is perfectly regular (it is $O(r)$ on the axis). If we evolve the variables u and u_r separately in a numerical code, this subtle relationship will fail to hold because of numerical errors, and the right-hand-side of (6.157) will blow up on the axis. Such combinations do occur in the

equations and so it is essential to address this problem. We enforce regularity of (6.157) by evolving instead of u_r the variable

$$\tilde{u}_r \equiv (r^{-1}u)_{,r}\,. \tag{6.158}$$

This implies the following redefinitions:

$$\begin{aligned} D_{rrz} &\rightarrow \tilde{D}_{rrz} \equiv \tfrac{1}{2}(r^{-1}H_{rz})_{,r} = r^{-1}D_{rrz} - \tfrac{1}{2}r^{-2}H_{rz}\,, \\ B_r{}^r &\rightarrow \tilde{B}_r{}^r \equiv \tfrac{1}{2}\alpha^{-1}(r^{-1}\beta^r)_{,r} = r^{-1}B_r{}^r - \tfrac{1}{2}\alpha^{-1}r^{-2}\beta^r\,, \\ s_r &\rightarrow \tilde{s}_r \equiv (r^{-1}s)_{,r} = r^{-1}s_r - r^{-2}s\,. \end{aligned} \tag{6.159}$$

6.5.2 Choice of gauge source functions

As pointed out in section 6.2, the right-hand-side of the evolution equations for the shift vector (6.47) is singular on the axis, unless the gauge source functions G^A in (6.48) are chosen appropriately. The offending term in (6.47) is

$$(2\mu - d)\partial^A \ln\lambda = (2\mu - d)L^A\,. \tag{6.160}$$

In terms of regularized variables,

$$L_A = rs_A + D_{Arr} + \delta_A{}^r(s + r^{-1})\,. \tag{6.161}$$

We can cancel the irregular term by subtracting r^{-1} from L_r. This corresponds to setting

$$G^r = -(2\mu - d)r^{-1}H^{rr} \tag{6.162}$$

in (6.48). For the remaining gauge source functions we choose

$$G^0 = G^z = 0\,. \tag{6.163}$$

Different choices of gauge source functions are of course possible. The one presented here is minimal in the sense that it precisely cancels the singular

$$H_{rr}, \underline{H_{rz}}, H_{zz}, \underline{s}, \alpha, \underline{\beta^r}, \beta^z,$$
$$\underline{D_{rrr}}, \underline{\tilde{D}_{rrz}}, \underline{D_{rzz}}, D_{zrr}, \underline{D_{zrz}}, D_{zzz}, \underline{\tilde{s}_r}, \underline{s_z}, \underline{A_r}, A_z, \underline{\tilde{B}_r{}^r}, \underline{B_r{}^z}, \underline{B_z{}^r}, B_z{}^z,$$
$$\chi_{rr}, \underline{\chi_{rz}}, \chi_{zz}, \underline{Y}, \underline{E^r}, E^z, \underline{B^\varphi}, \theta, \underline{Z_r}, Z_z, Z^\varphi,$$
$$\rho_H, \sigma, J^\varphi, \underline{J_r}, J_z,$$
$$\underline{\tilde{\tau}}, \underline{S_r}, S_z, \underline{\Sigma_r}, \Sigma_z, S_{rr}, \underline{S_{rz}}, S_{zz}.$$

Table 6.1: The regularized conserved variables $\tilde{\mathbf{u}}$ and their small-r behaviour. Underlined variables are $O(r)$ on the axis, all others are $O(1)$.

term in (6.47). We will see another application of gauge source functions in section 7.2 in the context of linearized theory.

A reasonable check for any gauge condition we choose is that Minkowski space in standard cylindrical polar coordinates is a solution. In this chart, it is given by

$$H_{AB} = \delta_{AB}\,, \qquad \lambda = r \;\Rightarrow\; s = 0\,, \qquad \alpha = 1\,, \qquad \beta^A = 0 \tag{6.164}$$

and of course $Z^A = 0$. It is easy to check that (6.48) is satisfied for the choice (6.162), but not for $G^r = 0$. Hence it it essential to include a gauge source function in order to be able to evolve flat space in standard coordinates!

6.5.3 Regularized conservation forms

It can now be verified with the help of a computer algebra programme (see appendix B) that in terms of the *regularized conserved variables* $\tilde{\mathbf{u}}$ (table 6.1), the Z(2+1)+1 equations can again be written in conservation form

$$\tilde{\mathbf{u}}_{,t} + \left[-\beta^D \tilde{\mathbf{u}} + \alpha \tilde{\mathcal{F}}^D(\tilde{\mathbf{u}})\right]_{,D} = \alpha \tilde{\mathcal{S}}(\tilde{\mathbf{u}})\,, \tag{6.165}$$

where now the fluxes $\tilde{\mathcal{F}}^D$ and sources $\tilde{\mathcal{S}}$ are regular on the axis, provided that the appropriate boundary conditions are enforced. For a variable $\underline{\tilde{u}}$ that is $O(r)$ on axis (the underlined variables in table 6.1), a Dirichlet condition

$$\underline{\tilde{u}}|_{r=0} = 0 \tag{6.166}$$

is needed, and for a variable $\tilde{u}$ that is $O(1)$ on axis (the remaining variables in table 6.1), we enforce a Neumann condition

$$\partial_r \tilde{u}|_{r=0} = 0\,. \tag{6.167}$$

This ensures that terms such as $r^{-1}\underline{\tilde{u}}$, $r^{-1}\partial_r\tilde{u}$, etc. are well-behaved on the axis. Numerically, this procedure works as long as we do not evaluate the fluxes and sources at $r = 0$. This is one of the reasons why we use a cell-centred grid (section 4.1.1), in which the centre of the innermost cell is half a grid spacing away from the axis.

In [119], the variables are further redefined by taking out the leading order of r, i.e.

$$\underline{\tilde{\tilde{u}}} \equiv r^{-1}\underline{\tilde{u}} \tag{6.168}$$

for the variables that are $O(r)$ on the axis (the remaining ones are unchanged). The equations can then be written in the form

$$\partial_t \tilde{\tilde{\mathbf{u}}} + \left[-2r^2\tilde{\tilde{\beta}}^r\tilde{\tilde{\mathbf{u}}} + \alpha\tilde{\tilde{\mathcal{F}}}^{(r^2)}(\tilde{\tilde{\mathbf{u}}})\right]_{,r^2} + \left[-\beta^z\tilde{\tilde{\mathbf{u}}} + \alpha\tilde{\tilde{\mathcal{F}}}^z(\tilde{\tilde{\mathbf{u}}})\right]_{,z} = \alpha\tilde{\tilde{\mathcal{S}}}(\tilde{\tilde{\mathbf{u}}})\,, \tag{6.169}$$

where now the fluxes $\tilde{\tilde{\mathcal{F}}}^D$ and the sources $\tilde{\tilde{\mathcal{S}}}$ are *manifestly* regular on the axis, i.e., no negative powers of r appear and they are even functions of r.

One might wonder whether one should discretize (6.169) on a grid that is uniform in r or on one that is uniform in r^2, since the derivatives are now taken with respect to r^2. On the former grid, one can enforce Neumann conditions for all the modified variables $\tilde{\tilde{\mathbf{u}}}$. On the latter grid, however, it

is not so clear what the boundary conditions should be. One might derive boundary conditions by restricting the evolution equations to $r = 0$, but those would include both time derivatives and spatial derivatives tangential and normal to the $r = 0$ boundary. An earlier attempt of Nakamura et al.[104] for a similar set of equations on an r^2 grid led to numerical instabilities on the axis, which could only be controlled by adding a large amount of artificial viscosity.

Another problem with the r^2 grid is that the characteristic speeds are non-uniform (proportional to r) because

$$\frac{\partial}{\partial(r^2)} = \frac{1}{2r}\frac{\partial}{\partial r}\,, \tag{6.170}$$

which means that a factor of $2r$ had to be taken out of the flux $\tilde{\mathcal{F}}^r$ in (6.165) in order to arrive at (6.169).

For these reasons, we choose to work on a grid that is uniform in r. Both regularized versions of the equations (6.165, 6.169) have been implemented, but at some stage we decided to focus on the first version, mainly for simplicity and because the ubiquitous factors of r^2 in the second version led to instabilities caused by the outer boundary conditions (chapter 8).

6.5.4 Hyperbolicity and the characteristic transformation

The question arises whether the regularization procedure outlined above affects the hyperbolicity of the system. This is not the case because we have merely performed a *linear* (position-dependent) transformation $\tilde{\mathbf{u}} = T\mathbf{u}$ of those variables that occur in the fluxes, namely

$$\tilde{D}_{rrz} = r^{-1} D_{rrz} + \dots , \tag{6.171}$$

$$\tilde{s}_r = r^{-2}(L_r - D_{rrr}) + \dots , \tag{6.172}$$

$$s_z = r^{-1}(L_z - D_{zrr}) , \tag{6.173}$$

$$\tilde{B}_r{}^r = r^{-1} B_r{}^r + \dots , \tag{6.174}$$

$$Y = r^{-1}(K_\varphi{}^\varphi - \frac{\chi_{rr}}{H_{rr}}) . \tag{6.175}$$

where the ellipses denote terms that have zero fluxes (and so has H_{rr} in (6.175)). Hence the characteristic structure is unchanged.

To compute the characteristic variables, one starts from the regularized variables $\tilde{\mathbf{u}}$, computes the original conserved variables $\mathbf{u}$ and evaluates the characteristic variables given in section 6.4. While this transformation is perfectly regular, the inverse transformation contains factors of r^{-1}, which might cause problems on the axis.

The transformation from characteristic variables to regularized conserved variables in the *z-direction* (i.e., $\mu_A \propto \delta_A{}^z$) turns out to be well-behaved at $r = 0$ provided that the characteristic variables have the correct leading order in r as summarized in table 6.2.[6] In turn, this small-r behaviour is manifest when expressing the characteristic variables in terms of the regularized conserved variables (using the conversions (6.171–6.175), again leaving out the lower-order terms). This is worked out explicitly in linearized theory in section 8.1.

However, the transformation from the characteristic variables in the *r-direction* (i.e., $\mu_A \propto \delta_A{}^r$) to regularized conserved variables is still singular on

[6]The basis of left eigenvectors in section 6.4 was chosen such that the regularity conditions on the characteristic variables have this simple form. For a different basis, they would involve linear combinations of characteristic variables.

$$\underline{l_{0,1}}, \overline{\underline{l_{0,2}}}, \underline{l_{0,3}}, \underline{l_{0,4}}, \underline{l_{0,5}}, \underline{l_{0,6}}, \overline{\underline{l_{0,7}}},$$
$$\overline{l^{\pm}_{1,1}}, \underline{l^{\pm}_{1,2}}, l^{\pm}_{1,3}, l^{\pm}_{1,4}, \underline{l^{\pm}_{1,5}}, l^{\pm}_{1,6},$$
$$l^{\pm}_{f}, \underline{l^{\pm}_{\mu}}, l^{\pm}_{d}\,.$$

Table 6.2: Small-r behaviour of the characteristic variables in the z-direction. Overlined variables are $O(r^2)$, underlined variables are $O(r)$ and the remaining variables are $O(1)$ on the axis.

the axis, and no simple regularity conditions on the characteristic variables as the above can cure this problem. To understand this, one should observe that unlike the characteristic variables in the z-direction, the characteristic variables in the r-direction do not have a definite r-parity (even and odd terms in r are mixed).

These results have two important numerical consequences. Firstly, numerical methods that operate in the space of characteristic variables (typically ones based on the solution of the Riemann problem[7] appear to be unusable near the axis because they require a transformation between conserved and characteristic variables *both* in the r *and* the z direction. Secondly, suppose that the computational domain has outer boundaries at $r = r_{\max}$ and $z = z_{\max}$. To set up boundary conditions, one typically only needs to transform between conserved and characteristic variables *normal* to the boundary. The $r = r_{\max}$ boundary is unproblematic because all points on it are far away from the axis at $r = 0$. At the $z = z_{\max}$ boundary, the characteristic transformation in the normal direction (i.e., the z direction) is well-behaved even near the axis, as pointed out above. Hence it should be possible to impose

[7]although there exist problems where the exact Riemann problem solution makes no reference to the characteristic structure, e.g., Euler's equations)

outer boundary conditions that respect regularity on axis. We shall see this explicitly in chapter 8.

6.6 Equation checks and code generation

We derived the regularized conservation forms (6.165) and (6.169) of the Z(2+1)+1 equations using the computer algebra language REDUCE [80]. As can be appreciated from appendix B, the resulting equations are rather lengthy. It is indispensable to perform some sort of consistency checks to make sure that they are correct. Here, we verify that the equations are satisfied for a variety of exact solutions of the field equations. We also generate C code implementing the equations directly from within REDUCE using a source code optimization package.

6.6.1 Checking the equations with exact solutions

The equations were checked with the following exact solutions, also considered in [14] for a different formulation. For all the solutions, we first computed the (2+1)+1 variables as described in chapter 3 and then the regularized conserved variables (section 6.5.3). These were then inserted directly into the regularized conservation form of the equations ((6.165) or alternatively (6.169)).

- A cylindrically symmetric Kasner metric [86]

$$\mathrm{d}s^2 = z^4(\mathrm{d}r^2 + r^2\mathrm{d}\varphi^2 + \mathrm{d}z^2) - z^{-2}\mathrm{d}t^2\,. \tag{6.176}$$

  This is a vacuum solution, it is static, and has zero twist.

- Another cylindrically symmetric Kasner metric [86]

$$\mathrm{d}s^2 = t^{\frac{4}{3}}(\mathrm{d}r^2 + r^2\mathrm{d}\varphi^2) + t^{-\frac{2}{3}}\mathrm{d}z^2 - \mathrm{d}t^2\,. \tag{6.177}$$

This is again matter- and twist-free, but not stationary.

- The JEKK metric [84, 91]

$$\mathrm{d}s^2 = -\mathrm{e}^{2(\gamma-\nu)}(\mathrm{d}t^2 - \mathrm{d}r^2) + \mathrm{e}^{2\nu}(\mathrm{d}z + \omega\mathrm{d}\varphi)^2 + r^2\mathrm{e}^{-2\nu}\mathrm{d}\varphi^2\,, \quad (6.178)$$

which is a cylindrically symmetric vacuum solution, with γ, ν and ω depending only on t and r. It has nonzero twist for $\omega \neq 0$ (for $\omega = 0$, it reduces to the Einstein-Rosen waves [140]). It is a solution of the Einstein equations if and only if

$$\begin{aligned}
\nu_{,tt} - r^{-1}\nu_{,r} - \nu_{,rr} &= \tfrac{1}{2}r^{-2}\mathrm{e}^{4\nu}\left({\omega_{,t}}^2 - {\omega_{,r}}^2\right)\,, & (6.179)\\
\omega_{,tt} + r^{-1}\omega_{,r} - \omega_{,rr} &= 4(\omega_{,r}\nu_{,r} - \omega_{,t}\nu_{,t}\,, & (6.180)\\
\gamma_{,r} &= r\left({\nu_{,t}}^2 + {\nu_{,r}}^2\right) \\
&\quad + \tfrac{1}{4}r^{-1}\mathrm{e}^{4\nu}\left({\omega_{,t}}^2 + {\omega_{,r}}^2\right)\,, & (6.181)\\
\gamma_{,t} &= 2r\nu_{,r}\nu_{,t} + \tfrac{1}{2}r^{-1}\mathrm{e}^{4\nu}\omega_{,r}\omega_{,t}\,. & (6.182)
\end{aligned}$$

- The Robertson-Walker metric [63]

$$\mathrm{d}s^2 = -\mathrm{d}t^2 + t^{\frac{2}{3}}(\mathrm{d}r^2 + \mathrm{d}z^2 + r^2\mathrm{d}\varphi^2)\,, \quad (6.183)$$

a non-rotating perfect fluid solution for the equation of state

$$p = \rho = \tfrac{1}{3}\kappa^{-1}t^{-2} \quad (6.184)$$

four-velocity

$$u_\alpha = -{\delta_\alpha}^t \quad (6.185)$$

and number density $N^\alpha = nu^\alpha$ with

$$n \propto t^{-1}\,. \quad (6.186)$$

- The Kramer metric [92]

$$\mathrm{d}s^2 = \mathrm{e}^{a^2r^2}\left(-\mathrm{d}t^2 + \mathrm{d}r^2\right) + \mathrm{d}z^2 + r^2\mathrm{d}\varphi^2\,, \tag{6.187}$$

a non-rotating static perfect fluid solution for

$$p = \rho = \kappa^{-1}a^2\mathrm{e}^{-a^2r^2}\,, \tag{6.188}$$

$$u_\alpha = -\mathrm{e}^{\frac{1}{2}a^2r^2}\delta_\alpha{}^t\,, \tag{6.189}$$

$$n = \text{const.}\,, \tag{6.190}$$

where a is a constant.

- The Tabensky-Taub metric [131]

$$\mathrm{d}s^2 = V(-\mathrm{d}t^2 + \mathrm{d}z^2) + z(\mathrm{d}r^2 + r^2\mathrm{d}\varphi^2)\,, \tag{6.191}$$

a non-rotating static perfect fluid solution for

$$p = \rho = \tfrac{1}{2}\kappa^{-1}a^2V^{-1}\,, \tag{6.192}$$

$$u_\alpha = -V^{\frac{1}{2}}\delta_\alpha{}^t\,, \tag{6.193}$$

$$n = \text{const.}\,, \tag{6.194}$$

where

$$V = z^{-\frac{1}{2}}\mathrm{e}^{-\frac{1}{2}a^2z^2} \tag{6.195}$$

and a is a constant.

- The solution given in equation (6.1) (taking $A = 1$) of Davidson [43],

$$\begin{aligned}\mathrm{d}s^2 &= -(1+r^2)\mathrm{d}t^2 + (1+r^2)^{\frac{1}{3}}\mathrm{d}r^2 + (1+r^2)^{-\frac{2}{3}}\mathrm{d}z^2 \\ &\quad + r^2(1 - \tfrac{5}{3}r^2 - \tfrac{8}{3}r^4)\mathrm{d}\varphi^2 - 2\sqrt{\tfrac{11}{3}}r^2(1+r^2)\mathrm{d}t\mathrm{d}\varphi\,,\end{aligned} \tag{6.196}$$

a rotating perfect fluid solution for

$$p = \tfrac{3}{5}\rho = 4\kappa^{-1}(1+r^2)^{-\frac{4}{3}}\,, \tag{6.197}$$

$$u^\alpha = (1+r^2)^{-\frac{1}{2}}\delta_t{}^\alpha\,, \tag{6.198}$$

$$n = \text{const.} \tag{6.199}$$

In addition, it was verified that the equations are satisfied by the solutions presented in chapter 7 in linearized theory.

6.6.2 Code generation

Since the equations that we would like to implement are very long, it is highly desirable to produce code directly from the computer algebra programme used to derive the equations. This is provided for REDUCE by the Source Code Optimization PackagE SCOPE [138], which in addition minimizes the number of algebraic operations in the output. We used SCOPE's straightforward `OPTIMIZE` command. A combination with the automatic code GENerator and TRANslator package GENTRAN [64], also described in [138], failed for very long expressions.

To make sure that the implementation is correct, we chose random data for all the variables and verified that the fluxes and sources computed with the C code agree with those computed within REDUCE.

Chapter 7

A test problem in linearized theory

To check that the implementation of the Z(2+1)+1 system is correct, it is highly desirable to have an exact solution which the numerical approximation can be compared with. In this thesis, we are mainly interested in asymptotically flat radiative vacuum spacetimes. Not many exact solutions of the fully nonlinear Einstein equations with those properties are known. The cylindrically symmetric Einstein-Rosen waves mentioned in section 6.6 as a special case of the JEKK solution are not asymptotically flat. In fact, as shown by Bičák and Schmidt [21], the only isometry in addition to axisymmetry admitting gravitational radiation and asymptotical flatness is boost symmetry. Examples of such boost-rotation-symmetric solutions can be found in [22].

Here, we take a different approach: we focus on axisymmetric gravitational wave solutions of the *linearized* field equations. We begin by writing out the linearized Z(2+1)+1 equations in terms of the regularized variables (section 7.1), which also serves as another illustration of regularity on axis. Next we discuss the transverse-traceless gauge and its compatibility with the

dynamical gauge conditions used in the Z(2+1)+1 system (section 7.2). The linearized quadrupole solution of Teukolsky [132] is then presented and the corresponding Z(2+1)+1 variables are computed (section 7.3). In addition, we derive an even-parity twisting octupole solution (section 7.4). Some features of the numerical implementation are described and convergence of the numerical solution to the exact one is demonstrated, both for vanishing and dynamical shift vector (section 7.5).

7.1 The linearized Z(2+1)+1 equations

We express the linearized Z(2+1)+1 equations in terms of the regularized variables (table 6.1). All variables u are linearized about their flat-space values u_0,

$$u = u_0 + \epsilon(\hat{u} - u_0)\,, \qquad \epsilon \ll 1\,, \tag{7.1}$$

and we shall omit the hats in the following. For $u \in \{H_{rr}, H_{zz}, \alpha\}$ we have $u_0 = 1$, for all remaining variables $u_0 = 0$. As a shorthand, we set

$$\begin{aligned} X_0 &\equiv f(2\chi_{rr} + \chi_{zz} - m\theta + rY)\,, && (7.2)\\ X_1 &\equiv aA_r - d(2D_{rrr} + D_{rzz} + r^2\tilde{s}_r) \\ &\quad +2\mu(D_{rrr} + D_{rzz} - D_{zrz} + r^2\tilde{s}_r - Z_r)\,, && (7.3)\\ X_2 &\equiv aA_z - d(2D_{zrr} + D_{zzz} + rs_z) \\ &\quad +2\mu(-r\tilde{D}_{rrz} + 2D_{zrr} + rs_z - Z_z)\,. && (7.4) \end{aligned}$$

Written in conservation form with sources, the linearized evolution equations are given by

$$\begin{aligned} \partial_t H_{rr} &= 2(2r\tilde{B}_r{}^r + r^{-1}\beta^r - \chi_{rr})\,, && (7.5)\\ \partial_t H_{rz} &= 2(B_r{}^z + B_z{}^r - \chi_{rz})\,, && (7.6) \end{aligned}$$

$$\partial_t H_{zz} = 2(2B_z{}^z - \chi_{zz})\,, \tag{7.7}$$

$$\partial_t s = -2\tilde{B}_r{}^r - Y\,, \tag{7.8}$$

$$\partial_t \alpha = -X_0\,, \tag{7.9}$$

$$\partial_t \beta^r = -X_1 - 2(2\mu - d)s\,, \tag{7.10}$$

$$\partial_t \beta^z = -X_2 + (3\mu - d)r^{-1}H_{rz}\,, \tag{7.11}$$

$$\partial_t D_{rrr} = -\partial_r[-2r\tilde{B}_r{}^r + \chi_{rr}] + 2\tilde{B}_r{}^r\,, \tag{7.12}$$

$$\partial_t \tilde{D}_{rrz} = -\partial_r[r^{-1}(-B_r{}^z - B_z{}^r + \chi_{rz})]\,, \tag{7.13}$$

$$\partial_t D_{rzz} = -\partial_r[-2B_z{}^z + \chi_{zz}]\,, \tag{7.14}$$

$$\partial_t D_{zrr} = -\partial_z[-2r\tilde{B}_r{}^r + \chi_{rr}] + 2r^{-1}B_z{}^r\,, \tag{7.15}$$

$$\partial_t D_{zrz} = -\partial_z[-B_r{}^z - B_z{}^r + \chi_{rz}]\,, \tag{7.16}$$

$$\partial_t D_{zzz} = -\partial_z[-2B_z{}^z + \chi_{zz}]\,, \tag{7.17}$$

$$\partial_t s_r = -\partial_r[r^{-1}(2\tilde{B}_r{}^r + Y)]\,, \tag{7.18}$$

$$\partial_t s_z = -\partial_z[2\tilde{B}_r{}^r + Y]\,, \tag{7.19}$$

$$\partial_t A_r = -\partial_r X_0\,, \tag{7.20}$$

$$\partial_t A_z = -\partial_z X_0\,, \tag{7.21}$$

$$\partial_t \tilde{B}_r{}^r = -\partial_r[\tfrac{1}{2}r^{-1}X_1] + (d - 2\mu)\tilde{s}_r\,, \tag{7.22}$$

$$\partial_t B_r{}^z = -\partial_r[\tfrac{1}{2}X_2] + (3\mu - d)\tilde{D}_{rrz}\,, \tag{7.23}$$

$$\partial_t B_z{}^r = -\partial_z[\tfrac{1}{2}X_1] + (d - 2\mu)s_z\,, \tag{7.24}$$

$$\partial_t B_z{}^z = -\partial_z[\tfrac{1}{2}X_2] + (3\mu - d)r^{-1}D_{zrz}\,, \tag{7.25}$$

$$\begin{aligned}\partial_t \chi_{rr} = {} & -\partial_r[A_r + D_{rrr} + D_{rzz} - 2D_{zrz} + r^2\tilde{s}_r - 2Z_r] \\ & -\partial_z D_{zrr} + r^{-1}(-D_{rrr} - 4r^2\tilde{s}_r - 6s)\,,\end{aligned} \tag{7.26}$$

$$\begin{aligned}\partial_t \chi_{rz} = {} & -\partial_r[\tfrac{1}{2}(A_z + 2D_{zrr} - D_{zzz} + rs_z - 2Z_z)] \\ & -\partial_z[\tfrac{1}{2}(A_r + D_{rzz} + r^2\tilde{s}_r - 2Z_r)] - 2s_z\,,\end{aligned} \tag{7.27}$$

$$\partial_t \chi_{zz} = -\partial_r D_{rzz} - \partial_z[A_z - 2r\tilde{D}_{rrz} + 2D_{zrr} + rs_z - 2Z_z]$$

$$
\begin{aligned}
& +r^{-1}(-D_{rzz}+4D_{zrz})\,, && (7.28)\\
\partial_t Y &= -\partial_r[r^{-1}(-A_r-D_{rzz}+2D_{zrz}+2Z_r)]-\partial_z s_z\,, && (7.29)\\
\partial_t E^r &= -\partial_r[-2Z^\varphi]-\partial_z[-B^\varphi] && (7.30)\\
\partial_t E^z &= -\partial_r B^\varphi-\partial_z[-2Z^\varphi]-3r^{-1}B^\varphi\,, && (7.31)\\
\partial_t B^\varphi &= -\partial_r E^z-\partial_z[-E^r]\,, && (7.32)\\
\partial_t\theta &= -\partial_r[D_{rrr}+D_{rzz}-D_{zrz}+r^2\tilde{s}_r-Z_r]\\
& \quad -\partial_z[-r\tilde{D}_{rrz}+2D_{zrr}+rs_z-Z_z]\\
& \quad +r^{-1}(-D_{rrr}-D_{rzz}+3D_{zrz}-4r^2\tilde{s}_r-6s+Z_r)\,, && (7.33)\\
\partial_t Z_r &= -\partial_r[\chi_{rr}+\chi_{zz}+rY-\theta]-\partial_z[-\chi_{rz}]-Y\,, && (7.34)\\
\partial_t Z_z &= -\partial_r[-\chi_{rz}]-\partial_z[2\chi_{rr}+rY-\theta]+r^{-1}\chi_{rz}\,, && (7.35)\\
\partial_t Z^\varphi &= -\partial_r[-\tfrac{1}{2}E^r]-\partial_z[-\tfrac{1}{2}E^z]+\tfrac{3}{2}r^{-1}E^r\,. && (7.36)
\end{aligned}
$$

We have used the minimal gauge source function (6.162) to cancel the singular term in (7.10). Note that all the above equations are regular on axis provided that the appropriate boundary conditions (table 6.1) are enforced. Another point to observe is that the evolution equations for the twist variables (7.30–7.32, 7.36) decouple completely from the remaining system, as already mentioned in section 6.3.

7.2 Transverse-traceless gauge

All the linearized solutions presented in this chapter adopt the *transverse-traceless (TT) gauge*, which is described in the following, stressing its relation to other familar gauges.

As usual in linearized theory, we write the metric as

$$g_{\alpha\beta} = \eta_{\alpha\beta} + h_{\alpha\beta}\,, \tag{7.37}$$

where $\eta_{\alpha\beta}$ is the Minkowski metric and $h_{\alpha\beta}$ is a small perturbation. $h_{\alpha\beta}$ is chosen to obey the *Lorentz gauge* condition

$$h^{\alpha\beta}{}_{|\beta} - \tfrac{1}{2}\partial^{\alpha} h = 0\,. \tag{7.38}$$

Here a vertical bar denotes a covariant derivative in flat space (where we will be using polar coordinates), indices are raised with $\eta^{\alpha\beta}$, and $h \equiv h_{\gamma}{}^{\gamma}$. We recognize in (7.38) the linearized version of the harmonic gauge condition (6.39). Hence it is not surprising that in this gauge the linearized vacuum Einstein equations become a flat-space wave equation,

$$h_{\alpha\beta|\gamma}{}^{\gamma} = 0\,. \tag{7.39}$$

The Lorentz gauge condition (7.38) is invariant under infinitesimal coordinate transformations

$$x^{\alpha} \to x^{\alpha} + \zeta^{\alpha} \tag{7.40}$$

provided that

$$\zeta^{\alpha}{}_{|\gamma}{}^{\gamma} = 0\,. \tag{7.41}$$

This remaining gauge freedom can be exploited to impose the additional conditions

$$h_{0\alpha} = 0\,, \tag{7.42}$$

$$h = 0\,, \tag{7.43}$$

i.e., $h_{\alpha\beta}$ is *transverse* to the time direction and *traceless*. Equations (7.42–7.43) are actually only four conditions because once (7.42) is enforced, the

time component of (7.38) implies that h is constant in time, and we can choose the initial conditions such that $h = 0$.

The question arises whether TT gauge is compatible with the dynamical gauge conditions (section 6.2) used in the Z(2+1)+1 system. In ADM language, (7.42) implies that to linear order

$$\alpha = 1\,, \qquad \beta^A = 0\,, \tag{7.44}$$

which is also known as *geodesic gauge*. In terms of regularized Z(2+1)+1 variables, the t, r and z components of (7.38) read

$$-\tfrac{1}{2}\partial_t(2H_{rr} + H_{zz} + 2rs) = 2\chi_{rr} + \chi_{zz} + rY \;=\; 0\,, \tag{7.45}$$

$$-D_{rzz} + 2D_{zrz} - r^2\tilde{s}_r - 4s \;=\; 0\,, \tag{7.46}$$

$$-2D_{zrr} + D_{zzz} - rs_z + 2r\tilde{D}_{rrz} + 2r^{-1}H_{rz} \;=\; 0\,. \tag{7.47}$$

Let us now compare these results with the linearized dynamical gauge conditions (7.9–7.11). The evolution equation for α (7.9) is satisfied for any choice of the parameter f. The evolution equation for β^z (7.11) is consistent if and only if we choose $\mu = d = 1$. This choice of parameters is also necessary for the evolution equation for β^r (7.10) to be satisfied, but not sufficient: the right-hand-side of (7.10) still fails to vanish by a term $2s$. To cancel this term, we have to add a gauge source function

$$G^r = -2s \tag{7.48}$$

to the right-hand-side of (7.10) (in addition to the minimal one, equation (6.162)). Note that this does not affect the principal parts of the system.

We conclude that our dynamical gauge conditions are compatible with the TT gauge used for the exact solutions if either the shift vector vanishes, or it is dynamical with parameters $\mu = d = 1$ (i.e., harmonic shift), in which case we need to include a gauge source function (7.48).

7.3 Teukolsky's quadrupole solution

General solutions of equations (7.38–7.39) and (7.42–7.43) can be constructed as multipole expansions using tensor spherical harmonics [35] with "quantum numbers" L and M. Teukolsky [132] focuses on quadrupole radiation ($L = 2$), which is likely to be the strongest mode from realistic sources (see, for example, [102]). Axisymmetry implies that the azimuthal quantum number is $M = 0$ in our case.

7.3.1 The even-parity solution

First we consider the solution that is symmetric under $\theta \to \pi - \theta$, or equivalently $z \to -z$. The line element can be written in spherical polar coordinates (t, R, θ, φ) as

$$\begin{aligned} \mathrm{d}s^2 &= -\mathrm{d}t^2 + (1 + Af_{RR})\mathrm{d}R^2 + (2Bf_{R\theta})R\,\mathrm{d}R\,\mathrm{d}\theta \\ &\quad + \left(1 + C\,f^{(1)}_{\theta\theta} + A\,f^{(2)}_{\theta\theta}\right) R^2\mathrm{d}\theta^2 \\ &\quad + \left(1 + C\,f^{(1)}_{\varphi\varphi} + A\,f^{(2)}_{\varphi\varphi}\right) R^2\sin^2\theta\,\mathrm{d}\varphi^2\,. \end{aligned} \tag{7.49}$$

The functions f only depend on the polar angle θ and are given by

$$f_{RR} = 2 - 3\sin^2\theta\,, \tag{7.50}$$

$$f_{R\theta} = -3\sin\theta\cos\theta\,, \tag{7.51}$$

$$f^{(1)}_{\theta\theta} = 3\sin^2\theta\,, \tag{7.52}$$

$$f^{(2)}_{\theta\theta} = -1\,, \tag{7.53}$$

$$f^{(1)}_{\varphi\varphi} = -3\sin^2\theta\,, \tag{7.54}$$

$$f^{(2)}_{\varphi\varphi} = 3\sin^2\theta - 1\,. \tag{7.55}$$

The functions A, B and C only depend on t and R and can be expressed as

$$A = 3\left(\frac{F^{(2)}}{R^3} \pm \frac{3F^{(1)}}{R^4} + \frac{3F}{R^5}\right), \tag{7.56}$$

$$B = -\left(\pm\frac{F^{(3)}}{R^2} + \frac{3F^{(2)}}{R^3} \pm \frac{6F^{(1)}}{R^4} + \frac{6F}{R^5}\right), \tag{7.57}$$

$$C = \frac{1}{4}\left(\frac{F^{(4)}}{R} \pm \frac{2F^{(3)}}{R^2} + \frac{9F^{(2)}}{R^3} \pm \frac{21F^{(1)}}{R^4} + \frac{21F}{R^5}\right), \tag{7.58}$$

where

$$F = F(t \mp R), \qquad F^{(n)} \equiv \frac{\mathrm{d}^n F(x)}{\mathrm{d}x^n}\Big|_{x=t\mp R}. \tag{7.59}$$

The mode function F can be freely specified. The upper sign in (7.56–7.59) corresponds to an outgoing solution, the lower sign to an ingoing one. Clearly, linear combinations of outgoing and ingoing solutions are also solutions. Using a Taylor expansion of F about $R = 0$, one can show that the only linear combination that is regular at $R = 0$ is (up to an overall factor)

$$\mathbf{u}_{\mathrm{reg}} = \mathbf{u}_{\mathrm{out}} - \mathbf{u}_{\mathrm{in}}, \tag{7.60}$$

where $\mathbf{u}_{\mathrm{out}}$ and $\mathbf{u}_{\mathrm{in}}$ are out- and ingoing solutions with the *same* mode function F.

Given the line element, we can now compute the regularized Z(2+1)+1 variables. To obtain the 2-metric H_{AB}, the metric tensor has to be transformed to cylindrical polar components r, z given by

$$r = R\sin\theta, \quad z = R\cos\theta \quad \Leftrightarrow \quad R = \sqrt{r^2+z^2}, \quad \theta = \tan^{-1}\frac{r}{z}. \tag{7.61}$$

We find

$$H_{rr} = 1 - A + 3\sin^2\theta\cos^2\theta(A - 2B + C), \tag{7.62}$$

$$H_{rz} = 3\sin\theta\cos\theta[\cos^2\theta(A - B) + \sin^2\theta(B - C)], \tag{7.63}$$

$$H_{zz} = 1 + 2A + 3\sin^2\theta(C - A) - 3\sin^2\theta\cos^2\theta(A - 2B + C) \tag{7.64}$$

To compute the variable s, we use its definition

$$s = r^{-1} \ln \left(\frac{\lambda}{r\sqrt{H_{rr}}} \right) , \tag{7.65}$$

first linearize the right-hand-side and then insert the results for H_{rr} and $\lambda^2 = g_{\varphi\varphi}$, obtaining

$$s = \tfrac{3}{2} R^{-1} \sin\theta [\sin^2\theta (A - C) + 2\cos^2\theta (B - C)] . \tag{7.66}$$

The spatial derivatives of the 2-metric and the extrinsic curvature variables can be computed from their definitions and using

$$\chi_{AB} = -\tfrac{1}{2} \partial_t H_{AB} , \tag{7.67}$$

$$Y = -\partial_t s . \tag{7.68}$$

As explained in section 7.2, the gauge variables are

$$\alpha = 1 , \qquad \beta^r = \beta^z = 0 , \tag{7.69}$$

and clearly

$$\theta = Z^r = Z^z = Z^\varphi = 0 \tag{7.70}$$

for an exact solution.

The important point to observe is that the twist variables vanish for the even-parity solution,

$$E^r = E^z = B^\varphi = 0 , \tag{7.71}$$

because there are no $(R\varphi)$ and $(\theta\varphi)$ components in the line element (7.49).

As with all the solutions presented in this chapter, it has been checked with REDUCE that the above solution obeys equations (7.38–7.39) and (7.42–7.43) as well as the linearized Z(2+1)+1 equations (section 7.1).

7.3.2 The odd-parity solution

Next we consider the solution that is antisymmetric under $\theta \to \pi - \theta$. Its line element is

$$\begin{aligned} \mathrm{d}s^2 &= -\mathrm{d}t^2 + \mathrm{d}R^2 + R^2\mathrm{d}\theta^2 + R^2\sin^2\theta\mathrm{d}\varphi^2 \\ &\quad +2K d_{R\varphi} R\sin\theta\,\mathrm{d}R\,\mathrm{d}\varphi + 2L d_{\theta\varphi} R^2\sin\theta\,\mathrm{d}\theta\,\mathrm{d}\varphi\,. \end{aligned} \tag{7.72}$$

The angular functions are

$$d_{R\varphi} = -4\cos\theta\sin\theta\,, \tag{7.73}$$

$$d_{\theta\varphi} = -\sin^2\theta\,. \tag{7.74}$$

The functions K and L are given by

$$K = \frac{G^{(2)}}{R^2} \pm \frac{3G^{(1)}}{R^3} + \frac{3G}{R^4}\,, \tag{7.75}$$

$$L = \pm\frac{G^{(3)}}{R} + \frac{2G^{(2)}}{R^2} \pm \frac{3G^{(1)}}{R^3} + \frac{3G}{R^4}\,, \tag{7.76}$$

where

$$G = G(t \mp R)\,, \qquad G^{(n)} \equiv \frac{\mathrm{d}^n G(x)}{\mathrm{d}x^n}\Big|_{x=t\mp R}\,. \tag{7.77}$$

The mode function G can be freely specified. Again, the upper sign corresponds to an outgoing solution and the lower sign to an ingoing one, and superpositions of the two are also solutions. To obtain a regular solution at $R = 0$, one has to form the combination

$$\mathbf{u}_{\mathrm{reg}} = \mathbf{u}_{\mathrm{out}} - \mathbf{u}_{\mathrm{in}}\,, \tag{7.78}$$

where $\mathbf{u}_{\mathrm{out}}$ and $\mathbf{u}_{\mathrm{in}}$ are out- and ingoing solutions with the same mode function G.

In the odd-parity case, the twist variables do not vanish:

$$E^r = R^{-1}\sin\theta\cos\theta\,\partial_t(L + 4K)\,, \tag{7.79}$$

$$E^z = R^{-1}\left[-\partial_t L + \cos^2\theta\,\partial_t(L + 4K)\right]\,, \tag{7.80}$$

$$B^\varphi = -R^{-2}\sin\theta(R\,\partial_R L + 4K)\,. \tag{7.81}$$

To obtain these, one first computes the twist vector (3.6) and then uses definitions (3.47–3.48). We have checked that when expressed in cylindrical polar coordinates (t, r, z, φ), the variables (7.79–7.81) are manifestly regular on the axis $r = 0$.

The remaining Z(2+1)+1 variables are found to be trivial:

$$H_{AB} = \delta_{AB}\,, \qquad s = 0 \tag{7.82}$$

and thus

$$D_{CAB} = s_A = \chi_{AB} = Y = 0\,. \tag{7.83}$$

Hence the odd-parity solution only involves the twist geometry, whereas the even-parity solution involves the remaining variables: the two polarization states can be understood as a twisting state and a non-twisting one. This reflects a similar decoupling of the evolution equations, section 7.1.

7.4 An even-parity twisting octupole solution

The twisting solution presented in section 7.3.2 is antisymmetric under reflection about the $z = 0$ plane. However, we would like to impose reflection symmetry about $z = 0$ so that we only need to evolve the upper half of the (r, z)-plane. It would thus be interesting to find an *even*-parity solution that is purely twisting. It turns out that the even polarization state of the octupole solution ($L = 3$) has that property.

The line element can again be written in the form (7.72). However, the angular functions are different:

$$d_{R\varphi} = \sin\theta(4 - 5\sin^2\theta)\,, \tag{7.84}$$

$$d_{\theta\varphi} = \sin^2\theta\cos\theta\,. \tag{7.85}$$

The radial functions are also modified:

$$K = \pm\frac{G^{(3)}}{R^2} + \frac{6G^{(2)}}{R^3} \pm \frac{15G^{(1)}}{R^4} + \frac{15G}{R^5}\,, \tag{7.86}$$

$$L = \frac{G^{(4)}}{R} \pm \frac{5G^{(3)}}{R^2} + \frac{15G^{(2)}}{R^3} \pm \frac{30G^{(1)}}{R^4} + \frac{30G}{R^5}\,, \tag{7.87}$$

where as before

$$G = G(t \mp R)\,, \qquad G^{(n)} \equiv \frac{\mathrm{d}^n G(x)}{\mathrm{d}x^n}\Big|_{x=t\mp R}\,, \tag{7.88}$$

and a regular solution can be obtained by forming

$$\mathbf{u}_{\mathrm{reg}} = \mathbf{u}_{\mathrm{out}} - \mathbf{u}_{\mathrm{in}}\,, \tag{7.89}$$

where $\mathbf{u}_{\mathrm{out}}$ and $\mathbf{u}_{\mathrm{in}}$ are out- and ingoing solutions with the same mode function G.

The twist variables are found to be

$$E^r = R^{-1}\sin\theta(\cos^2\theta\,\partial_t(L+4K) - \sin^2\theta\,\partial_t K)\,, \tag{7.90}$$

$$E^z = R^{-1}\cos\theta(4\cos^2\theta\,\partial_t K - \sin^2\theta\,\partial_t(L+K)\,, \tag{7.91}$$

$$B^\varphi = R^{-2}\sin\theta\cos\theta(R\,\partial_R L + 10K)\,. \tag{7.92}$$

Noting the transformation (7.61), these have both the desired r and z parities (tables 6.1, and 7.1 in the following section). The remaining Z(2+1)+1 variables are trivial, as in section 7.3.2.

It is worth explaining how we derived this solution. Instead of using tensor spherical harmonics as in [132], it is easier to work directly with the twist subsystem of the linearized Z(2+1)+1 equations. One can begin by postulating the desired angular behaviour, i.e.,

$$E^r \propto \sin\theta\,, \qquad E^z \propto \cos\theta\,, \qquad B^\varphi \propto \sin\theta\cos\theta\,. \tag{7.93}$$

For the spherical polar components, this means

$$E^R \propto (4 - 5\sin^2\theta)\,, \qquad E^\theta \propto \sin\theta\cos\theta\,, \qquad B^\varphi \propto \sin\theta\cos\theta\,. \tag{7.94}$$

One now makes an ansatz of a form similar to the previously found solutions,

$$E^R = (4 - 5\sin^2\theta)\, R^{-p} \sum_{n=0}^{N} a_n^{\pm} R^n G^{(n)}(t \pm R)\,, \tag{7.95}$$

$$E^\theta = \sin\theta\cos\theta\, R^{-(p+1)} \sum_{n=0}^{N} b_n^{\pm} R^n G^{(n)}(t \pm R)\,, \tag{7.96}$$

$$B^\varphi = \sin\theta\cos\theta\, R^{-p} \sum_{n=0}^{N} c_n^{\pm} R^n G^{(n)}(t \pm R) \tag{7.97}$$

and inserts it into the spherical polar version of equations (7.30–7.32, 7.36) (with $Z^\varphi = 0$),

$$0 = E^R{}_{,t} + R^{-1} B^\varphi{}_{,\theta} + 3R^{-1}\cot\theta\, B^\varphi\,, \tag{7.98}$$

$$0 = E^\theta{}_{,t} - R^{-1} B^\varphi{}_{,R} - 3R^{-2} B^\varphi\,, \tag{7.99}$$

$$0 = E^\theta{}_{,t} - R^{-1} B^\varphi{}_{,R} - 3R^{-2} B^\varphi\,, \tag{7.100}$$

$$0 = E^R{}_{,R} + R^{-1} E^R + E^\theta{}_{,\theta} + 3(R^{-1} E^R + \cot\theta\, E^\theta)\,. \tag{7.101}$$

After some experimentation one finds that $p = 6$ and $N = 4$ are required and that the only nontrivial solution for the constants $a_n^{\pm}, b_n^{\pm}, c_n^{\pm}$ is (up to an overall factor)

$$a_n^{\pm} = (15, \mp 15, 6, \mp 1, 0)\,, \tag{7.102}$$

$$b_n^{\pm} = (30, \mp 30, 15, \mp 5, 1)\,, \tag{7.103}$$

$$c_n^{\pm} = (0, -15, \pm 15, -6, \pm 1)\,. \tag{7.104}$$

Transforming back to cylindrical polar coordinates, one arrives at (7.90–7.92).

7.5 Numerical evolutions

We are now ready to perform numerical evolutions and compare them with the exact solutions.

The initial data is taken to be that of the exact solutions at $t = 0$. The even-parity non-twisting quadrupole solution (section 7.3.1) and the even-parity twisting octupole solution (section 7.4) are considered separately. The mode functions are taken to be

$$F(x) = F_0 x \mathrm{e}^{-x^2}, \qquad G(x) = G_0 x \mathrm{e}^{-x^2}, \tag{7.105}$$

and in both cases we form a regular combination of outgoing and ingoing solutions as described in the preceding sections. Although the exact solutions are only valid in linearized theory, we evolve them using the fully nonlinear Z(2+1)+1 system. This is consistent if the amplitudes $F_0, G_0 \ll 1$ in (7.105). The amplitudes we choose are $F_0 = G_0 = 10^{-4}$.

The gauge parameters are taken to be those of harmonic gauge, $f = d = \mu = a = 1$, $m = 2$. Both vanishing and dynamical shift are considered.

We impose the appropriate Dirichlet or Neumann conditions on the axis $r = 0$ (table 6.1). Because the exact solutions we consider are reflection-symmetric about $z = 0$, we only evolve the upper half of the (r, z)-plane and impose either a Dirichlet or a Neumann condition at $z = 0$, depending on the z-parity of the variables (table 7.1). The outer boundaries are placed at $r_{\max} = z_{\max} = 5$. In this chapter, we impose the exact solution at the outer boundaries (chapter 8 is devoted entirely to general outer boundary conditions).

7.5.1 Numerical method

The equations are discretized using second-order accurate finite differencing on a single cell-centred grid that is uniform in r and z (section 4.1). The conservative form of the equations is retained on the discrete level, i.e.,

$$\partial_t \mathbf{u} = -\partial_r \mathcal{F}^r(\mathbf{u}) - \partial_z \mathcal{F}^z(\mathbf{u}) + \mathcal{S}(\mathbf{u}) \tag{7.106}$$

$$
\begin{aligned}
& H_{rr}, \underline{H_{rz}}, H_{zz}, s, \alpha, \beta^r, \underline{\beta^z}, \\
D_{rrr}, \underline{\tilde{D}_{rrz}}, D_{rzz}, \underline{D_{zrr}}, D_{zrz}, \underline{D_{zzz}}, \tilde{s}_r, \underline{s_z}, A_r, \underline{A_z}, \tilde{B_r}^r, \underline{B_r}^z, \underline{B_z}^r, B_z{}^z, & \\
& \chi_{rr}, \underline{\chi_{rz}}, \chi_{zz}, Y, E^r, \underline{E^z}, \underline{B^\varphi}, \theta, Z_r, \underline{Z_z}, Z^\varphi, \\
& J^\varphi, J_r, \underline{J_z}, \rho_H, \tilde{\tau}, S_r, \underline{S_z}, S_{rr}, \underline{S_{rz}}, S_{zz}.
\end{aligned}
$$

Table 7.1: z-parity of the regularized Z(2+1)+1 variables if reflection symmetry is assumed. Underlined variables are odd functions of z, the remaining ones are even.

is discretized as

$$
\begin{aligned}
\partial_t \mathbf{u}_{ij} &= -\tfrac{1}{2h}\left[\mathcal{F}^r(\mathbf{u})_{i+1,j} - \mathcal{F}^r(\mathbf{u})_{i-1,j} + \mathcal{F}^z(\mathbf{u})_{i,j+1} - \mathcal{F}^z(\mathbf{u})_{i,j-1}\right] \\
&\quad + \mathcal{S}(\mathbf{u})_{ij}\,. \qquad (7.107)
\end{aligned}
$$

The numerical solution is advanced in time using the method of lines with the third-order Runge-Kutta scheme (4.38b). The Courant number is taken to be $\Delta t/h = 0.8$. Fourth-order Kreiss-Oliger dissipation (4.64) with amplitude $\epsilon_D = 0.5$ is added at all interior points. The boundary conditions are implemented using the method of ghost cells (section 4.1.3). The ghosts at the outer boundaries are filled with the exact solution.

7.5.2 Snapshots of the evolution

As an example, figure 7.1 shows the variable s of the even-parity quadrupole solution (section 7.3.1) with vanishing shift at a number of consecutive times. The numerical approximation and the exact solution are overlaid. The resolution is very coarse (32 points) – for higher resolutions, the difference between the exact solution and the numerical approximation is hardly visible. Note that the numerical evolution is perfectly regular on the axis.

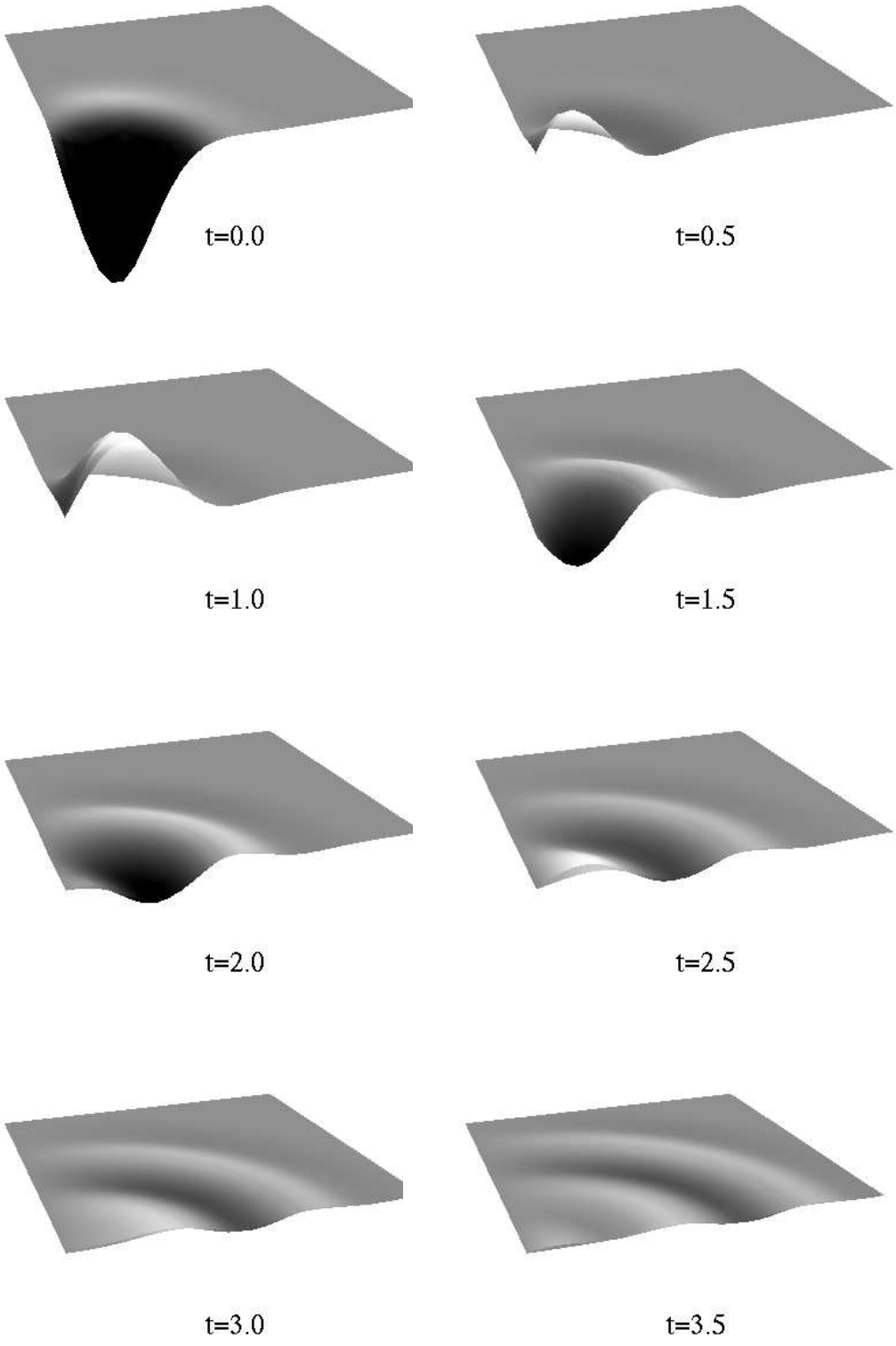

Figure 7.1: Evolution of the variable s for the even-parity quadrupole solution with vanishing shift. The numerical approximation and the exact solution are overlaid.

7.5.3 Convergence tests

An important touchstone for a numerical code is a convergence test. Because our implementation uses second-order accurate finite-differencing and at least a second-order accurate time integrator, the numerical error with respect to the exact solution should behave like $\sim h^2$, where h is the grid spacing. That is, if we double the number of points per spatial dimension, the error should decrease by a factor of 4. The following plots show for three different resolutions (32, 64 and 128 points) the total (discrete) L^2 norm of the error $\mathbf{e} = \mathbf{u} - \mathbf{u}_{\rm exact}$ as a function of time,

$$e_{L^2}(t) \equiv h \left(\sum_{ijn} e^n_{ij}(t)^2 \right)^{1/2} , \tag{7.108}$$

where the index n labels the component of the solution (all the Z(2+1)+1 variables are included), and the indices i, j refer to the grid point. Alternatively, we have tried the supremum norm

$$e_{\rm sup}(t) \equiv \max_{ijn} |e^n_{ij}(t)| , \tag{7.109}$$

which leads to the same qualitative results.

Consider first the even-parity non-twisting quadrupole solution (section 7.3.1). This was evolved both with vanishing shift (figure 7.2) and with dynamical shift (figure 7.4). Both evolutions show approximate (not perfect) second-order convergence. The average convergence factor of the vanishing shift evolution is shown in figure 7.3. In order to study the influence of the boundary location, we have performed the same run with twice the domain size. Discrepancies between the convergence factors can be observed from $t \approx 4$ onwards, when the wave is about to arrive at the boundary of the smaller domain. However, this does not lead to a significant loss of convergence at later times.

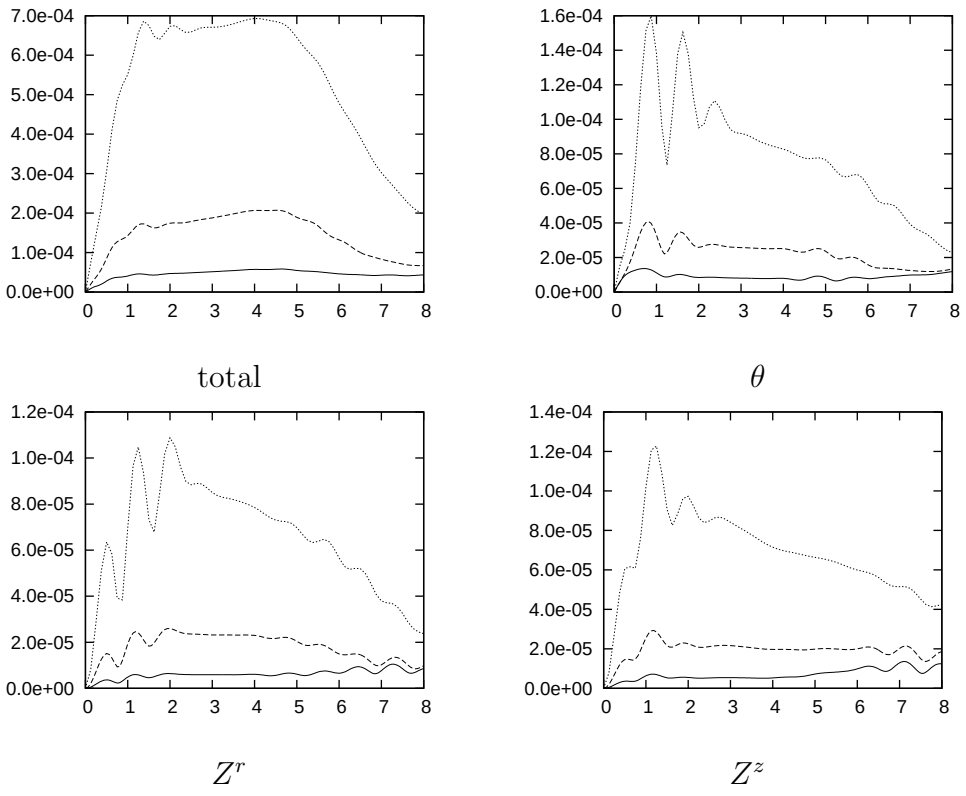

Figure 7.2: Convergence test for the even-parity quadrupole solution using vanishing shift. L^2 norm of the error as a function of time for 32 (dotted), 64 (dashed) and 128 (solid) points per dimension. The total error of all the Z(2+1)+1 variables and the components of the Z vector are shown separately.

Note that in the vanishing shift case, the error decays with time and all the variables assume (very nearly) their flat-space values after the wave has left the computational domain. In contrast, the dynamical shift evolution suffers from a growth of the error, which also affects the constraints. We have verified that the growth rates are virtually independent of the boundary location (the results for twice the domain size are visually indistinguishable from the plots in figure 7.4). It would be interesting to investigate the origin of this growth in future work.

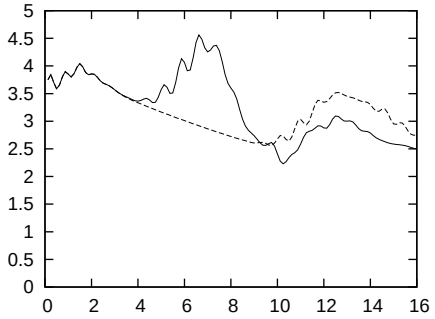

Figure 7.3: Average convergence factor of the Z(2+1)+1 variables as a function of time for the even-parity quadrupole solution using vanishing shift. Solid line: $r_{\max} = z_{\max} = 5$ as in figure 7.2, dashed line: $r_{\max} = z_{\max} = 10$.

Figure 7.5 shows a similar convergence test for the even-parity twisting octupole solution (section 7.4). Here it does not matter whether we use vanishing or dynamical shift because the right-hand-side of the evolution equations for the shift (7.10–7.11) is zero anyway. We see approximate second-order convergence up to $t \approx 3$. After this, the constraint Z^φ begins to grow. In this particular case, the onset and growth rate of the instability depend on the location of the outer boundary, as demonstrated by figure 7.6.

7.5.4 Conclusions

To summarize, we have demonstrated second-order convergence of the code (at least at early times) for two different exact solutions of linearized theory and two different shift conditions, which strongly indicates that the implementation is correct. An unexpected growth of the error occurs in the dynamical shift case.

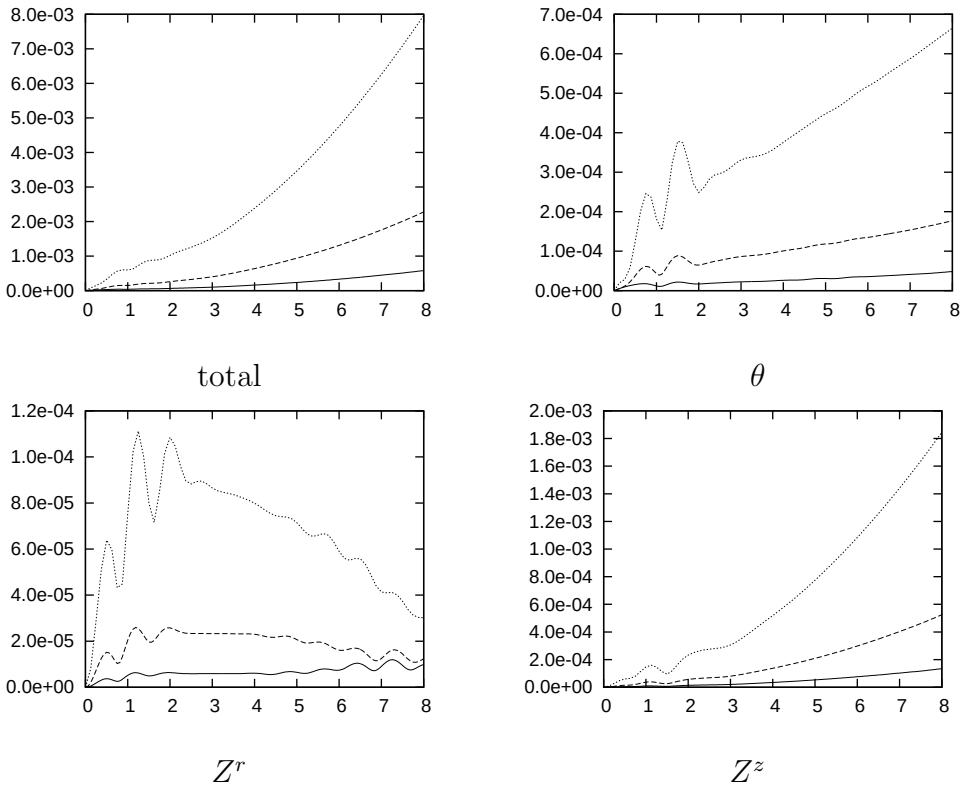

Figure 7.4: Convergence test for the even-parity quadrupole solution using dynamical shift. L^2 norm of the error as a function of time for 32 (dotted), 64 (dashed) and 128 (solid) points per dimension. The total error of all the Z(2+1)+1 variables and the components of the Z vector are shown separately.

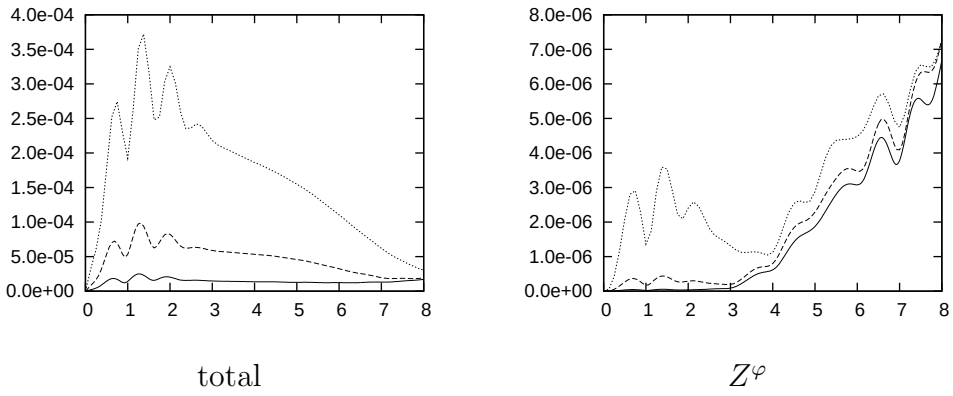

Figure 7.5: Convergence test for the even-parity octupole solution. L^2 norm of the error as a function of time for 32 (dotted), 64 (dashed) and 128 (solid) points per dimension. Total error of all the Z(2+1)+1 variables and the constraint Z^φ.

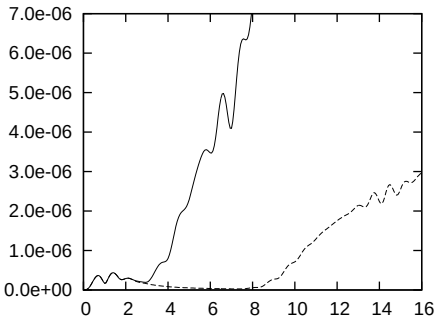

Figure 7.6: Dependence of the constraint growth on the boundary location for the even-parity octupole solution. Shown is the variable Z^φ as a function of time. Solid line: $r_{\max} = z_{\max} = 5$ as in figure 7.5, dashed line: $r_{\max} = z_{\max} = 10$. The resolution is taken to be 64 points per dimension.

Chapter 8

Outer boundary conditions

Having derived the appropriate boundary conditions on the axis $r = 0$ (table 6.1) and at $z = 0$ if reflection symmetry is assumed (table 7.1), we now turn to the question of how to impose boundary conditions at the outer boundaries of the computational domain.

Outer boundary conditions are currently a very active field of research in numerical relativity, particularly since hyperbolic formulations of the Einstein equations were introduced. In such formulations, one knows the characteristic variables and their propagation speeds with respect to the boundary, and one can use this information to construct boundary conditions.

Throughout this thesis we assume that spacetime is asymptotically flat, by which we mean in a broad sense that the metric approaches the Minkowski metric towards spacelike infinity (no precise definition of asymptotic flatness is required for our purposes). By placing the outer boundary sufficiently far out, we may assume that linearized theory is valid near the boundary. Hence all the calculations in this chapter are performed in linearized theory.

We begin by writing down the characteristic variables in terms of the regularized Z(2+1)+1 variables (section 8.1), which we shall need throughout

the following. As a first class of boundary conditions, we discuss dissipative boundary conditions (section 8.2), for which well-posedness theorems of the initial boundary value problem are known. In an alternative approach to the problem, we begin with certain physical considerations, which are then translated into a prescription for the characteristic variables. These considerations fall into three different groups: outgoing radiation boundary conditions based on the Newman-Penrose scalars (section 8.3), constraint-preserving boundary conditions based on the so-called subsidiary system (section 8.4), and gauge boundary conditions (section 8.5). Stability of the thus derived boundary conditions is analysed using the Fourier-Laplace transform technique (section 8.6). We perform numerical evolutions of the exact linearized solutions of chapter 7 to compare the various boundary conditions with regard to their stability and efficiency in avoiding spurious reflections from the outer boundaries (section 8.7).

8.1 Linearized characteristic variables

The linearized Z(2+1)+1 equations have already been expressed in terms of regularized variables in section 7.1. Here we derive the characteristic variables of that system. One starts from the results in section 6.4 and makes the replacements (6.171–6.175). Note that the terms with zero fluxes (the ellipses in (6.171–6.175)) are not to be included because they do not enter the principal parts of the regularized evolution equations. Finally we linearize the characteristic variables about flat space. We have checked explicitly with REDUCE that the results below are indeed the characteristic variables of the system stated in section 7.1.

For the characteristic variables in the r-direction we find in the dynamical shift case

$$
\begin{aligned}
l_{0,1} &= D_{zrr}\,, && (8.1)\\
l_{0,2} &= D_{zrz}\,, && (8.2)\\
l_{0,3} &= D_{zzz}\,, && (8.3)\\
l_{0,4} &= rs_z + D_{zrr} - D_{zzz}\,, && (8.4)\\
l_{0,5} &= A_z\,, && (8.5)\\
l_{0,6} &= B_z{}^r\,, && (8.6)\\
l_{0,7} &= B_z{}^z\,, && (8.7)\\
l^{\pm}_{1,1} &= rY + \chi_{rr} - \chi_{zz} + 2B_z{}^z \pm (r^2\tilde{s}_r + D_{rrr} - D_{rzz})\,, && (8.8)\\
l^{\pm}_{1,2} &= E^z \pm B^\varphi\,, && (8.9)\\
l^{\pm}_{1,3} &= \theta - 2B_z{}^z \pm (D_{rzz} + r^2\tilde{s}_r + D_{rrr} - D_{zrz} - Z_r)\,, && (8.10)\\
l^{\pm}_{1,4} &= rY + \chi_{rr} + \chi_{zz} - \theta \pm (D_{zrz} + Z_r)\,, && (8.11)\\
l^{\pm}_{1,5} &= \chi_{rz} \pm \tfrac{1}{2}(A_z + 2D_{zrr} - D_{zzz} + rs_z - 2Z_z)\,, && (8.12)\\
l^{\pm}_{1,6} &= E^r \mp 2Z^\varphi\,, && (8.13)\\
l^{\pm}_{f} &= A_r - fc_1(D_{rzz} + r^2\tilde{s}_r + D_{rrr} - D_{zrz} - Z_r)\\
&\quad \pm\sqrt{f}(2\chi_{rr} + \chi_{zz} + rY - (fc_1 + 2)\theta + 2c_1B_z{}^z)\,, && (8.14)\\
l^{\pm}_{\mu} &= aA_z + 2\mu(rs_z + 2D_{zrr} - r\tilde{D}_{rrz} - Z_z)\\
&\quad -d(2D_{zrr} + D_{zzz} + rs_z) \pm 2\sqrt{\mu}(B_r{}^z + B_z{}^r)\,, && (8.15)\\
l^{\pm}_{d} &= (fc_2 + 1)(2\chi_{rr} + \chi_{zz} + rY) + (fc_2c_3 + 2c_4)(2B_z{}^z - \theta)\\
&\quad -fmc_2\theta - 2(r\tilde{B}_r{}^r + B_z{}^z)\\
&\quad \pm\sqrt{d}[2D_{rrr} + D_{rzz} + r^2\tilde{s}_r + c_2A_r) && (8.16)\\
&\qquad -(fc_2c_3 + 2c_4)(r^2\tilde{s}_r + D_{rrr} + D_{rzz} - D_{zrz} - Z_r)]\,.
\end{aligned}
$$

In the vanishing shift case, $l_{0,6}$ and $l_{0,7}$ are replaced with

$$\begin{aligned} l_{0,6} &= fm(D_{rzz} + r^2\tilde{s}_r + D_{rrr} - D_{zrz} - Z_r) \\ &\quad -f(2D_{rrr} + D_{rzz} + r^2\tilde{s}_r) + A_r \,, \end{aligned} \tag{8.17}$$

$$\begin{aligned} l_{0,7} &= fm(2D_{zrr} + rs_z - r\tilde{D}_{rrz} - Z_z) \\ &\quad -f(2D_{zrr} + D_{zzz} + rs_z) + A_z \,. \end{aligned} \tag{8.18}$$

The characteristic variables in the z-direction for dynamical shift are found to be

$$l_{0,1} = D_{rzz} \,, \tag{8.19}$$

$$l_{0,2} = r\tilde{D}_{rrz} \,, \tag{8.20}$$

$$l_{0,3} = D_{rrr} \,, \tag{8.21}$$

$$l_{0,4} = r^2\tilde{s}_r \,, \tag{8.22}$$

$$l_{0,5} = A_r \,, \tag{8.23}$$

$$l_{0,6} = B_r{}^z \,, \tag{8.24}$$

$$l_{0,7} = r\tilde{B}_r{}^r \,, \tag{8.25}$$

$$l^{\pm}_{1,1} = r(Y + 2\tilde{B}_r{}^r \pm s_z) \,, \tag{8.26}$$

$$l^{\pm}_{1,2} = E^r \mp B^{\varphi} \,, \tag{8.27}$$

$$l^{\pm}_{1,3} = \theta - 2r\tilde{B}_r{}^r \pm (2D_{zrr} + rs_z - r\tilde{D}_{rrz} - Z_z) \,, \tag{8.28}$$

$$l^{\pm}_{1,4} = rY + 2\chi_{rr} - \theta \pm (r\tilde{D}_{rrz} + Z_z) \,, \tag{8.29}$$

$$l^{\pm}_{1,5} = \chi_{rz} \pm \tfrac{1}{2}(A_r + D_{rzz} + r^2\tilde{s}_r - 2Z_r) \,, \tag{8.30}$$

$$l^{\pm}_{1,6} = E^z \mp 2Z^{\varphi} \,, \tag{8.31}$$

$$\begin{aligned} l^{\pm}_{f} &= A_z - fc_1(2D_{zrr} + rs_z - r\tilde{D}_{rrz} - Z_z) \\ &\quad \pm\sqrt{f}(\chi_{zz} + 2\chi_{rr} + rY - (fc_1 + 2)\theta + 2c_1 r\tilde{B}_r{}^r) \,, \end{aligned} \tag{8.32}$$

$$\begin{aligned} l^{\pm}_{\mu} &= aA_r + 2\mu(r^2\tilde{s}_r + D_{rrr} + D_{rzz} - D_{zrz} - Z_r) \\ &\quad -d(D_{rzz} + 2D_{rrr} + r^2\tilde{s}_r) \pm 2\sqrt{\mu}(B_z{}^r + B_r{}^z) \,, \end{aligned} \tag{8.33}$$

$$
\begin{aligned}
l_d^{\pm} &= (fc_2+1)(\chi_{zz}+2\chi_{rr}+rY)+(fc_2c_3+2c_4)(2r\tilde{B}_r{}^r-\theta) \\
&\quad -fmc_2\theta-2(B_z{}^z+r\tilde{B}_r{}^r) \\
&\quad \pm\sqrt{d}(D_{zzz}+2D_{zrr}+rs_z+c_2A_z) \\
&\qquad -(fc_2c_3+2c_4)(rs_z+2D_{zrr}-r\tilde{D}_{rrz}-Z_z)\,.
\end{aligned} \tag{8.34}
$$

In the vanishing shift case, $l_{0,6}$ and $l_{0,7}$ are replaced with

$$
\begin{aligned}
l_{0,6} &= fm(2D_{zrr}+rs_z-r\tilde{D}_{rrz}-Z_z) \\
&\quad -f(2D_{zrr}+D_{zzz}+rs_z)+A_z\,, \qquad (8.35) \\
l_{0,7} &= fm(D_{rzz}+r^2\tilde{s}_r+D_{rrr}-D_{zrz}-Z_r) \\
&\quad -f(2D_{rrr}+D_{rzz}+r^2\tilde{s}_r)+A_r\,. \qquad (8.36)
\end{aligned}
$$

For the numerical implementation of the characteristic transformation in the z-direction, we replace $l_{0,2}$, $l_{0,4}$, the dynamical-shift version of $l_{0,7}$, and $l_{1,1}^{\pm}$ with

$$
\begin{aligned}
\tilde{l}_{0,2} &\equiv r^{-1}l_{0,2}=\tilde{D}_{rrz}\,, \qquad (8.37) \\
\tilde{l}_{0,4} &\equiv r^{-2}l_{0,4}=\tilde{s}_r\,, \qquad (8.38) \\
\tilde{l}_{0,7} &\equiv r^{-1}l_{0,7}=\tilde{B}_r{}^r\,, \qquad (8.39) \\
\tilde{l}_{1,1}^{\pm} &\equiv r^{-1}l_{1,1}^{\pm}=Y+2\tilde{B}_r{}^r\pm s_z \qquad (8.40)
\end{aligned}
$$

because then the inverse transformation from z-characteristic to regularized conserved variables does not involve any negative powers of r.

8.2 Dissipative boundary conditions

Let $\mathbf{v}^-$ be the vector of ingoing characteristic variables in the direction normal to the boundary under consideration and $\mathbf{v}^+$ the vector of the remaining

(outgoing and zero-speed) characteristic variables. In this section, we consider *(homogeneous) dissipative boundary conditions* of the form

$$\mathbf{v}^- \doteq M\mathbf{v}^+ \,, \tag{8.41}$$

where M is a constant real matrix and here and in the following $\doteq$ denotes equality on the boundary.

Under certain additional assumptions, there exist theorems that guarantee the well-posedness of the initial boundary value problem (IBVP) for such boundary conditions, which we shall outline in the following.

8.2.1 Well-posedness of the IBVP

We focus on a single boundary here and so we take the spatial domain $\Omega \subset \mathbb{R}^2$ to be a bounded open set lying on one side of its boundary Γ. Suppose we have a linear symmetric hyperbolic system

$$\partial_t \mathbf{u} + A^A \partial_A \mathbf{u} + B\mathbf{u} = 0 \,, \tag{8.42}$$

in $[0,\infty) \times \Omega$, i.e., the matrices A^A can be assumed to be symmetric (after a suitable symmetrization). The boundary conditions are taken to be of the form (8.41) on $[0,\infty) \times \Gamma$. Assume first that the boundary is *non-characteristic*, i.e. that $A^\perp \equiv A^A \mu_A$ is invertible on the entire boundary Γ, where μ_A is the boundary normal. One can prove [73] that the above initial boundary-value problem is *strongly well-posed* in the following sense: for every initial data $\mathbf{f} \in C^\infty(x^A)$, $\mathbf{u}(0, x^A) = f(x^A)$, there exists a unique solution $\mathbf{u}(t, x^A) \in C^\infty(t, x^A)$ such that

$$\|\mathbf{u}(t,\cdot)\| \leqslant K \mathrm{e}^{\alpha t} \|\mathbf{f}(\cdot)\| \,, \tag{8.43}$$

where the constants K and α are independent of f, and we are using L^2 norms (this is the same type of estimate as in section 6.4).

This result has been generalized by Majda and Osher [101] to the case of a *uniformly characteristic boundary*, which means that $A^{\perp}$ has constant (not necessarily maximal) rank across the whole boundary Γ. This wider class includes many important examples in physics such as Maxwell's equations and the linearized Einstein equations. Finally, Rauch [115] and Secchi [124] generalized the well-posedness theorem to quasilinear systems (such as the fully nonlinear Z(2+1)+1 system). In this case, however, the estimate (8.43) only holds for a finite time in general and the solution cannot be taken to be C^{∞} (instead, it lies in an appropriate Sobolev space, see [124] for details).

Since the above theorems all require a symmetric hyperbolic system, they are only applicable to the zero-shift version of the Z(2+1)+1 equations with parameters ($f = 1, m = 2$). In practice, however, dissipative boundary conditions work well for most strongly hyperbolic systems, too. We would like to stress that in the dynamical shift case, the boundary is uniformly characteristic only in linearized theory because otherwise the speed of the normal modes depends on the shift vector, which may change sign along the boundary.

8.2.2 Absorbing boundary conditions

The simplest example of dissipative boundary conditions are *absorbing boundary conditions*

$$\mathbf{v}^{-} \doteq 0\,, \tag{8.44}$$

i.e., the incoming modes are set to zero at the outer boundaries. These boundary conditions have proven to be very stable in numerical experiments (section 8.7).

One might ask to what extent absorbing boundary conditions are satisfied by the exact linearized solutions of chapter 7. Even if they are not satisfied

identically, one can still evaluate the residuals of the boundary conditions (i.e., the incoming modes) and expand them into a series in inverse powers of r (for the outer boundary at $r = r_{\max}$) or z (for the outer boundary at $z = z_{\max}$). One finds that the incoming modes vanish to leading order except for $l^{\pm}_{1,3}, l^{\pm}_{1,4}, l^{\pm}_{1,5}$ and $l^{\pm}_{1,6}$.

Can we construct "better" boundary conditions of dissipative type?

8.2.3 Zero-Z boundary conditions

A different boundary condition one might impose is the vanishing of the algebraic constraints

$$\theta \doteq Z_r \doteq Z_Z \doteq Z^{\varphi} \doteq 0\,, \tag{8.45}$$

which is clearly satisfied by a solution of Einstein's equations. Using the expressions for the characteristic variables (section 8.1), we can rewrite (8.45) in dissipative form:

$$l^{-}_{1,3} \doteq -l^{+}_{1,3} - 4l_{0,7}\,, \tag{8.46}$$

$$l^{-}_{1,4} \doteq l^{+}_{1,4} - 2l_{0,2}\,, \tag{8.47}$$

$$l^{-}_{1,5} \doteq l^{+}_{1,5} - l_{0,1} - l_{0,4} - l_{0,5}\,, \tag{8.48}$$

$$l^{-}_{1,6} \doteq l^{+}_{1,6} \tag{8.49}$$

(the equations are the same in the r- and in the z-direction). Supplemented with absorbing boundary conditions for the remaining incoming modes, we obtain a set of boundary conditions that are all satisfied by the exact solutions at least to leading order in the respective inverse coordinate. In this sense, they would appear to be superior to pure absorbing boundary conditions. However, we shall see in section 8.4 that the Z vector obeys a wave equation (8.99). The boundary conditions (8.46–8.49) are Dirichlet boundary conditions and hence any violations of the $Z_\alpha = 0$ constraints hitting

the outer boundaries will be reflected. This is confirmed by our numerical experiments in section 8.7.

8.3 Outgoing-radiation boundary conditions

We now start to look for a different set of boundary conditions based on more physical considerations. A reasonable requirement for an isolated system is that no gravitational radiation should enter the computational domain from the outside. If we were dealing with a scalar wave equation

$$\Box u = 0\,, \tag{8.50}$$

the appropriate outgoing-radiation boundary condition would be a *Sommerfeld condition*

$$u = \frac{f(t-R)}{R} \Rightarrow (\partial_t + \partial_R)(Ru) = 0\,, \tag{8.51}$$

where $R = \sqrt{r^2+z^2}$. This is the condition we imposed componentwise on all the variables evolved with the hyperbolic-elliptic system (section 5.7). However, the gravitational field has only two degrees of freedom (the two polarization states, cf. chapter 7) and hence we are only allowed to impose two conditions.

8.3.1 Newman-Penrose scalars and the peeling theorem

More insight can be obtained by looking at the asymptotic behaviour of the *Weyl tensor*

$$\begin{aligned} C_{\alpha\beta\gamma\delta} &= R_{\alpha\beta\gamma\delta} - \tfrac{1}{2}(g_{\alpha\gamma}R_{\delta\beta} + g_{\beta\delta}R_{\gamma\alpha} - g_{\alpha\delta}R_{\gamma\beta} - g_{\beta\gamma}R_{\delta\alpha}) \\ &\quad + \tfrac{1}{6}R(g_{\alpha\gamma}g_{\delta\beta} - g_{\alpha\delta}g_{\gamma\beta})\,. \end{aligned} \tag{8.52}$$

The Weyl tensor is the tracefree part of the Riemann tensor, i.e., the part that is not determined by the matter sources via Einstein's equations. It thus contains the gravitational-wave information, and it reduces to the Riemann tensor in vacuum.

In the *Newman-Penrose (NP) formalism* [108, 128], one forms a complex null tetrad $(l, k, m, \bar{m})$ consisting of two real null vectors l and k, a complex null vector m and its complex conjugate $\bar{m}$ satisfying

$$l \cdot k = -1\,, \qquad m \cdot \bar{m} = 1\,. \tag{8.53}$$

Here we adapt the null tetrad to the boundary under consideration in the following way: first we choose an orthonormal basis $\{e_0, e_1, e_2, e_3\}$ with the properties

$$e_0 \propto n \qquad \text{(future-directed timelike normal)}\,, \tag{8.54}$$

$$e_1 \propto \mu \qquad \text{(spacelike outward-pointing normal to the boundary)}\,, \tag{8.55}$$

$$e_2 \propto \pi \qquad \text{(tangent to the boundary, } \mu_A \pi^A = 0)\,, \tag{8.56}$$

$$e_3 \propto \xi \qquad \text{(Killing vector)}\,. \tag{8.57}$$

Then we define the NP tetrad by

$$l \equiv \tfrac{1}{\sqrt{2}}(e_0 + e_1)\,, \tag{8.58}$$

$$k \equiv \tfrac{1}{\sqrt{2}}(e_0 - e_1)\,, \tag{8.59}$$

$$m \equiv \tfrac{1}{\sqrt{2}}(e_2 - i e_3)\,, \tag{8.60}$$

which satisfies the relations (8.53).

One now forms the five independent complex projections of the Weyl tensor with respect to the NP tetrad,

$$\Psi_0 \equiv C_{\alpha\beta\gamma\delta} l^\alpha m^\beta l^\gamma m^\delta\,, \tag{8.61}$$

$$\Psi_1 \equiv C_{\alpha\beta\gamma\delta} l^\alpha k^\beta l^\gamma m^\delta \,, \tag{8.62}$$

$$\Psi_2 \equiv C_{\alpha\beta\gamma\delta} l^\alpha m^\beta \bar{m}^\gamma k^\delta \,, \tag{8.63}$$

$$\Psi_3 \equiv C_{\alpha\beta\gamma\delta} l^\alpha k^\beta \bar{m}^\gamma k^\delta \,, \tag{8.64}$$

$$\Psi_4 \equiv C_{\alpha\beta\gamma\delta} k^\alpha \bar{m}^\beta k^\gamma \bar{m}^\delta \,. \tag{8.65}$$

The *peeling theorem* implies that

$$\Psi_i \sim x^{-5+i} \,, \quad i = 0, 1, 2, 3, 4 \tag{8.66}$$

as future null infinity is approached along the outgoing null geodesics with tangent l and affine parameter x. For the $r = r_{\max}$ ($z = z_{\max}$) boundary, x may be taken to be the coordinate r (z). Strictly speaking, (8.66) is only valid for solutions of the Einstein equations that are algebraically general. We have checked that all the linearized solutions in chapter 7 have the peeling behaviour (8.66), as expected for generic gravitational radiation.

One can use the peeling theorem to derive an outgoing radiation condition at the outer boundaries: because x is large there, $\Psi_0 \sim x^{-5}$ is suppressed as compared with the other Weyl scalars and so it is reasonable to impose

$$\Psi_0 \doteq 0 \tag{8.67}$$

at the outer boundaries. This condition was used by Friedrich and Nagy [58] in their well-posed initial boundary value formulation of the Einstein equations, and similar conditions have recently been applied to numerical relativity (e.g., [88, 121]). Because Ψ_0 is complex, (8.67) constitute two real conditions, as desired. They correspond to the two gravitational degrees of freedom, as we will see explicitly in the following.

8.3.2 Construction of the NP tetrad

We begin by setting up the orthormal basis (8.54–8.57). For this we need the full four metric $g_{\alpha\beta}$ and its inverse $g^{\alpha\beta}$. In linearized theory, we may set

$$\alpha = 1 + \delta\alpha\,, \tag{8.68}$$

$$H_{AB} = \delta_{AB} + \delta H_{AB}\,, \tag{8.69}$$

$$\lambda = r(1 + \delta\lambda)\,, \tag{8.70}$$

where $\delta\alpha$, δH_{AB} and $\delta\lambda$ as well as the shift vector β^A and the components ξ_t, ξ_A of the Killing vector are small quantities. In (t, r, z, φ) coordinates, the linearized 4-metric then takes the form

$$g_{\alpha\beta} = \begin{pmatrix} -1 - 2\delta\alpha & \beta^r & \beta^z & \xi_t \\ \beta^r & 1 + \delta H_{rr} & \delta H_{rz} & \xi_r \\ \beta^z & \delta H_{rz} & 1 + \delta H_{zz} & \xi_z \\ \xi_t & \xi_r & \xi_z & r^2(1 + 2\delta\lambda) \end{pmatrix} \tag{8.71}$$

and its inverse is

$$g^{\alpha\beta} = \begin{pmatrix} -1 + 2\delta\alpha & \beta^r & \beta^z & r^{-2}\xi_t \\ \beta^r & 1 - \delta H_{rr} & -\delta H_{rz} & -r^{-2}\xi_r \\ \beta^z & -\delta H_{rz} & 1 - \delta H_{zz} & -r^{-2}\xi_z \\ r^{-2}\xi_t & -r^{-2}\xi_r & -r^{-2}\xi_z & r^{-2}(1 - 2\delta\lambda) \end{pmatrix}. \tag{8.72}$$

Note that ξ_t, ξ_r and ξ_z are *not* in the Geroch space $\mathcal{N}$ (section 3.1).

The Killing vector is $\xi^\alpha = \delta_\varphi{}^\alpha$ and so we have

$$e_3{}^\alpha = (0, 0, 0, r^{-1}(1 - \delta\lambda))\,, \tag{8.73}$$

normalized such that $e_3{}^\alpha e_{3\,\alpha} = 1$. Lowering indices with $g_{\alpha\beta}$, the covariant version becomes to linear order

$$e_{3\,\alpha} = (r^{-1}\xi_t, r^{-1}\xi_r, r^{-1}\xi_z, r(1 + \delta\lambda))\,. \tag{8.74}$$

The timelike normal n satisfies $n_a = -\alpha {\delta_a}^t$ and $n_\alpha \xi^\alpha = 0$, which yields

$$e_{0\,\alpha} = (-1 - \delta\alpha, 0, 0, 0)\,, \tag{8.75}$$

and raising indices with $g^{\alpha\beta}$,

$$e_0{}^\alpha = (-1 + \delta\alpha, \beta^r, \beta^z, r^{-2}\xi_t)\,. \tag{8.76}$$

Consider first the $r = r_{\max}$ boundary. Its spacelike normal satisfies $\mu_A \propto {\delta_A}^r$, $\mu_a n^a = 0$ and $\mu_\alpha \xi^\alpha = 0$, which implies

$$e_{1\,\alpha} = (\beta^r, 1 + \tfrac{1}{2}\delta H_{rr}, 0, 0) \tag{8.77}$$

and so

$$e_1{}^\alpha = (0, 1 - \tfrac{1}{2}\delta H_{rr}, -\delta H_{rz}, -r^{-2}\xi_r)\,. \tag{8.78}$$

The tangent to the boundary, π^A satisfies $\pi^A \mu_A = 0$, $\pi^a n_a = 0$ and $\pi^\alpha \xi_\alpha = 0$, which together with the normalization fixes

$$e_2{}^\alpha = (0, 0, 1 - \tfrac{1}{2}\delta H_{zz}, -r^{-2}\xi_z) \tag{8.79}$$

and thus finally

$$e_{2\,\alpha} = (\beta^z, \delta H_{rz}, 1 + \tfrac{1}{2}\delta H_{zz}, 0)\,. \tag{8.80}$$

For the $z = z_{\max}$ boundary we have instead

$$e_{1\,\alpha} = (\beta^z, 0, 1 + \tfrac{1}{2}\delta H_{zz}, 0)\,, \tag{8.81}$$

$$e_1{}^\alpha = (0, -\delta H_{rz}, 1 - \tfrac{1}{2}H_{zz}, -r^{-2}\xi_z) \tag{8.82}$$

and

$$e_2{}^\alpha = (0, 1 - \tfrac{1}{2}\delta H_{rr}, 0, -r^{-2}\xi_r)\,, \tag{8.83}$$

$$e_{2\,\alpha} = (\beta^r, 1 + \tfrac{1}{2}\delta H_{rr}, \delta H_{rz}, 0)\,. \tag{8.84}$$

From the orthonormal basis, we finally form the NP tetrad as defined by equations (8.58–8.60).

8.3.3 Computation of Ψ_0

Having constructed the NP tetrad in covariant and contravariant form, we can compute the Weyl scalars (8.61–8.65) using, for example, the algorithm of Campbell and Wainwright [39].[1]

The resulting expressions contain various (up to second-order) time and spatial derivatives of δH_{AB}, $\delta\lambda$, $\delta\alpha$, β^A and ξ_t, ξ_A, which we need to translate into (2+1)+1 language. In particular, one might worry about the components of the Killing vector ξ because they are not in $\mathcal{N}$. Fortunately, they only appear in the following combinations:

$$2r^{-2}(\xi_{[r,t]} + r^{-1}\xi_t) = E^r\,, \tag{8.85}$$

$$2r^{-2}\xi_{[z,t]} = E^z\,, \tag{8.86}$$

$$2r^{-2}(\xi_{[r,z]} + r^{-1}\xi_z) = B^\varphi\,, \tag{8.87}$$

so that we recover the twist variables, which are in $\mathcal{N}$ (we have used definitions (3.6) and (3.47–3.48)). This was to be expected, of course, because Ψ_0 is a spacetime scalar and as such is in $\mathcal{N}$. The remaining time derivatives in the expressions for the NP scalars are eliminated using the linearized evolution equations (section 7.1). The spatial derivatives of $\delta H_{AB}, \delta\lambda, \delta\alpha$ and β^A are substituted using the definitions of the first-order variables (6.51–6.54).[2] Everything is expressed in terms of regularized variables; e.g., one should note that

$$\delta\lambda = rs + \tfrac{1}{2}\delta H_{rr} \tag{8.88}$$

in linearized theory.

[1] A REDUCE version of this algorithm was written by John Stewart.

[2] The ordering of the second spatial derivatives must be chosen carefully so that the results below obtain.

For the $r = r_{\max}$ boundary, we find

$$\begin{aligned}
\mathrm{Re}\Psi_0 &= \tfrac{1}{2}\{-\partial_r[rY + \chi_{rr} - \chi_{zz} - r^2\tilde{s}_r - D_{rrr} + D_{rzz}] \\
&\quad +\partial_z[-\chi_{rz} + 2r\tilde{D}_{rrz} - D_{zrr}] \qquad (8.89)\\
&\quad +r^{-1}D_{rrr} + 2r^{-1}D_{zrz} - 2Y + 4r\tilde{s}_r + 6r^{-1}s\}\,, \\
\mathrm{Im}\Psi_0 &= \tfrac{r}{4}\{2\partial_r[E^z - B^\varphi] - \partial_z E^r - 6r^{-1}B^\varphi + 3r^{-1}E^z\}\,. \qquad (8.90)
\end{aligned}$$

Thus the imaginary part of Ψ_0 involves only the twist variables and the real part only the remaining variables. Recall from chapter 7 that these two subsystems correspond to the two polarization states of the gravitational field so that we obtain one separate boundary condition for each polarization, as desired. Note also that (8.89–8.90) are manifestly gauge-independent (they do not contain the lapse, shift or derivatives thereof).

Next observe that the r-fluxes in (8.89–8.90) are proportional to the incoming modes $l^-_{1,1}$ (8.8) and $l^-_{1,2}$ (8.9)! Hence we can express the boundary conditions $\Psi_0 \doteq 0$ as conditions on the normal derivatives of two of the incoming modes:

$$\begin{aligned}
\partial_r\, l^-_{1,1} &\doteq \partial_z[-\chi_{rz} + 2r\tilde{D}_{rrz} - D_{zrr} + 2B_r{}^z] \\
&\quad +r^{-1}D_{rrr} + 2r^{-1}D_{zrz} - Y + 4r\tilde{s}_r + 6r^{-1}s\,, \qquad (8.91)\\
\partial_r\, l^-_{1,2} &\doteq \tfrac{1}{2}\partial_z E^r + 3r^{-1}B^\varphi - \tfrac{3}{2}r^{-1}E^z\,. \qquad (8.92)
\end{aligned}$$

Similarly, we find for the $z = z_{\max}$ boundary

$$\begin{aligned}
\mathrm{Re}\Psi_0 &= \tfrac{1}{2}\{-\partial_z[r(Y - s_z)] + \partial_r[r^{-1}(-\chi_{rz} - D_{rzz} + 2D_{zrz})]\}\,, \qquad (8.93)\\
\mathrm{Im}\Psi_0 &= \tfrac{r}{4}\{2\partial_z[E^r + B^\varphi] - \partial_r E^z\}\,. \qquad (8.94)
\end{aligned}$$

We identify $l^-_{1,1}$ (8.26) and $l^-_{1,2}$ (8.27) in the z-fluxes so that $\Psi_0 \doteq 0$ can be written as

$$\begin{aligned}
\partial_z \tilde{l}^-_{1,1} &\doteq \partial_r[r^{-1}(-\chi_{rz} - D_{rzz} + 2D_{zrz} + 2B_z{}^r)]\,, \qquad (8.95)\\
\partial_z\, l^-_{1,2} &\doteq \tfrac{1}{2}\partial_r E^z\,, \qquad (8.96)
\end{aligned}$$

where $\tilde{l}^-_{1,1}$ was defined in (8.40), and here we see very clearly the reason for that definition: written in the form (8.95), the boundary condition is regular at $r = 0$ because of table 6.1.

We have checked that the residuals of the boundary conditions (8.91–8.92) are indeed of the order r^{-5} when evaluated for the exact linearized solutions of chapter 7. However, this fall-off is not uniform in z: the leading-order coefficient of the expansion of the residual in inverse powers of r has a z-dependence of $\sim z^4$ or lower, depending on which solution we choose. A similar statement with r and z interchanged holds for equations (8.95–8.96). This means that if the size of the grid is doubled both in the r and in the z direction, the supremum of the residual evaluated along the entire boundary will not decrease by a factor of $2^5 = 32$ but only 2 (in the worst case).

In order to improve on this, one could consider an NP tetrad that points in the R-direction, where $R = \sqrt{r^2 + z^2}$, for this coordinate is large everywhere on the outer boundary. The residual then falls off like R^{-5}. However, in this case we cannot translate the boundary conditions into a prescription for the normal derivatives of the incoming modes as done above.

8.4 Constraint-preserving boundary conditions

Further boundary conditions can be obtained by requiring that no violations of the constraints enter the computational domain from the outside. The basic strategy for deriving such *constraint-preserving boundary conditions* was first developed by Stewart [129], and there has been much recent work on this subject (e.g., [37, 38, 25]).

In the Z4 formalism, the standard Einstein or ADM constraints are re-

placed with the algebraic constraints

$$Z_\alpha = 0\,. \tag{8.97}$$

If those hold at all times, the Einstein constraints are automatically satisfied by virtue of the evolution equations for the Z vector (6.31–6.33). In order to set up constraint-preserving boundary conditions, we need to understand how the constraints propagate. By applying the contracted Bianchi identities

$$\nabla_\beta G^{\alpha\beta} = 0 \tag{8.98}$$

to the Z4-Einstein equations (6.1), we obtain a homogeneous wave equation for the Z vector:

$$\nabla_\beta \nabla^\beta Z_\alpha + R_{\alpha\beta} Z^\beta = 0\,. \tag{8.99}$$

This equation forms the *constraint propagation* or *subsidiary system*.

The (2+1)+1 reduction of (8.99) can be obtained by simply taking a second time derivative of the evolution equations for the Z vector (6.31–6.33). As we would like to write the resulting system in first-order form, we have to introduce new variables for the first-order space and time derivatives of the Z vector,

$$\theta_A \equiv \partial_A \theta\,, \qquad Z_{BA} \equiv \partial_B Z_A\,, \qquad Z_A{}^\varphi \equiv \partial_A Z^\varphi\,, \tag{8.100}$$

$$\theta_0 \equiv \mathfrak{d}_t \theta\,, \qquad Z_{0A} \equiv \mathfrak{d}_t Z_A\,, \qquad Z_0{}^\varphi \equiv \mathfrak{d}_t Z^\varphi\,, \tag{8.101}$$

where

$$\mathfrak{d}_t \equiv \alpha^{-1}(\partial_t - \beta^A \partial_A)\,. \tag{8.102}$$

We also need the *ordering constraints*

$$\mathcal{D}_{ABCD} \equiv 2\partial_{[A}D_{B]CD}\,, \tag{8.103}$$

$$\mathcal{L}_{AB} \equiv 2\partial_{[A}L_{B]}\,, \tag{8.104}$$

$$\mathcal{A}_{AB} \equiv 2\partial_{[A}A_{B]}\,, \tag{8.105}$$

$$\mathcal{B}_{AB}{}^{C} \equiv 2\partial_{[A}B_{B]}{}^{C}\,, \tag{8.106}$$

which vanish because of the definitions of the first-order variables (6.51–6.54).

The subsidiary system now takes the form

$$\partial_t\theta_0 - \partial_B\theta^B \simeq -2\partial_B\mathcal{B}^B{}_A{}^A\,, \tag{8.107}$$

$$\partial_t Z_{0A} - \partial_B Z^B{}_A \simeq \tfrac{1}{2}\partial_B\left(\mathcal{A}_A{}^B + \mathcal{L}_A{}^B + \mathcal{D}_A{}^{BC}{}_C - 2\mathcal{D}_C{}^{BC}{}_A\right)\,, \tag{8.108}$$

$$\partial_t Z_0{}^{\varphi} - \partial_B Z^{B\varphi} \simeq 0\,, \tag{8.109}$$

to principal parts ($\simeq$). We clearly recognize the wave operator of equation (8.99) on the left-hand-sides of (8.107–8.109). The ordering constraints on the right-hand-sides of (8.107–8.108) are not present in (8.99); they are a consequence of the first-order reduction we used to derive the Z(2+1)+1 system. Analytically of course, the ordering constraints vanish, but this may not obtain numerically and so we have to include them in the subsidiary system. Fortunately, the ordering constraints propagate along the normal lines:

$$\partial_t\mathcal{D}_{ABCD} = \partial_t\mathcal{L}_{AB} = \partial_t\mathcal{A}_{AB} = \partial_t\mathcal{B}_{AB}{}^{C} = 0\,. \tag{8.110}$$

Constraint-preserving boundary conditions are obtained by requiring the incoming modes of the subsidiary system to vanish at the boundary. If μ_A is the unit outward-pointing normal to the boundary and $\perp$ denotes contraction

with μ_A (cf. section 6.4), the conditions read

$$\theta_0 + \theta_\perp - 2\mathcal{B}_{\perp A}{}^A \doteq 0\,, \tag{8.111}$$

$$Z_{0A} + Z_{\perp A} + \tfrac{1}{2}(\mathcal{A}_{A\perp} + \mathcal{L}_{A\perp} + \mathcal{D}_{A\perp C}{}^C - 2\mathcal{D}_{C\perp}{}^C{}_A) \doteq 0\,, \tag{8.112}$$

$$Z_0{}^\varphi + Z_\perp{}^\varphi \doteq 0\,. \tag{8.113}$$

We now express these conditions in terms of regularized Z(2+1)+1 variables and in linearized theory. The time derivatives of the Z vector (8.101) are substituted using the evolution equations (6.31–6.33). The boundary conditions at $r = r_{\max}$ can be written as

$$\begin{aligned}
\partial_r l^-_{1,3} &= \partial_r[\theta - 2B_z{}^z - D_{rzz} - r^2\tilde{s}_r - D_{rrr} + D_{zrz} + Z_r] \\
&\doteq \partial_z[-2B_r{}^z - r\tilde{D}_{rrz} + 2D_{zrr} + rs_z - Z_z] \qquad (8.114)\\
&\quad + r^{-1}(D_{rrr} + D_{rzz} - 3D_{zrz} - Z_r + 6s) + 4r\tilde{s}_r\,, \\
\partial_r l^-_{1,4} &= \partial_r[rY + \chi_{rr} + \chi_{zz} - \theta - D_{zrz} - Z_r] \\
&\doteq \partial_z[\chi_{rz} - r\tilde{D}_{rrz}] - Y - r^{-1}D_{zrz}\,, \qquad (8.115)\\
\partial_r l^-_{1,5} &= \partial_r[\chi_{rz} - \tfrac{1}{2}(A_z + 2D_{zrr} - D_{zzz} + rs_z - 2Z_z)] \\
&\doteq \partial_z[2\chi_{rr} + rY - \theta - \tfrac{1}{2}(A_r - D_{rzz} + 2D_{rrr} + r^2\tilde{s}_r)] \qquad (8.116)\\
&\quad - r^{-1}\chi_{rz} - s_z\,, \\
\partial_r l^-_{1,6} &= \partial_r[E^r + 2Z^\varphi] \doteq -\partial_z E^z - 3r^{-1}E^r\,. \qquad (8.117)
\end{aligned}$$

For the $z = z_{\max}$ boundary we find

$$\begin{aligned}
\partial_z l^-_{1,3} &= \partial_z[\theta - 2r\tilde{B}_r{}^r - 2D_{zrr} - rs_z + r\tilde{D}_{rrz} + Z_z] \\
&\doteq \partial_r[-2B_z{}^r + D_{rrr} + D_{rzz} - D_{zrz} - Z_r + r^2\tilde{s}_r] \qquad (8.118)\\
&\quad + r^{-1}(B_z{}^r + D_{rrr} + D_{rzz} - 3D_{zrz} - Z_r + 6s) + 4r\tilde{s}_r\,, \\
\partial_z l^-_{1,4} &= \partial_z[rY + 2\chi_{rr} - \theta - r\tilde{D}_{rrz} - Z_z] \\
&\doteq \partial_r[\chi_{rz} - D_{zrz}] + r^{-1}(\chi_{rz} + D_{zrz})\,, \qquad (8.119)
\end{aligned}$$

$$\begin{aligned}
\partial_z l^-_{1,5} &= \partial_z[\chi_{rz} - \tfrac{1}{2}(A_r + D_{rzz} + r^2\tilde{s}_r - 2Z_r)] \\
&\doteq \partial_r[rY + \chi_{rr} + \chi_{zz} - \theta - \tfrac{1}{2}(A_z + D_{zzz} + rs_z)] \qquad (8.120) \\
&\quad +Y + s_z\,, \\
\partial_z l^-_{1,6} &= \partial_z[E^z + 2Z^\varphi] \doteq -\partial_r E^r - 3r^{-1}E^r\,. \qquad (8.121)
\end{aligned}$$

As in section 8.3, these boundary conditions are again prescriptions for the normal derivatives of the incoming modes. The conditions at the $z = z_{\max}$ boundary are regular at $r = 0$ provided that the on-axis conditions hold (table 6.1). We have verified that equations (8.114–8.117) and (8.118–8.121) are satisfied identically by the exact solutions of chapter 7. This is as it should be because the constraints vanish for an exact solution and so do the incoming modes of the subsidiary system.

8.5 Gauge boundary conditions and summary

To complete the boundary conditions derived so far in sections 8.3 and 8.4, we have to prescribe boundary conditions for the gauge variables α and β^A. Because we are free to specify the gauge in any way we like, this procedure is essentially arbitrary. The simplest choice would be absorbing boundary conditions for the gauge modes,

$$l^-_f \doteq 0\,, \qquad (8.122)$$

$$l^-_\mu \doteq l^-_d \doteq 0\,. \qquad (8.123)$$

Provided that the gauge parameters are chosen to be those of harmonic gauge ($f = \mu = d = a = 1, m = 2$), equation (8.122) is satisfied identically by the exact solutions of chapter 7, but equations (8.123) only hold to leading order in r^{-1} (z^{-1}).

Can we construct gauge boundary conditions that are all satisfied identically by the exact solutions? In harmonic gauge, the lapse α and the components of the shift β^A each satisfy a wave equation to principal parts: in linearized theory,

$$\partial_t^2 \alpha - \partial_B \partial^B \alpha \simeq 0 \,, \tag{8.124}$$

$$\partial_t^2 \beta^A - \partial_B \partial^B \beta^A \simeq 0 \,. \tag{8.125}$$

This is clear from the harmonic gauge condition (6.39) but can also be verified directly from the linearized Z(2+1)+1 equations (section 7.1). It is important to note that harmonic gauge is the only choice of gauge parameters for which one obtains a *closed* evolution system for the gauge variables.

We can now construct boundary conditions for (8.124–8.125) in a similar way as we did for the constraint evolution system (8.99), which also formed a wave equation. In order that the waves in the gauge variables leave the computational domain without causing reflections, it is reasonable to set the incoming modes of (8.124–8.125) to zero at the outer boundaries, i.e.

$$\partial_t \alpha + \partial_\perp \alpha \doteq 0 \,, \tag{8.126}$$

$$\partial_t \beta^A + \partial_\perp \beta^A \doteq 0 \,, \tag{8.127}$$

where as usual $\perp$ denotes a derivative normal to the boundary.

Substituting the time derivatives using the evolution equations (7.9–7.11)

we obtain in the r-direction

$$\begin{aligned}
0 &\doteq A_r - 2\chi_{rr} - \chi_{zz} - rY + 2\theta \\
&= l_f^- \,, \qquad (8.128) \\
0 &\doteq 2r\tilde{B}_r{}^r + r^{-1}\beta^r - A_r - D_{rzz} + 2D_{zrz} - r^2\tilde{s}_r - 4s + 2Z_r \\
&= -l_d^- - l_f^- + 2l_{1,3}^- + 2l_{0,7} + r^{-1}\beta^r - 4s \,, \qquad (8.129) \\
0 &\doteq 2B_r{}^z - A_z + 2r\tilde{D}_{rrz} - 2D_{zrr} + D_{zzz} + 2r^{-1}H_{rz} \\
&\quad -rs_z + 2Z_z \qquad (8.130) \\
&= -l_\mu^- - 2l_{0,6} + 2r^{-1}H_{rz} \,.
\end{aligned}$$

Equation (8.128) is simply an absorbing boundary condition for l_f^-. However, (8.129) is more problematic because it specifies l_d^- in terms of $l_{1,3}^-$, of which only the normal derivative is known if we impose constraint-preserving boundary conditions (8.114). What happens though if we take a time derivative of (8.128–8.130)? Equation (8.128) becomes

$$\partial_r l_f^- = -\partial_z A_z - r^{-1}A_r \,. \qquad (8.131)$$

As for (8.129), terms $\partial_r l_f^-$ and $\partial_r l_{1,3}^-$ will appear (recall that l_f^- and $l_{1,3}^-$ are eigenfields in the r-direction both with speed 1 in the harmonic case). These can be eliminated using (8.131) and (8.114). The result is

$$\begin{aligned}
\partial_r l_d^- &\doteq \partial_z[A_z + 2(-B_r{}^z + B_z{}^r - r\tilde{D}_{rrz} + 2D_{zrr} + rs_z - Z_z)] \\
&\quad + r^{-1}[A_r + 2(2r\tilde{B}_r{}^r + D_{rrr} + D_{rzz} - 3D_{zrz} - Z_r \qquad (8.132) \\
&\quad + 2r^2\tilde{s}_r + 4s)] \,.
\end{aligned}$$

Thus we have managed to obtain a prescription for the normal derivative of l_d^- in terms of tangential derivatives and source terms. The time derivative of (8.130) becomes

$$\partial_r l_\mu^- = \partial_z[2(B_z{}^z - r\tilde{B}_r{}^r)] + 4\tilde{D}_{rrz} + 2r^{-1}(B_r{}^z - B_z{}^r) \,. \qquad (8.133)$$

Applying the same procedure in the z-direction yields

$$\partial_z l_f^- \doteq -\partial_r A_r - r^{-1} A_r \,, \tag{8.134}$$

$$\begin{aligned} \partial_z l_d^- \doteq\ & \partial_r [A_r + 2(B_r{}^z + D_{rrr} + D_{rzz} - D_{zrz} + r^2 \tilde{s}_r - Z_r)] \\ & + r^{-1} [A_r + 2(B_r{}^z + 2D_{zrz} + D_{rrr} + D_{rzz} - 3D_{zrz} \\ & \quad + 4r^2 \tilde{s}_r + 6s - Z_r)] \,, \end{aligned} \tag{8.135}$$

$$\partial_z l_\mu^- \doteq \partial_z [2(r\tilde{B}_r{}^r - B_z{}^z)] + 4(\tilde{B}_r{}^r - s_z) \,. \tag{8.136}$$

These equations are regular on axis because of table 6.1.

As expected, the boundary conditions (8.131–8.133) and (8.134–8.136) are now satisfied identically by the exact solutions.

Summary. Using information about the Newman-Penrose scalar Ψ_0 (section 8.3), the constraint propagation system (section 8.4) and the gauge propagation system (section 8.5), we have obtained a total of 9 boundary conditions for each outer boundary. The conditions all specify the normal derivatives of the incoming modes in terms of tangential derivatives and source terms.

We have checked that the boundary conditions are satisfied identically by the exact linearized solutions of chapter 7, except for the two outgoing-radiation boundary conditions, whose residuals are of the optimal order of r^{-5} (z^{-5}).

Since the linearized Z(2+1)+1 system with dynamical shift has 9 incoming modes, we have a complete set of boundary conditions specifying all the incoming modes of the system. In the vanishing shift case, one deletes the boundary conditions for l_d^- and l_μ^- and obtains a total of 7 conditions, which is again the required number.

It is a fortunate coincidence of axisymmetry that the numbers work out

in such a convenient way. In the case without symmetries, there are more characteristic variables and hence more boundary conditions are required. For instance, there are 6 additional pairs of light cone modes [23]. This problem can be addressed by considering instead of Ψ_0 the evolution system of the electric and magnetic parts of the Weyl tensor, which leads to the right number of boundary conditions for the light cone modes [88].

8.6 Fourier-Laplace analysis

Having derived a set of boundary conditions in sections 8.3–8.5, the question arises whether the associated initial boundary value problem is well-posed. Because the boundary conditions are not of the dissipative type (8.41), the standard theorems mentioned in section 8.2.1 do not apply.

We now prove a necessary condition for well-posedness of the IBVP in the high-frequency limit using the Fourier-Laplace technique [73]. This limit is also known as the WKB approximation, or geometrical optics. It implies that we may neglect the source terms in the linearized Z(2+1)+1 equations against the flux terms. Harmonic slicing is used ($f = 1, m = 2$), and we consider first the case of a vanishing shift vector.

To begin with, it is convenient to rewrite the linearized Z(2+1)+1 equations (section 7.1) in characteristic space, i.e., as evolution equations for the characteristic variables. This can easily be done with the help of a computer algebra programme using the transformation between conserved and characteristic variables (section 8.1). The characteristic form of the equations has the advantage that it is the same both for characteristic variables in the r-direction and in the z-direction (this has been checked explicitly). Hence we use general indices $\perp$ and $\parallel$, where either $(x^\perp, x^\parallel) = (r, z)$ or $(x^\perp, x^\parallel) = (z, r)$.

The coordinate normal to the boundary under consideration is $x^\perp$ and the one parallel to it is $x^\parallel$. The characteristic variables refer to the $x^\perp$-direction. Neglecting the source terms, we find

$$\begin{aligned}
\partial_t l_{0,1} &= -\tfrac{1}{2}\partial_\parallel(l^-_{1,3} + l^+_{1,3} - l^-_{1,4} - l^+_{1,4} - l^-_f + l^+_f)\,, && (8.137)\\
\partial_t l_{0,2} &= -\tfrac{1}{2}\partial_\parallel(l^-_{1,5} + l^+_{1,5})\,, && (8.138)\\
\partial_t l_{0,3} &= -\tfrac{1}{4}\partial_\parallel(-l^-_{1,1} - l^+_{1,1} + l^-_{1,3} + l^+_{1,3} + l^-_{1,4} + l^+_{1,4})\,, && (8.139)\\
\partial_t l_{0,4} &= -\tfrac{1}{2}\partial_\parallel(l^-_{1,1} + l^+_{1,1})\,, && (8.140)\\
\partial_t l_{0,5} &= -\tfrac{1}{2}\partial_\parallel(-l^-_f + l^+_f)\,, && (8.141)\\
\partial_t l_{0,6} &= 0\,, && (8.142)\\
\partial_t l_{0,7} &= 0\,, && (8.143)\\
\partial_t l^\pm_{1,1} &= \mp\partial_\perp l^\pm_{1,1} - \partial_\parallel(l_{0,4} - l_{0,7})\,, && (8.144)\\
\partial_t l^\pm_{1,2} &= \mp\partial_\perp l^\pm_{1,2} \pm \partial_\parallel l^\mp_{1,6}\,, && (8.145)\\
\partial_t l^\pm_{1,3} &= \mp\partial_\perp l^\pm_{1,3} - \tfrac{1}{2}\partial_\parallel(l_{0,1} + 2l_{0,3} + l_{0,4} - l_{0,5} + l_{0,7})\,, && (8.146)\\
\partial_t l^\pm_{1,4} &= \mp\partial_\perp l^\pm_{1,4} - \tfrac{1}{2}\partial_\parallel(-l_{0,1} + 2l_{0,3} + l_{0,4} + l_{0,5} + l_{0,7})\,, && (8.147)\\
\partial_t l^\pm_{1,5} &= \mp\partial_\perp l^\pm_{1,5} - \tfrac{1}{2}\partial_\parallel(2l_{0,2} + l_{0,6})\,, && (8.148)\\
\partial_t l^\pm_{1,6} &= \mp\partial_\perp l^\pm_{1,6} \mp \partial_\parallel l^\mp_{1,2}\,, && (8.149)\\
\partial_t l^\pm_f &= \mp\partial_\perp l^\pm_f \mp \partial_\parallel l_{0,5}\,. && (8.150)
\end{aligned}$$

We can solve these equations by means of a Laplace transformation in time and a Fourier transformation in the $x^\parallel$ direction. That is, we write the solution as a superposition of modes of the form

$$\mathbf{u}(t, x^\perp, x^\parallel) = \hat{\mathbf{u}}(x^\perp)\mathrm{e}^{st+i\omega x^\parallel}\,, \qquad (8.151)$$

where $s \in \mathbb{C}$, $\mathrm{Re}(s) > 0$. Substituting this into (8.137–8.150), we obtain a set

of ordinary differential equations in the coordinate $x^\perp$ coupled to algebraic conditions. For simplicity we set

$$\xi \equiv \omega x^\perp\,, \qquad \zeta \equiv \frac{s}{\omega}\,, \tag{8.152}$$

(we may assume $\omega > 0$ because we are only interested in high frequencies) and we leave out the hats on the transformed variables.

Substituting (8.152) into (8.137–8.143) yields the following algebraic conditions for the zero-speed modes:

$$\begin{aligned}
l_{0,1} &= -\tfrac{i}{2\zeta}(l^-_{1,3} + l^+_{1,3} - l^-_{1,4} - l^+_{1,4} - l^-_f + l^+_f)\,, && (8.153)\\
l_{0,2} &= -\tfrac{i}{2\zeta}(l^-_{1,5} + l^+_{1,5})\,, && (8.154)\\
l_{0,3} &= -\tfrac{i}{4\zeta}(-l^-_{1,1} - l^+_{1,1} + l^-_{1,3} + l^+_{1,3} + l^-_{1,4} + l^+_{1,4})\,, && (8.155)\\
l_{0,4} &= -\tfrac{i}{2\zeta}(l^-_{1,1} + l^+_{1,1})\,, && (8.156)\\
l_{0,5} &= -\tfrac{i}{2\zeta}(-l^-_f + l^+_f)\,, && (8.157)\\
l_{0,6} &= 0\,, && (8.158)\\
l_{0,7} &= 0\,. && (8.159)
\end{aligned}$$

These can now be used to eliminate the zero-speed modes in the Fourier-Laplace transform of (8.144–8.150):

$$\begin{aligned}
\partial_\xi l^\pm_{1,1} &= \mp\zeta l^\pm_{1,1} \mp i(l_{0,4} - l_{0,7})\\
&= \mp\zeta l^\pm_{1,1} \mp \tfrac{1}{2\zeta}(l^-_{1,1} + l^+_{1,1})\,, && (8.160)\\
\partial_\xi l^\pm_{1,2} &= \mp\zeta l^\pm_{1,2} + i l^\mp_{1,6}\,, && (8.161)\\
\partial_\xi l^\pm_{1,3} &= \mp\zeta l^\pm_{1,3} \mp \tfrac{i}{2}(l_{0,1} + 2l_{0,3} + l_{0,4} - l_{0,5} + l_{0,7})\\
&= \mp\zeta l^\pm_{1,3} \mp \tfrac{1}{2\zeta}(l^-_{1,3} + l^+_{1,3})\,, && (8.162)\\
\partial_\xi l^\pm_{1,4} &= \mp\zeta l^\pm_{1,4} \mp \tfrac{i}{2}(-l_{0,1} + 2l_{0,3} + l_{0,4} + l_{0,5} + l_{0,7})\\
&= \mp\zeta l^\pm_{1,4} \mp \tfrac{1}{2\zeta}(l^-_{1,4} + l^+_{1,4})\,, && (8.163)
\end{aligned}$$

$$\begin{aligned}
\partial_\xi l^\pm_{1,5} &= \mp\zeta l^\pm_{1,5} \mp \tfrac{i}{2}(2l_{0,2} + l_{0,6}) \\
&= \mp\zeta l^\pm_{1,5} \mp \tfrac{1}{2\zeta}(l^-_{1,5} + l^+_{1,5})\,, && (8.164)\\
\partial_\xi l^\pm_{1,6} &= \mp\zeta l^\pm_{1,6} - i l^\mp_{1,2}\,, && (8.165)\\
\partial_\xi l^\pm_{f} &= \mp\zeta l^\pm_{f} - i l_{0,5} \\
&= \mp\zeta l^\pm_{f} - \tfrac{1}{2\zeta}(-l^-_f + l^+_f)\,. && (8.166)
\end{aligned}$$

This system of ODEs decouples into the following 2×2 blocks:

$$\begin{aligned}
\partial_\xi (l^-_{1,1}, l^+_{1,1})^T &= M_1 (l^-_{1,1}, l^+_{1,1})^T\,, && (8.167)\\
\partial_\xi (l^-_{1,3}, l^+_{1,3})^T &= M_1 (l^-_{1,3}, l^+_{1,3})^T\,, && (8.168)\\
\partial_\xi (l^-_{1,4}, l^+_{1,4})^T &= M_1 (l^-_{1,4}, l^+_{1,4})^T\,, && (8.169)\\
\partial_\xi (l^-_{1,5}, l^+_{1,5})^T &= M_1 (l^-_{1,5}, l^+_{1,5})^T\,, && (8.170)\\
\partial_\xi (l^-_{f}, l^+_{f})^T &= M_2 (l^-_{f}, l^+_{f})^T\,, && (8.171)\\
\partial_\xi (l^-_{1,2}, l^+_{1,6})^T &= M_3 (l^-_{1,2}, l^+_{1,6})^T\,, && (8.172)\\
\partial_\xi (l^+_{1,2}, l^-_{1,6})^T &= M_4 (l^+_{1,2}, l^-_{1,6})^T\,, && (8.173)
\end{aligned}$$

where the matrices M_i are given by

$$\begin{aligned}
M_1 &= \begin{pmatrix} \zeta + \frac{1}{2\zeta} & \frac{1}{2\zeta} \\ -\frac{1}{2\zeta} & -\zeta - \frac{1}{2\zeta} \end{pmatrix}\,, \qquad M_2 = \begin{pmatrix} \zeta + \frac{1}{2\zeta} & -\frac{1}{2\zeta} \\ \frac{1}{2\zeta} & -\zeta - \frac{1}{2\zeta} \end{pmatrix}\,, \\
M_3 &= \begin{pmatrix} \zeta & i \\ -i & -\zeta \end{pmatrix}\,, \qquad M_4 = \begin{pmatrix} -\zeta & i \\ -i & \zeta \end{pmatrix}\,. && (8.174)
\end{aligned}$$

Each matrix M_i has eigenvalues $\pm\lambda$ where

$$\lambda = \sqrt{1 + \zeta^2}\,, \qquad (8.175)$$

with the sign of the square root chosen such that $\mathrm{Re}(\lambda) > 0$ for $\mathrm{Re}(\zeta) > 0$. The corresponding solutions of the ODEs have a ξ-dependence of $\exp(\pm\lambda\xi)$.

We only admit solutions that are L^2 in the interior and so we have to exclude the $\exp(-\lambda\xi)$ solutions[3] because they blow up as $\xi \to -\infty$. The (right) eigenvectors of the M_i with eigenvalue $+\lambda$ and hence the admissible solutions of the ODEs are found to be

$$(l^-_{1,1}, l^+_{1,1})^T = a_1 \mathrm{e}^{\lambda\xi}(-1, (\zeta-\lambda)^2)^T\,, \tag{8.176}$$

$$(l^-_{1,3}, l^+_{1,3})^T = a_2 \mathrm{e}^{\lambda\xi}(-1, (\zeta-\lambda)^2)^T\,, \tag{8.177}$$

$$(l^-_{1,4}, l^+_{1,4})^T = a_3 \mathrm{e}^{\lambda\xi}(-1, (\zeta-\lambda)^2)^T\,, \tag{8.178}$$

$$(l^-_{1,5}, l^+_{1,5})^T = a_4 \mathrm{e}^{\lambda\xi}(-1, (\zeta-\lambda)^2)^T\,, \tag{8.179}$$

$$(l^-_{f}, l^+_{f})^T = a_5 \mathrm{e}^{\lambda\xi}(1, (\zeta-\lambda)^2)^T\,, \tag{8.180}$$

$$(l^-_{1,2}, l^+_{1,6})^T = a_6 \mathrm{e}^{\lambda\xi}(-i, \zeta-\lambda)^T\,, \tag{8.181}$$

$$(l^+_{1,2}, l^-_{1,6})^T = a_7 \mathrm{e}^{\lambda\xi}(i, \zeta+\lambda)^T\,, \tag{8.182}$$

and the general admissible solution is a superposition of these with arbitrary complex constants a_i.

In order for the IBVP to be well-posed, the constants a_i have to be uniquely determined by the boundary conditions, for all $\zeta \in \mathbb{C}$ with $\mathrm{Re}(\zeta) > 0$. Otherwise, there exists a nontrivial solution for some ζ with $\mathrm{Re}(\zeta) > 0$, which after reversing the Fourier-Laplace transformation takes the form

$$\mathbf{u}(t, x^\perp, x^\parallel) = \hat{\mathbf{u}}(x^\perp)\mathrm{e}^{\omega(\zeta t + i x^\parallel)}\,. \tag{8.183}$$

Here ω can be arbitrarily large. Hence no estimate of the form (8.43) holds, and the IBVP is ill-posed.

The boundary conditions we want to impose consist of the outgoing-radiation conditions ((8.91–8.92) and (8.95–8.96)), the constraint-preserving

[3]It is more common in the literature to have the boundary at $\xi = 0$, with $\xi > 0$ being in the interior, in which case the opposite sign of λ has to be chosen here.

conditions ((8.114–8.117) and (8.118–8.121)) and the gauge boundary condition for the lapse function ((8.131) and (8.134)). In characteristic space and after performing the Fourier-Laplace transformation, these boundary conditions can be written as

$$\begin{aligned}
\partial_\xi l^-_{1,1} &\doteq -\tfrac{i}{2}(2l_{0,1} + 2l_{0,7} + 3l^-_{1,5} - l^+_{1,5}) \\
&= -\tfrac{1}{2\zeta}(l^-_{1,3} + l^+_{1,3} - l^-_{1,4} - l^+_{1,4} - l^-_f + l^+_f) \\
&\quad -\tfrac{i}{2}(3l^-_{1,5} - l^+_{1,5})\,, \qquad (8.184)\\
\partial_\xi l^-_{1,2} &\doteq \tfrac{i}{4}(l^+_{1,6} + l^-_{1,6})\,, \qquad (8.185)\\
\partial_\xi l^-_{1,3} &\doteq -\tfrac{i}{2}(-l_{0,1} - 2l_{0,3} - l_{0,4} + l_{0,5} - l_{0,7}) \\
&= \tfrac{1}{2\zeta}(l^-_{1,3} + l^+_{1,3})\,, \qquad (8.186)
\end{aligned}$$

$$\begin{aligned}
\partial_\xi l^-_{1,4} &\doteq -\tfrac{i}{2}(-l_{0,7} - 2l^-_{1,5}) \\
&= il^-_{1,5}\,, \qquad (8.187)\\
\partial_\xi l^-_{1,5} &\doteq -\tfrac{i}{2}(-l_{0,6} - l^-_{1,1} - l^-_{1,3} + l^-_{1,4} + 2l^-_f) \\
&= -\tfrac{i}{2}(-l^-_{1,1} - l^-_{1,3} + l^-_{1,4} + 2l^-_f)\,, \qquad (8.188)\\
\partial_\xi l^-_{1,6} &\doteq -\tfrac{i}{2}(l^-_{1,2} + l^+_{1,2})\,, \qquad (8.189)\\
\partial_\xi l^-_f &\doteq -il_{0,7} \\
&= -\tfrac{1}{2\zeta}(-l^-_f + l^+_f)\,, \qquad (8.190)
\end{aligned}$$

where we have again used the algebraic conditions (8.153–8.159) to eliminate the incoming modes. (It does not matter whether we choose $(\perp, \parallel) = (r, z)$ or $(\perp, \parallel) = (z, r)$, the result is the same.) Inserting the superposition of (8.176–8.182) into (8.184–8.190), we obtain the following relations for the coefficients a_i. Equation (8.186) yields

$$0 = -\lambda a_2 + \tfrac{1}{2\zeta}[1 - (\zeta - \lambda)^2]a_2 = \zeta a_2\,, \qquad (8.191)$$

where we have used (8.175). Hence $a_2 = 0$ because $\mathrm{Re}(\zeta) > 0$. Similarly, (8.190) becomes

$$0 = \lambda a_5 + \tfrac{1}{2\zeta}[-1 + (\zeta - \lambda)^2]a_5 = -\zeta a_5 \tag{8.192}$$

so that $a_5 = 0$. Equation (8.188) tells us that

$$a_4 = -i\lambda a_3 \,. \tag{8.193}$$

Inserting the results for a_2, a_4 and a_5 into equations (8.184) and (8.188) leads to the following linear system for the coefficients a_1 and a_3:

$$\begin{pmatrix} -\lambda & -\lambda + \zeta^2(\zeta - \lambda) \\ \frac{i}{2} & \frac{i}{2}(2\zeta^2 + 1) \end{pmatrix} \begin{pmatrix} a_1 \\ a_3 \end{pmatrix} = 0 \,. \tag{8.194}$$

Its determinant is found to be

$$D_1(\zeta) = -\tfrac{i}{2}\zeta^2(\zeta + \lambda) \,. \tag{8.195}$$

$D_1(\zeta) \neq 0$ because $\mathrm{Re}(\zeta) > 0$ and $\mathrm{Re}(\lambda) > 0$. Hence $a_1 = a_3 = 0$ is the only solution. The twist subsystem ((8.185) and (8.189)) implies that

$$\begin{pmatrix} \lambda + \frac{1}{4}(\zeta - \lambda) & \frac{1}{4}(\zeta + \lambda) \\ \frac{1}{2} & \lambda(\zeta + \lambda) - \frac{1}{2} \end{pmatrix} \begin{pmatrix} a_6 \\ a_7 \end{pmatrix} = 0 \,. \tag{8.196}$$

Its determinant is

$$D_2(\zeta) = \tfrac{1}{4}[\zeta(4\zeta^2 + 3) + \lambda(4\zeta^2 + 1)] \,. \tag{8.197}$$

Let us multiply this with

$$\hat{D}_2(\zeta) \equiv \tfrac{1}{4}[\zeta(4\zeta^2 + 3) - \lambda(4\zeta^2 + 1)] \,, \tag{8.198}$$

obtaining

$$D_2(\zeta)\hat{D}_2(\zeta) = \tfrac{1}{16}[\zeta^2(4\zeta^2 + 3)^2 - (1 + \zeta^2)(4\zeta^2 + 1)^2] = -\tfrac{1}{16} \neq 0 \,. \tag{8.199}$$

Hence also $D_2(\zeta) \neq 0$ for all $\zeta \in \mathbb{C}$.

We conclude that the only solution that satisfies the boundary conditions is the trivial one ($a_i = 0 \, \forall i$), and thus we have proven a necessary condition for well-posedness of the IBVP in the high-frequency limit.

It should be stressed that the above *determinant condition* is necessary but not sufficient for well-posedness. If the boundary conditions are algebraic, a stronger condition called the *Kreiss condition* [93] is sufficient: the IBVP is well-posed if the determinant of the coefficient matrix is uniformly bounded away from zero for $\mathrm{Re}(\zeta) \geqslant 0$. This condition is not satisfied in our example, as equation (8.195) clearly shows. Even if the Kreiss condition is satisfied, this does not guarantee well-posedness of the IBVP if the boundary conditions are differential as in our case. A counter-example can be found in [117]. Furthermore, we have only investigated the limit of high-frequencies. There could well be an instability for low frequencies where the source terms may not be neglected.

In the above analysis, we have assumed that the shift vector vanishes. The algebra in the dynamical shift case turns out to be considerably more complicated – the system of ODEs no longer decouples into simple 2×2 blocks as in equations (8.167–8.173). A REDUCE programme has been written to carry out the calculation in this case. Of course, the twist subsystem is unchanged. Remarkably, the determinant of the coefficient matrix for the remaining system turns out to be (up to a constant factor) again D_1 defined above (8.195)! Hence the same stability result applies in the dynamical shift case.

8.7 Numerical experiments

In the preceding sections, we have developed three different sets of boundary conditions:

- absorbing boundary conditions (section 8.2.2)
- dissipative boundary conditions with zero Z vector (section 8.2.3)
- differential boundary conditions (the combination of sections 8.3, 8.4 and 8.5)

We now perform some numerical experiments to assess the performance of these boundary conditions in practice. The ideal boundary conditions would be numerically stable (i.e., no "blow-up" of the numerical solution occurs) and they would minimize spurious reflections. These originate when the wave arrives at the outer boundaries. The reflections then propagate in and grow in amplitude as a consequence of cylindrical polar coordinates (the time-reverse, an outgoing wave, loses amplitude as it travels out in these coordinates). The maximum of the reflections occurs when they reach the origin, i.e., approximately two light-crossing times after the pulse is emitted from the origin.

To measure the reflections, we use the exact linearized solutions of chapter 7 as a test problem and monitor the numerical error. The three test problems we look at are

- the even-parity non-twisting quadrupole solution (section 7.3.1) evolved with vanishing shift
- the same evolved with dynamical shift

- the even-parity twisting octupole solution (section 7.4; here the shift does not enter the linearized evolution equations)

For all the runs, the resolution is taken to be 32 points in both spatial dimensions and the outer boundaries are placed at $r_{\max} = z_{\max} = 5$. The mode functions are of the form (7.105) with amplitudes $F_0 = G_0 = 10^{-4}$. The outer boundaries are not very far out compared with the width of the initial pulse (≈ 1) and the resolution is rather low, but this suffices for our purposes here. The amplitude of the reflections decreases approximately linearly as $r_{\max}$ and $z_{\max}$ are increased and it is nearly independent of the resolution. The qualitative comparisons we draw between the different boundary conditions below are robust under changes of these parameters.

8.7.1 Numerical method

The interior grid points are evolved in the same way as in section 7.5. In particular, fourth-order numerical dissipation is added at all interior points unless otherwise stated. This implies that we need two layers of ghost cells at each boundary.

In all cases, the outgoing and zero-speed characteristic variables $\mathbf{v}^+$ are computed from the conserved variables $\mathbf{u}$ at the outermost interior cells and are linearly extrapolated to the ghost cells.

For the dissipative (absorbing and zero-Z) boundary conditions, the incoming modes at the ghost cells are then set in terms of the outgoing and zero-speed modes there using the dissipative boundary conditions ((8.44) or (8.46–8.49), respectively). Finally the ghost cells are transformed back to conserved variables.

The differential boundary conditions have the form (we write out the

r-direction, the z-direction follows by symmetry)

$$\partial_r v^- = \partial_z f + s \tag{8.200}$$

and are discretized as described in section 4.1.3, equation (4.23). We have also implemented the second-order discretization (4.26) but in the cases in which the boundary conditions were unstable, the instability showed up earlier when using that discretization.

8.7.2 Numerical results

The quadrupole solution with vanishing shift. Consider first the non-twisting quadrupole solution (section 7.3.1) evolved with vanishing shift vector. Figure 8.1 shows the L^2 norm of the error for the variable s and the constraint θ (the qualitative results are similar for the remaining variables).

As expected, the reflection-induced peak of the error occurs after two light-crossing times, at $t \approx 10$. The zero-Z dissipative boundary conditions cause much stronger reflections than the absorbing boundary conditions, particularly for the constraints. This is somewhat surprising because we argued in section 8.2.3 that the zero-Z boundary conditions are satisfied by the exact solution, in contrast to absorbing ones. However, the zero-Z boundary conditions are not constraint-preserving and are indeed highly reflective because they form Dirichlet conditions for the wave equation (8.99). Both types of dissipative boundary conditions (absorbing and zero-Z) are stable.

The differential boundary conditions perform best in minimizing the reflections. However, at late times ($t \gtrsim 20$) the error begins to grow exponentially. In an attempt to cure this instability, we tried applying second-order dissipation (4.69) instead of fourth-order dissipation (4.64) near the boundaries (at the outermost interior cells and along the first ghost layer). This

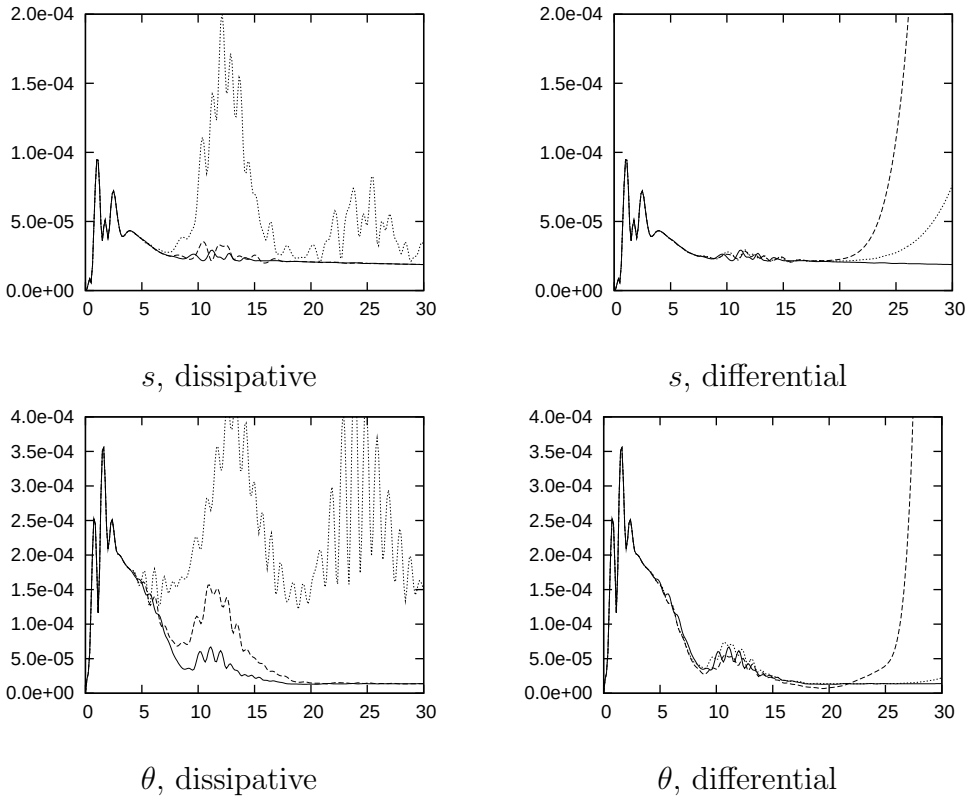

Figure 8.1: Test of boundary conditions for the quadrupole solution with vanishing shift. L^2 norm of the error as a function of time for the variables s (top panels) and θ (bottom panels). Left panels: absorbing (dashed) and zero-Z (dotted) boundary conditions, right panels: differential boundary conditions without (dashed) and with (dotted) modified dissipation near the boundaries. For comparison, the solid lines show the error if the exact solution is imposed at the boundaries.

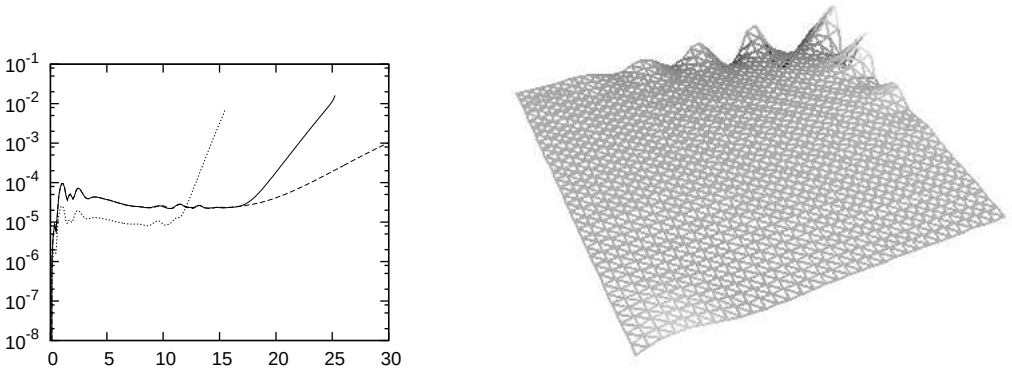

(a) (b)

Figure 8.2: Instability of the differential boundary conditions (quadrupole solution with vanishing shift). (a) L^2 norm of the error as a function of time for the variable s. Solid line: without modified dissipation near the boundaries, dashed line: with modified dissipation near the boundaries, dotted line: same as solid line but with twice the resolution. (b) The variable s at $t = 25$.

postponed the blow-up to a later time but could not eliminate it completely (see the right half of figure 8.1).

In order to determine the nature of the instability, we performed the same evolution again but with twice the resolution. Figure 8.2a shows that the instability sets in earlier and with a higher exponential growth rate. The ratio of the growth rates is found to be 2.00 ± 0.02. This suggests that the numerical solution behaves like $\sim \exp(at/h)$ at late times. The dependence on the grid spacing h means that the instability is not present in the continuum problem but is caused by the finite-differencing used. Modified second-order dissipation near the boundaries reduces the growth rate but cannot eliminate the instability (for no value of $0 \leqslant \epsilon_D \leqslant 1$). So far we have not found a stable discretization. Figure 8.2b indicates that the instability might emanate from the outer corner. A more careful treatment of the discretization at the corner

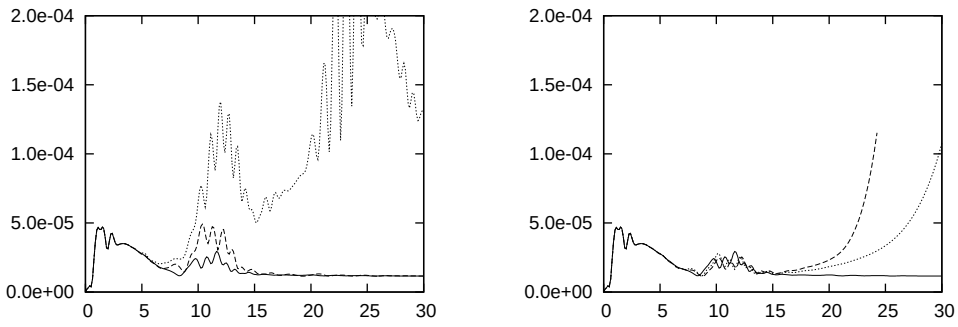

s, dissipative s, differential

Figure 8.3: Test of boundary conditions for the quadrupole solution with dynamical shift. L^2 norm of the error as a function of time for the variable s. Left panel: absorbing (dashed) and zero-Z (dotted) boundary conditions. Right panel: differential boundary conditions without (dashed) and with (dotted) modified dissipation near the boundaries. The solid lines show the error if the exact solution is imposed at the boundaries.

will be required (one-sided differences are used in (4.23)).

The quadrupole solution with dynamical shift. The results for the evolution with a dynamical shift vector are similar (figure 8.3). With regard to the avoidance of reflections, the differential boundary conditions perform better than the absorbing ones, which in turn are better than the zero-Z dissipative boundary conditions. (We do not display the constraint θ here because it is affected by the linear drift of the error (section 7.5) and differences between the boundary conditions are hardly visible.) Again, a late-time instability occurs for the differential boundary conditions, which can be postponed but not eliminated by modifying the numerical dissipation near the boundaries.

The twisting octupole solution. The twisting octupole solution (section 7.4) is the only test problem for which the zero-Z dissipative boundary con-

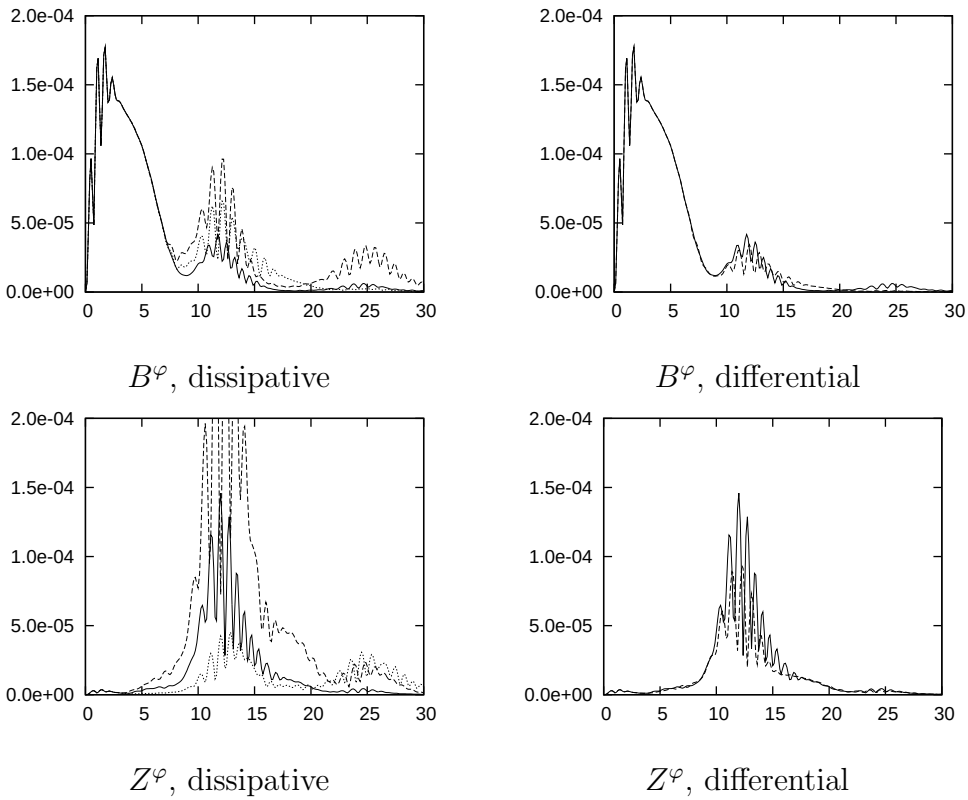

Figure 8.4: Test of boundary conditions for the octupole solution. L^2 norm of the error as a function of time for the variables B^φ (top panels) and Z^φ (bottom panels). Left panels: absorbing (dashed) and zero-Z (dotted) boundary conditions. Right panels: differential boundary conditions (dashed). The solid lines show the error if the exact solution is imposed at the boundaries.

ditions outperform the absorbing ones (figure 8.4). The differential boundary conditions are about as good, and in this case they are also stable.

8.7.3 Conclusions

We conclude that in all cases, the differential boundary conditions do the best job in reducing reflections from the outer boundaries. However, their non-twisting part suffers from a late-time instability, which appears to be caused

by the particular discretization that is currently used. For the time being, the differential boundary conditions cannot be used in numerical simulations, at least not for a long time (one might switch to more stable boundary conditions at late times, see section 9.2).

As expected, the boundary conditions of dissipative type are stable in all cases. With regard to reflections, absorbing boundary conditions clearly outperform the zero-Z ones for the nontwisting subsystem. For the twist subsystem, the zero-Z boundary conditions are marginally better.

In section 9.2, the boundary conditions are further tested from the point of view of mass conservation.

Chapter 9

Adaptive evolutions of nonlinear generalized Brill waves

The numerical evolutions with the Z(2+1)+1 system presented so far were all linear. In this final chapter, we turn to nonlinear evolutions of axisymmetric gravitational waves in vacuum. A nonzero twist is included and hence we refer to the problem investigated here as *generalized Brill waves*.

We begin by explaining our choices of initial data and gauge in section 9.1. The pros and cons of the different gauge conditions are discussed and the need for adaptive mesh refinement (AMR) is demonstrated. A 3-grid convergence test is performed in section 9.2, indicating the accuracy of our implementation. Once we form a black hole in supercritical Brill wave evolutions, we would like to detect it, and so we describe our method of finding apparent horizons in section 9.3. Our results on adaptive evolutions of both sub- and supercritical generalized Brill waves are presented in section 9.4.

9.1 Initial data and gauge choices

Our method of generating initial data is similar to the formalism used in chapter 5. We take the initial 2-metric to be conformally flat,

$$H_{AB} = \psi^4 \delta_{AB} \,. \tag{9.1}$$

Free data is prescribed for the Z(2+1)+1 variables[1] s, α and

$$\hat{B}^\varphi \equiv \psi^{9/2} B^\varphi \,. \tag{9.2}$$

We choose Gaussian profiles

$$\begin{aligned} s &= -A_s \, r \, \exp\left[-(\tfrac{r}{\sigma_{r,s}})^2 - (\tfrac{z}{\sigma_{z,s}})^2\right] , & (9.3)\\ \hat{B}^\varphi &= A_B \, rz \, \exp\left[-(\tfrac{r}{\sigma_{r,B}})^2 - (\tfrac{z}{\sigma_{z,B}})^2\right] , & (9.4)\\ \alpha &= 1 - A_\alpha \exp\left[-(\tfrac{r}{\sigma_{r,\alpha}})^2 - (\tfrac{z}{\sigma_{z,\alpha}})^2\right] . & (9.5) \end{aligned}$$

Note that the factors of r and z have to be included for the correct behaviour at small r and z (as before, we impose reflection symmetry about $z = 0$). Unless otherwise stated, we take all the widths σ to be 1 and $A_\alpha = 0$. The variables χ_{AB}, Y and E^A are chosen to vanish initially. As already mentioned in section 5.7, this initial data is more general than Brill's orginial one [32] (which has zero twist, $A_B = 0$) but is still time-symmetric, so that the term *generalized Brill waves* is justified.

The momentum constraints (3.51) and the Geroch constraint (3.52) are automatically satisfied for this choice of initial data. The Hamiltonian constraint (3.50) takes the form

$$\begin{aligned} 0 &= \psi_{,rr} + \psi_{,zz} + (s + rs_{,r} + r^{-1})\psi_{,r} + rs_{,z}\psi_{,z} \\ &\quad + \tfrac{1}{4}[rs_{,rr} + 4s_{,r} + 2r^{-1}s + (s + rs_{,r})^2 + rs_{,zz} + r^2 {s_{,z}}^2]\psi \\ &\quad + \tfrac{1}{16} r^2 \mathrm{e}^{2rs} {\hat{B}^\varphi}^2 \,. \end{aligned} \tag{9.6}$$

[1] Note that the Z(2+1)+1 definition of s differs from the one in chapter 5 by a minus sign.

This elliptic equation is solved for the conformal factor ψ using Multigrid (section 4.3). Note that the variable B^φ has been conformally rescaled (9.2). Otherwise B^φ would be multiplied with a positive power of ψ in (9.6), the equation would not be linearization-stable, and Multigrid would fail to converge (cf. section 5.5). After solving the Hamiltonian constraint, the original variable B^φ is formed and the derivatives of the 2-metric are computed numerically.

Next the question arises which gauge in the family of generalized harmonic gauge conditions (section 6.2) one should use in order to evolve this initial data. The vanishing shift case and the dynamical shift case turn out to behave in a completely different way, as illustrated by figure 9.1: whereas the variables clearly show a wavelike behaviour and eventually assume their flat-space values in the dynamical shift case, they settle down to a non-trivial static solution in the vanishing shift case (we shall see below that this is also Minkowski space, but in non-standard coordinates). A similar residual "lump of gauge" for harmonic slicing with zero shift has also been reported by Eppley [49]. The explanation for this lies in the fact that in pure harmonic gauge (i.e., including a dynamical shift), all the variables obey the wave equation to principal parts (section 6.2), which does not hold in the vanishing shift case. The linear evolutions in chapter 7 were wavelike even for vanishing shift only because the initial data was taken to be that of the exact solution. It is not clear which restrictions one has to impose on general initial data such that this property extends to the nonlinear case. These difficulties were our main motivation for adding dynamical shift conditions to our original paper [119].

In order to convince ourselves that the final state of the vanishing-shift evolution is indeed Minkowski space, we need to compute the curvature. A

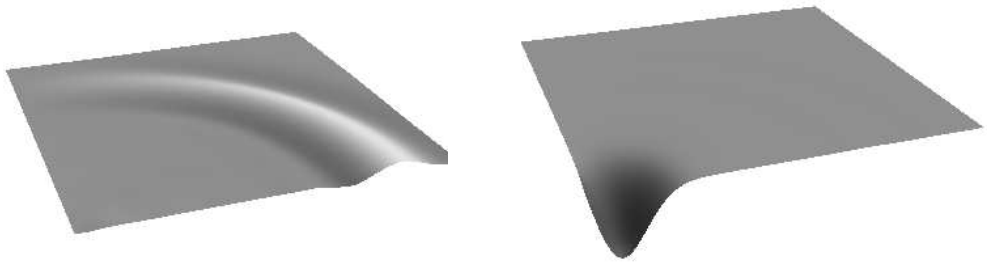

(a) dynamical shift (b) vanishing shift

Figure 9.1: The variable s at time $t = 8.75$ for a Brill wave with amplitudes $A_s = 1$ and $A_B = 0$ using harmonic gauge with (a) dynamical and (b) vanishing shift vector (gauge parameters $f = d = \mu = a = 1$, $m = 2$). Single grid with 64 points in each dimension, $r_{\max} = z_{\max} = 5$.

useful quantity to look at is the *Kretschmann scalar*

$$I \equiv {}^{(4)}R_{\alpha\beta\gamma\delta}{}^{(4)}R^{\alpha\beta\gamma\delta} \tag{9.7}$$

evaluated at the origin $r = z = 0$, where we expect the curvature to be maximal. To simplify the calculation, one can first note that when computing the Riemann tensor for a general metric of the form (2.26) and finally setting $r = 0$, the φt, φr and φz components do not contribute. We also assume that the shift vanishes. Hence we consider the metric

$$g_{\alpha\beta} = \begin{pmatrix} -\alpha^2 & 0 & 0 & 0 \\ 0 & H_{rr} & H_{rz} & 0 \\ 0 & H_{rz} & H_{zz} & 0 \\ 0 & 0 & 0 & r^2 H_{rr} \mathrm{e}^{2rs} \end{pmatrix} . \tag{9.8}$$

For this we compute the Riemann tensor directly using REDUCE, substituting the evolution equations for the time derivatives. The resulting expression

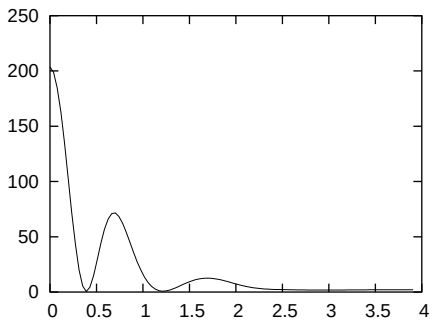

Figure 9.2: The Kretschmann scalar I as a function of time for a Brill wave with amplitudes $A_s = 1$ and $A_B = 0$ using harmonic slicing with vanishing shift.

is manifestly regular. It contains up to second-order spatial derivatives of the metric, i.e., first-order derivatives of the first-order variables (6.51–6.53). To second order in the grid spacing h, it is consistent to evaluate I at the innermost grid point $r = z = h/2$ and to set $u_{,r} = 0$ for a variable that is even in r and $u_{,r} = 2u/h$ for a variable that is odd in r (and similarly for z). Figure 9.2 shows that I for the above evolution starts off at a large value of ≈ 200, then drops rapidly and after a few bounces settles down at a constant small value of ≈ 2 (this is mainly determined by the time step and decays as it is decreased). This suggests that the curvature of the final state indeed vanishes.

Unexpected difficulties occur for strong waves (amplitudes $A_s \gtrsim 3$, irrespective of A_B). In the dynamical shift case, the solution blows up exponentially as the waves travel out. The first variables to grow are the constraints θ, Z_r, Z_z, and soon after all the remaining variables are affected. The blow-up occurs at $z = 0$ (where most of the variables have their extrema), well away from the axis $r = 0$. We have checked that the location and growth rate are essentially unchanged as the resolution is increased. Hence it is likely that we are faced with a continuum instability.

Motivated by work of Brodbeck et al. [33], Gundlach et al. [70] have recently proposed the addition of *constraint-damping* terms to the Z4 equations (6.1),

$$R_{\alpha\beta} + 2\nabla_{(\alpha} Z_{\beta)} - \kappa_{\rm CD}(2n_{(\alpha} Z_{\beta)} - g_{\alpha\beta} n^\gamma Z_\gamma) = 0\,, \tag{9.9}$$

where n_α is the unit timelike normal to the foliation and $\kappa_{\rm CD} > 0$ is a constant. After performing the Geroch and ADM reductions, this implies that we should add the following terms to the right-hand-sides of the Z(2+1)+1 equations:

$$\mathcal{L}_n\theta = \ldots - 2\kappa_{\rm CD}\,\theta\,, \tag{9.10}$$

$$\mathcal{L}_n Z_A = \ldots - \kappa_{\rm CD}\, Z_A\,, \tag{9.11}$$

$$\mathcal{L}_n Z^\varphi = \ldots - \kappa_{\rm CD}\, Z^\varphi\,, \tag{9.12}$$

$$\mathcal{L}_n \chi_{AB} = \ldots - \kappa_{\rm CD}\,\theta H_{AB}\,. \tag{9.13}$$

The authors of [70] showed that in the high-frequency (or geometrical optics) approximation, all constraints are damped exponentially if the damping terms are included, except modes that are constant in space. Recently, constraint damping has been used successfully in binary black hole simulations [112]. However, we found that it could not eliminate the blow-up in the gravitational wave evolutions with dynamical shift considered here, for any value of $\kappa_{\rm CD}$. It should be stressed that the analysis in [70] is only valid for high-frequency constraint violations. It is unclear if the inclusion of such damping terms renders the constraint manifold $Z_\alpha = 0$ an attractor if the wavelength of the constraint violations becomes comparable with the curvature scale, as is expected in nonlinear gravitational wave evolutions. We have also tried eliminating all nonlinear couplings with the Z vector in the source terms of the Z(2+1)+1 equations, again without any improvements. Hence harmonic gauge with dynamical shift appears to be unusable for the problem at hand.

One is faced with a different obstruction when using a vanishing shift vector: the occurrence of steep gradients and highly distorted waves. This is not surprising if we recall that the *coordinate* characteristic speeds depend on the spatial metric: the *physical* speeds in section 6.4 were computed for the projection of the flux vector along the *unit* normal to the boundary, $\mathcal{F}^{\perp} = \mathcal{F}^{A}\mu_{A}$. For the $r = r_{\max}$ boundary, for example, $\mu_{A} = \delta_{A}{}^{r}/\sqrt{H^{rr}}$. Hence the coordinate speeds in the r-direction (corresponding to the r-component of the flux vector, $\mathcal{F}^{r}$) are obtained from the physical speeds by multiplying with $\sqrt{H^{rr}}$. If the metric is wavelike as in the dynamical shift case, then it is essentially constant when averaged in time, and the characteristic speeds should be uniform across the grid on average. If however the metric is essentially static and non-constant as in the vanishing shift case, then there can well be regions in which the characteristics converge (signals to the left travel faster than those to the right for a right-moving wave), and steep gradients can build up.

It has been claimed by Alcubierre [4, 8, 5] that under certain circumstances, true discontinuities can develop when using hyperbolic gauge conditions, so-called *gauge shocks*. Our results strongly suggest that this is not the case in our problem, provided that we choose the gauge parameter to be $f = 1$. We do observe a steep gradient in the profile of the lapse function α, or equivalently, a sharp peak in the variable $A_{r} = \alpha^{-1}\alpha_{,r}$, which travels out at the speed of light. However, if we switch on the adaptive mesh refinement (section 4.5) and sufficiently refine the region around the gradient, we can show that the peak is completely smooth (figure 9.3). Its height increases as one increases the amplitude A_{s}. We have checked that the peak is well-resolved during the entire evolution even for for the largest amplitudes considered in section 9.4. This would not be possible on a single coarse

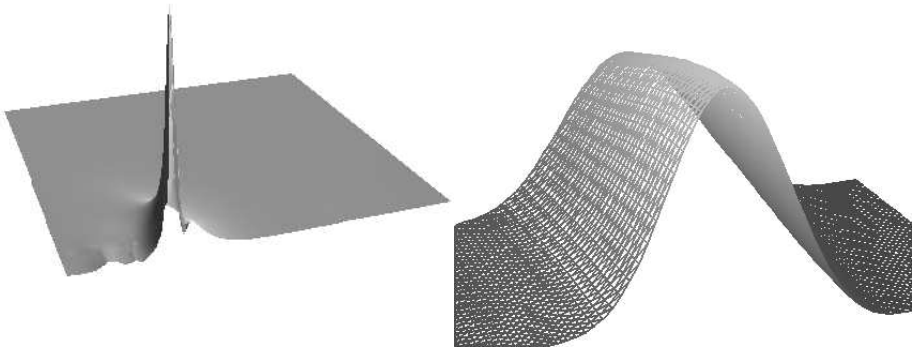

(a) (b)

Figure 9.3: The variable $A_r = \alpha^{-1}\alpha_{,r}$ at time $t = 1.72$ when the spike reaches its maximum height, for a Brill wave with amplitudes $A_s = 4$ and $A_B = 0$, using harmonic slicing with vanishing shift. (a) shows the base grid, (b) the finest grid containing the spike. The base grid resolution is 64 points and 4 levels of refinement are added.

grid: there the feature *looks* like a "delta-function" and the finite-difference code would crash because of the Gibbs oscillations that this causes. Hence adaptive mesh refinement appears to be crucial in order to be able to evolve radiative spacetimes with harmonic slicing and zero shift. Preliminary results indicate that for parameters $f \neq 1$, the peak in the gradient of the lapse becomes narrower and narrower during the evolution, which ultimately crashes the code. This is in agreement with the work of Alcubierre, who showed that generalized harmonic slicing will always develop gauge shocks for $f < 1$.

9.2 Convergence test

Unlike in linearized theory, no exact solutions are known for nonlinear Brill waves and so the method of testing the convergence of the code used in

section 7.5 is not applicable. However, we can perform a 3-grid convergence test based on Richardson extrapolation. As explained in section 4.5, we estimate the error $\mathbf{e}^h$ on a grid G^h with grid spacing h by

$$\mathbf{e}^h \approx \tfrac{1}{3}(\mathbf{u}^{2h} - \mathbf{u}^h)\,, \tag{9.14}$$

where $\mathbf{u}^h$ denotes the numerical approximation on G^h. This involves interpolating the approximation from G^{2h} to G^h, and it is important to use an interpolation scheme that is more than second-order accurate in order not to affect the leading order of the error estimate (we use biquadratic interpolation). Similarly, we can estimate the error on G^{2h} by

$$\mathbf{e}^{2h} \approx \tfrac{1}{3}(\mathbf{u}^{4h} - \mathbf{u}^{2h})\,. \tag{9.15}$$

For a second-order accurate code, the ratio of the errors should be

$$\|\mathbf{e}^{2h}\|/\|\mathbf{e}^h\| \approx 4\,, \tag{9.16}$$

where we use the discrete L^2 norm and all variables are summed over.

We evolve a twisting Brill wave with amplitudes $A_s = A_B = 1$ using harmonic slicing ($f = 1$, $m = 2$) with vanishing shift. The coarsest grid has a resolution of 32 points, with the outer boundaries placed at $r_{max} = z_{max} = 5$. The Courant number is taken to be 0.5. First we can check that the initial data solver works correctly. The estimated errors on the two finest grids obtained via Richardson extrapolation are 9.91×10^{-3} and 2.25×10^{-3}, yielding a ratio of 4.40. The constraint residuals (evaluated independently from the Multigrid solver) are 5.11×10^{-2}, 1.28×10^{-2} and 3.23×10^{-3}, with ratios 3.99 and 3.96. This is perfectly second-order convergent. Next we look at the evolution of the errors and constraints. Figure 9.4 shows the estimated errors as well as the residuals of the Einstein constraints (3.50–3.52), the Z constraints $\theta = Z_r = Z_z = Z^\varphi = 0$ and the differential constraints associated with the

definitions of the first-order variables (6.51–6.53). The results indicate not perfect, but approximate second-order convergence up to one light-crossing time ($t = 5$). At this point we switched from differential boundary conditions to absorbing ones (chapter 8) in order to avoid the instability of the former at late times. This leads to a loss of convergence and an increase particularly of the constraint residuals – this is what we expect because the absorbing boundary conditions are not constraint-preserving. However, we do achieve a stable evolution in this way.

A useful quantity to monitor during the evolution is the *ADM mass*, the mass of an asymptotically flat spacetime measured at spacelike infinity. This can be derived by writing the Hamiltonian constraint (3.50) in linearized theory in conservation form

$$\kappa\rho = \tilde{\nabla}_A J^A \,, \tag{9.17}$$

where $\tilde{\nabla}$ denotes the flat-space connection and the current J^A is given in our variables by

$$J^r = -D_{rrr} - D_{rzz} + D_{zrz} - r^2\tilde{s}_r - 3s \,, \tag{9.18}$$

$$J^z = r\tilde{D}_{rrz} - 2D_{zrr} + r^{-1}H_{rz} - rs_z \,. \tag{9.19}$$

The ADM mass is then defined by an integral over a 2-surface S_∞ at spacelike infinity,

$$M_{\rm ADM} = \kappa^{-1}\int_{S_\infty} J^A \mathrm{d}^2 S_A \,, \tag{9.20}$$

$\mathrm{d}^2 S_A$ denoting the area element on S_∞. We choose the S_∞ to be aligned with the grid boundaries,

$$M_{\rm ADM} = \lim_{r_0,z_0\to\infty} \tfrac{1}{2}\left(\int_0^{r_0} rJ^z \mathrm{d}r\big|_{z=z_0} + r_0\int_0^{z_0} J^r \mathrm{d}z\big|_{r=r_0}\right) . \tag{9.21}$$

We have verified that we obtain the same result for the ADM mass if we start from the standard expression found in the literature [102], which is

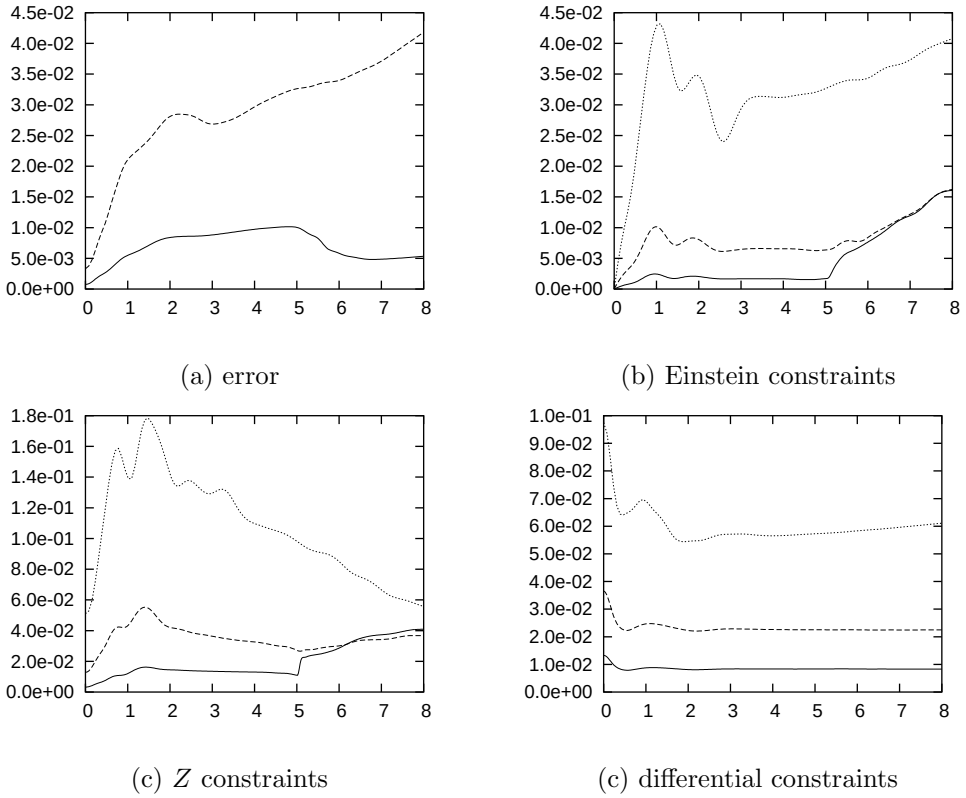

(a) error (b) Einstein constraints

(c) Z constraints (c) differential constraints

Figure 9.4: 3-grid convergence test for a Brill wave with $A_s = A_B = 1$. The resolutions are 32 points (dotted), 64 points (dashed) and 128 points (solid) per dimension. Shown are as functions of time the L^2 norms of (a) the estimated error on the two finest grids; (b) the Einstein constraints, (c) the Z constraints and (d) the differential constraints on all three grids.

only valid in *Cartesian* coordinates, and carefully transform it to cylindrical polar coordinates.

In the numerical implementation, we evaluate the integrals in (9.21) at $r_0 = 0.9 r_{\max}$, $z_0 = 0.9 z_{\max}$ (a few grid points away from the outer boundaries in order to reduce the influence of possible reflections). One would expect the ADM mass to be constant until the wave reaches the outer boundaries of the computational domain and to drop afterwards. This is confirmed by figure 9.5a, which shows the ADM mass as a function of time on the three

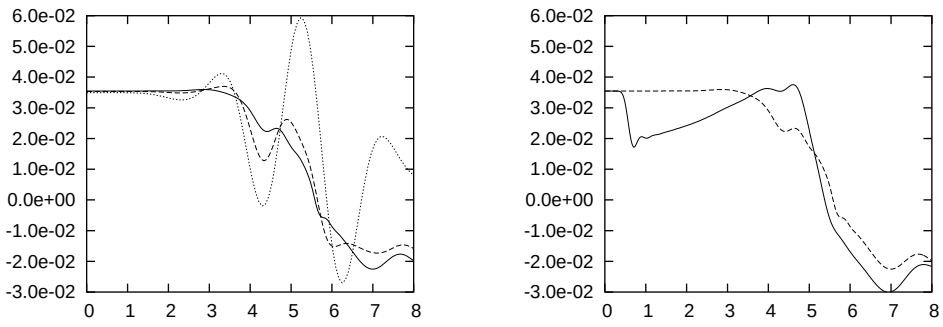

Figure 9.5: The ADM mass as a function of time for a Brill wave with $A_s = A_B = 1$. (a) 3-grid convergence test as in figure 9.4, (b) absorbing (solid) vs. differential (dashed) boundary conditions on the finest grid.

grids. The higher the resolution, the longer the mass is conserved. In order to study the influence of the boundary, we perform another run with twice the domain size, leaving the surface of integration (the "detector") at the same location (figure 9.6). This shows that the initial drop of the numerically evaluated ADM mass at $t \approx 4$ is indeed caused by the wave passing through the detector rather than by reflections from the boundary. However, the (unphysical) negative value of the ADM mass at $t \gtrsim 6$ appears to be a boundary effect – this is less severe in the run with twice the domain size.

It turns out that the ADM mass is extremely sensitive to the outer boundary conditions we impose, and we can use this to assess the various choices of boundary conditions that are available. Figure 9.5b shows that the differential boundary conditions of chapter 8 perform very well in this respect but that absorbing boundary conditions are not very mass-conserving at all. This is what we expect because the differential boundary conditions are designed such that no incoming radiation enters the domain from the outside, whereas this does not hold for absorbing boundary conditions. For this reason, we

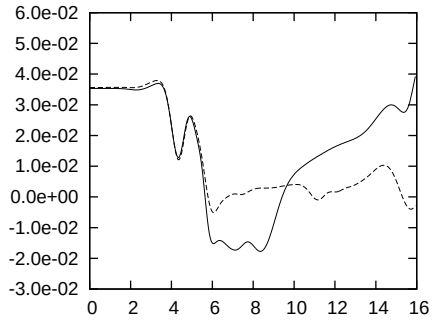

Figure 9.6: Dependence of the numerically evaluated ADM mass on the location of the outer boundary for a Brill wave with $A_s = A_B = 1$. Solid line: $r_{\max} = z_{\max} = 5$, dashed line: $r_{\max} = z_{\max} = 10$. In both cases, the integral (9.21) is evaluated at $r_0 = z_0 = 4.5$. The resolution is 64 points per dimension and differential boundary conditions are used.

henceforth use differential boundary conditions as long as we can and switch to absorbing ones at late times just before the instability sets in.

9.3 Apparent horizon finder

Once a black hole has formed in our numerical spacetime, we would like to be able to detect it. An indication of black hole formation is the existence of *trapped surfaces*, i.e., closed two-surfaces whose outgoing null geodesics have zero expansion ("light cannot escape"). The outermost[2] trapped surface in a given spacelike slice is called the *apparent horizon*. Since only the data on a given spacelike slice is required, apparent horizons can be determined at each time step during a numerical simulation.

The *(future) event horizon* is defined to be the boundary of the causal past of future null infinity. This is a global property of spacetime: in contrast

[2]It can be very difficult to verify that a trapped surface is the outermost one. Often the terms "apparent horizon" and "trapped surface" are used synonymously.

to an apparent horizon, the event horizon can only be determined if the entire future development of the given slice is known, i.e., at the end of a numerical simulation.

Under certain technical assumptions, the existence of an apparent horizon implies the existence of an event horizon containing the apparent horizon in its interior [79]. Unfortunately, the converse is not true: one can construct slicings of Schwarzschild spacetime such that there is no apparent horizon [139], although an event horizon does of course exist. However, generally an apparent horizon is a good approximation to the event horizon. In particular, the two coincide in stationary spacetimes.

In the following, we shall focus on apparent horizons and derive an equation determining the horizon in the $(2+1)+1$ formalism.

Suppose we are given an apparent horizon $\mathcal{H}$ on a *three*-dimensional spacelike hypersurface ${}^{(3)}\Sigma$. Let s^α be the outward-pointing unit normal to the horizon, ${}^{(3)}g_{\alpha\beta}$ the metric on ${}^{(3)}\Sigma$,

$$ {}^{(3)}g_{\alpha\beta} = g_{\alpha\beta} + n_\alpha n_\beta \,, \tag{9.22} $$

${}^{(3)}\nabla$ the covariant derivative of that metric, and ${}^{(3)}K_{\alpha\beta}$ the second fundamental form,

$$ {}^{(3)}K_{\alpha\beta} = -{}^{(3)}g_\alpha{}^\gamma \, {}^{(3)}g_\beta{}^\delta \, n_{(\gamma;\delta)} \,. \tag{9.23} $$

From the unit spatial normal s^α to the horizon and the unit timelike normal n^α to ${}^{(3)}\Sigma$, we can construct the future-pointing outgoing null vector field

$$ l^\alpha = n^\alpha + s^\alpha \,. \tag{9.24} $$

The expansion Θ of the null vectors is given by the (four-)divergence of l^α projected into the hypersurface $\mathcal{H}$,

$$ \Theta = ({}^{(3)}g^{\alpha\beta} - s^\alpha s^\beta)\nabla_\beta l_\alpha \,. \tag{9.25} $$

Substituting (9.24) into (9.25) and using the definition of the second fundamental form (9.23), we obtain [145]

$$\Theta = {}^{(3)}\nabla_\alpha s^\alpha + {}^{(3)}K_{\alpha\beta}s^\alpha s^\beta - {}^{(3)}K\,. \tag{9.26}$$

For an apparent horizon, this quantity has to vanish.

We would like to write equation (9.26) in $(2+1)+1$ form. The first term on the right-hand-side can be rewritten as

$${}^{(3)}\nabla_\alpha s^\alpha = \mathrm{d}_A s^A + \lambda^{-1}s^A\partial_A\lambda\,. \tag{9.27}$$

Using the definitions of ${}^{(3)}K_{\alpha\beta}$ (9.23) and $\chi_{\alpha\beta}$ (3.36), we can express ${}^{(3)}K_{\alpha\beta}$ in terms of $(2+1)+1$ quantities:

$${}^{(3)}K_{\alpha\beta} = \chi_{\alpha\beta} + \lambda^{-2}\xi_{(\alpha}\epsilon_{\beta)\gamma}\omega^\gamma + \lambda^{-2}\xi_\alpha\xi_\beta K_\varphi{}^\varphi\,. \tag{9.28}$$

Hence we obtain the *apparent horizon equation* in $(2+1)+1$ form,

$$\mathrm{d}_A s^A + \lambda^{-1}s^A\partial_A\lambda + \chi_{AB}s^As^B - \chi - K_\varphi{}^\varphi = 0\,, \tag{9.29}$$

which is clearly an equation in $\mathcal{N}$.

Since the horizon is a closed *curve* in ${}^{(3)}\Sigma\cap\mathcal{N}$, we can parametrize its coordinates as $x^A = x^A(\tau)$. The horizon normal is then given by

$$s^A = NH^{AB}\epsilon_{BC}\frac{\mathrm{d}x^C}{\mathrm{d}\tau}\,,\quad N \equiv \left(H_{AB}\frac{\mathrm{d}x^A}{\mathrm{d}\tau}\frac{\mathrm{d}x^B}{\mathrm{d}\tau}\right)^{-1/2}\,. \tag{9.30}$$

Let us also introduce the unit tangent to the horizon,

$$t^A = N\frac{\mathrm{d}x^A}{\mathrm{d}\tau}\,. \tag{9.31}$$

Clearly, $t^As_A = 0$. Differentiating that relation, we obtain

$$\begin{aligned} 0 &= \mathrm{d}_B(t^As_A) = s_A\mathrm{d}_Bt^A + t^A\mathrm{d}_Bs_A \\ \Rightarrow 0 &= t^Bs_A\mathrm{d}_Bt^A + t^Bt^A\mathrm{d}_Bs_A = t^Bs_A\mathrm{d}_Bt^A + H^{AB}\mathrm{d}_Bs_A\,, \end{aligned} \tag{9.32}$$

where in the last step we have used that the two-metric can be written as $H^{AB} = s^A s^B + t^A t^B$ and that $s_A s^A = 1$. Hence we find

$$\begin{aligned} d_A s^A &= -t^B s_A \mathrm{d}_B t^A = -t^B s_A \left(\partial_B t^A + \Gamma^A{}_{BC} t^C\right) \\ &= -N^3 \left[\epsilon_{AB} \frac{\mathrm{d}^2 x^A}{\mathrm{d}\tau^2} \frac{\mathrm{d}x^B}{\mathrm{d}\tau} + \epsilon_{AB} \frac{\mathrm{d}x^B}{\mathrm{d}\tau} \frac{\mathrm{d}x^C}{\mathrm{d}\tau} \frac{\mathrm{d}x^D}{\mathrm{d}\tau} \Gamma^A{}_{CD}\right] , \end{aligned} \tag{9.33}$$

which agrees with [104, eqn. $(2 \cdot 23)$].

In practice, we choose the parameter τ to be the spherical polar angle θ.[3] The cylindrical polar coordinates of the horizon are

$$x^1 \equiv r = R(\theta) \sin\theta \,, \quad x^2 \equiv z = R(\theta) \cos\theta \,, \tag{9.34}$$

where the spherical polar radius $R(\theta)$ is the unknown function we need to determine.

With these definitions, (9.29) becomes a nonlinear second-order ODE for $R(\theta)$,

$$f\big(\theta, R(\theta), R'(\theta), R''(\theta), \mathbf{u}(R(\theta), \theta)\big) = 0 \,. \tag{9.35}$$

Here $\mathbf{u}$ denotes the vector of (2+1)+1 variables. We require that the horizon be smooth on the axes, which implies Neumann boundary conditions

$$R'(0) = R'(\tfrac{\pi}{2}) = 0 \tag{9.36}$$

(note again that we impose reflection symmetry about $z = 0 \Leftrightarrow \theta = \frac{\pi}{2}$).

We cover the interval $[0, \frac{\pi}{2}]$ with a uniform cell-centred grid consisting of N_H points with grid spacing $h_H = \frac{\pi}{2N_H}$. Second-order accurate centred finite differences are used to discretize the derivatives of $R(\theta)$,

$$\begin{aligned} R'_i &\to \tfrac{1}{2h_H}(R_{i+1} - R_{i-1}) \,, \\ R''_i &\to \tfrac{1}{{h_H}^2}(R_{i+1} - 2R_i + R_{i-1}) \,, \end{aligned} \tag{9.37}$$

[3] This parametrization only works when the apparent horizon forms a star-shaped domain with respect to the centre.

where $1 \leqslant i \leqslant N_H$, and ghost cells are employed to implement the boundary conditions (9.36),

$$R_0 = R_1 \,, \qquad R_{N_H+1} = R_{N_H} \,. \tag{9.38}$$

The nonlinear two-point boundary value problem (9.35–9.36) is solved using the Newton-Raphson method. At each step of the iteration, we approximate the Jacobian matrix

$$J_{ij} = \frac{\partial f_i}{\partial R_j} \tag{9.39}$$

numerically by a difference quotient

$$J_{ij} \approx \tfrac{1}{2\Delta R} \left[f_i(R_j + \Delta R) - f_i(R_j - \Delta R) \right] \,. \tag{9.40}$$

Fortunately, the discretization (9.37–9.38) yields a tridiagonal Jacobian matrix, which can be solved exactly in $O(N_H)$ operations using the Thomas algorithm [109].

We have tested our apparent horizon finder for a Schwarzschild black hole of mass M in isotropic coordinates,

$$\mathrm{d}s^2 = -\left(\frac{M-2R}{M+2R}\right)^2 \mathrm{d}t^2 + \left(1+\frac{M}{2R}\right)^4 (\mathrm{d}r^2 + \mathrm{d}z^2 + r^2 \mathrm{d}\varphi^2) \,. \tag{9.41}$$

Its horizon is a sphere of radius $R = M/2$.

Figure 9.7 shows the convergence of the Newton iteration. Here we have chosen the mass to be $M = 4$ and the initial guess for the horizon to be a sphere of radius $R_0 = 1$. The algorithm converged for initial radii $R_0 \in [0.05, 4.5]$. One could probably enlarge the radius of convergence by including a line search in Newton's method [109]. The radius and rate of convergence turn out to depend crucially on the displacement ΔR used to evaluate the Jacobian matrix (9.40). The best performance was achieved by choosing $\Delta R \approx 0.5 {N_H}^{-1} R$. As seen in figure 9.7, the final error and residual settle down at a constant level after a few iterations. This is mainly determined

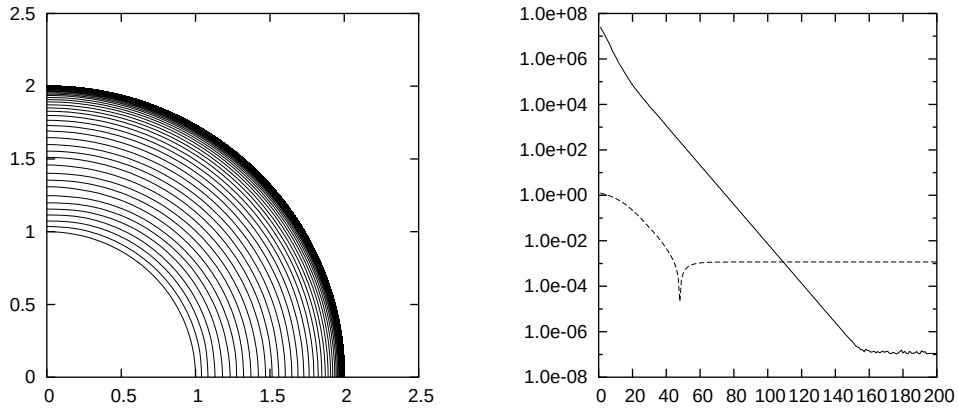

(a) (b)

Figure 9.7: Test of the apparent horizon finder for a Schwarzschild black hole of mass $M = 1$ and initial guess $R = 1$ for the horizon radius. The horizon grid resolution is 64 points, the data grid resolution 128 points in each dimension, with $r_{\max} = z_{\max} = 5$. Shown are (a) the approximation to the horizon shape after each Newton iteration and (b) the L^2 norms of the residual of the apparent horizon equation (solid) and the error with respect to the exact solution (dashed) as functions of the iteration number.

by the resolution of the grid holding the (2+1)+1 variables, from which the data is interpolated.

If a spacelike slice does not contain an apparent horizon, the approximation typically shrinks to a point and we stop the iteration once its radius is smaller than one grid spacing.

If an apparent horizon is found, one can compute the mass M of the black hole via the (proper) horizon area A_H: the area radius is defined as

$$R_A = \sqrt{\frac{A_H}{4\pi}} \tag{9.42}$$

and the horizon mass is then given by

$$M = \tfrac{1}{2} R_A \,. \tag{9.43}$$

The area can be calculated as

$$A_H = 2\pi \int_{\theta=0}^{\pi} \lambda \, \mathrm{d}s \,, \tag{9.44}$$

where λ is the norm of the Killing vector and $\mathrm{d}s$ is the line element of the horizon curve,

$$\mathrm{d}s^2 = H_{AB} \frac{\mathrm{d}x^A}{\mathrm{d}\theta} \frac{\mathrm{d}x^B}{\mathrm{d}\theta} \mathrm{d}\theta^2 \,. \tag{9.45}$$

For our test problem above, the algorithm determined the mass to be $M = 4.00014$, corresponding to a relative error of 3×10^{-5}.

One should remark here that formula (9.43) only holds for non-rotating black holes. For rotating black holes, it has to be replaced with

$$M = \frac{1}{2R_A} \sqrt{R_A^4 + 4J^4} \,, \tag{9.46}$$

where J is the angular momentum of the black hole (see e.g. [45] for a discussion in the isolated horizon framework). However, axisymmetric initial data on a spacelike slice Σ that does not contain any trapped surfaces has zero angular momentum in vacuum. (Angular momentum in axisymmetry can be defined in an unambiguous way by the Komar integral [90] associated with the Killing vector ξ,

$$J = \kappa^{-1} \oint_{\partial\Sigma} \mathrm{d}S_{\alpha\beta} \nabla^\alpha \xi^\beta \,, \tag{9.47}$$

and a little calculation shows that this vanishes in vacuum by virtue of the angular momentum or Geroch constraint (3.52)). Angular momentum conservation implies that if a black hole forms when evolving such initial data, it must also have zero angular momentum.

With regard to the relation between angular momentum and twist, one should note that a nonzero angular momentum implies a nonzero twist, but not the other way around.

9.4 Adaptive collapse simulations

In this final section, we present some evolutions of strong Brill waves close to the threshold of black hole formation. The initial data is taken to be that of section 9.1. We focus on non-twisting waves here ($A_B = 0$). Amplitudes A_s in the range $4 \leqslant A_s \leqslant 6$ are considered. The width of the pulse is taken to be $\sigma_{r,s} = \sigma_{z,s} = 1$. The same initial data was chosen (in a 3D code) by Alcubierre et al. [6] and (in an axisymmetric code) by Garfinkle and Duncan [62]. The former authors determined the critical amplitude of black hole formation to be $A_s^* = 4.85 \pm 0.15$ and the latter reported $4 \leqslant A_s^* \leqslant 6$.

The two codes used different gauge conditions (maximal slicing with zero shift vs. maximal slicing with Wilson shift (cf. section 5.1)) but the critical amplitude should of course be independent of the gauge. Our gauge condition is again different: we use harmonic slicing ($f = 1, m = 2$) with zero shift. It is found empirically that by choosing the initial lapse function to have a slight dip at the origin, $A_\alpha \sim 0.5$ in (9.5), the initial rise of the peak in the gradient A_r of the lapse function is less drastic (about half the growth rate), making it easier for the code to cope with this feature.

Adaptive mesh refinement is used with a refinement criterion based on truncation error estimation as described in section 4.5.3. A reasonable value for the threshold of the L^2 norm of the error appears to be 0.1. The largest values attained by the variables during the evolutions are of the order of 10^2 so that the threshold corresponds to a relative error of $\sim 10^{-3}$. We have also experimented with "ad hoc" refinement indicators such as a combination of the quantities $h^2 A_r$ and $h^2\theta$ (some power of the grid spacing h has to be included here so that the algorithm does not refine indefinitely). The first quantity ensures that the gauge peak is tracked during the evolution, the second one takes highly oscillatory features close to the origin into account

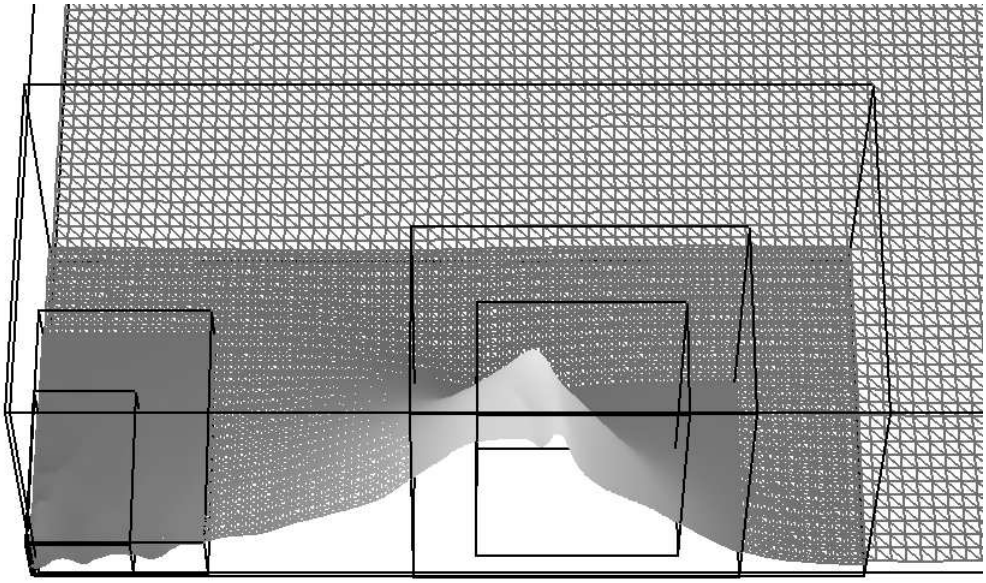

Figure 9.8: Typical AMR hierarchy in strong Brill wave evolutions: the variable Y at time $t \approx 3$ for the amplitude $A_s = 5$. Only a quarter of the base grid is shown. The high resolution region on the right coincides with the position of the gauge peak.

that typically lead to constraint violations, particularly of the variable θ. This refinement criterion gave similar results as the one based on truncation error estimation. We decided to use the latter in order not to lose track of features that cannot be controlled with the "ad hoc" criterion. Figure 9.8 shows a typical AMR hierarchy. The resolution of the base grid is taken to be 128 points in each dimension and up to three levels of refinement are added. This is the minimum number of levels needed in order to keep all features well resolved. Two levels are used *ab initio* in order to keep the residual of the Hamiltonian constraint at a tolerable level close to the origin.

The outer boundaries are placed at $r_{\max} = z_{\max} = 5$. This is sufficient for supercritical evolutions $A_s \gtrsim 5$, which do not produce much gravitational radiation because the wave essentially collapses. For the dispersing waves

with $A_s \lesssim 5$, the results should only be trusted until times $t \sim 10$, after which the solution becomes dominated by reflections from the outer boundaries. As explained in section 9.2, we start with differential boundary conditions and switch to absorbing ones at $t = 3.5$.

All the parameters – resolution, location of the outer boundaries, evolution time – should be enlarged considerably in the future if more powerful computer equipment is available. The runtime for the strongest wave ($A_s = 6$) presented here was ≈ 6 hours on a 3 GHz single-processor machine, and the code is still in the testing phase. The code would have to be parallelized in order to make efficient use of multi-processor architectures.

The following plots refer to Brill waves with amplitudes $A_s = 4$, 5 and 6. The corresponding ADM masses are $M_{\rm ADM} = 0.48$, 0.67 and 0.94. Figure 9.9a shows the logarithm of the lapse function at the origin as a function of time. Whereas the lapse eventually returns to its flat-space value for the $A_s = 4$ evolution as the wave disperses, it continues to collapse for the $A_s = 6$ evolution. The code could not be run long enough (for reasons discussed below) to determine the final fate of the $A_s = 5$ wave. This qualitative behaviour of the lapse in the three evolutions is consistent with the results of section 5.7 (figure 5.3), where a very different formulation was used. It also agrees with [6] and [62]. The claim that the $A_s = 4$ wave disperses and the $A_s = 6$ wave collapses is further substantiated by figure 9.9b, which shows the evolution of the Kretschmann scalar I (9.7) evaluated at the origin. This quantity decays at late times in the $A_s = 4$ case and grows exponentially in the $A_s = 6$ case, which indicates that a singularity is approached. The Kretschmann scalar is still highly oscillatory at the end of the runtime of the near-critical $A_s = 5$ evolution.

No apparent horizon was found in the supercritical $A_s = 6$ evolution

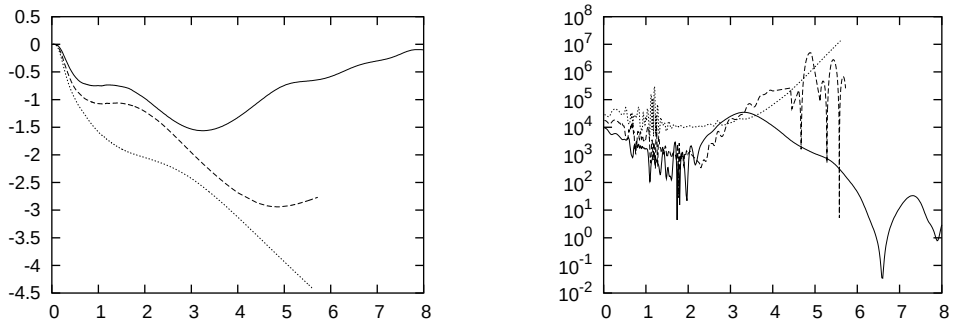

(a) (b)

Figure 9.9: (a) Logarithm of the lapse function at the origin and (b) Kretschmann scalar at the origin as functions of time for amplitudes $A_s = 4$ (solid), 5 (dashed) and 6 (dotted).

during the runtime of the simulation (until $t \approx 5.7$). To make sure that this is not caused by bad convergence of the apparent horizon finder, we used a sequence of circular trial curves spanning the entire domain of interest as initial guesses. There appeared to be a trend for the average expansion of curves with radius ≈ 1 to decrease but we would have to wait a little longer for it to pass through zero. Alcubierre et al. [6] report the formation of the apparent horizon at $t = 7.7$ in their coordinates.

In order to see why the simulations crashed, we display the L^2 norm of the Z vector as a function of time in figure 9.10a (the remaining constraints behave in a similar way). For near- and supercritical evolutions, the constraints begin to grow exponentially fast at late times. This growth then affects all the other variables and ultimately leads to a breakdown of the numerical evolution. The growth mainly occurs close to the origin across a rather large spatial scale (again, this is not a high-frequency instability). The growth rate is robust under variations of the Courant number (we used $\Delta t/h = 0.5$ for the results presented here) and of the resolution, which indicates that we are

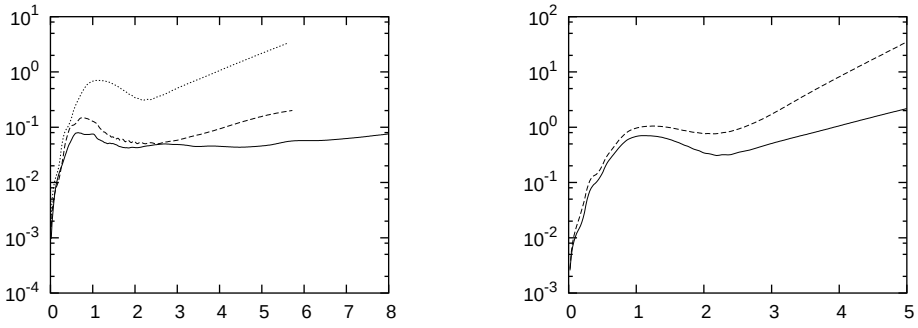

(a) (b)

Figure 9.10: L^2 norm of the Z vector as a function of time. (a) The $A_s = 4$ (solid), 5 (dashed) and 6 (dotted) evolutions with constraint-damping constant $\kappa_{\rm CD} = 4$, (b) the $A_s = 6$ evolution with $\kappa_{\rm CD} = 4$ (solid) and 0 (dashed).

faced with a continuum instability. Figure 9.11 demonstrates that the onset and growth rate of the instability depend only weakly on the location of the outer boundary. This suggests that the predominant source of the constraint growth is the formulation of the equations in the bulk, not the boundary conditions.

We included constraint-damping terms in the evolution equations as described in section 9.1. Figure 9.10b shows that this does have a positive effect: the growth rate of the constraints is smaller if a nonzero $\kappa_{\rm CD} > 0$ is chosen. For large values $\kappa_{\rm CD} \gtrsim 10$, however, instabilities at the outer boundaries quickly developed. A good compromise appeared to be $\kappa_{CD} \approx 4$. For no value of $\kappa_{\rm CD}$ could constraint-damping eliminate the exponential growth completely. We also tried setting $Z^\alpha = 0$ every few timesteps (a simple example of "constraint projection" [83]). However, the increase in the constraint variables became increasingly rapid after the projections, again ultimately leading to a blow-up of the numerical solution.

The development of more sophisticated methods for controlling the growth

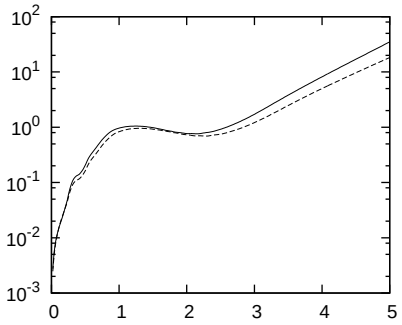

Figure 9.11: Dependence of the constraint growth on the location of the outer boundary. Shown is the L^2 norm of the Z vector as a function of time for a Brill wave with amplitude $A_s = 6$. Solid line: $r_{\max} = z_{\max} = 5$, dashed line: $r_{\max} = z_{\max} = 7.5$. (No constraint damping is included here.)

of the constraints in this formulation of the Einstein equations will be crucial in order to be able to evolve long enough such that interesting physical phenomena can be studied. The work of Abrahams and Evans [1] suggests that critical behaviour will not set in before $t \gtrsim 20$ (although this will be gauge-dependent).

To close on a more positive note, we demonstrate that we can evolve twisting spacetimes as well. Figure 9.12 shows a few snapshots of the variable B^φ for an evolution with amplitudes $A_s = 4$ and $A_B = 2$. As pointed out in section 3.2, the evolution equations for the twist variables are essentially Maxwell's equations and as expected, we see a wavelike behaviour, although a rather complicated one because the twist system is now coupled to the remaining evolution equations in a nonlinear way.

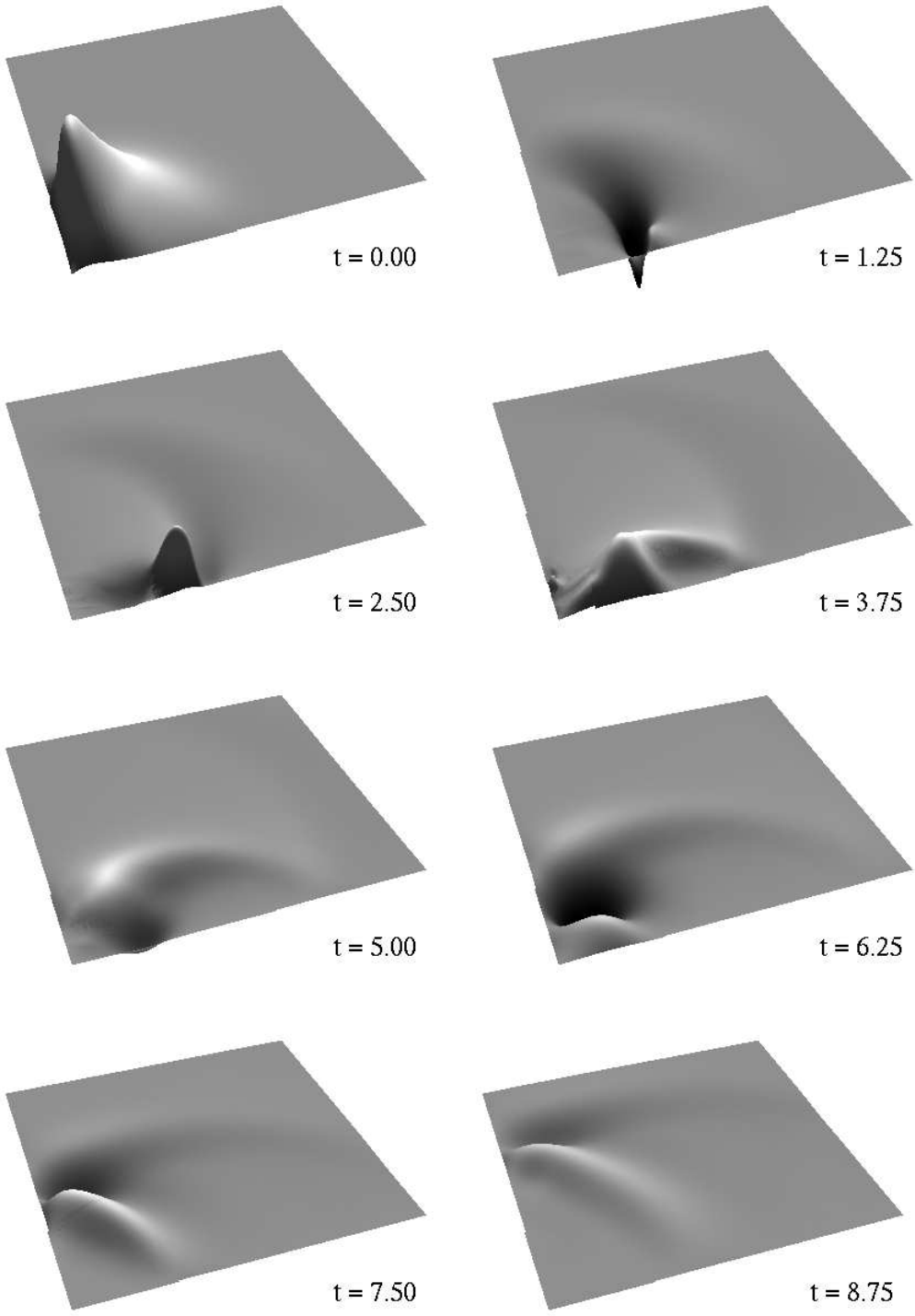

Figure 9.12: Evolution of the twist variable B^{φ} for a strong generalized Brill wave with amplitudes $A_s = 4$ and $A_B = 2$.

Chapter 10

Conclusions and outlook

10.1 Conclusions

This thesis has been concerned with formulations of the Einstein equations suitable for the numerical evolution of axisymmetric spacetimes, mainly focusing on the vacuum geometry.

We started out by trying to understand why many previous attempts to evolve these spacetimes failed because of instabilities on the axis. This led to a detailed study of the behaviour of the components of axisymmetric tensor fields with respect to cylindrical polar coordinates, given that the components with respect to Cartesian coordinates were regular in a neighbourhood of the axis.

In order to exploit the axisymmetry and simplify the system of equations as much as possible, we first performed a dimensional reduction to the Lorentzian three-manifold formed by the trajectories of the Killing vector. This manifold was then foliated into spacelike hypersurfaces by an ADM decomposition, arriving at what is known as the (2+1)+1 formalism [100]. We included general matter sources and rotational degrees of freedom, which

have been neglected in previous numerical studies.

The first evolution system we presented adopted elliptic gauge conditions arising from maximal slicing and conformal flatness of the two-metric, as previously considered in [49, 62, 41]. The hyperbolic evolution equations were integrated using the method of lines with second-order finite differencing, and the elliptic equations were solved using an efficient Multigrid algorithm. In strong field situations the Multigrid solver failed when trying solve the Hamiltonian constraint and the slicing condition during the evolution. This was explained in terms of a lack of diagonal dominance of the discretization matrix. In addition, an analytical investigation indicated that the equations concerned might actually be ill-posed in the sense that they are not linearization-stable. If on the other hand we used free evolution, the constraints suffered from a severe numerical violation. We showed that the constraint evolution system was in fact ill-posed in this case. These observations led us to consider a partially constrained evolution scheme, in which only the momentum constraints were solved but not the Hamiltonian constraint and for which the elliptic equations were well-posed. Using this modified scheme, we were able to evolve strong Brill waves and estimated the critical amplitude of black hole formation by looking at the collapse of the lapse function. For the first time, a nonzero twist was included. The runtime of the code for near-critical evolutions is at present limited by the resolution. Adaptive mesh refinement would be needed to explore the critical behaviour more closely.

The problems we experienced with this mixed hyperbolic-elliptic system motivated the search for a completely hyperbolic formulation of the Einstein equations. We used the Z4 formalism developed by Bona et al. [23] but applied it to the (2+1)+1 formalism, arriving at what we called the Z(2+1)+1

system. Generalized harmonic gauge conditions were included, both with vanishing and dynamical shift vector. We wrote the equations in first-order form as conservation laws with sources. The system was shown to be strongly hyperbolic and, for one choice of parameters, symmetric hyperbolic. By a judicious choice of dependent variables based on our study of the behavior of axisymmetric tensor fields, we were able to write the equations in a form that was well-behaved on the axis and suitable for numerical evolutions. The incompatibility of the harmonic shift conditions with axisymmetry was addressed by adding a suitable gauge source function.

As a first test problem for our implementation, we considered exact solutions of linearized theory. The quadrupole waves of Teukolsky [132] were expressed in terms of Z(2+1)+1 variables and the two polarization states were understood in terms of twisting and non-twisting solutions. In addition, we derived a new even-parity twisting solution with octupolar angular dependence. The solutions were shown to satisfy the Z(2+1)+1 equations provided that the gauge parameters and gauge source functions were chosen such that transverse-traceless gauge and (generalized) harmonic gauge are compatible. Second-order convergence of our code to the exact solutions was demonstrated up to the point when the waves interacted with the boundary. Whereas the error decayed with time in the vanishing shift case, it grew linearly if a dynamical shift was used, the cause of which would need further investigation.

Next we discussed various choices of outer boundary conditions. The dissipative boundary conditions we considered included absorbing boundary conditions and boundary conditions with vanishing Z vector. A study of the Newman-Penrose scalars and the constraint and gauge propagation systems led to a set of differential boundary conditions, where the normal derivatives

of the incoming modes were prescribed. Whereas dissipative boundary conditions have been proven to be stable subject to certain restrictions on the hyperbolic system [115, 124], those theorems do not apply to the differential boundary conditions. Hence we analyzed the latter using the Fourier-Laplace technique. This suggested that our differential boundary conditions were stable in the high-frequency limit, although it could not rule out a low-frequency instability. Numerical evolutions of the linearized solutions showed that the dissipative boundary conditions were stable as expected but that (the non-twisting part of) the differential boundary conditions suffered from a late-time instability, which appeared to be a finite-difference instability rather than a continuum one. In minimizing spurious reflections from the outer boundaries, the differential boundary conditions performed better than the absorbing ones, which in turn outperformed the zero-Z boundary conditions in most cases.

Finally, we turned to nonlinear evolutions of generalized Brill waves (including twist). Initial data was generated in the same way as for the hyperbolic-elliptic system by requiring that the 2-metric be conformally flat and that the extrinsic curvature be zero initially. When using harmonic slicing with zero shift, subcritical initial data of this type evolved to a nontrivial representation of Minkowski space. Adaptive mesh refinement turned out to be essential in order to resolve the highly distorted waveforms that occurred as a consequence of this. We showed that for pure harmonic slicing ($f = 1$), no gauge shocks appeared. A 3-grid convergence test was carried out for a moderately strong Brill wave, and a study of the numerical conservation of the ADM mass showed that differential boundary conditions are superior to those of dissipative type in this respect. Adaptive evolutions of near-critical Brill waves were then performed. We obtained bounds on the critical ampli-

tude by looking at the evolution of the lapse function and the Kretschmann scalar at the origin. These are consistent with the results obtained with our hyperbolic-elliptic system and by other authors. The simulations could not be run long enough yet for an apparent horizon to form in the supercritical case. The main limitation to the runtime is currently an exponential growth of the constraints. The inclusion of constraint-damping terms [70] in the evolution equations decreased the growth rate but could not eliminate the blow-up completely.

In a sense, the situation is more complicated in Z4-like formulations than in different approaches because extra constraint variables (the Z vector) are introduced. Only solutions with $Z = 0$ are solutions of the Einstein equations, but it is not at all clear whether the constraint manifold $Z = 0$ is an attractor in the fully nonlinear case. On the other hand, terms homogeneous in the Z vector can easily be added to the evolution equations without affecting the characteristic structure (in general, this is not possible in more conventional approaches). It is quite possible that constraint additions will be found in the future that eliminate the constraint blow-up completely.

10.2 Outlook on future work

Once the growth of the constraints is under control, we will hopefully be able to tune closer to the critical point of black hole formation and to evolve long enough so that the potentially interesting physics that occurs at the threshold can be studied. Apart from comparing with the results of Abrahams and Evans [1, 2], we would like to find out whether a nonzero twist might modify the critical behaviour. Another question that should be addressed is whether highly distorted initial data can lead to the formation of naked singularities

in Brill wave collapse [3, 62].

Our long-term goal is to include matter in the form of a perfect fluid. This is much more interesting physically because perfect fluid spacetimes can carry angular momentum. When studying the gravitational collapse of a rotating fluid, the question arises what happens with the angular momentum at the threshold of black hole formation. A perturbation analysis by Gundlach [68] predicts that for a slightly non-spherical and slowly rotating fluid, the critical solution will be the spherically symmetric one, which for the ultrarelativistic equation of state was found by Evans and Coleman [51]. According to Gundlach, the angular momentum in supercritical evolutions will obey a similar power-law as the black hole mass (1.1), and an expression for the dependence of the angular momentum exponent on the mass exponent and the equation of state has been derived. It would be very interesting to probe those results numerically.

Appendix A

Perfect fluid

In section 3.3, we derived the evolution equations for general matter in the (2+1)+1 formalism. Here, we specify the matter model to be a perfect fluid. We write the equations in conservation form and work out their characteristic decomposition. The transformation from conserved to primitive variables is cast in a form that helps avoid superluminal speeds in numerical simulations.

A.1 Conservation form

The matter evolution equations (3.69–3.71, 3.81) can clearly be written in conservation form (with sources and a common advection term),

$$\partial_t \mathbf{u} + \left[-\beta^A \mathbf{u} + \alpha \mathcal{F}^D(\mathbf{u})\right]_{,D} = \alpha \mathcal{S}(\mathbf{u})\,. \tag{A.1}$$

Following [13], we replace ρ_H with $\rho_K = \rho_H - \sigma$ (kinetic energy) and regard as the set of conserved variables

$$\mathbf{u} = (\rho_K, J_A, J^\varphi, \sigma)^T\,. \tag{A.2}$$

The fluxes are

$$\mathcal{F}^D{}_{\rho_K} = J^D - \Sigma^D\,, \tag{A.3}$$

$$\mathcal{F}^D{}_{J_A} = S_A{}^D\,, \tag{A.4}$$

$$\mathcal{F}^D{}_{J^\varphi} = S^D\,, \tag{A.5}$$

$$\mathcal{F}^D{}_{\sigma} = \Sigma^D\,, \tag{A.6}$$

and the source terms are

$$\begin{aligned}\mathcal{S}_{\rho_K} &= (\Sigma^A - J^A)(D^{\mathrm{I}}{}_A + L_A) + K_\varphi{}^\varphi(\tau + \rho_K) + \chi_{AB}S^{AB} \\ &\quad -J^A A_A + \chi\rho_K + \lambda^2 E^A S_A\,, \end{aligned}\tag{A.7}$$

$$\begin{aligned}\mathcal{S}_{J_A} &= -S_{AB}(A^B + L^B) + J_A(\chi + K_\varphi{}^\varphi) + 2B_A{}^B J_B \\ &\quad -A_A\rho_H + L_A\tau + \lambda^2(E_A J^\varphi + \epsilon_{AB}S^B B^\varphi)\,, \end{aligned}\tag{A.8}$$

$$\mathcal{S}_{J^\varphi} = -(D^{\mathrm{I}}{}_A + 3L_A)S^A + J^\varphi(\chi + 3K_\varphi{}^\varphi)\,, \tag{A.9}$$

$$\mathcal{S}_{\sigma} = -(D^{\mathrm{I}}{}_A + L_A)\Sigma^A + \sigma(\chi + K_\varphi{}^\varphi)\,. \tag{A.10}$$

We use the notation of section 6.3 for the first-order derivatives of the metric.

A.2 Matter model

To evaluate the characteristic structure, we need to specify the matter model. Here, we consider a perfect fluid with four-velocity u^α, normalized such that

$$u_\alpha u^\alpha = -1\,, \tag{A.11}$$

rest mass density ρ, pressure p and internal energy ϵ. The dependence of the pressure on the density and the internal energy is given by the *equation of state*

$$p = p(\rho, \epsilon)\,. \tag{A.12}$$

With those definitions, the number density is

$$N^\alpha = \rho u^\alpha \tag{A.13}$$

and the energy-momentum tensor is given by

$$T^{\alpha\beta} = \rho h u^\alpha u^\beta + p g^{\alpha\beta}\,, \tag{A.14}$$

where h is the specific enthalpy,

$$h = 1 + \epsilon + \frac{p}{\rho}\,. \tag{A.15}$$

The Lorentz factor is defined as

$$W \equiv -u^\alpha n_\alpha\,. \tag{A.16}$$

Observers who are at rest in a slice $\Sigma(t)$ (i.e., who have four-velocity n^α) measure a coordinate velocity

$$v^A = W^{-1} h_\alpha{}^A u^\alpha\,, \tag{A.17}$$

and the angular velocity is

$$v^\varphi = W^{-1}\lambda^{-2}\xi_\alpha u^\alpha\,. \tag{A.18}$$

Hence we obtain the familiar relation

$$W = (1 - v^2)^{-1/2}\,, \tag{A.19}$$

where

$$v^2 = v_A v^A + \lambda^2 v^{\varphi 2}\,. \tag{A.20}$$

The variables

$$\mathbf{w} = (v_A, v^\varphi, \rho, p, \epsilon, h, W)^T \tag{A.21}$$

are called *primitive variables*. Note only five of these are independent because of (A.12), (A.15) and (A.19). The conserved variables can be expressed in terms of the primitive variables as

$$\begin{aligned} \rho_K &= \rho h W^2 - p - \rho W \,, \\ J_A &= \rho h W^2 v_A \,, \\ J^\varphi &= \rho h W^2 v^\varphi \,, \\ \sigma &= \rho W \,, \end{aligned} \tag{A.22}$$

and the remaining matter variables are

$$\begin{aligned} \tau &= \rho h W^2 \lambda^2 v^{\varphi 2} + p \,, \\ S_A &= \rho h W^2 v^\varphi v_A \,, \\ S_{AB} &= \rho h W^2 v_A v_B + p H_{AB} \,, \\ \Sigma_A &= \rho W v_A \,. \end{aligned} \tag{A.23}$$

A.3 Characteristic decomposition

The characteristic decomposition for 3+1 general relativistic hydrodynamics was first derived by the Valencia group [13]. The application to our (2+1)+1 system is straightforward. Note however the additional source terms that occur in our case. Our method differs slightly from [13] in that we choose a general orthonormal basis (μ^A, π^A) in two-space as in section 6.4 and project vectors along μ (index $\perp$) and π (index $\|$).

Following the notation of [54], we introduce a few abbreviations. From the equation of state (A.12), we form

$$\chi \equiv \frac{\partial p}{\partial \rho} \,, \qquad \kappa \equiv \frac{\partial p}{\partial \epsilon} \,, \qquad h c_s^2 \equiv \chi + \frac{p}{\rho^2} \kappa \,, \tag{A.24}$$

where c_s is known as the *sound speed*. Also set

$$\mathcal{K}^{-1} = 1 - \frac{c_s^2 \rho}{\kappa}\,, \qquad \mathcal{V}^{\pm} = \frac{v_\perp - \lambda_s^{\pm}}{1 - v_\perp \lambda_s^{\pm}}\,, \qquad \mathcal{A}^{\pm} = \frac{1 - v_\perp^2}{1 - v_\perp \lambda_s^{\pm}}\,,$$

$$\mathcal{C}^{\pm} = v_\perp - \mathcal{V}^{\pm}\,, \qquad \xi = 1 - v_\perp^2\,, \tag{A.25}$$

$$\Delta = h^3 W (1 - \mathcal{K}^{-1})(\mathcal{C}^{+} - \mathcal{C}^{-})\xi\,.$$

Our definitions of ξ and Δ differ from those in [54] by a factor of λ^2 to ensure regularity on axis. We have defined $\mathcal{K}^{-1}$ instead of $\mathcal{K}$ to allow for the special case of the ultrarelativistic equation of state (A.37), for which $\mathcal{K}^{-1} = 0$. As a consequence, Δ above has been multiplied by $\mathcal{K}^{-1}$ and the characteristic variable $l_{0,1}$ has been divided by $\mathcal{K}^{-1}$.

The system is found to be strongly hyperbolic. The characteristic speeds in the μ-direction are

$$\begin{aligned} \lambda_0 &= v_\perp\,, \\ \lambda_s^{\pm} &= \frac{1}{1 - v^2 c_s^2}\Big\{ v_\perp (1 - c_s^2) \\ &\qquad \pm c_s \sqrt{(1 - v^2)\left[(1 - v^2 c_s^2) - v_\perp^2 (1 - c_s^2)\right]} \Big\}\,. \end{aligned} \tag{A.26}$$

The characteristic variables l (corresponding to the left eigenvectors) are

$$\begin{aligned} l_{0,1} &= \frac{W}{1 - \mathcal{K}^{-1}}\Big\{ h\sigma - W(\sigma + \rho_K) \\ &\qquad + W(v_\perp J_\perp + v_\parallel J_\parallel + \lambda^2 v^\varphi J^\varphi) \Big\}\,, \end{aligned} \tag{A.27}$$

$$l_{0,2} = \frac{1}{h\xi}\left\{ -v_\parallel(\sigma + \rho_K) + v_\perp v_\parallel J_\perp + (1 - v_\perp^2) J_\parallel \right\}\,, \tag{A.28}$$

$$l_{0,3} = \frac{1}{h\xi}\left\{ -v^\varphi(\sigma + \rho_K) + v^\varphi v_\perp J_\perp + (1 - v_\perp^2) J^\varphi \right\}\,, \tag{A.29}$$

$$
\begin{aligned}
l_s^{\mp} &= \frac{h^2}{\Delta}\Big\{\mathcal{K}^{-1}hW\mathcal{V}^{\pm}\xi\sigma + \left[\mathcal{K}^{-1} - \mathcal{A}^{\pm} - (2-\mathcal{K}^{-1})v_\perp\right] J_\perp \\
&\quad +(2-\mathcal{K}^{-1})\mathcal{V}^{\pm}W^2\xi(v_\perp J_\perp + v_\parallel J_\parallel + \lambda^2 v^\varphi J^\varphi) \qquad \text{(A.30)} \\
&\quad + \left[(\mathcal{K}^{-1}-1)\left(-v_\perp + \mathcal{V}^{\pm}(W^2\xi - 1)\right)\right. \\
&\quad \left. -W^2\mathcal{V}^{\pm}\xi\right](\sigma + \rho_K)\Big\}. \qquad \text{(A.31)}
\end{aligned}
$$

The inverse transformation (corresponding to the right eigenvectors) is given by

$$
\begin{aligned}
\sigma &= \frac{1}{hW}l_{0,1} + W(v_\parallel l_{0,2} + \lambda^2 v^\varphi l_{0,3}) + l_s^+ + l_s^-\,, \qquad \text{(A.32)} \\
J_\perp &= \mathcal{K}^{-1}v_\perp l_{0,1} + 2hW^2 v_\perp(v_\parallel l_{0,2} + \lambda^2 v^\varphi l_{0,3}) \\
&\quad +hW(\mathcal{C}^+ l_s^+ + \mathcal{C}^- l_s^-)\,, \qquad \text{(A.33)} \\
J_\parallel &= \mathcal{K}^{-1}v_\parallel l_{0,1} + h l_{0,2} + 2hW^2 v_\parallel(v_\parallel l_{0,2} + \lambda^2 v^\varphi l_{0,3}) \\
&\quad +hW v_\parallel(l_s^+ + l_s^-)\,, \qquad \text{(A.34)} \\
J^\varphi &= \mathcal{K}^{-1}v^\varphi l_{0,1} + h l_{0,3} + 2hW^2 v^\varphi(v_\parallel l_{0,2} + \lambda^2 v^\varphi l_{0,3}) \\
&\quad +hW v^\varphi(l_s^+ + l_s^-)\,, \qquad \text{(A.35)} \\
\rho_K &= \left(\mathcal{K}^{-1} - \frac{1}{hW}\right) l_{0,1} + W(2hW-1)(v_\parallel l_{0,2} + \lambda^2 v^\varphi l_{0,3}) \\
&\quad +hW(\mathcal{A}^+ l_s^+ + \mathcal{A}^- l_s^-) - l_s^+ - l_s^-\,. \qquad \text{(A.36)}
\end{aligned}
$$

A.4 Transformation from conserved to primitive variables

The conserved matter variables (A.2) are the ones that are evolved in a numerical algorithm. To compute the remaining matter variables (A.23) and the eigenvectors, the primitive variables have to be calculated from the

conserved variables in an intermediate step. This transformation is much more involved than the opposite direction (A.22). To make it explicit, we have to specify an equation of state. Here, we consider the ultrarelativistic equation of state,

$$p = (\Gamma - 1)\rho_{tot} = (\Gamma - 1)\rho(\epsilon + 1) = \frac{\Gamma - 1}{\Gamma}\rho h\,, \tag{A.37}$$

where ρ_{tot} is the total energy density.

Suppose we are given the conserved variables, and also form $\rho_H = \rho_K + \sigma$. Consider the quantity

$$J^2 \equiv J_A J^A + \lambda^2 J^{\varphi 2}\,. \tag{A.38}$$

Using (A.22), (A.37) and (A.19), we can express J^2 and ρ_H in terms of the primitive variables as

$$\begin{aligned} J^2 &= \left(\frac{\Gamma}{\Gamma - 1}\right)^2 p^2 W^2 (W^2 - 1)\,, \\ \rho_H &= p\left(\frac{\Gamma}{\Gamma - 1} W^2 - 1\right)\,. \end{aligned} \tag{A.39}$$

Eliminating W yields an equation for the pressure in terms of conserved variables:

$$p = -2\beta\rho_H + \sqrt{4\beta^2\rho_H^2 + (\Gamma - 1)(\rho_H^2 - J^2)}\,, \tag{A.40}$$

where $\beta \equiv (2 - \Gamma)/4$. Next define

$$\chi_A \equiv \frac{(\Gamma - 1)J_A}{\Gamma p}\,, \qquad \chi^\varphi \equiv \frac{(\Gamma - 1)J^\varphi}{\Gamma p}\,, \qquad \chi^2 \equiv \chi_A \chi^A + \lambda^2 \chi^{\varphi 2}\,. \tag{A.41}$$

We identify $\chi^A = W^2 v^A$ and $\chi^\varphi = W^2 v^\varphi$ and hence with (A.19) we obtain

$$W^{-2} = \frac{1}{2\chi^2}\left(\sqrt{1 + 4\chi^2} - 1\right)\,. \tag{A.42}$$

This now enables us to calculate the velocities,

$$v_A = W^{-2}\chi_A\,, \qquad v^\varphi = W^{-2}\chi^\varphi\,. \tag{A.43}$$

The form of W^{-2} in (A.42) guarantees that $|v_A|$, $|v^\varphi| \leqslant 1$. This is most important since evolved speeds greater than unity (i.e., greater than the speed of light) can easily cause the numerical code to crash.

Finally, we can calculate the specific enthalpy and rest mass energy density from (A.22) and (A.37),

$$h = \frac{J^\varphi}{\sigma v^\varphi W}\,, \qquad \rho = \frac{\Gamma p}{(\Gamma - 1)h}\,. \tag{A.44}$$

A similar method of calculating the primitive variables to the one described here is used by Choptuik and Neilsen [106, 105] and Hawke [77].

Appendix B

Regularized conservation form

In this appendix we write out the fluxes and sources of the regularized conservation form (6.165) of the Z(2+1)+1 equations. The equations were generated with the computer algebra language REDUCE [80], from which we created LaTeX code using the TeX-REDUCE Interface TRI [10].

To demonstrate regularity on axis, we define

$$\underline{\hat{u}} \equiv r^{-1}\underline{u} \tag{B.1}$$

for a variable $\underline{u}$ that is $O(r)$ on the axis (see table 5.2). In terms of the hatted variables, the fluxes and sources are manifestly regular on axis. They are either even or odd functions of r. As a shorthand, we introduce

$$H \equiv H_{rr}H_{zz} - {H_{rz}}^2 \tag{B.2}$$

for the determinant of the 2-metric. We use the minimal gauge source function (6.162).

B.1 Fluxes in the r direction

$$\tilde{\mathcal{F}}^r\left(H_{rr}\right) = 0$$

$$\tilde{\mathcal{F}}^r\left(H_{rz}\right) = 0$$

$$\tilde{\mathcal{F}}^r\left(H_{zz}\right) = 0$$

$$\tilde{\mathcal{F}}^r\left(s\right) = 0$$

$$\tilde{\mathcal{F}}^r\left(\alpha\right) = 0$$

$$\tilde{\mathcal{F}}^r\left(\beta^r\right) = 0$$

$$\tilde{\mathcal{F}}^r\left(\beta^z\right) = 0$$

$$\tilde{\mathcal{F}}^r\left(D_{rrr}\right) = \alpha\chi_{rr} - 2\alpha r^2\left(\hat{\tilde{B}}_r{}^r H_{rr} + \hat{B}_r{}^z\hat{H}_{rz}\right) - \hat{D}_{rrr}r^2\hat{\beta}^r$$

$$\begin{aligned}\tilde{\mathcal{F}}^r\left(\tilde{D}_{rrz}\right) = \alpha\Big(&-r^2\hat{\tilde{B}}_r{}^r\hat{H}_{rz} - \hat{B}_r{}^z H_{zz} \\ &- \hat{B}_z{}^r H_{rr} - B_z{}^z\hat{H}_{rz} + \hat{\chi}_{rz}\Big) - \hat{\tilde{D}}_{rrz}r^2\hat{\beta}^r\end{aligned}$$

$$\tilde{\mathcal{F}}^r\left(D_{rzz}\right) = \alpha\chi_{zz} - 2\alpha\left(r^2\hat{B}_z{}^r\hat{H}_{rz} + B_z{}^z H_{zz}\right) - \hat{D}_{rzz}r^2\hat{\beta}^r$$

$$\tilde{\mathcal{F}}^r\left(D_{zrr}\right) = -D_{zrr}r\hat{\beta}^r$$

$$\tilde{\mathcal{F}}^r\left(D_{zrz}\right) = -\hat{D}_{zrz}r^2\hat{\beta}^r$$

$$\tilde{\mathcal{F}}^r\left(D_{zzz}\right) = -D_{zzz}r\hat{\beta}^r$$

$$\tilde{\mathcal{F}}^r\left(\tilde{s}_r\right) = \alpha\left(2\hat{\tilde{B}}_r{}^r + 2\hat{B}_r{}^z H_{rr}^{-1}\hat{H}_{rz} + \hat{Y}\right) - r^2\hat{\beta}^r\hat{\tilde{s}}_r$$

$$\tilde{\mathcal{F}}^r\left(s_z\right) = -r^2\hat{\beta}^r\hat{s}_z$$

$$\begin{aligned}\tilde{\mathcal{F}}^r\left(A_r\right) = {} & 2\alpha\chi_{rr}fH_{rr}^{-1} + H^{-1}\alpha\chi_{rr}r^2fH_{rr}^{-1}\hat{H}_{rz}^2 + H^{-1}\alpha\chi_{zz}fH_{rr} \\ & + \alpha f\left(r^2\hat{Y} - m\theta\right) - 2H^{-1}\alpha r^2\hat{\chi}_{rz}f\hat{H}_{rz} - r^2\hat{A}_r\hat{\beta}^r\end{aligned}$$

$$\tilde{\mathcal{F}}^r\left(A_z\right) = -rA_z\hat{\beta}^r$$

$$\begin{aligned}\tilde{\mathcal{F}}^r\left(\tilde{B}_r{}^r\right) = {} & H^{-1}\alpha\hat{D}_{rrr}H_{rr}^{-1}H_{zz}\left(-d+\mu\right) \\ & - \frac{1}{2}H^{-2}\alpha\hat{D}_{rrr}r^2dH_{rr}^{-1}\hat{H}_{rz}^2H_{zz} + H^{-1}\alpha\hat{\tilde{D}}_{rrz}r^2dH_{rr}^{-1}\hat{H}_{rz} \\ & + H^{-2}\alpha\hat{\tilde{D}}_{rrz}r^4dH_{rr}^{-1}\hat{H}_{rz}^3 + H^{-1}\alpha\hat{D}_{rzz}\left(-\frac{1}{2}d+\mu\right) \\ & - \frac{1}{2}H^{-2}\alpha\hat{D}_{rzz}r^2d\hat{H}_{rz}^2 + H^{-1}\alpha D_{zrr}H_{rr}^{-1}\hat{H}_{rz}\left(d-\mu\right) \\ & + \frac{1}{2}H^{-2}\alpha D_{zrr}r^2dH_{rr}^{-1}\hat{H}_{rz}^3 - H^{-1}\alpha\hat{D}_{zrz}\mu \\ & - H^{-2}\alpha\hat{D}_{zrz}r^2d\hat{H}_{rz}^2 + \frac{1}{2}H^{-2}\alpha D_{zzz}dH_{rr}\hat{H}_{rz} \\ & + \alpha H_{rr}^{-1}\left(-\frac{1}{2}r^2d\hat{\tilde{s}}_r + r^2\mu\hat{\tilde{s}}_r + \frac{1}{2}a\hat{A}_r - \mu\hat{Z}_r\right) \\ & + H^{-1}\alpha\hat{H}_{rz}\left(-\frac{1}{2}r^4dH_{rr}^{-1}\hat{H}_{rz}\hat{\tilde{s}}_r + r^4H_{rr}^{-1}\hat{H}_{rz}\mu\hat{\tilde{s}}_r\right. \\ & \qquad + \frac{1}{2}r^2a\hat{A}_rH_{rr}^{-1}\hat{H}_{rz} + \frac{1}{2}r^2d\hat{s}_z - r^2H_{rr}^{-1}\hat{H}_{rz}\mu\hat{Z}_r \\ & \qquad \left. - r^2\mu\hat{s}_z - \frac{1}{2}aA_z + \mu Z_z\right) - r^2\hat{\beta}^r\hat{\tilde{B}}_r{}^r\end{aligned}$$

$$\begin{aligned}\tilde{\mathcal{F}}^r\left(B_r{}^z\right) = {} & H^{-1}\alpha\hat{D}_{rrr}r^2H_{rr}^{-1}\hat{H}_{rz}\left(d-\mu\right)\\ & + \frac{1}{2}H^{-2}\alpha\hat{D}_{rrr}r^4dH_{rr}^{-1}\hat{H}_{rz}^3 - H^{-1}\alpha\hat{\hat{D}}_{rrz}r^2\mu\\ & - H^{-2}\alpha\hat{\hat{D}}_{rrz}r^4d\hat{H}_{rz}^2 + \frac{1}{2}H^{-2}\alpha\hat{D}_{rzz}r^2dH_{rr}\hat{H}_{rz}\\ & + H^{-1}\alpha D_{zrr}\left(-d+2\mu\right) - \frac{1}{2}H^{-2}\alpha D_{zrr}r^2d\hat{H}_{rz}^2\\ & + H^{-2}\alpha\hat{D}_{zrz}r^2dH_{rr}\hat{H}_{rz} - \frac{1}{2}H^{-2}\alpha D_{zzz}dH_{rr}^2\\ & + H^{-1}\alpha\left(\frac{1}{2}r^4d\hat{H}_{rz}\hat{\hat{s}}_r - r^4\hat{H}_{rz}\mu\hat{\hat{s}}_r - \frac{1}{2}r^2a\hat{A}_r\hat{H}_{rz}\right.\\ & \qquad - \frac{1}{2}r^2dH_{rr}\hat{s}_z + r^2H_{rr}\mu\hat{s}_z + r^2\hat{H}_{rz}\mu\hat{Z}_r\\ & \qquad \left. + \frac{1}{2}aA_zH_{rr} - H_{rr}\mu Z_z\right) - r^2\hat{\beta}^r\hat{B}_r{}^z\end{aligned}$$

$$\tilde{\mathcal{F}}^r\left(B_z{}^r\right) = -r^2\hat{\beta}^r\hat{B}_z{}^r$$

$$\tilde{\mathcal{F}}^r\left(B_z{}^z\right) = -r\hat{\beta}^rB_z{}^z$$

$$\begin{aligned}\tilde{\mathcal{F}}^r\left(\chi_{rr}\right) = {} & \alpha\hat{D}_{rrr}rH_{rr}^{-1} + H^{-1}\alpha\hat{D}_{rzz}rH_{rr} + H^{-1}\alpha D_{zrr}r\hat{H}_{rz}\\ & - 2H^{-1}\alpha\hat{D}_{zrz}rH_{rr} + \alpha r\left(r^2\hat{\hat{s}}_r + \hat{A}_r - 2\hat{Z}_r\right) - \chi_{rr}r\hat{\beta}^r\end{aligned}$$

$$\begin{aligned}\tilde{\mathcal{F}}^r\left(\chi_{rz}\right) = {} & H^{-1}\alpha\hat{D}_{rzz}r^2\hat{H}_{rz} + \alpha D_{zrr}H_{rr}^{-1}\\ & + \frac{1}{2}H^{-1}\alpha D_{zrr}r^2H_{rr}^{-1}\hat{H}_{rz}^2 - H^{-1}\alpha\hat{D}_{zrz}r^2\hat{H}_{rz}\\ & - \frac{1}{2}H^{-1}\alpha D_{zzz}H_{rr} + \alpha\left(\frac{1}{2}r^2\hat{s}_z + \frac{1}{2}A_z - Z_z\right) - r^2\hat{\beta}^r\hat{\chi}_{rz}\end{aligned}$$

$$\tilde{\mathcal{F}}^r\left(\chi_{zz}\right) = H^{-1}\alpha\hat{D}_{rzz}rH_{zz} - H^{-1}\alpha D_{zzz}r\hat{H}_{rz} - \chi_{zz}r\hat{\beta}^r$$

$$\begin{aligned}\tilde{\mathcal{F}}^r\left(Y\right) = {} & H^{-1}\alpha\hat{D}_{rrr}r^2H_{rr}^{-2}\hat{H}_{rz}^2 - H^{-1}\alpha\hat{D}_{rzz} - 2H^{-1}\alpha D_{zrr}H_{rr}^{-1}\hat{H}_{rz}\\ & + 2H^{-1}\alpha\hat{D}_{zrz} + \alpha H_{rr}^{-1}\left(-\hat{A}_r + 2\hat{Z}_r\right)\\ & + H^{-1}\alpha r^2\hat{H}_{rz}\left(r^2H_{rr}^{-1}\hat{H}_{rz}\hat{\hat{s}}_r - \hat{s}_z\right) - r^2\hat{\beta}^r\hat{Y}\end{aligned}$$

$$\tilde{\mathcal{F}}^r\left(E^r\right) = -2H^{-1}\alpha H_{zz}Z^\varphi - r^2\hat{\beta}^r\hat{E}^r$$

$$\tilde{\mathcal{F}}^r\left(E^z\right) = 2H^{-1}\alpha r\hat{H}_{rz}Z^\varphi - r\hat{\beta}^r E^z + \left(\sqrt{H}\right)^{-1}\alpha r\hat{B}^\varphi$$

$$\tilde{\mathcal{F}}^r\left(B^\varphi\right) = -r^2\hat{\beta}^r\hat{B}^\varphi + \left(\sqrt{H}\right)^{-1}\alpha\left(r^2\hat{E}^r\hat{H}_{rz} + E^z H_{zz}\right)$$

$$\begin{aligned}\tilde{\mathcal{F}}^r\left(\theta\right) = {} & H^{-1}\alpha\hat{D}_{rrr}rH_{rr}^{-1}H_{zz} + H^{-1}\alpha\hat{D}_{rzz}r - H^{-1}\alpha D_{zrr}rH_{rr}^{-1}\hat{H}_{rz} \\ & - H^{-1}\alpha\hat{D}_{zrz}r + \alpha rH_{rr}^{-1}\left(r^2\hat{\tilde{s}}_r - \hat{Z}_r\right) \\ & + H^{-1}\alpha r\hat{H}_{rz}\left(r^4H_{rr}^{-1}\hat{H}_{rz}\hat{\tilde{s}}_r - r^2H_{rr}^{-1}\hat{H}_{rz}\hat{Z}_r\right. \\ & \left. - r^2\hat{s}_z + Z_z\right) - r\hat{\beta}^r\theta\end{aligned}$$

$$\begin{aligned}\tilde{\mathcal{F}}^r\left(Z_r\right) = {} & \alpha\chi_{rr}H_{rr}^{-1} + H^{-1}\alpha\chi_{zz}H_{rr} \\ & + \alpha\left(r^2\hat{Y} - \theta\right) - H^{-1}\alpha r^2\hat{\chi}_{rz}\hat{H}_{rz} - r^2\hat{\beta}^r\hat{Z}_r\end{aligned}$$

$$\tilde{\mathcal{F}}^r\left(Z_z\right) = H^{-1}\alpha\chi_{zz}r\hat{H}_{rz} - H^{-1}\alpha r\hat{\chi}_{rz}H_{zz} - r\hat{\beta}^r Z_z$$

$$\tilde{\mathcal{F}}^r\left(Z^\varphi\right) = -\frac{1}{2}\alpha r\hat{E}^r - r\hat{\beta}^r Z^\varphi$$

B.2 Fluxes in the z direction

$$\tilde{\mathcal{F}}^z\left(H_{rr}\right) = 0$$

$$\tilde{\mathcal{F}}^z\left(H_{rz}\right) = 0$$

$$\tilde{\mathcal{F}}^z\left(H_{zz}\right) = 0$$

$$\tilde{\mathcal{F}}^z\left(s\right) = 0$$

$$\tilde{\mathcal{F}}^z(\alpha) = 0$$

$$\tilde{\mathcal{F}}^z(\beta^r) = 0$$

$$\tilde{\mathcal{F}}^z(\beta^z) = 0$$

$$\tilde{\mathcal{F}}^z(D_{rrr}) = -\hat{D}_{rrr} r \beta^z$$

$$\tilde{\mathcal{F}}^z\left(\tilde{D}_{rrz}\right) = -\hat{\tilde{D}}_{rrz} r \beta^z$$

$$\tilde{\mathcal{F}}^z(D_{rzz}) = -\hat{D}_{rzz} r \beta^z$$

$$\tilde{\mathcal{F}}^z(D_{zrr}) = \alpha\chi_{rr} - 2\alpha r^2 \left(\hat{\tilde{B}}_r{}^r H_{rr} + \hat{B}_r{}^z \hat{H}_{rz}\right) - D_{zrr}\beta^z$$

$$\begin{aligned}\tilde{\mathcal{F}}^z(D_{zrz}) = \alpha r \Big(&-r^2 \hat{\tilde{B}}_r{}^r \hat{H}_{rz} - \hat{B}_r{}^z H_{zz} \\ &- \hat{B}_z{}^r H_{rr} - B_z{}^z \hat{H}_{rz} + \hat{\chi}_{rz}\Big) - \hat{D}_{zrz} r \beta^z\end{aligned}$$

$$\tilde{\mathcal{F}}^z(D_{zzz}) = \alpha\chi_{zz} - 2\alpha \left(r^2 \hat{B}_z{}^r \hat{H}_{rz} + B_z{}^z H_{zz}\right) - D_{zzz}\beta^z$$

$$\tilde{\mathcal{F}}^z(\tilde{s}_r) = -r\beta^z \hat{\tilde{s}}_r$$

$$\tilde{\mathcal{F}}^z(s_z) = \alpha r \left(2\hat{\tilde{B}}_r{}^r + 2\hat{B}_r{}^z H_{rr}^{-1} \hat{H}_{rz} + \hat{Y}\right) - r\beta^z \hat{s}_z$$

$$\tilde{\mathcal{F}}^z(A_r) = -r\hat{A}_r \beta^z$$

$$\begin{aligned}\tilde{\mathcal{F}}^z(A_z) = {}& 2\alpha\chi_{rr} f H_{rr}^{-1} + H^{-1}\alpha\chi_{rr} r^2 f H_{rr}^{-1} \hat{H}_{rz}^2 + H^{-1}\alpha\chi_{zz} f H_{rr} \\ &+ \alpha f \left(r^2 \hat{Y} - m\theta\right) - 2H^{-1}\alpha r^2 \hat{\chi}_{rz} f \hat{H}_{rz} - A_z \beta^z\end{aligned}$$

$$\tilde{\mathcal{F}}^z\left(\tilde{B}_r{}^r\right) = -r\beta^z \hat{\tilde{B}}_r{}^r$$

$$\tilde{\mathcal{F}}^z\left(B_r{}^z\right) = -r\beta^z \hat{B}_r{}^z$$

$$\begin{aligned}
\tilde{\mathcal{F}}^z\left(B_z{}^r\right) = {} & H^{-1}\alpha\hat{D}_{rrr}rH_{rr}^{-1}H_{zz}\left(-d+\mu\right) \\
& - \frac{1}{2}H^{-2}\alpha\hat{D}_{rrr}r^3dH_{rr}^{-1}\hat{H}_{rz}^2H_{zz} \\
& + H^{-1}\alpha\hat{\tilde{D}}_{rrz}r^3dH_{rr}^{-1}\hat{H}_{rz} + H^{-2}\alpha\hat{\tilde{D}}_{rrz}r^5dH_{rr}^{-1}\hat{H}_{rz}^3 \\
& + H^{-1}\alpha\hat{D}_{rzz}r\left(-\frac{1}{2}d+\mu\right) - \frac{1}{2}H^{-2}\alpha\hat{D}_{rzz}r^3d\hat{H}_{rz}^2 \\
& + H^{-1}\alpha D_{zrr}rH_{rr}^{-1}\hat{H}_{rz}\left(d-\mu\right) \\
& + \frac{1}{2}H^{-2}\alpha D_{zrr}r^3dH_{rr}^{-1}\hat{H}_{rz}^3 - H^{-1}\alpha\hat{D}_{zrz}r\mu \\
& - H^{-2}\alpha\hat{D}_{zrz}r^3d\hat{H}_{rz}^2 + \frac{1}{2}H^{-2}\alpha D_{zzz}rdH_{rr}\hat{H}_{rz} \\
& + \alpha rH_{rr}^{-1}\left(-\frac{1}{2}r^2d\hat{\tilde{s}}_r + r^2\mu\hat{\tilde{s}}_r + \frac{1}{2}a\hat{A}_r - \mu\hat{Z}_r\right) \\
& + H^{-1}\alpha r\hat{H}_{rz}\left(-\frac{1}{2}r^4dH_{rr}^{-1}\hat{H}_{rz}\hat{\tilde{s}}_r + r^4H_{rr}^{-1}\hat{H}_{rz}\mu\hat{\tilde{s}}_r\right. \\
& \qquad + \frac{1}{2}r^2a\hat{A}_rH_{rr}^{-1}\hat{H}_{rz} + \frac{1}{2}r^2d\hat{s}_z - r^2H_{rr}^{-1}\hat{H}_{rz}\mu\hat{Z}_r \\
& \qquad \left. - r^2\mu\hat{s}_z - \frac{1}{2}aA_z + \mu Z_z\right) - r\beta^z\hat{B}_z{}^r
\end{aligned}$$

$$\begin{aligned}\tilde{\mathcal{F}}^z\left(B_z{}^z\right) = {} & H^{-1}\alpha\hat{D}_{rrr}r^2H_{rr}^{-1}\hat{H}_{rz}\left(d-\mu\right)\\ & + \frac{1}{2}H^{-2}\alpha\hat{D}_{rrr}r^4dH_{rr}^{-1}\hat{H}_{rz}^3 - H^{-1}\alpha\hat{\tilde{D}}_{rrz}r^2\mu\\ & - H^{-2}\alpha\hat{\tilde{D}}_{rrz}r^4d\hat{H}_{rz}^2 + \frac{1}{2}H^{-2}\alpha\hat{D}_{rzz}r^2dH_{rr}\hat{H}_{rz}\\ & + H^{-1}\alpha D_{zrr}\left(-d+2\mu\right) - \frac{1}{2}H^{-2}\alpha D_{zrr}r^2d\hat{H}_{rz}^2\\ & + H^{-2}\alpha\hat{D}_{zrz}r^2dH_{rr}\hat{H}_{rz} - \frac{1}{2}H^{-2}\alpha D_{zzz}dH_{rr}^2\\ & + H^{-1}\alpha\left(\frac{1}{2}r^4d\hat{H}_{rz}\hat{\tilde{s}}_r - r^4\hat{H}_{rz}\mu\hat{\tilde{s}}_r - \frac{1}{2}r^2a\hat{A}_r\hat{H}_{rz}\right.\\ & \qquad - \frac{1}{2}r^2dH_{rr}\hat{s}_z + r^2H_{rr}\mu\hat{s}_z + r^2\hat{H}_{rz}\mu\hat{Z}_r\\ & \qquad \left. + \frac{1}{2}aA_zH_{rr} - H_{rr}\mu Z_z\right) - \beta^zB_z{}^z\end{aligned}$$

$$\tilde{\mathcal{F}}^z\left(\chi_{rr}\right) = -H^{-1}\alpha\hat{D}_{rrr}r^2\hat{H}_{rz} + H^{-1}\alpha D_{zrr}H_{rr} - \chi_{rr}\beta^z$$

$$\begin{aligned}\tilde{\mathcal{F}}^z\left(\chi_{rz}\right) = {} & -\frac{1}{2}H^{-1}\alpha\hat{D}_{rrr}r^3H_{rr}^{-1}\hat{H}_{rz}^2 - H^{-1}\alpha\hat{\tilde{D}}_{rrz}r^3\hat{H}_{rz}\\ & + \frac{1}{2}H^{-1}\alpha\hat{D}_{rzz}rH_{rr} + H^{-1}\alpha D_{zrr}r\hat{H}_{rz}\\ & + \alpha r\left(\frac{1}{2}r^2\hat{\tilde{s}}_r + \frac{1}{2}\hat{A}_r - \hat{Z}_r\right) - r\beta^z\hat{\chi}_{rz}\end{aligned}$$

$$\begin{aligned}\tilde{\mathcal{F}}^z\left(\chi_{zz}\right) = {} & -2\alpha\hat{\tilde{D}}_{rrz}r^2H_{rr}^{-1} - 2H^{-1}\alpha\hat{\tilde{D}}_{rrz}r^4H_{rr}^{-1}\hat{H}_{rz}^2\\ & + H^{-1}\alpha\hat{D}_{rzz}r^2\hat{H}_{rz} + 2\alpha D_{zrr}H_{rr}^{-1}\\ & + H^{-1}\alpha D_{zrr}r^2H_{rr}^{-1}\hat{H}_{rz}^2 + \alpha\left(r^2\hat{s}_z + A_z - 2Z_z\right) - \chi_{zz}\beta^z\end{aligned}$$

$$\tilde{\mathcal{F}}^z\left(Y\right) = H^{-1}\alpha r\left(-r^2\hat{H}_{rz}\hat{\tilde{s}}_r + H_{rr}\hat{s}_z\right) - r\beta^z\hat{Y}$$

$$\tilde{\mathcal{F}}^z\left(E^r\right) = 2H^{-1}\alpha r\hat{H}_{rz}Z^\varphi - r\beta^z\hat{E}^r - \left(\sqrt{H}\right)^{-1}\alpha r\hat{B}^\varphi$$

$$\tilde{\mathcal{F}}^z\left(E^z\right) = -2H^{-1}\alpha H_{rr}Z^\varphi - \beta^zE^z$$

$$\tilde{\mathcal{F}}^z\left(B^\varphi\right) = -r\beta^z\hat{B}^\varphi - \left(\sqrt{H}\right)^{-1}\alpha r\left(\hat{E}^r H_{rr} + E^z\hat{H}_{rz}\right)$$

$$\begin{aligned}\tilde{\mathcal{F}}^z\left(\theta\right) = &-H^{-1}\alpha\hat{D}_{rrr}r^2H_{rr}^{-1}\hat{H}_{rz} - H^{-1}\alpha\hat{\hat{D}}_{rrz}r^2 + 2H^{-1}\alpha D_{zrr}\\ &+ H^{-1}\alpha\left(-r^4\hat{H}_{rz}\hat{\hat{s}}_r + r^2H_{rr}\hat{s}_z + r^2\hat{H}_{rz}\hat{Z}_r - H_{rr}Z_z\right) - \beta^z\theta\end{aligned}$$

$$\tilde{\mathcal{F}}^z\left(Z_r\right) = H^{-1}\alpha\chi_{rr}r\hat{H}_{rz} - H^{-1}\alpha r\hat{\chi}_{rz}H_{rr} - r\beta^z\hat{Z}_r$$

$$\begin{aligned}\tilde{\mathcal{F}}^z\left(Z_z\right) = &2\alpha\chi_{rr}H_{rr}^{-1} + H^{-1}\alpha\chi_{rr}r^2H_{rr}^{-1}\hat{H}_{rz}^2\\ &+ \alpha\left(r^2\hat{Y} - \theta\right) - H^{-1}\alpha r^2\hat{\chi}_{rz}\hat{H}_{rz} - \beta^z Z_z\end{aligned}$$

$$\tilde{\mathcal{F}}^z\left(Z^\varphi\right) = -\frac{1}{2}\alpha E^z - \beta^z Z^\varphi$$

B.3 Sources

$$\begin{aligned}\tilde{\mathcal{S}}\left(H_{rr}\right) = &-2\alpha\chi_{rr} + 4\alpha r^2\left(\hat{\hat{B}}_r{}^r H_{rr} + \hat{B}_r{}^z\hat{H}_{rz}\right)\\ &+ 2\hat{D}_{rrr}r^2\hat{\beta}^r + 2D_{zrr}\beta^z + 2\hat{\beta}^r H_{rr}\end{aligned}$$

$$\begin{aligned}\tilde{\mathcal{S}}\left(H_{rz}\right) = &2\alpha r\left(r^2\hat{\hat{B}}_r{}^r\hat{H}_{rz} + \hat{B}_r{}^z H_{zz} + \hat{B}_z{}^r H_{rr} + B_z{}^z\hat{H}_{rz} - \hat{\chi}_{rz}\right)\\ &+ 2\hat{\hat{D}}_{rrz}r^3\hat{\beta}^r + 2\hat{D}_{zrz}r\beta^z + 2r\hat{\beta}^r\hat{H}_{rz}\end{aligned}$$

$$\tilde{\mathcal{S}}\left(H_{zz}\right) = -2\alpha\chi_{zz} + 4\alpha\left(r^2\hat{B}_z{}^r\hat{H}_{rz} + B_z{}^z H_{zz}\right) + 2\hat{D}_{rzz}r^2\hat{\beta}^r + 2D_{zzz}\beta^z$$

$$\tilde{\mathcal{S}}\left(s\right) = \alpha r\left(-2\hat{\hat{B}}_r{}^r - 2\hat{B}_r{}^z H_{rr}^{-1}\hat{H}_{rz} - \hat{Y}\right) + r\left(r^2\hat{\beta}^r\hat{\hat{s}}_r + 2\hat{\beta}^r\hat{s} + \beta^z\hat{s}_z\right)$$

$$\begin{aligned}\tilde{\mathcal{S}}\left(\alpha\right) = &-2\alpha^2\chi_{rr}fH_{rr}^{-1} - H^{-1}\alpha^2\chi_{rr}r^2fH_{rr}^{-1}\hat{H}_{rz}^2\\ &- H^{-1}\alpha^2\chi_{zz}fH_{rr} + \alpha^2 f\left(-r^2\hat{Y} + m\theta\right)\\ &+ 2H^{-1}\alpha^2r^2\hat{\chi}_{rz}f\hat{H}_{rz} + \alpha\left(r^2\hat{A}_r\hat{\beta}^r + A_z\beta^z\right)\end{aligned}$$

$$
\begin{aligned}
\tilde{\mathcal{S}}\left(\beta^{r}\right) = {} & 2H^{-1}\alpha^{2}\hat{D}_{rrr}rH_{rr}^{-1}H_{zz}\left(d-\mu\right)\\
& + H^{-2}\alpha^{2}\hat{D}_{rrr}r^{3}dH_{rr}^{-1}\hat{H}_{rz}^{2}H_{zz}\\
& - 2H^{-1}\alpha^{2}\hat{\tilde{D}}_{rrz}r^{3}dH_{rr}^{-1}\hat{H}_{rz} - 2H^{-2}\alpha^{2}\hat{\tilde{D}}_{rrz}r^{5}dH_{rr}^{-1}\hat{H}_{rz}^{3}\\
& + H^{-1}\alpha^{2}\hat{D}_{rzz}r\left(d-2\mu\right) + H^{-2}\alpha^{2}\hat{D}_{rzz}r^{3}d\hat{H}_{rz}^{2}\\
& + 2H^{-1}\alpha^{2}D_{zrr}rH_{rr}^{-1}\hat{H}_{rz}\left(-d+\mu\right)\\
& - H^{-2}\alpha^{2}D_{zrr}r^{3}dH_{rr}^{-1}\hat{H}_{rz}^{3} + 2H^{-1}\alpha^{2}\hat{D}_{zrz}r\mu\\
& + 2H^{-2}\alpha^{2}\hat{D}_{zrz}r^{3}d\hat{H}_{rz}^{2} - H^{-2}\alpha^{2}D_{zzz}rdH_{rr}\hat{H}_{rz}\\
& + \alpha^{2}rH_{rr}^{-1}\left(r^{2}d\hat{\tilde{s}}_{r} - 2r^{2}\mu\hat{\tilde{s}}_{r} - a\hat{A}_{r} + 2d\hat{s} - 4\mu\hat{s} + 2\mu\hat{Z}_{r}\right)\\
& + H^{-1}\alpha^{2}r\hat{H}_{rz}\left(r^{4}dH_{rr}^{-1}\hat{H}_{rz}\hat{\tilde{s}}_{r} - 2r^{4}H_{rr}^{-1}\hat{H}_{rz}\mu\hat{\tilde{s}}_{r}\right.\\
& \qquad - r^{2}a\hat{A}_{r}H_{rr}^{-1}\hat{H}_{rz} + 2r^{2}dH_{rr}^{-1}\hat{H}_{rz}\hat{s} - r^{2}d\hat{s}_{z}\\
& \qquad - 4r^{2}H_{rr}^{-1}\hat{H}_{rz}\mu\hat{s} + 2r^{2}H_{rr}^{-1}\hat{H}_{rz}\mu\hat{Z}_{r}\\
& \qquad \left. + 2r^{2}\mu\hat{s}_{z} + aA_{z} - dH_{rr}^{-1}\hat{H}_{rz} - 2\mu Z_{z}\right)\\
& - H^{-2}\alpha^{2}r^{3}dH_{rr}^{-1}\hat{H}_{rz}^{4} + 2\alpha r\left(r^{2}\hat{\beta}^{r}\hat{\tilde{B}}_{r}{}^{r} + \beta^{z}\hat{B}_{z}{}^{r}\right) + r\hat{\beta}^{r^{2}}
\end{aligned}
$$

$$
\begin{aligned}
\tilde{\mathcal{S}}\left(\beta^{z}\right) = {} & 2H^{-1}\alpha^{2}\hat{D}_{rrr}r^{2}H_{rr}^{-1}\hat{H}_{rz}\left(-d+\mu\right)\\
& - H^{-2}\alpha^{2}\hat{D}_{rrr}r^{4}dH_{rr}^{-1}\hat{H}_{rz}^{3} + 2H^{-1}\alpha^{2}\hat{\tilde{D}}_{rrz}r^{2}\mu\\
& + 2H^{-2}\alpha^{2}\hat{\tilde{D}}_{rrz}r^{4}d\hat{H}_{rz}^{2} - H^{-2}\alpha^{2}\hat{D}_{rzz}r^{2}dH_{rr}\hat{H}_{rz}\\
& + 2H^{-1}\alpha^{2}D_{zrr}\left(d-2\mu\right) + H^{-2}\alpha^{2}D_{zrr}r^{2}d\hat{H}_{rz}^{2}\\
& - 2H^{-2}\alpha^{2}\hat{D}_{zrz}r^{2}dH_{rr}\hat{H}_{rz} + H^{-2}\alpha^{2}D_{zzz}dH_{rr}^{2}\\
& + H^{-1}\alpha^{2}\left(-r^{4}d\hat{H}_{rz}\hat{\tilde{s}}_{r} + 2r^{4}\hat{H}_{rz}\mu\hat{\tilde{s}}_{r} + r^{2}a\hat{A}_{r}\hat{H}_{rz} + r^{2}dH_{rr}\hat{s}_{z}\right.\\
& \qquad - 2r^{2}d\hat{H}_{rz}\hat{s} - 2r^{2}H_{rr}\mu\hat{s}_{z} + 4r^{2}\hat{H}_{rz}\mu\hat{s} - 2r^{2}\hat{H}_{rz}\mu\hat{Z}_{r}\\
& \qquad \left. - aA_{z}H_{rr} - d\hat{H}_{rz} + 2H_{rr}\mu Z_{z} + 3\hat{H}_{rz}\mu\right)\\
& + H^{-2}\alpha^{2}r^{2}d\hat{H}_{rz}^{3} + 2\alpha\left(r^{2}\hat{\beta}^{r}\hat{B}_{r}{}^{z} + \beta^{z}B_{z}{}^{z}\right)
\end{aligned}
$$

$$
\tilde{\mathcal{S}}\left(D_{rrr}\right) = -2\alpha\hat{D}_{rrr}rB_{z}{}^{z} + 2\alpha D_{zrr}r\hat{B}_{r}{}^{z} + 2\alpha r\hat{\tilde{B}}_{r}{}^{r}H_{rr} + 2\hat{D}_{rrr}r\hat{\beta}^{r}
$$

$$\tilde{\mathcal{S}}\left(\tilde{D}_{rrz}\right) = -2\alpha\hat{\tilde{D}}_{rrz}rB_z{}^z + 2\alpha\hat{D}_{zrz}r\hat{B}_r{}^z + 2\alpha r\hat{\tilde{B}}_r{}^r\hat{H}_{rz} + 2\hat{\tilde{D}}_{rrz}r\hat{\beta}^r$$

$$\tilde{\mathcal{S}}\left(D_{rzz}\right) = -2\alpha\hat{D}_{rzz}rB_z{}^z + 2\alpha D_{zzz}r\hat{B}_r{}^z$$

$$\tilde{\mathcal{S}}\left(D_{zrr}\right) = 2\alpha\hat{D}_{rrr}r^2\hat{B}_z{}^r - 2\alpha D_{zrr}r^2\hat{\tilde{B}}_r{}^r + 2\alpha\hat{B}_z{}^rH_{rr} + D_{zrr}\hat{\beta}^r$$

$$\tilde{\mathcal{S}}\left(D_{zrz}\right) = 2\alpha\hat{\tilde{D}}_{rrz}r^3\hat{B}_z{}^r - 2\alpha\hat{D}_{zrz}r^3\hat{\tilde{B}}_r{}^r + 2\alpha r\hat{B}_z{}^r\hat{H}_{rz}$$

$$\tilde{\mathcal{S}}\left(D_{zzz}\right) = 2\alpha\hat{D}_{rzz}r^2\hat{B}_z{}^r - 2\alpha D_{zzz}r^2\hat{\tilde{B}}_r{}^r - D_{zzz}\hat{\beta}^r$$

$$\tilde{\mathcal{S}}\left(\tilde{s}_r\right) = 2\alpha r\left(2\hat{\tilde{B}}_r{}^r\hat{s} + \hat{B}_r{}^z\hat{s}_z - B_z{}^z\hat{\tilde{s}}_r\right) + 2r\hat{\beta}^r\hat{\tilde{s}}_r$$

$$\tilde{\mathcal{S}}\left(s_z\right) = 2\alpha r\left(-r^2\hat{\tilde{B}}_r{}^r\hat{s}_z + r^2\hat{B}_z{}^r\hat{\tilde{s}}_r + 2\hat{B}_z{}^r\hat{s}\right)$$

$$\tilde{\mathcal{S}}\left(A_r\right) = 2\alpha r\left(-\hat{A}_rB_z{}^z + A_z\hat{B}_r{}^z\right)$$

$$\tilde{\mathcal{S}}\left(A_z\right) = 2\alpha r^2\left(\hat{A}_r\hat{B}_z{}^r - A_z\hat{\tilde{B}}_r{}^r\right) - A_z\hat{\beta}^r$$

$$
\begin{aligned}
\tilde{\mathcal{S}}\left(\tilde{B}_r{}^r\right) = {} & 2\alpha\chi_{rr} r \hat{\tilde{B}}_r{}^r f H_{rr}^{-1} \\
& + H^{-1}\alpha\chi_{rr} r^3 \hat{\tilde{B}}_r{}^r f H_{rr}^{-1} \hat{H}_{rz}^2 + H^{-1}\alpha\chi_{zz} r \hat{\tilde{B}}_r{}^r f H_{rr} \\
& + H^{-1}\alpha\hat{D}_{rrr} r H_{rr}^{-1} H_{zz}\left(\hat{A}_r d - \hat{A}_r \mu - 2d\hat{s} + 4\mu\hat{s}\right) \\
& + H^{-2}\alpha\hat{D}_{rrr} r H_{rr}^{-1} \hat{H}_{rz}^2 H_{zz}\left(\frac{1}{2} r^2 \hat{A}_r d - 2r^2 d\hat{s} + 4r^2\mu\hat{s} + 2d\right) \\
& + 2H^{-3}\alpha\hat{D}_{rrr} r^3 d H_{rr}^{-1} \hat{H}_{rz}^4 H_{zz} \\
& + H^{-1}\alpha\hat{\tilde{D}}_{rrz} r H_{rr}^{-1} \hat{H}_{rz}\left(-r^2 \hat{A}_r d + 4r^2 d\hat{s} - 8r^2\mu\hat{s} - 2d\right) \\
& + H^{-2}\alpha\hat{\tilde{D}}_{rrz} r^3 H_{rr}^{-1} \hat{H}_{rz}^3\left(-r^2 \hat{A}_r d + 4r^2 d\hat{s} - 8r^2\mu\hat{s} - 6d\right) \\
& - 4H^{-3}\alpha\hat{\tilde{D}}_{rrz} r^5 d H_{rr}^{-1} \hat{H}_{rz}^5 + H^{-1}\alpha\hat{D}_{rzz} r \hat{A}_r\left(\frac{1}{2} d - \mu\right) \\
& + H^{-2}\alpha\hat{D}_{rzz} r \hat{H}_{rz}^2\left(\frac{1}{2} r^2 \hat{A}_r d - 2r^2 d\hat{s} + 4r^2\mu\hat{s} + d\right) \\
& + 2H^{-3}\alpha\hat{D}_{rzz} r^3 d\hat{H}_{rz}^4 + H^{-1}\alpha D_{zrr} r \hat{A}_r H_{rr}^{-1} \hat{H}_{rz}\left(-d + \mu\right) \\
& - \frac{1}{2} H^{-2}\alpha D_{zrr} r^3 \hat{A}_r d H_{rr}^{-1} \hat{H}_{rz}^3 + H^{-1}\alpha\hat{D}_{zrz} r \hat{A}_r \mu \\
& + H^{-2}\alpha\hat{D}_{zrz} r^3 \hat{A}_r d\hat{H}_{rz}^2 - \frac{1}{2} H^{-2}\alpha D_{zzz} r \hat{A}_r d H_{rr} \hat{H}_{rz} \\
& + \alpha r\left(\frac{1}{2} r^2 \hat{A}_r d H_{rr}^{-1} \hat{\tilde{s}}_r - r^2 \hat{A}_r H_{rr}^{-1} \mu \hat{\tilde{s}}_r + r^2 \hat{\tilde{B}}_r{}^r f\hat{Y}\right. \\
& \quad - \frac{1}{2} a \hat{A}_r^2 H_{rr}^{-1} + 2\hat{A}_r d H_{rr}^{-1}\hat{s} - 4\hat{A}_r H_{rr}^{-1}\mu\hat{s} \\
& \quad + \hat{A}_r H_{rr}^{-1}\mu\hat{Z}_r - 2\hat{\tilde{B}}_r{}^r B_z{}^z - \hat{\tilde{B}}_r{}^r f m\theta \\
& \quad \left. + 2\hat{B}_r{}^z \hat{B}_z{}^r + d H_{rr}^{-1}\hat{\tilde{s}}_r - 2H_{rr}^{-1}\mu\hat{\tilde{s}}_r\right)
\end{aligned}
$$

$$
\begin{aligned}
&+H^{-1}\alpha r\hat{H}_{rz}\left(\frac{1}{2}r^4\hat{A}_r d H_{rr}^{-1}\hat{H}_{rz}\hat{\tilde{s}}_r - r^4\hat{A}_r H_{rr}^{-1}\hat{H}_{rz}\mu\hat{\tilde{s}}_r\right.\\
&\qquad -\frac{1}{2}r^2 a\hat{A}_r^2 H_{rr}^{-1}\hat{H}_{rz} + 2r^2\hat{A}_r d H_{rr}^{-1}\hat{H}_{rz}\hat{s}\\
&\qquad -\frac{1}{2}r^2\hat{A}_r d\hat{s}_z - 4r^2\hat{A}_r H_{rr}^{-1}\hat{H}_{rz}\mu\hat{s}\\
&\qquad + r^2\hat{A}_r H_{rr}^{-1}\hat{H}_{rz}\mu\hat{Z}_r + r^2\hat{A}_r\mu\hat{s}_z - 2r^2\hat{\tilde{B}}_r{}^r\hat{\chi}_{rz}f\\
&\qquad + r^2 d H_{rr}^{-1}\hat{H}_{rz}\hat{\tilde{s}}_r - 2r^2 H_{rr}^{-1}\hat{H}_{rz}\mu\hat{\tilde{s}}_r\\
&\qquad +\frac{1}{2}a\hat{A}_r A_z - \hat{A}_r d H_{rr}^{-1}\hat{H}_{rz} - \hat{A}_r\mu Z_z\\
&\qquad \left. + 2d H_{rr}^{-1}\hat{H}_{rz}\hat{s} - 4H_{rr}^{-1}\hat{H}_{rz}\mu\hat{s}\right)\\
&+ H^{-2}\alpha r H_{rr}^{-1}\hat{H}_{rz}^4\left(-r^2\hat{A}_r d + 2r^2 d\hat{s} - 4r^2\mu\hat{s} - 2d\right)\\
&- 2H^{-3}\alpha r^3 d H_{rr}^{-1}\hat{H}_{rz}^6 + 2r\hat{\beta}^r\hat{\tilde{B}}_r{}^r
\end{aligned}
$$

$$
\begin{aligned}
\tilde{\mathcal{S}}\left(B_r{}^z\right) = {} & 2\alpha\chi_{rr} r \hat{B}_r{}^z f H_{rr}^{-1} \\
& + H^{-1}\alpha\chi_{rr} r^3 \hat{B}_r{}^z f H_{rr}^{-1} \hat{H}_{rz}^2 + H^{-1}\alpha\chi_{zz} r \hat{B}_r{}^z f H_{rr} \\
& + H^{-1}\alpha \hat{D}_{rrr} r H_{rr}^{-1} \hat{H}_{rz} \Big(-r^2 \hat{A}_r d + r^2 \hat{A}_r \mu \\
& \qquad + 2r^2 d\hat{s} - 4r^2 \mu \hat{s} + d - 3\mu \Big) \\
& + H^{-2}\alpha \hat{D}_{rrr} r^3 H_{rr}^{-1} \hat{H}_{rz}^3 \left(-\frac{1}{2} r^2 \hat{A}_r d + 2r^2 d\hat{s} - 4r^2 \mu \hat{s} - d - 3\mu \right) \\
& - 2H^{-3}\alpha \hat{D}_{rrr} r^5 d H_{rr}^{-1} \hat{H}_{rz}^5 \\
& + H^{-1}\alpha \hat{\tilde{D}}_{rrz} r \left(r^2 \hat{A}_r \mu - 2r^2 d\hat{s} + 4r^2 \mu \hat{s} - d + 3\mu \right) \\
& + H^{-2}\alpha \hat{\tilde{D}}_{rrz} r^3 \hat{H}_{rz}^2 \left(r^2 \hat{A}_r d - 4r^2 d\hat{s} + 8r^2 \mu \hat{s} + d + 6\mu \right) \\
& + 4H^{-3}\alpha \hat{\tilde{D}}_{rrz} r^5 d \hat{H}_{rz}^4 \\
& + H^{-2}\alpha \hat{D}_{rzz} r H_{rr} \hat{H}_{rz} \left(-\frac{1}{2} r^2 \hat{A}_r d + 2r^2 d\hat{s} - 4r^2 \mu \hat{s} + d - 3\mu \right) \\
& - 2H^{-3}\alpha \hat{D}_{rzz} r^3 d H_{rr} \hat{H}_{rz}^3 + H^{-1}\alpha D_{zrr} r \hat{A}_r \left(d - 2\mu \right) \\
& + \frac{1}{2} H^{-2}\alpha D_{zrr} r^3 \hat{A}_r d \hat{H}_{rz}^2 - H^{-2}\alpha \hat{D}_{zrz} r^3 \hat{A}_r d H_{rr} \hat{H}_{rz} \\
& + \frac{1}{2} H^{-2}\alpha D_{zzz} r \hat{A}_r d H_{rr}^2 + \alpha r \hat{B}_r{}^z f \left(r^2 \hat{Y} - m\theta \right) \\
& + H^{-1}\alpha r \left(-\frac{1}{2} r^4 \hat{A}_r d \hat{H}_{rz} \hat{\tilde{s}}_r + r^4 \hat{A}_r \hat{H}_{rz} \mu \hat{\tilde{s}}_r + \frac{1}{2} r^2 a \hat{A}_r^2 \hat{H}_{rz} \right. \\
& \qquad + \frac{1}{2} r^2 \hat{A}_r d H_{rr} \hat{s}_z - 2r^2 \hat{A}_r d \hat{H}_{rz} \hat{s} - r^2 \hat{A}_r H_{rr} \mu \hat{s}_z \\
& \qquad + 4r^2 \hat{A}_r \hat{H}_{rz} \mu \hat{s} - r^2 \hat{A}_r \hat{H}_{rz} \mu \hat{Z}_r - 2r^2 \hat{B}_r{}^z \hat{\chi}_{rz} f \hat{H}_{rz} \\
& \qquad - r^2 d \hat{H}_{rz} \hat{\tilde{s}}_r + 2r^2 \hat{H}_{rz} \mu \hat{\tilde{s}}_r - \frac{1}{2} a \hat{A}_r A_z H_{rr} - \hat{A}_r d \hat{H}_{rz} \\
& \qquad \left. + \hat{A}_r H_{rr} \mu Z_z + 3\hat{A}_r \hat{H}_{rz} \mu - 2d \hat{H}_{rz} \hat{s} + 4\hat{H}_{rz} \mu \hat{s} \right) \\
& + H^{-2}\alpha r \hat{H}_{rz}^3 \left(r^2 \hat{A}_r d - 2r^2 d\hat{s} + 4r^2 \mu \hat{s} + 3\mu \right) + 2H^{-3}\alpha r^3 d \hat{H}_{rz}^5
\end{aligned}
$$

$$
\begin{aligned}
\tilde{\mathcal{S}}\left(B_z{}^r\right) = {} & 2\alpha\chi_{rr} r \hat{B}_z{}^r f H_{rr}^{-1} + H^{-1}\alpha\chi_{rr} r^3 \hat{B}_z{}^r f H_{rr}^{-1} \hat{H}_{rz}^2 \\
& + H^{-1}\alpha\chi_{zz} r \hat{B}_z{}^r f H_{rr} + H^{-1}\alpha \hat{D}_{rrr} r A_z H_{rr}^{-1} H_{zz} \left(d - \mu\right) \\
& + \frac{1}{2} H^{-2}\alpha \hat{D}_{rrr} r^3 A_z d H_{rr}^{-1} \hat{H}_{rz}^2 H_{zz} \\
& - H^{-1}\alpha \hat{\tilde{D}}_{rrz} r^3 A_z d H_{rr}^{-1} \hat{H}_{rz} - H^{-2}\alpha \hat{\tilde{D}}_{rrz} r^5 A_z d H_{rr}^{-1} \hat{H}_{rz}^3 \\
& + H^{-1}\alpha \hat{D}_{rzz} r A_z \left(\frac{1}{2} d - \mu\right) + \frac{1}{2} H^{-2}\alpha \hat{D}_{rzz} r^3 A_z d \hat{H}_{rz}^2 \\
& + H^{-1}\alpha D_{zrr} r H_{rr}^{-1} \Big(-A_z d \hat{H}_{rz} + A_z \hat{H}_{rz} \mu \\
& \qquad - 2 d H_{zz} \hat{s} + 4 H_{zz} \mu \hat{s} \Big) \\
& + H^{-2}\alpha D_{zrr} r H_{rr}^{-1} \hat{H}_{rz}^2 \Big(-\frac{1}{2} r^2 A_z d \hat{H}_{rz} - 2 r^2 d H_{zz} \hat{s} \\
& \qquad + 4 r^2 H_{zz} \mu \hat{s} + 2 d H_{zz} \Big) \\
& + 2 H^{-3}\alpha D_{zrr} r^3 d H_{rr}^{-1} \hat{H}_{rz}^4 H_{zz} \\
& + H^{-1}\alpha \hat{D}_{zrz} r \Big(4 r^2 d H_{rr}^{-1} \hat{H}_{rz} \hat{s} - 8 r^2 H_{rr}^{-1} \hat{H}_{rz} \mu \hat{s} \\
& \qquad + A_z \mu - 2 d H_{rr}^{-1} \hat{H}_{rz} \Big) \\
& + H^{-2}\alpha \hat{D}_{zrz} r^3 \hat{H}_{rz}^2 \Big(4 r^2 d H_{rr}^{-1} \hat{H}_{rz} \hat{s} - 8 r^2 H_{rr}^{-1} \hat{H}_{rz} \mu \hat{s} \\
& \qquad + A_z d - 6 d H_{rr}^{-1} \hat{H}_{rz} \Big) \\
& - 4 H^{-3}\alpha \hat{D}_{zrz} r^5 d H_{rr}^{-1} \hat{H}_{rz}^5 \\
& + H^{-2}\alpha D_{zzz} r \hat{H}_{rz} \Big(-2 r^2 d \hat{H}_{rz} \hat{s} + 4 r^2 \hat{H}_{rz} \mu \hat{s} - \frac{1}{2} A_z d H_{rr} \\
& \qquad + d \hat{H}_{rz} \Big) + 2 H^{-3}\alpha D_{zzz} r^3 d \hat{H}_{rz}^4 \\
& + \alpha r \Big(\frac{1}{2} r^2 A_z d H_{rr}^{-1} \hat{\tilde{s}}_r - r^2 A_z H_{rr}^{-1} \mu \hat{\tilde{s}}_r + r^2 \hat{B}_z{}^r f \hat{Y} \\
& \quad - \frac{1}{2} a \hat{A}_r A_z H_{rr}^{-1} + 2 A_z d H_{rr}^{-1} \hat{s} - 4 A_z H_{rr}^{-1} \mu \hat{s} \\
& \quad + A_z H_{rr}^{-1} \mu \hat{Z}_r - \hat{B}_z{}^r f m \theta + d H_{rr}^{-1} \hat{s}_z - 2 H_{rr}^{-1} \mu \hat{s}_z \Big)
\end{aligned}
$$

$$
\begin{aligned}
&+H^{-1}\alpha r\hat{H}_{rz}\left(\frac{1}{2}r^4A_z dH_{rr}^{-1}\hat{H}_{rz}\hat{\hat{s}}_r - r^4A_zH_{rr}^{-1}\hat{H}_{rz}\mu\hat{\hat{s}}_r\right.\\
&\qquad -\frac{1}{2}r^2a\hat{A}_rA_zH_{rr}^{-1}\hat{H}_{rz} + 2r^2A_zdH_{rr}^{-1}\hat{H}_{rz}\hat{s}\\
&\qquad -\frac{1}{2}r^2A_zd\hat{s}_z - 4r^2A_zH_{rr}^{-1}\hat{H}_{rz}\mu\hat{s}\\
&\qquad + r^2A_zH_{rr}^{-1}\hat{H}_{rz}\mu\hat{Z}_r + r^2A_z\mu\hat{s}_z - 2r^2\hat{B}_z{}^r\hat{\chi}_{rz}f\\
&\qquad + r^2dH_{rr}^{-1}\hat{H}_{rz}\hat{s}_z - 2r^2H_{rr}^{-1}\hat{H}_{rz}\mu\hat{s}_z\\
&\qquad \left.+\frac{1}{2}aA_z^2 - A_zdH_{rr}^{-1}\hat{H}_{rz} - A_z\mu Z_z\right)\\
&- H^{-2}\alpha r^3A_zdH_{rr}^{-1}\hat{H}_{rz}^4
\end{aligned}
$$

$$
\begin{aligned}
\tilde{\mathcal{S}}\left(B_z{}^z\right) = {} & 2\alpha\chi_{rr}B_z{}^z f H_{rr}^{-1} + H^{-1}\alpha\chi_{rr}r^2 B_z{}^z f H_{rr}^{-1}\hat{H}_{rz}^2 \\
& + H^{-1}\alpha\chi_{zz}B_z{}^z f H_{rr} + H^{-1}\alpha\hat{D}_{rrr}r^2 A_z H_{rr}^{-1}\hat{H}_{rz}\left(-d+\mu\right) \\
& - \frac{1}{2}H^{-2}\alpha\hat{D}_{rrr}r^4 A_z d H_{rr}^{-1}\hat{H}_{rz}^3 + H^{-1}\alpha\hat{\tilde{D}}_{rrz}r^2 A_z\mu \\
& + H^{-2}\alpha\hat{\tilde{D}}_{rrz}r^4 A_z d\hat{H}_{rz}^2 - \frac{1}{2}H^{-2}\alpha\hat{D}_{rzz}r^2 A_z d H_{rr}\hat{H}_{rz} \\
& + H^{-1}\alpha D_{zrr}\Big(2r^2 d H_{rr}^{-1}\hat{H}_{rz}\hat{s} - 4r^2 H_{rr}^{-1}\hat{H}_{rz}\mu\hat{s} + A_z d \\
& \qquad - 2A_z\mu + d H_{rr}^{-1}\hat{H}_{rz} - 3H_{rr}^{-1}\hat{H}_{rz}\mu\Big) \\
& + H^{-2}\alpha D_{zrr}r^2\hat{H}_{rz}^2\Big(2r^2 d H_{rr}^{-1}\hat{H}_{rz}\hat{s} - 4r^2 H_{rr}^{-1}\hat{H}_{rz}\mu\hat{s} \\
& \qquad + \frac{1}{2}A_z d - d H_{rr}^{-1}\hat{H}_{rz} - 3H_{rr}^{-1}\hat{H}_{rz}\mu\Big) \\
& - 2H^{-3}\alpha D_{zrr}r^4 d H_{rr}^{-1}\hat{H}_{rz}^5 \\
& + H^{-1}\alpha\hat{D}_{zrz}\left(-2r^2 d\hat{s} + 4r^2\mu\hat{s} - d + 3\mu\right) \\
& + H^{-2}\alpha\hat{D}_{zrz}r^2\hat{H}_{rz}\Big(-4r^2 d\hat{H}_{rz}\hat{s} + 8r^2\hat{H}_{rz}\mu\hat{s} - A_z d H_{rr} + d\hat{H}_{rz} \\
& \qquad + 6\hat{H}_{rz}\mu\Big) + 4H^{-3}\alpha\hat{D}_{zrz}r^4 d\hat{H}_{rz}^4 \\
& + H^{-2}\alpha D_{zzz}H_{rr}\Big(2r^2 d\hat{H}_{rz}\hat{s} - 4r^2\hat{H}_{rz}\mu\hat{s} + \frac{1}{2}A_z d H_{rr} + d\hat{H}_{rz} \\
& \qquad - 3\hat{H}_{rz}\mu\Big) - 2H^{-3}\alpha D_{zzz}r^2 d H_{rr}\hat{H}_{rz}^3 \\
& + \alpha\Big(-2r^2\hat{\tilde{B}}_r{}^r B_z{}^z + 2r^2\hat{B}_r{}^z\hat{B}_z{}^r + r^2 B_z{}^z f\hat{Y} - B_z{}^z f m\theta\Big) \\
& + H^{-1}\alpha\Big(-\frac{1}{2}r^4 A_z d\hat{H}_{rz}\hat{\tilde{s}}_r + r^4 A_z\hat{H}_{rz}\mu\hat{\tilde{s}}_r + \frac{1}{2}r^2 a\hat{A}_r A_z\hat{H}_{rz} \\
& \qquad + \frac{1}{2}r^2 A_z d H_{rr}\hat{s}_z - 2r^2 A_z d\hat{H}_{rz}\hat{s} - r^2 A_z H_{rr}\mu\hat{s}_z \\
& \qquad + 4r^2 A_z\hat{H}_{rz}\mu\hat{s} - r^2 A_z\hat{H}_{rz}\mu\hat{Z}_r - 2r^2 B_z{}^z\hat{\chi}_{rz}f\hat{H}_{rz} \\
& \qquad - r^2 d\hat{H}_{rz}\hat{s}_z + 2r^2\hat{H}_{rz}\mu\hat{s}_z - \frac{1}{2}a A_z^2 H_{rr} \\
& \qquad - A_z d\hat{H}_{rz} + A_z H_{rr}\mu Z_z + 3A_z\hat{H}_{rz}\mu\Big) \\
& + H^{-2}\alpha r^2 A_z d\hat{H}_{rz}^3 - \hat{\beta}^r B_z{}^z
\end{aligned}
$$

$$
\begin{aligned}
\tilde{\mathcal{S}}\left(\chi_{rr}\right) = \kappa\alpha H_{rr}&\left(\frac{1}{2}r^2\hat{\tilde{\tau}} - \frac{1}{2}\rho_K - \frac{1}{2}\sigma\right)\\
&+ H^{-1}\kappa\alpha\left(-r^2 H_{rr}\hat{H}_{rz}\hat{S}_{rz} + \frac{1}{2}r^2\hat{H}_{rz}^2 S_{rr} + \frac{1}{2}H_{rr}^2 S_{zz}\right)\\
&- H^{-1}\alpha\chi_{rr}^2 r^2 H_{rr}^{-1}\hat{H}_{rz}^2 + H^{-1}\alpha\chi_{rr}\chi_{zz}H_{rr}\\
&+ \alpha\chi_{rr}\left(2r^2\hat{\tilde{B}}_r{}^r + r^2\hat{Y} - 2B_z{}^z - 2\theta\right)\\
&+ 2H^{-1}\alpha\chi_{rr}r^2\hat{\chi}_{rz}\hat{H}_{rz} + H^{-1}\alpha\hat{D}_{rrr}^2 r^4 H_{rr}^{-2}\hat{H}_{rz}^2\\
&- 2H^{-1}\alpha\hat{D}_{rrr}\hat{\tilde{D}}_{rrz}r^4 H_{rr}^{-1}\hat{H}_{rz} + H^{-1}\alpha\hat{D}_{rrr}\hat{D}_{rzz}r^2\\
&- H^{-2}\alpha\hat{D}_{rrr}\hat{D}_{rzz}r^4\hat{H}_{rz}^2 - 4H^{-1}\alpha\hat{D}_{rrr}\hat{D}_{zrz}r^2\\
&- 2H^{-2}\alpha\hat{D}_{rrr}\hat{D}_{zrz}r^4\hat{H}_{rz}^2 + 3H^{-2}\alpha\hat{D}_{rrr}D_{zzz}r^2 H_{rr}\hat{H}_{rz}\\
&+ \alpha\hat{D}_{rrr}H_{rr}^{-1}\left(-r^4\hat{\tilde{s}}_r + 2r^2\hat{A}_r - 2r^2\hat{s} - 2r^2\hat{Z}_r - 1\right)\\
&+ H^{-1}\alpha\hat{D}_{rrr}r^2\hat{H}_{rz}\left(r^4 H_{rr}^{-1}\hat{H}_{rz}\hat{\tilde{s}}_r + r^2\hat{A}_r H_{rr}^{-1}\hat{H}_{rz}\right.\\
&\qquad + 2r^2 H_{rr}^{-1}\hat{H}_{rz}\hat{s} - 2r^2 H_{rr}^{-1}\hat{H}_{rz}\hat{Z}_r\\
&\qquad \left. - r^2\hat{s}_z - 2A_z + 2Z_z\right)\\
&+ 2H^{-2}\alpha\hat{\tilde{D}}_{rrz}\hat{D}_{rzz}r^4 H_{rr}\hat{H}_{rz}\\
&+ 4H^{-1}\alpha\hat{\tilde{D}}_{rrz}D_{zrr}r^2 + 4H^{-2}\alpha\hat{\tilde{D}}_{rrz}D_{zrr}r^4\hat{H}_{rz}^2\\
&- 4H^{-2}\alpha\hat{\tilde{D}}_{rrz}\hat{D}_{zrz}r^4 H_{rr}\hat{H}_{rz} - 2H^{-2}\alpha\hat{\tilde{D}}_{rrz}D_{zzz}r^2 H_{rr}^2\\
&+ 2H^{-1}\alpha\hat{\tilde{D}}_{rrz}r^2\left(-r^4\hat{H}_{rz}\hat{\tilde{s}}_r - r^2\hat{A}_r\hat{H}_{rz} + r^2 H_{rr}\hat{s}_z - 2r^2\hat{H}_{rz}\hat{s}\right.\\
&\qquad \left. + 2r^2\hat{H}_{rz}\hat{Z}_r + A_z H_{rr} - 2H_{rr}Z_z - \hat{H}_{rz}\right)\\
&- H^{-2}\alpha\hat{D}_{rzz}^2 r^2 H_{rr}^2 - 3H^{-2}\alpha\hat{D}_{rzz}D_{zrr}r^2 H_{rr}\hat{H}_{rz}\\
&+ 4H^{-2}\alpha\hat{D}_{rzz}\hat{D}_{zrz}r^2 H_{rr}^2 + H^{-1}\alpha\hat{D}_{rzz}r^2\hat{A}_r H_{rr}\\
&+ H^{-2}\alpha\hat{D}_{rzz}r^2 H_{rr}\hat{H}_{rz}^2 - H^{-2}\alpha D_{zrr}^2 r^2\hat{H}_{rz}^2\\
&+ 2H^{-2}\alpha D_{zrr}\hat{D}_{zrz}r^2 H_{rr}\hat{H}_{rz} - H^{-2}\alpha D_{zrr}D_{zzz}H_{rr}^2
\end{aligned}
$$

$$
\begin{aligned}
&+H^{-1}\alpha D_{zrr}\Big(r^4\hat{H}_{rz}\hat{\tilde{s}}_r+2r^2\hat{A}_r\hat{H}_{rz}-r^2H_{rr}\hat{s}_z+2r^2\hat{H}_{rz}\hat{s}\\
&\qquad\qquad-2r^2\hat{H}_{rz}\hat{Z}_r+2H_{rr}Z_z+3\hat{H}_{rz}\Big)\\
&+2H^{-2}\alpha D_{zrr}r^2\hat{H}_{rz}^3-2H^{-1}\alpha\hat{D}_{zrz}r^2\hat{A}_rH_{rr}\\
&-2H^{-2}\alpha\hat{D}_{zrz}r^2H_{rr}\hat{H}_{rz}^2-H^{-2}\alpha D_{zzz}H_{rr}^2\hat{H}_{rz}\\
&+\alpha e^{2r^2\hat{s}}r^4H_{rr}\left(-\frac{1}{2}\hat{B^\varphi}^2H_{rr}+\frac{1}{2}\hat{E^r}^2H_{rr}^2\right.\\
&\qquad\qquad\left.+\hat{E^r}E^zH_{rr}\hat{H}_{rz}+\frac{1}{2}E^{z2}\hat{H}_{rz}^2\right)\\
&+\alpha\Big(-r^6\hat{\tilde{s}}_r^2+r^4\hat{A}_r\hat{\tilde{s}}_r-4r^4\hat{s}\hat{\tilde{s}}_r-2r^2\hat{A}_r\hat{Z}_r\\
&\quad+4r^2\hat{B_r}^z\hat{\chi}_{rz}-4r^2\hat{s}^2-4r^2\hat{\tilde{s}}_r-6\hat{s}\Big)\\
&+H^{-1}\alpha\Big(-r^4\hat{H}_{rz}^2\hat{\tilde{s}}_r-r^2\hat{A}_r\hat{H}_{rz}^2-2r^2\hat{\chi}_{rz}^2H_{rr}\\
&\qquad+r^2H_{rr}\hat{H}_{rz}\hat{s}_z-2r^2\hat{H}_{rz}^2\hat{s}+2r^2\hat{H}_{rz}^2\hat{Z}_r\\
&\qquad+A_zH_{rr}\hat{H}_{rz}-2H_{rr}\hat{H}_{rz}Z_z-\hat{H}_{rz}^2\Big)+\chi_{rr}\hat{\beta}^r
\end{aligned}
$$

$$
\begin{aligned}
\tilde{\mathcal{S}}\left(\chi_{rz}\right) = \kappa\alpha r\left(\frac{1}{2}r^2\hat{H}_{rz}\hat{\tilde{\tau}} + H_{rr}^{-1}\hat{H}_{rz}S_{rr} - \frac{1}{2}\hat{H}_{rz}\rho_K - \frac{1}{2}\hat{H}_{rz}\sigma - \hat{S}_{rz}\right) \\
+ H^{-1}\kappa\alpha r\hat{H}_{rz}\left(\frac{1}{2}r^2H_{rr}^{-1}\hat{H}_{rz}^2S_{rr} - r^2\hat{H}_{rz}\hat{S}_{rz} + \frac{1}{2}H_{rr}S_{zz}\right) \\
+ 2H^{-1}\alpha\chi_{rr}\chi_{zz}r\hat{H}_{rz} + 2\alpha\chi_{rr}r\hat{B}_z{}^r \\
- H^{-1}\alpha\chi_{rr}r^3\hat{\chi}_{rz}H_{rr}^{-1}\hat{H}_{rz}^2 + 2\alpha\chi_{zz}r\hat{B}_r{}^z \\
- H^{-1}\alpha\chi_{zz}r\hat{\chi}_{rz}H_{rr} - 2H^{-1}\alpha\hat{D}_{rrr}\hat{D}_{rzz}r^3H_{rr}^{-1}\hat{H}_{rz} \\
- H^{-2}\alpha\hat{D}_{rrr}\hat{D}_{rzz}r^5H_{rr}^{-1}\hat{H}_{rz}^3 \\
+ H^{-1}\alpha\hat{D}_{rrr}D_{zrr}r^3H_{rr}^{-2}\hat{H}_{rz}^2 \\
- 2H^{-1}\alpha\hat{D}_{rrr}\hat{D}_{zrz}r^3H_{rr}^{-1}\hat{H}_{rz} \\
- 2H^{-2}\alpha\hat{D}_{rrr}\hat{D}_{zrz}r^5H_{rr}^{-1}\hat{H}_{rz}^3 \\
+ 3H^{-2}\alpha\hat{D}_{rrr}D_{zzz}r^3\hat{H}_{rz}^2 - \alpha\hat{D}_{rrr}r^3H_{rr}^{-1}\hat{s}_z \\
- \frac{1}{2}H^{-1}\alpha\hat{D}_{rrr}r^3A_zH_{rr}^{-1}\hat{H}_{rz}^2 + 2H^{-1}\alpha\hat{\tilde{D}}_{rrz}\hat{D}_{rzz}r^3 \\
+ 2H^{-2}\alpha\hat{\tilde{D}}_{rrz}\hat{D}_{rzz}r^5\hat{H}_{rz}^2 + 4H^{-1}\alpha\hat{\tilde{D}}_{rrz}D_{zrr}r^3H_{rr}^{-1}\hat{H}_{rz} \\
+ 4H^{-2}\alpha\hat{\tilde{D}}_{rrz}D_{zrr}r^5H_{rr}^{-1}\hat{H}_{rz}^3 - 4H^{-1}\alpha\hat{\tilde{D}}_{rrz}\hat{D}_{zrz}r^3 \\
- 4H^{-2}\alpha\hat{\tilde{D}}_{rrz}\hat{D}_{zrz}r^5\hat{H}_{rz}^2 - 2H^{-2}\alpha\hat{\tilde{D}}_{rrz}D_{zzz}r^3H_{rr}\hat{H}_{rz} \\
- H^{-1}\alpha\hat{\tilde{D}}_{rrz}r^3A_z\hat{H}_{rz} - H^{-2}\alpha\hat{D}_{rzz}^2r^3H_{rr}\hat{H}_{rz} \\
+ H^{-1}\alpha\hat{D}_{rzz}D_{zrr}r - 3H^{-2}\alpha\hat{D}_{rzz}D_{zrr}r^3\hat{H}_{rz}^2 \\
+ 4H^{-2}\alpha\hat{D}_{rzz}\hat{D}_{zrz}r^3H_{rr}\hat{H}_{rz} \\
+ H^{-1}\alpha\hat{D}_{rzz}r\left(-r^4\hat{H}_{rz}\hat{\tilde{s}}_r + r^2H_{rr}\hat{s}_z - 2r^2\hat{H}_{rz}\hat{s}\right. \\
\left. + 2r^2\hat{H}_{rz}\hat{Z}_r + \frac{3}{2}A_zH_{rr} - 2H_{rr}Z_z\right) \\
+ H^{-2}\alpha\hat{D}_{rzz}r^3\hat{H}_{rz}^3 - 2H^{-1}\alpha D_{zrr}^2rH_{rr}^{-1}\hat{H}_{rz} \\
- H^{-2}\alpha D_{zrr}^2r^3H_{rr}^{-1}\hat{H}_{rz}^3 + 2H^{-1}\alpha D_{zrr}\hat{D}_{zrz}r \\
+ 2H^{-2}\alpha D_{zrr}\hat{D}_{zrz}r^3\hat{H}_{rz}^2 - H^{-2}\alpha D_{zrr}D_{zzz}rH_{rr}\hat{H}_{rz} \\
+ 2\alpha D_{zrr}rH_{rr}^{-1}\left(\hat{A}_r - \hat{Z}_r\right)
\end{aligned}
$$

$$
\begin{aligned}
&+H^{-1}\alpha D_{zrr} r \hat{H}_{rz} \Big(r^4 H_{rr}^{-1} \hat{H}_{rz} \hat{\hat{s}}_r + \frac{3}{2} r^2 \hat{A}_r H_{rr}^{-1} \hat{H}_{rz} \\
&\qquad + 2r^2 H_{rr}^{-1} \hat{H}_{rz} \hat{s} - 2r^2 H_{rr}^{-1} \hat{H}_{rz} \hat{Z}_r \\
&\qquad - r^2 \hat{s}_z + 2 H_{rr}^{-1} \hat{H}_{rz} + 2 Z_z \Big) \\
&+ H^{-2} \alpha D_{zrr} r^3 H_{rr}^{-1} \hat{H}_{rz}^4 - H^{-1} \alpha \hat{D}_{zrz} r^3 \hat{A}_r \hat{H}_{rz} \\
&- \frac{1}{2} H^{-1} \alpha D_{zzz} r \hat{A}_r H_{rr} - 2 H^{-2} \alpha D_{zzz} r H_{rr} \hat{H}_{rz}^2 \\
&+ \frac{1}{2} \alpha e^{2r^2 \hat{s}} H r^3 E^z \left(\hat{E}^r H_{rr} + E^z \hat{H}_{rz} \right) \\
&+ \alpha e^{2r^2 \hat{s}} r^5 \hat{H}_{rz} \Big(-\frac{1}{2} \hat{B}^{\varphi\,2} H_{rr} + \frac{1}{2} \hat{E}^{r\,2} H_{rr}^2 \\
&\qquad + \hat{E}^r E^z H_{rr} \hat{H}_{rz} + \frac{1}{2} E^{z2} \hat{H}_{rz}^2 \Big) \\
&+ \alpha r \Big(-r^4 \hat{\hat{s}}_r \hat{s}_z + \frac{1}{2} r^2 \hat{A}_r \hat{s}_z + \frac{1}{2} r^2 A_z \hat{\hat{s}}_r + r^2 \hat{\chi}_{rz} \hat{Y} \\
&\quad - 2r^2 \hat{s} \hat{s}_z - \hat{A}_r Z_z - A_z \hat{Z}_r - 2 \hat{\chi}_{rz} \theta - 2 \hat{s}_z \Big)
\end{aligned}
$$

$$
\begin{aligned}
\tilde{\mathcal{S}}\left(\chi_{zz}\right) = \kappa\alpha H H_{rr}^{-2}&\left(\frac{1}{2}r^2 H_{rr}\hat{\tilde{\tau}} - \frac{1}{2}H_{rr}\rho_K - \frac{1}{2}H_{rr}\sigma + S_{rr}\right)\\
&+ \kappa\alpha\left(\frac{1}{2}r^4 H_{rr}^{-1}\hat{H}_{rz}^2\hat{\tilde{\tau}} - \frac{1}{2}r^2 H_{rr}^{-1}\hat{H}_{rz}^2\rho_K - \frac{1}{2}r^2 H_{rr}^{-1}\hat{H}_{rz}^2\sigma\right.\\
&\qquad\left. - r^2 H_{rr}^{-1}\hat{H}_{rz}\hat{S}_{rz} + \frac{3}{2}r^2 H_{rr}^{-2}\hat{H}_{rz}^2 S_{rr} - \frac{1}{2}S_{zz}\right)\\
&+ H^{-1}\kappa\alpha r^2\hat{H}_{rz}^2\left(-r^2 H_{rr}^{-1}\hat{H}_{rz}\hat{S}_{rz} + \frac{1}{2}r^2 H_{rr}^{-2}\hat{H}_{rz}^2 S_{rr}\right.\\
&\qquad\left. + \frac{1}{2}S_{zz}\right) + 2\alpha\chi_{rr}\chi_{zz}H_{rr}^{-1}\\
&+ H^{-1}\alpha\chi_{rr}\chi_{zz}r^2 H_{rr}^{-1}\hat{H}_{rz}^2 - H^{-1}\alpha\chi_{zz}^2 H_{rr}\\
&+ \alpha\chi_{zz}\left(-2r^2\hat{\tilde{B}}_r{}^r + r^2\hat{Y} + 2B_z{}^z - 2\theta\right) + 2H^{-1}\alpha\chi_{zz}r^2\hat{\chi}_{rz}\hat{H}_{rz}\\
&- 2\alpha\hat{D}_{rrr}\hat{D}_{rzz}r^2 H_{rr}^{-2} - 3H^{-1}\alpha\hat{D}_{rrr}\hat{D}_{rzz}r^4 H_{rr}^{-2}\hat{H}_{rz}^2\\
&- H^{-2}\alpha\hat{D}_{rrr}\hat{D}_{rzz}r^6 H_{rr}^{-2}\hat{H}_{rz}^4\\
&- 2H^{-1}\alpha\hat{D}_{rrr}\hat{D}_{zrz}r^4 H_{rr}^{-2}\hat{H}_{rz}^2\\
&- 2H^{-2}\alpha\hat{D}_{rrr}\hat{D}_{zrz}r^6 H_{rr}^{-2}\hat{H}_{rz}^4\\
&+ 2H^{-1}\alpha\hat{D}_{rrr}D_{zzz}r^2 H_{rr}^{-1}\hat{H}_{rz}\\
&+ 3H^{-2}\alpha\hat{D}_{rrr}D_{zzz}r^4 H_{rr}^{-1}\hat{H}_{rz}^3\\
&+ 2H^{-1}\alpha\hat{\tilde{D}}_{rrz}\hat{D}_{rzz}r^4 H_{rr}^{-1}\hat{H}_{rz}\\
&+ 2H^{-2}\alpha\hat{\tilde{D}}_{rrz}\hat{D}_{rzz}r^6 H_{rr}^{-1}\hat{H}_{rz}^3\\
&+ 4\alpha\hat{\tilde{D}}_{rrz}D_{zrr}r^2 H_{rr}^{-2} + 8H^{-1}\alpha\hat{\tilde{D}}_{rrz}D_{zrr}r^4 H_{rr}^{-2}\hat{H}_{rz}^2\\
&+ 4H^{-2}\alpha\hat{\tilde{D}}_{rrz}D_{zrr}r^6 H_{rr}^{-2}\hat{H}_{rz}^4\\
&- 4H^{-1}\alpha\hat{\tilde{D}}_{rrz}\hat{D}_{zrz}r^4 H_{rr}^{-1}\hat{H}_{rz}\\
&- 4H^{-2}\alpha\hat{\tilde{D}}_{rrz}\hat{D}_{zrz}r^6 H_{rr}^{-1}\hat{H}_{rz}^3 - 4H^{-1}\alpha\hat{\tilde{D}}_{rrz}D_{zzz}r^2\\
&- 2H^{-2}\alpha\hat{\tilde{D}}_{rrz}D_{zzz}r^4\hat{H}_{rz}^2 - 2\alpha\hat{\tilde{D}}_{rrz}r^2 A_z H_{rr}^{-1}\\
&- 2H^{-1}\alpha\hat{\tilde{D}}_{rrz}r^4 A_z H_{rr}^{-1}\hat{H}_{rz}^2 + H^{-1}\alpha\hat{D}_{rzz}^2 r^2\\
&- H^{-2}\alpha\hat{D}_{rzz}^2 r^4\hat{H}_{rz}^2 - 2H^{-1}\alpha\hat{D}_{rzz}D_{zrr}r^2 H_{rr}^{-1}\hat{H}_{rz}\\
&- 3H^{-2}\alpha\hat{D}_{rzz}D_{zrr}r^4 H_{rr}^{-1}\hat{H}_{rz}^3
\end{aligned}
$$

$$
\begin{aligned}
&+2H^{-1}\alpha\hat{D}_{rzz}\hat{D}_{zrz}r^2+4H^{-2}\alpha\hat{D}_{rzz}\hat{D}_{zrz}r^4\hat{H}_{rz}^2\\
&+\alpha\hat{D}_{rzz}H_{rr}^{-1}\left(-r^4\hat{\tilde{s}}_r-2r^2\hat{s}+2r^2\hat{Z}_r-1\right)\\
&+H^{-1}\alpha\hat{D}_{rzz}r^2\hat{H}_{rz}\left(-r^4H_{rr}^{-1}\hat{H}_{rz}\hat{\tilde{s}}_r-2r^2H_{rr}^{-1}\hat{H}_{rz}\hat{s}\right.\\
&\qquad\left.+2r^2H_{rr}^{-1}\hat{H}_{rz}\hat{Z}_r+r^2\hat{s}_z+2A_z-2Z_z\right)\\
&+H^{-2}\alpha\hat{D}_{rzz}r^4H_{rr}^{-1}\hat{H}_{rz}^4-2\alpha D_{zrr}^2H_{rr}^{-2}\\
&-2H^{-1}\alpha D_{zrr}^2r^2H_{rr}^{-2}\hat{H}_{rz}^2-H^{-2}\alpha D_{zrr}^2r^4H_{rr}^{-2}\hat{H}_{rz}^4\\
&+2H^{-2}\alpha D_{zrr}\hat{D}_{zrz}r^4H_{rr}^{-1}\hat{H}_{rz}^3\\
&+2H^{-1}\alpha D_{zrr}D_{zzz}-H^{-2}\alpha D_{zrr}D_{zzz}r^2\hat{H}_{rz}^2\\
&+2\alpha D_{zrr}H_{rr}^{-1}\left(-r^2\hat{s}_z+A_z\right)+H^{-1}\alpha D_{zrr}r^2A_zH_{rr}^{-1}\hat{H}_{rz}^2\\
&+2\alpha\hat{D}_{zrz}H_{rr}^{-1}\left(r^4\hat{\tilde{s}}_r+r^2\hat{A}_r+2r^2\hat{s}-2r^2\hat{Z}_r+2\right)\\
&+2H^{-1}\alpha\hat{D}_{zrz}r^2\hat{H}_{rz}\left(r^4H_{rr}^{-1}\hat{H}_{rz}\hat{\tilde{s}}_r+r^2\hat{A}_rH_{rr}^{-1}\hat{H}_{rz}\right.\\
&\qquad+2r^2H_{rr}^{-1}\hat{H}_{rz}\hat{s}-2r^2H_{rr}^{-1}\hat{H}_{rz}\hat{Z}_r\\
&\qquad\left.-r^2\hat{s}_z-A_z+3H_{rr}^{-1}\hat{H}_{rz}+2Z_z\right)\\
&+2H^{-2}\alpha\hat{D}_{zrz}r^4H_{rr}^{-1}\hat{H}_{rz}^4\\
&+H^{-1}\alpha D_{zzz}\left(-r^4\hat{H}_{rz}\hat{\tilde{s}}_r-2r^2\hat{A}_r\hat{H}_{rz}+r^2H_{rr}\hat{s}_z-2r^2\hat{H}_{rz}\hat{s}\right.\\
&\qquad\left.+2r^2\hat{H}_{rz}\hat{Z}_r+A_zH_{rr}-2H_{rr}Z_z-3\hat{H}_{rz}\right)\\
&-3H^{-2}\alpha D_{zzz}r^2\hat{H}_{rz}^3+\frac{1}{2}\alpha e^{2r^2\hat{s}}H^2r^2E^{z2}H_{rr}^{-1}\\
&+\alpha e^{2r^2\hat{s}}Hr^4\left(-\frac{1}{2}\hat{B^{\varphi}}^2+\hat{E^r}E^z\hat{H}_{rz}+E^{z2}H_{rr}^{-1}\hat{H}_{rz}^2\right)\\
&+\alpha e^{2r^2\hat{s}}r^6\hat{H}_{rz}^2\left(-\frac{1}{2}\hat{B^{\varphi}}^2+\frac{1}{2}\hat{E^r}^2H_{rr}\right.\\
&\qquad\left.+\hat{E^r}E^z\hat{H}_{rz}+\frac{1}{2}E^{z2}H_{rr}^{-1}\hat{H}_{rz}^2\right)\\
&+\alpha\left(-r^4\hat{s}_z^2+r^2A_z\hat{s}_z+4r^2\hat{B_z}^r\hat{\chi}_{rz}-2r^2\hat{\chi}_{rz}^2H_{rr}^{-1}\right.\\
&\quad\left.-2A_zZ_z\right)-2H^{-1}\alpha r^4\hat{\chi}_{rz}^2H_{rr}^{-1}\hat{H}_{rz}^2-\chi_{zz}\hat{\beta^r}
\end{aligned}
$$

$$
\begin{aligned}
\tilde{\mathcal{S}}\left(Y\right) = & -\kappa\alpha r\hat{\tilde{\tau}} + 2H^{-1}\alpha\chi_{rr}^{2} r H_{rr}^{-2}\hat{H}_{rz}^{2} \\
& + 2\alpha\chi_{rr} r H_{rr}^{-2}\left(2\hat{B}_{r}{}^{z}\hat{H}_{rz} + H_{rr}\hat{Y}\right) \\
& + H^{-1}\alpha\chi_{rr} r H_{rr}^{-1}\hat{H}_{rz}\left(r^{2}\hat{H}_{rz}\hat{Y} - 4\hat{\chi}_{rz}\right) \\
& + H^{-1}\alpha\chi_{zz} r H_{rr}\hat{Y} - 4H^{-1}\alpha\hat{D}_{rrr}^{2} r^{3} H_{rr}^{-3}\hat{H}_{rz}^{2} \\
& - H^{-2}\alpha\hat{D}_{rrr}^{2} r^{5} H_{rr}^{-3}\hat{H}_{rz}^{4} + 4H^{-1}\alpha\hat{D}_{rrr}\hat{\tilde{D}}_{rrz} r^{3} H_{rr}^{-2}\hat{H}_{rz} \\
& + 2H^{-2}\alpha\hat{D}_{rrr}\hat{\tilde{D}}_{rrz} r^{5} H_{rr}^{-2}\hat{H}_{rz}^{3} + 4H^{-1}\alpha\hat{D}_{rrr} D_{zrr} r H_{rr}^{-2}\hat{H}_{rz} \\
& + 2H^{-2}\alpha\hat{D}_{rrr} D_{zrr} r^{3} H_{rr}^{-2}\hat{H}_{rz}^{3} - 2H^{-2}\alpha\hat{D}_{rrr} D_{zzz} r\hat{H}_{rz} \\
& + H^{-1}\alpha\hat{D}_{rrr} r H_{rr}^{-2}\hat{H}_{rz}\left(-5r^{4}\hat{H}_{rz}\hat{\tilde{s}}_{r} - r^{2}\hat{A}_{r}\hat{H}_{rz} + 4r^{2}H_{rr}\hat{s}_{z}\right. \\
& \qquad\qquad - 2r^{2}\hat{H}_{rz}\hat{s} + 4r^{2}\hat{H}_{rz}\hat{Z}_{r} \\
& \qquad\qquad \left. + 2A_{z}H_{rr} - 4H_{rr}Z_{z}\right) \\
& + H^{-2}\alpha\hat{D}_{rrr} r^{3} H_{rr}^{-2}\hat{H}_{rz}^{3}\left(-r^{4}\hat{H}_{rz}\hat{\tilde{s}}_{r} + r^{2}H_{rr}\hat{s}_{z}\right. \\
& \qquad\qquad \left. + 2r^{2}\hat{H}_{rz}\hat{s} + 2\hat{H}_{rz}\right) \\
& - 2H^{-2}\alpha\hat{\tilde{D}}_{rrz}\hat{D}_{rzz} r^{3}\hat{H}_{rz} - 4H^{-1}\alpha\hat{\tilde{D}}_{rrz} D_{zrr} r H_{rr}^{-1} \\
& - 6H^{-2}\alpha\hat{\tilde{D}}_{rrz} D_{zrr} r^{3} H_{rr}^{-1}\hat{H}_{rz}^{2} \\
& + 4H^{-2}\alpha\hat{\tilde{D}}_{rrz}\hat{D}_{zrz} r^{3}\hat{H}_{rz} + 2H^{-2}\alpha\hat{\tilde{D}}_{rrz} D_{zzz} r H_{rr} \\
& + 2H^{-1}\alpha\hat{\tilde{D}}_{rrz} r\left(2r^{4}H_{rr}^{-1}\hat{H}_{rz}\hat{\tilde{s}}_{r} + r^{2}\hat{A}_{r}H_{rr}^{-1}\hat{H}_{rz}\right. \\
& \qquad\qquad \left. - 2r^{2}H_{rr}^{-1}\hat{H}_{rz}\hat{Z}_{r} - r^{2}\hat{s}_{z} - A_{z} + 2Z_{z}\right) \\
& + 2H^{-2}\alpha\hat{\tilde{D}}_{rrz} r^{3}\hat{H}_{rz}^{2}\left(r^{4}H_{rr}^{-1}\hat{H}_{rz}\hat{\tilde{s}}_{r} - 2r^{2}H_{rr}^{-1}\hat{H}_{rz}\hat{s}\right. \\
& \qquad\qquad \left. - r^{2}\hat{s}_{z} - H_{rr}^{-1}\hat{H}_{rz}\right) \\
& + H^{-2}\alpha\hat{D}_{rzz}^{2} r H_{rr} + 4H^{-2}\alpha\hat{D}_{rzz} D_{zrr} r\hat{H}_{rz} \\
& - 4H^{-2}\alpha\hat{D}_{rzz}\hat{D}_{zrz} r H_{rr} + H^{-1}\alpha\hat{D}_{rzz} r\left(-r^{2}\hat{\tilde{s}}_{r} - \hat{A}_{r} - 2\hat{s}\right) \\
& + H^{-2}\alpha\hat{D}_{rzz} r^{3}\hat{H}_{rz}\left(-r^{2}\hat{H}_{rz}\hat{\tilde{s}}_{r} + H_{rr}\hat{s}_{z} + 2\hat{H}_{rz}\hat{s}\right) \\
& + 2H^{-1}\alpha D_{zrr} r\left(r^{2}H_{rr}^{-1}\hat{H}_{rz}\hat{\tilde{s}}_{r} - \hat{A}_{r}H_{rr}^{-1}\hat{H}_{rz} - \hat{s}_{z}\right)
\end{aligned}
$$

$$
\begin{aligned}
&+H^{-2}\alpha D_{zrr} r \hat{H}_{rz}^2 \Big(r^4 H_{rr}^{-1} \hat{H}_{rz} \hat{\hat{s}}_r - 2r^2 H_{rr}^{-1} \hat{H}_{rz} \hat{s} - r^2 \hat{s}_z \\
&\qquad - 4 H_{rr}^{-1} \hat{H}_{rz} \Big) + 2H^{-1} \alpha \hat{D}_{zrz} r \left(\hat{A}_r + 2\hat{s} \right) \\
&+ 2H^{-2} \alpha \hat{D}_{zrz} r \hat{H}_{rz} \left(-r^4 \hat{H}_{rz} \hat{\hat{s}}_r + r^2 H_{rr} \hat{s}_z + 2r^2 \hat{H}_{rz} \hat{s} + 2\hat{H}_{rz} \right) \\
&+H^{-2} \alpha D_{zzz} r H_{rr} \left(r^2 \hat{H}_{rz} \hat{\hat{s}}_r - H_{rr} \hat{s}_z - 2\hat{H}_{rz} \hat{s} \right) - \frac{1}{2} \alpha e^{2r^2 \hat{s}} H r E^{z2} \\
&+ \alpha e^{2r^2 \hat{s}} r^3 \left(\hat{B^{\varphi}}^2 H_{rr} - \hat{E^r}^2 H_{rr}^2 - 2\hat{E^r} E^z H_{rr} \hat{H}_{rz} - E^{z2} \hat{H}_{rz}^2 \right) \\
&+ \alpha r \Big(-r^2 \hat{A}_r H_{rr}^{-1} \hat{\hat{s}}_r - 2r^2 \hat{\hat{B}}_r{}^r \hat{Y} + 2r^2 H_{rr}^{-1} \hat{\hat{s}}_r \hat{Z}_r \\
&\qquad + r^2 \hat{Y}^2 - 2\hat{A}_r H_{rr}^{-1} \hat{s} + 2\hat{A}_r H_{rr}^{-1} \hat{Z}_r \\
&\qquad - 4\hat{B_r}^z \hat{\chi}_{rz} H_{rr}^{-1} - 2B_z{}^z \hat{Y} + 4H_{rr}^{-1} \hat{s} \hat{Z}_r - 2\theta \hat{Y} \Big) \\
&+ H^{-1} \alpha r \Big(-r^6 H_{rr}^{-1} \hat{H}_{rz}^2 \hat{\hat{s}}_r^2 - 4r^4 H_{rr}^{-1} \hat{H}_{rz}^2 \hat{s} \hat{\hat{s}}_r \\
&\qquad + 2r^4 H_{rr}^{-1} \hat{H}_{rz}^2 \hat{\hat{s}}_r \hat{Z}_r + 2r^4 \hat{H}_{rz} \hat{\hat{s}}_r \hat{s}_z \\
&\qquad - 2r^2 \hat{A}_r H_{rr}^{-1} \hat{H}_{rz}^2 \hat{s} - 2r^2 \hat{\chi}_{rz} \hat{H}_{rz} \hat{Y} - r^2 H_{rr} \hat{s}_z^2 \\
&\qquad - 4r^2 H_{rr}^{-1} \hat{H}_{rz}^2 \hat{s}^2 + 4r^2 H_{rr}^{-1} \hat{H}_{rz}^2 \hat{s} \hat{Z}_r \\
&\qquad - 3r^2 H_{rr}^{-1} \hat{H}_{rz}^2 \hat{\hat{s}}_r + 4r^2 \hat{H}_{rz} \hat{s} \hat{s}_z - 2r^2 \hat{H}_{rz} \hat{\hat{s}}_r Z_z \\
&\qquad - 2r^2 \hat{H}_{rz} \hat{s}_z \hat{Z}_r + 2A_z \hat{H}_{rz} \hat{s} + 2\hat{\chi}_{rz}^2 + 2H_{rr} \hat{s}_z Z_z \\
&\qquad - 6H_{rr}^{-1} \hat{H}_{rz}^2 \hat{s} - 4\hat{H}_{rz} \hat{s} Z_z + 4\hat{H}_{rz} \hat{s}_z \Big) \\
&+ H^{-2} \alpha r \hat{H}_{rz}^3 \Big(r^4 H_{rr}^{-1} \hat{H}_{rz} \hat{\hat{s}}_r - 2r^2 H_{rr}^{-1} \hat{H}_{rz} \hat{s} \\
&\qquad - r^2 \hat{s}_z - H_{rr}^{-1} \hat{H}_{rz} \Big)
\end{aligned}
$$

$$
\begin{aligned}
\tilde{\mathcal{S}}\left(E^r\right) = & -2\kappa\alpha r H_{rr}^{-1}\hat{S}_r + 2H^{-1}\kappa\alpha r\hat{H}_{rz}\left(-r^2 H_{rr}^{-1}\hat{H}_{rz}\hat{S}_r + S_z\right) \\
& + 4\alpha\chi_{rr} r\hat{E}^r H_{rr}^{-1} + H^{-1}\alpha\chi_{rr} r^3\hat{E}^r H_{rr}^{-1}\hat{H}_{rz}^2 \\
& + H^{-1}\alpha\chi_{zz} r\hat{E}^r H_{rr} + 4H^{-1}\alpha\hat{D}_{rrr} r H_{rr}^{-1} H_{zz} Z^{\varphi} \\
& + 4H^{-2}\alpha\hat{D}_{rrr} r^3 H_{rr}^{-1}\hat{H}_{rz}^2 H_{zz} Z^{\varphi} \\
& - 8H^{-1}\alpha\hat{\tilde{D}}_{rrz} r^3 H_{rr}^{-1}\hat{H}_{rz} Z^{\varphi} - 8H^{-2}\alpha\hat{\tilde{D}}_{rrz} r^5 H_{rr}^{-1}\hat{H}_{rz}^3 Z^{\varphi} \\
& + 4H^{-2}\alpha\hat{D}_{rzz} r^3\hat{H}_{rz}^2 Z^{\varphi} - 4H^{-1}\alpha D_{zrr} r H_{rr}^{-1}\hat{H}_{rz} Z^{\varphi} \\
& - 4H^{-2}\alpha D_{zrr} r^3 H_{rr}^{-1}\hat{H}_{rz}^3 Z^{\varphi} + 4H^{-1}\alpha\hat{D}_{zrz} r Z^{\varphi} \\
& + 8H^{-2}\alpha\hat{D}_{zrz} r^3\hat{H}_{rz}^2 Z^{\varphi} - 4H^{-2}\alpha D_{zzz} r H_{rr}\hat{H}_{rz} Z^{\varphi} \\
& + \alpha r\left(-4r^2\hat{\tilde{B}}_r{}^r\hat{E}^r + 3r^2\hat{E}^r\hat{Y} - 2\hat{A}_r H_{rr}^{-1} Z^{\varphi}\right. \\
& \qquad \left. - 2\hat{B}_z{}^r E^z - 2B_z{}^z\hat{E}^r - 2\hat{E}^r\theta\right) \\
& + 2H^{-1}\alpha r\hat{H}_{rz}\left(-r^2\hat{A}_r H_{rr}^{-1}\hat{H}_{rz} Z^{\varphi} - r^2\hat{\chi}_{rz}\hat{E}^r\right. \\
& \qquad\qquad \left. + A_z Z^{\varphi} - 2H_{rr}^{-1}\hat{H}_{rz} Z^{\varphi}\right) \\
& - 4H^{-2}\alpha r^3 H_{rr}^{-1}\hat{H}_{rz}^4 Z^{\varphi} - 2r\hat{\beta}^r\hat{E}^r \\
& + 4\left(\sqrt{H}\right)^{-1}\alpha D_{zrr} r\hat{B}^{\varphi} H_{rr}^{-1} \\
& + H^{-1}\left(\sqrt{H}\right)^{-1}\alpha D_{zrr} r^3\hat{B}^{\varphi} H_{rr}^{-1}\hat{H}_{rz}^2 \\
& - 2H^{-1}\left(\sqrt{H}\right)^{-1}\alpha\hat{D}_{zrz} r^3\hat{B}^{\varphi}\hat{H}_{rz} \\
& + H^{-1}\left(\sqrt{H}\right)^{-1}\alpha D_{zzz} r\hat{B}^{\varphi} H_{rr} + \left(\sqrt{H}\right)^{-1}\alpha r\hat{B}^{\varphi}\left(3r^2\hat{s}_z - 2Z_z\right)
\end{aligned}
$$

$$
\begin{aligned}
\tilde{\mathcal{S}}\left(E^z\right) = {} & 2H^{-1}\kappa\alpha\left(r^2\hat{H}_{rz}\hat{S}_r - H_{rr}S_z\right) + 4\alpha\chi_{rr}E^z H_{rr}^{-1} \\
& + H^{-1}\alpha\chi_{rr}r^2E^z H_{rr}^{-1}\hat{H}_{rz}^2 + H^{-1}\alpha\chi_{zz}E^z H_{rr} \\
& - 4H^{-1}\alpha\hat{D}_{rrr}r^2H_{rr}^{-1}\hat{H}_{rz}Z^\varphi - 4H^{-2}\alpha\hat{D}_{rrr}r^4H_{rr}^{-1}\hat{H}_{rz}^3Z^\varphi \\
& + 4H^{-1}\alpha\hat{\tilde{D}}_{rrz}r^2Z^\varphi + 8H^{-2}\alpha\hat{\tilde{D}}_{rrz}r^4\hat{H}_{rz}^2Z^\varphi \\
& - 4H^{-2}\alpha\hat{D}_{rzz}r^2H_{rr}\hat{H}_{rz}Z^\varphi + 4H^{-2}\alpha D_{zrr}r^2\hat{H}_{rz}^2Z^\varphi \\
& - 8H^{-2}\alpha\hat{D}_{zrz}r^2H_{rr}\hat{H}_{rz}Z^\varphi + 4H^{-2}\alpha D_{zzz}H_{rr}^2Z^\varphi \\
& + \alpha\left(-2r^2\hat{\tilde{B}}_r{}^rE^z - 2r^2\hat{B}_r{}^z\hat{E}^r + 3r^2E^z\hat{Y} - 4B_z{}^zE^z - 2E^z\theta\right) \\
& + 2H^{-1}\alpha\left(r^2\hat{A}_r\hat{H}_{rz}Z^\varphi - r^2\hat{\chi}_{rz}E^z\hat{H}_{rz} - A_zH_{rr}Z^\varphi + \hat{H}_{rz}Z^\varphi\right) \\
& + 4H^{-2}\alpha r^2\hat{H}_{rz}^3Z^\varphi - \hat{\beta}^rE^z - 4\left(\sqrt{H}\right)^{-1}\alpha\hat{D}_{rrr}r^2\hat{B}^\varphi H_{rr}^{-1} \\
& - H^{-1}\left(\sqrt{H}\right)^{-1}\alpha\hat{D}_{rrr}r^4\hat{B}^\varphi H_{rr}^{-1}\hat{H}_{rz}^2 \\
& + 2H^{-1}\left(\sqrt{H}\right)^{-1}\alpha\hat{\tilde{D}}_{rrz}r^4\hat{B}^\varphi\hat{H}_{rz} - H^{-1}\left(\sqrt{H}\right)^{-1}\alpha\hat{D}_{rzz}r^2\hat{B}^\varphi H_{rr} \\
& + \left(\sqrt{H}\right)^{-1}\alpha\hat{B}^\varphi\left(-3r^4\hat{\tilde{s}}_r - 6r^2\hat{s} + 2r^2\hat{Z}_r - 3\right) \\
& + H^{-1}\left(\sqrt{H}\right)^{-1}\alpha r^2\hat{B}^\varphi\hat{H}_{rz}^2
\end{aligned}
$$

$$
\begin{aligned}
\tilde{\mathcal{S}}\left(B^{\varphi}\right) = {} & H^{-1}\alpha\chi_{rr}r\hat{B}^{\varphi}H_{zz} + H^{-1}\alpha\chi_{zz}r\hat{B}^{\varphi}H_{rr} \\
& - 2\alpha r\hat{B}^{\varphi}\left(r^{2}\hat{\tilde{B}}_{r}{}^{r} + B_{z}{}^{z}\right) - 2H^{-1}\alpha r^{3}\hat{B}^{\varphi}\hat{\chi}_{rz}\hat{H}_{rz} \\
& - r\hat{\beta}^{r}\hat{B}^{\varphi} - H^{-1}\left(\sqrt{H}\right)^{-1}\alpha\hat{D}_{rrr}rH_{zz}\left(r^{2}\hat{E}^{r}\hat{H}_{rz} + E^{z}H_{zz}\right) \\
& + 2H^{-1}\left(\sqrt{H}\right)^{-1}\alpha\hat{\tilde{D}}_{rrz}r^{3}\hat{H}_{rz}\left(r^{2}\hat{E}^{r}\hat{H}_{rz} + E^{z}H_{zz}\right) \\
& - \left(\sqrt{H}\right)^{-1}\alpha\hat{D}_{rzz}rE^{z} \\
& - H^{-1}\left(\sqrt{H}\right)^{-1}\alpha\hat{D}_{rzz}r^{3}\hat{H}_{rz}\left(\hat{E}^{r}H_{rr} + E^{z}\hat{H}_{rz}\right) \\
& + \left(\sqrt{H}\right)^{-1}\alpha D_{zrr}r\hat{E}^{r} \\
& + H^{-1}\left(\sqrt{H}\right)^{-1}\alpha D_{zrr}r\hat{H}_{rz}\left(r^{2}\hat{E}^{r}\hat{H}_{rz} + E^{z}H_{zz}\right) \\
& - 2H^{-1}\left(\sqrt{H}\right)^{-1}\alpha\hat{D}_{zrz}r^{3}\hat{H}_{rz}\left(\hat{E}^{r}H_{rr} + E^{z}\hat{H}_{rz}\right) \\
& + H^{-1}\left(\sqrt{H}\right)^{-1}\alpha D_{zzz}rH_{rr}\left(\hat{E}^{r}H_{rr} + E^{z}\hat{H}_{rz}\right) \\
& + H^{-1}\left(\sqrt{H}\right)^{-1}\alpha r\hat{H}_{rz}^{2}\left(r^{2}\hat{E}^{r}\hat{H}_{rz} + E^{z}H_{zz}\right)
\end{aligned}
$$

$$
\begin{aligned}
\tilde{\mathcal{S}}(\theta) = &-\kappa\alpha(\rho_K+\sigma) + \alpha\chi_{rr}^2 H_{rr}^{-2} + H^{-1}\alpha\chi_{rr}^2 r^2 H_{rr}^{-2}\hat{H}_{rz}^2 \\
&+ 2H^{-1}\alpha\chi_{rr}\chi_{zz} + \alpha\chi_{rr}H_{rr}^{-1}\left(r^2\hat{Y} - 2\theta\right) \\
&+ H^{-1}\alpha\chi_{rr}r^2 H_{rr}^{-1}\hat{H}_{rz}\left(r^2\hat{H}_{rz}\hat{Y} - 2\hat{\chi}_{rz} - \hat{H}_{rz}\theta\right) \\
&+ H^{-1}\alpha\chi_{zz}H_{rr}\left(r^2\hat{Y} - \theta\right) - 2H^{-1}\alpha\hat{D}_{rrr}^2 r^2 H_{rr}^{-2}H_{zz} \\
&- H^{-2}\alpha\hat{D}_{rrr}^2 r^4 H_{rr}^{-2}\hat{H}_{rz}^2 H_{zz} + 2H^{-1}\alpha\hat{D}_{rrr}\hat{\hat{D}}_{rrz}r^4 H_{rr}^{-2}\hat{H}_{rz} \\
&+ 2H^{-2}\alpha\hat{D}_{rrr}\hat{\hat{D}}_{rrz}r^6 H_{rr}^{-2}\hat{H}_{rz}^3 - 2H^{-1}\alpha\hat{D}_{rrr}\hat{D}_{rzz}r^2 H_{rr}^{-1} \\
&- 2H^{-2}\alpha\hat{D}_{rrr}\hat{D}_{rzz}r^4 H_{rr}^{-1}\hat{H}_{rz}^2 \\
&+ 4H^{-1}\alpha\hat{D}_{rrr}D_{zrr}r^2 H_{rr}^{-2}\hat{H}_{rz} + 2H^{-2}\alpha\hat{D}_{rrr}D_{zrr}r^4 H_{rr}^{-2}\hat{H}_{rz}^3 \\
&- 2H^{-2}\alpha\hat{D}_{rrr}\hat{D}_{zrz}r^4 H_{rr}^{-1}\hat{H}_{rz}^2 + 2H^{-2}\alpha\hat{D}_{rrr}D_{zzz}r^2\hat{H}_{rz} \\
&+ \alpha\hat{D}_{rrr}H_{rr}^{-2}\left(-3r^4\hat{\hat{s}}_r + r^2\hat{A}_r - 2r^2\hat{s} + 2r^2\hat{Z}_r - 1\right) \\
&+ H^{-1}\alpha\hat{D}_{rrr}r^2 H_{rr}^{-2}\hat{H}_{rz}\Big(-4r^4\hat{H}_{rz}\hat{\hat{s}}_r + r^2\hat{A}_r\hat{H}_{rz} \\
&\qquad + 3r^2 H_{rr}\hat{s}_z + 3r^2\hat{H}_{rz}\hat{Z}_r \\
&\qquad - A_z H_{rr} - 2H_{rr}Z_z + \hat{H}_{rz}\Big) \\
&+ H^{-2}\alpha\hat{D}_{rrr}r^4 H_{rr}^{-2}\hat{H}_{rz}^3\Big(-r^4\hat{H}_{rz}\hat{\hat{s}}_r + r^2 H_{rr}\hat{s}_z + 2r^2\hat{H}_{rz}\hat{s} \\
&\qquad + r^2\hat{H}_{rz}\hat{Z}_r - H_{rr}Z_z + 2\hat{H}_{rz}\Big) \\
&+ 2H^{-2}\alpha\hat{\hat{D}}_{rrz}\hat{D}_{rzz}r^4\hat{H}_{rz} \\
&+ 2H^{-1}\alpha\hat{\hat{D}}_{rrz}D_{zrr}r^2 H_{rr}^{-1} - 4H^{-2}\alpha\hat{\hat{D}}_{rrz}\hat{D}_{zrz}r^4\hat{H}_{rz} \\
&+ H^{-1}\alpha\hat{\hat{D}}_{rrz}r^2\Big(2r^4 H_{rr}^{-1}\hat{H}_{rz}\hat{\hat{s}}_r - 4r^2 H_{rr}^{-1}\hat{H}_{rz}\hat{s} \\
&\qquad - 2r^2 H_{rr}^{-1}\hat{H}_{rz}\hat{Z}_r - A_z - 2H_{rr}^{-1}\hat{H}_{rz}\Big) \\
&+ 2H^{-2}\alpha\hat{\hat{D}}_{rrz}r^4\hat{H}_{rz}^2\Big(r^4 H_{rr}^{-1}\hat{H}_{rz}\hat{\hat{s}}_r - 2r^2 H_{rr}^{-1}\hat{H}_{rz}\hat{s} \\
&\qquad - r^2 H_{rr}^{-1}\hat{H}_{rz}\hat{Z}_r - r^2\hat{s}_z \\
&\qquad - H_{rr}^{-1}\hat{H}_{rz} + Z_z\Big) \\
&- H^{-2}\alpha\hat{D}_{rzz}^2 r^2 H_{rr} + 2H^{-2}\alpha\hat{D}_{rzz}\hat{D}_{zrz}r^2 H_{rr} \\
&\quad + H^{-1}\alpha\hat{D}_{rzz}\left(-r^4\hat{\hat{s}}_r + r^2\hat{A}_r - 2r^2\hat{s} + r^2\hat{Z}_r - 1\right)
\end{aligned}
$$

$$
\begin{aligned}
&+ H^{-2}\alpha\hat{D}_{rzz}r^2\hat{H}_{rz}\Big(-r^4\hat{H}_{rz}\hat{\tilde{s}}_r + r^2H_{rr}\hat{s}_z + 2r^2\hat{H}_{rz}\hat{s} \\
&\qquad + r^2\hat{H}_{rz}\hat{Z}_r - H_{rr}Z_z + 2\hat{H}_{rz}\Big) \\
&- 3H^{-1}\alpha D^2_{zrr}H^{-1}_{rr} - 2H^{-2}\alpha D^2_{zrr}r^2H^{-1}_{rr}\hat{H}^2_{rz} \\
&+ 4H^{-2}\alpha D_{zrr}\hat{D}_{zrz}r^2\hat{H}_{rz} - 2H^{-2}\alpha D_{zrr}D_{zzz}H_{rr} \\
&+ H^{-1}\alpha D_{zrr}\Big(3r^4H^{-1}_{rr}\hat{H}_{rz}\hat{\tilde{s}}_r - r^2\hat{A}_rH^{-1}_{rr}\hat{H}_{rz} \\
&\qquad + 2r^2H^{-1}_{rr}\hat{H}_{rz}\hat{s} - 2r^2H^{-1}_{rr}\hat{H}_{rz}\hat{Z}_r \\
&\qquad - 3r^2\hat{s}_z + 2A_z + H^{-1}_{rr}\hat{H}_{rz} + 2Z_z\Big) \\
&+ H^{-2}\alpha D_{zrr}r^2\hat{H}^2_{rz}\Big(r^4H^{-1}_{rr}\hat{H}_{rz}\hat{\tilde{s}}_r - 2r^2H^{-1}_{rr}\hat{H}_{rz}\hat{s} \\
&\qquad - r^2H^{-1}_{rr}\hat{H}_{rz}\hat{Z}_r - r^2\hat{s}_z \\
&\qquad - 2H^{-1}_{rr}\hat{H}_{rz} + Z_z\Big) \\
&+ H^{-1}\alpha\hat{D}_{zrz}\Big(-r^2\hat{A}_r + 4r^2\hat{s} + 3\Big) \\
&+ 2H^{-2}\alpha\hat{D}_{zrz}r^2\hat{H}_{rz}\Big(-r^4\hat{H}_{rz}\hat{\tilde{s}}_r + r^2H_{rr}\hat{s}_z + 2r^2\hat{H}_{rz}\hat{s} \\
&\qquad + r^2\hat{H}_{rz}\hat{Z}_r - H_{rr}Z_z + \hat{H}_{rz}\Big) \\
&+ H^{-2}\alpha D_{zzz}H_{rr}\Big(r^4\hat{H}_{rz}\hat{\tilde{s}}_r - r^2H_{rr}\hat{s}_z - 2r^2\hat{H}_{rz}\hat{s} - r^2\hat{H}_{rz}\hat{Z}_r \\
&\qquad + H_{rr}Z_z - 2\hat{H}_{rz}\Big) - \frac{1}{4}\alpha e^{2r^2\hat{s}}Hr^2E^{z2} \\
&+ \alpha e^{2r^2\hat{s}}r^4\Big(-\frac{1}{4}\hat{B^\varphi}^2H_{rr} - \frac{1}{4}\hat{E^r}^2H^2_{rr} - \frac{1}{2}\hat{E^r}E^zH_{rr}\hat{H}_{rz} \\
&\qquad - \frac{1}{4}E^{z2}\hat{H}^2_{rz}\Big) \\
&+ \alpha\Big(-r^6H^{-1}_{rr}\hat{\tilde{s}}^2_r + r^4\hat{A}_rH^{-1}_{rr}\hat{\tilde{s}}_r - 4r^4H^{-1}_{rr}\hat{s}\hat{\tilde{s}}_r \\
&\quad + r^4H^{-1}_{rr}\hat{\tilde{s}}_r\hat{Z}_r - 2r^2\hat{A}_rH^{-1}_{rr}\hat{Z}_r - 2r^2\hat{\tilde{B}}_r{}^r\theta \\
&\quad - 4r^2H^{-1}_{rr}\hat{s}^2 + 2r^2H^{-1}_{rr}\hat{s}\hat{Z}_r - 4r^2H^{-1}_{rr}\hat{\tilde{s}}_r \\
&\quad - r^2\theta\hat{Y} - 2B_z{}^z\theta - 6H^{-1}_{rr}\hat{s} + H^{-1}_{rr}\hat{Z}_r\Big)
\end{aligned}
$$

$$
\begin{aligned}
&+H^{-1}\alpha\Big(-r^8H_{rr}^{-1}\hat{H}_{rz}^2\hat{\tilde{s}}_r^2+r^6\hat{A}_rH_{rr}^{-1}\hat{H}_{rz}^2\hat{\tilde{s}}_r\\
&\quad-4r^6H_{rr}^{-1}\hat{H}_{rz}^2\hat{s}\hat{\tilde{s}}_r+r^6H_{rr}^{-1}\hat{H}_{rz}^2\hat{\tilde{s}}_r\hat{Z}_r\\
&\quad+2r^6\hat{H}_{rz}\hat{\tilde{s}}_r\hat{s}_z-2r^4\hat{A}_rH_{rr}^{-1}\hat{H}_{rz}^2\hat{Z}_r-r^4\hat{A}_r\hat{H}_{rz}\hat{s}_z\\
&\quad-r^4A_z\hat{H}_{rz}\hat{\tilde{s}}_r-2r^4\hat{\chi}_{rz}\hat{H}_{rz}\hat{Y}-r^4H_{rr}\hat{s}_z^2\\
&\quad-4r^4H_{rr}^{-1}\hat{H}_{rz}^2\hat{s}^2+2r^4H_{rr}^{-1}\hat{H}_{rz}^2\hat{s}\hat{Z}_r\\
&\quad-3r^4H_{rr}^{-1}\hat{H}_{rz}^2\hat{\tilde{s}}_r+4r^4\hat{H}_{rz}\hat{s}\hat{s}_z-r^4\hat{H}_{rz}\hat{\tilde{s}}_rZ_z\\
&\quad-r^4\hat{H}_{rz}\hat{s}_z\hat{Z}_r+2r^2\hat{A}_r\hat{H}_{rz}Z_z+r^2A_zH_{rr}\hat{s}_z\\
&\quad+2r^2A_z\hat{H}_{rz}\hat{Z}_r-r^2\hat{\chi}_{rz}^2+2r^2\hat{\chi}_{rz}\hat{H}_{rz}\theta\\
&\quad+r^2H_{rr}\hat{s}_zZ_z-8r^2H_{rr}^{-1}\hat{H}_{rz}^2\hat{s}-2r^2\hat{H}_{rz}\hat{s}Z_z\\
&\quad+4r^2\hat{H}_{rz}\hat{s}_z-2A_zH_{rr}Z_z-H_{rr}^{-1}\hat{H}_{rz}^2-\hat{H}_{rz}Z_z\Big)\\
&+H^{-2}\alpha r^2\hat{H}_{rz}^3\Big(r^4H_{rr}^{-1}\hat{H}_{rz}\hat{\tilde{s}}_r-2r^2H_{rr}^{-1}\hat{H}_{rz}\hat{s}\\
&\qquad-r^2H_{rr}^{-1}\hat{H}_{rz}\hat{Z}_r-r^2\hat{s}_z\\
&\qquad-H_{rr}^{-1}\hat{H}_{rz}+Z_z\Big)-\hat{\beta}^r\theta
\end{aligned}
$$

$$
\begin{aligned}
\tilde{\mathcal{S}}\left(Z_r\right) = & -\kappa\alpha r\hat{J}_r - \frac{1}{2}\sqrt{H}\alpha e^{2r^2\hat{s}} r^3 \hat{B}^{\varphi} E^z H_{rr} + H^{-1}\alpha\chi_{rr}\hat{D}_{rrr} r^3 H_{rr}^{-2}\hat{H}_{rz}^2 \\
& + H^{-1}\alpha\chi_{rr}\hat{D}_{rzz} r - 2H^{-1}\alpha\chi_{rr} D_{zrr} r H_{rr}^{-1}\hat{H}_{rz} \\
& - H^{-2}\alpha\chi_{rr} D_{zrr} r^3 H_{rr}^{-1}\hat{H}_{rz}^3 + 2H^{-2}\alpha\chi_{rr}\hat{D}_{zrz} r^3 \hat{H}_{rz}^2 \\
& - H^{-2}\alpha\chi_{rr} D_{zzz} r H_{rr}\hat{H}_{rz} + \alpha\chi_{rr} r H_{rr}^{-1}\left(\hat{A}_r - 2\hat{Z}_r\right) \\
& + H^{-1}\alpha\chi_{rr} r\hat{H}_{rz}\Big(r^4 H_{rr}^{-1}\hat{H}_{rz}\hat{\tilde{s}}_r + 2r^2 H_{rr}^{-1}\hat{H}_{rz}\hat{s} \\
& \qquad - 2r^2 H_{rr}^{-1}\hat{H}_{rz}\hat{Z}_r - r^2\hat{s}_z \\
& \qquad + A_z + H_{rr}^{-1}\hat{H}_{rz} + 2Z_z\Big) \\
& - H^{-2}\alpha\chi_{zz}\hat{D}_{rrr} r^3 \hat{H}_{rz}^2 + 2H^{-2}\alpha\chi_{zz}\hat{\tilde{D}}_{rrz} r^3 H_{rr}\hat{H}_{rz} \\
& - H^{-2}\alpha\chi_{zz}\hat{D}_{rzz} r H_{rr}^2 + H^{-1}\alpha\chi_{zz} r\hat{A}_r H_{rr} \\
& + H^{-2}\alpha\chi_{zz} r H_{rr}\hat{H}_{rz}^2 - \alpha\hat{D}_{rrr} r^3 H_{rr}^{-1}\hat{Y} \\
& + H^{-2}\alpha\hat{D}_{rrr} r^5 \hat{\chi}_{rz} H_{rr}^{-1}\hat{H}_{rz}^3 - 2H^{-1}\alpha\hat{\tilde{D}}_{rrz} r^3\hat{\chi}_{rz} \\
& - 2H^{-2}\alpha\hat{\tilde{D}}_{rrz} r^5\hat{\chi}_{rz}\hat{H}_{rz}^2 + H^{-2}\alpha\hat{D}_{rzz} r^3\hat{\chi}_{rz} H_{rr}\hat{H}_{rz} \\
& + 2H^{-1}\alpha D_{zrr} r\hat{\chi}_{rz} + H^{-2}\alpha D_{zrr} r^3\hat{\chi}_{rz}\hat{H}_{rz}^2 \\
& - 2H^{-2}\alpha\hat{D}_{zrz} r^3\hat{\chi}_{rz} H_{rr}\hat{H}_{rz} + H^{-2}\alpha D_{zzz} r\hat{\chi}_{rz} H_{rr}^2 \\
& + \alpha r\Big(-r^4\hat{\tilde{s}}_r\hat{Y} + r^2\hat{A}_r\hat{Y} - 2r^2\hat{s}\hat{Y} - 2\hat{A}_r\theta \\
& \qquad + 2\hat{B}_r{}^z Z_z - 2B_z{}^z\hat{Z}_r - \hat{Y}\Big) \\
& + H^{-1}\alpha r\hat{\chi}_{rz}\Big(-r^4\hat{H}_{rz}\hat{\tilde{s}}_r - r^2\hat{A}_r\hat{H}_{rz} + r^2 H_{rr}\hat{s}_z - 2r^2\hat{H}_{rz}\hat{s} \\
& \qquad + 2r^2\hat{H}_{rz}\hat{Z}_r - A_z H_{rr} - 2H_{rr}Z_z \\
& \qquad - 2\hat{H}_{rz}\Big) - H^{-2}\alpha r^3\hat{\chi}_{rz}\hat{H}_{rz}^3
\end{aligned}
$$

$$
\begin{aligned}
\tilde{\mathcal{S}}\left(Z_z\right) = & -\kappa\alpha J_z + \frac{1}{2}\sqrt{H}\alpha e^{2r^2\hat{s}} r^4 \hat{B}^{\varphi}\hat{E}^{r} H_{rr} - 2\alpha\chi_{rr} D_{zrr} H_{rr}^{-2} \\
& - 2H^{-1}\alpha\chi_{rr} D_{zrr} r^2 H_{rr}^{-2}\hat{H}_{rz}^2 - H^{-2}\alpha\chi_{rr} D_{zrr} r^4 H_{rr}^{-2}\hat{H}_{rz}^4 \\
& + 2H^{-1}\alpha\chi_{rr}\hat{D}_{zrz} r^2 H_{rr}^{-1}\hat{H}_{rz} + 2H^{-2}\alpha\chi_{rr}\hat{D}_{zrz} r^4 H_{rr}^{-1}\hat{H}_{rz}^3 \\
& - H^{-2}\alpha\chi_{rr} D_{zzz} r^2 \hat{H}_{rz}^2 + \alpha\chi_{rr} H_{rr}^{-1}\left(-r^2\hat{s}_z + 2A_z\right) \\
& + H^{-1}\alpha\chi_{rr} r^2 A_z H_{rr}^{-1}\hat{H}_{rz}^2 - 2H^{-1}\alpha\chi_{zz}\hat{D}_{rrr} r^2 H_{rr}^{-1}\hat{H}_{rz} \\
& - H^{-2}\alpha\chi_{zz}\hat{D}_{rrr} r^4 H_{rr}^{-1}\hat{H}_{rz}^3 + 2H^{-2}\alpha\chi_{zz}\hat{\hat{D}}_{rrz} r^4 \hat{H}_{rz}^2 \\
& - H^{-2}\alpha\chi_{zz}\hat{D}_{rzz} r^2 H_{rr}\hat{H}_{rz} + 2H^{-1}\alpha\chi_{zz} D_{zrr} \\
& + H^{-1}\alpha\chi_{zz}\Big(-r^4\hat{H}_{rz}\hat{\hat{s}}_r + r^2\hat{A}_r\hat{H}_{rz} + r^2 H_{rr}\hat{s}_z - 2r^2\hat{H}_{rz}\hat{s} \\
& \qquad + 2r^2\hat{H}_{rz}\hat{Z}_r - 2H_{rr}Z_z - \hat{H}_{rz}\Big) \\
& + H^{-2}\alpha\chi_{zz} r^2\hat{H}_{rz}^3 + 2\alpha\hat{D}_{rrr} r^2\hat{\chi}_{rz} H_{rr}^{-2} \\
& + 3H^{-1}\alpha\hat{D}_{rrr} r^4\hat{\chi}_{rz} H_{rr}^{-2}\hat{H}_{rz}^2 \\
& + H^{-2}\alpha\hat{D}_{rrr} r^6\hat{\chi}_{rz} H_{rr}^{-2}\hat{H}_{rz}^4 - 2H^{-1}\alpha\hat{\hat{D}}_{rrz} r^4\hat{\chi}_{rz} H_{rr}^{-1}\hat{H}_{rz} \\
& - 2H^{-2}\alpha\hat{\hat{D}}_{rrz} r^6\hat{\chi}_{rz} H_{rr}^{-1}\hat{H}_{rz}^3 + H^{-1}\alpha\hat{D}_{rzz} r^2\hat{\chi}_{rz} \\
& + H^{-2}\alpha\hat{D}_{rzz} r^4\hat{\chi}_{rz}\hat{H}_{rz}^2 - \alpha D_{zrr} r^2 H_{rr}^{-1}\hat{Y} \\
& + H^{-2}\alpha D_{zrr} r^4\hat{\chi}_{rz} H_{rr}^{-1}\hat{H}_{rz}^3 - 2H^{-1}\alpha\hat{D}_{zrz} r^2\hat{\chi}_{rz} \\
& - 2H^{-2}\alpha\hat{D}_{zrz} r^4\hat{\chi}_{rz}\hat{H}_{rz}^2 + H^{-2}\alpha D_{zzz} r^2\hat{\chi}_{rz} H_{rr}\hat{H}_{rz} \\
& + \alpha\Big(r^4\hat{\chi}_{rz} H_{rr}^{-1}\hat{\hat{s}}_r - r^4\hat{s}_z\hat{Y} - r^2\hat{A}_r\hat{\chi}_{rz} H_{rr}^{-1} \\
& \quad + r^2 A_z\hat{Y} - 2r^2\hat{\hat{B}}_r{}^r Z_z + 2r^2\hat{B}_z{}^r\hat{Z}_r + 2r^2\hat{\chi}_{rz} H_{rr}^{-1}\hat{s} \\
& \quad - 2r^2\hat{\chi}_{rz} H_{rr}^{-1}\hat{Z}_r - 2A_z\theta + \hat{\chi}_{rz} H_{rr}^{-1}\Big) \\
& + H^{-1}\alpha r^2\hat{\chi}_{rz}\hat{H}_{rz}\Big(r^4 H_{rr}^{-1}\hat{H}_{rz}\hat{\hat{s}}_r - r^2\hat{A}_r H_{rr}^{-1}\hat{H}_{rz} \\
& \qquad + 2r^2 H_{rr}^{-1}\hat{H}_{rz}\hat{s} - 2r^2 H_{rr}^{-1}\hat{H}_{rz}\hat{Z}_r \\
& \qquad - r^2\hat{s}_z - A_z + 2Z_z\Big) \\
& - H^{-2}\alpha r^4\hat{\chi}_{rz} H_{rr}^{-1}\hat{H}_{rz}^4 - \hat{\beta}^r Z_z
\end{aligned}
$$

$$\begin{aligned}\tilde{\mathcal{S}}\left(Z^{\varphi}\right) = &-\kappa\alpha J^{\varphi} + 2\alpha\hat{D}_{rrr}r^2\hat{E}^r H_{rr}^{-1} + \frac{1}{2}H^{-1}\alpha\hat{D}_{rrr}r^4\hat{E}^r H_{rr}^{-1}\hat{H}_{rz}^2 \\ &- H^{-1}\alpha\hat{\tilde{D}}_{rrz}r^4\hat{E}^r\hat{H}_{rz} + \frac{1}{2}H^{-1}\alpha\hat{D}_{rzz}r^2\hat{E}^r H_{rr} \\ &+ 2\alpha D_{zrr}E^z H_{rr}^{-1} + \frac{1}{2}H^{-1}\alpha D_{zrr}r^2E^z H_{rr}^{-1}\hat{H}_{rz}^2 \\ &- H^{-1}\alpha\hat{D}_{zrz}r^2E^z\hat{H}_{rz} + \frac{1}{2}H^{-1}\alpha D_{zzz}E^z H_{rr} \\ &+ \alpha\left(\frac{3}{2}r^4\hat{E}^r\hat{\tilde{s}}_r - \frac{1}{2}r^2\hat{A}_r\hat{E}^r - 2r^2\hat{\tilde{B}}_r{}^r Z^{\varphi} + 3r^2\hat{E}^r\hat{s}\right. \\ &\quad - r^2\hat{E}^r\hat{Z}_r + \frac{3}{2}r^2E^z\hat{s}_z - \frac{1}{2}A_zE^z - 2B_z{}^z Z^{\varphi} \\ &\quad \left. + \frac{3}{2}\hat{E}^r - E^z Z_z\right) - \frac{1}{2}H^{-1}\alpha r^2\hat{E}^r\hat{H}_{rz}^2 - \hat{\beta}^r Z^{\varphi}\end{aligned}$$

Bibliography

[1] A.M. Abrahams and C.R. Evans. Critical Behaviour and Scaling in Vacuum Axisymmetric Gravitational Collapse. *Phys. Rev. Lett.*, 70(20):2980–2983, 1993.

[2] A.M. Abrahams and C.R. Evans. Universality in axisymmetric vacuum collapse. *Phys. Rev. D*, 49(8):3998–4003, 1994.

[3] A.M. Abrahams, K.R. Heiderich, S.L. Shapiro, and S.A. Teukolsky. Vacuum initial data, singularities, and cosmic censorship. *Phys. Rev. D*, 46(6):2452–2463, 1992.

[4] M. Alcubierre. Appearance of coordinate shocks in hyperbolic formalisms of general relativity. *Phys. Rev. D*, 55(10):5981–5991, 1997.

[5] M. Alcubierre. Hyperbolic slicings of spacetime: singularity avoidance and gauge shocks. *Class. Quantum Grav.*, 20:607–623, 2003.

[6] M. Alcubierre, G. Allen, B. Brügmann, G. Lanfermann, W. Seidel, W.-M. Suen, and M. Tobias. Gravitational collapse of gravitational waves in 3D numerical relativity. *Phys. Rev. D*, 61(041501), 2000.

[7] M. Alcubierre, S. Brandt, B. Brügmann, D. Holz, E. Seidel, R. Takahashi, and J. Thornburg. Symmetry without symmetry: Numerical

simulation of axisymmetric systems using Cartesian grids. *Int. J. Mod. Phys.*, 10(3):273–290, 2001.

[8] M. Alcubierre and J. Massó. Pathologies of hyperbolic gauges in general relativity amd other field theories. *Phys. Rev. D*, 57(8):R4511–15, 1998.

[9] P. Anninos, K. Camarda, J. Massó, E. Seidel, W.-M. Suen, and J. Towns. Three-dimensional numerical relativity: The evolution of black holes. *Phys. Rev. D*, 52(4):2059–2082, 1995.

[10] W. Antweiler, A. Strotmann, and V. Winkelmann. *Typesetting REDUCE output with TeX – A REDUCE-TeX-Interface*. University of Cologne, Computer Centre, 1995.

[11] D.N. Arnold, A. Mukherjee, and L. Pouly. Adaptive finite elements and colliding black holes. *Preprint, arXiv::gr-qc*, (9709038), 1997.

[12] R. Arnowitt, S. Deser, and C. W. Misner. The dynamics of general relativity. In L. Witten, editor, *Gravitation: an introduction to current research*, chapter 7, pages 227–265. Wiley, 1962.

[13] F. Banyuls, J.A. Font, J.M. Ibáñez, J.M. Martí, and J.A. Miralles. Numerical 3+1 general relativistic hydrodynamics: A local characteristic approach. *Astrophys. J.*, 476:221–231, 1997.

[14] A. Barnes. *Numerical Relativistic Hydrodynamics in Planar and Axisymmetric Spacetimes*. PhD thesis, University of Cambridge, August 2004.

[15] A.P. Barnes, P.G. Lefloch, B.G. Schmidt, and J.M. Stewart. The Glimm scheme for perfect fluids on plane-symmetric Gowdy spacetimes. *Class. Quantum Grav.*, 21:5043–5074, 2004.

[16] T. W. Baumgarte and S. Shapiro. Numerical integration of Einstein's field equations. *Phys. Rev. D*, 59(024007), 1998.

[17] M. Berger and I. Rigoutsos. An Algorithm for Point Clustering and Grid Generation. *IEEE Transactions on Systems, Man, and Cybernetics*, 21(5):1278–1286, 1991.

[18] M.J. Berger and P. Colella. Local Adaptive Mesh Refinement for Shock Hydrodynamics. *J. Comp. Phys*, 82:64–84, 1988.

[19] M.J. Berger and J. Oliger. Adaptive mesh refinement for hyperbolic partial differential equations. *J. Comput. Phys.*, 53:484–512, 1984.

[20] G.D. Birkhoff. *Relativity and Modern Physics*. Harvard University Press, 1923.

[21] J. Bičák and B.G. Schmidt. Isometries compatible with gravitational radiation. *J. Math. Phys.*, 25(3):606–606, 1984.

[22] J. Bičák and B.G. Schmidt. Asymptotically flat radiative space-times with boost-rotation symmetry. *Phys. Rev. D*, 40:1827–1853, 1989.

[23] C. Bona, T. Ledvinka, C. Palenzuela, and M. Žáček. General-covariant evolution formalism for numerical relativity. *Phys. Rev. D*, 67(104005), 2003.

[24] C. Bona, T. Ledvinka, C. Palenzuela, and M. Žáček. A symmetry-breaking mechanism for the Z4 general-covariant evolution system. *Phys. Rev. D*, 69(064036), 2004.

[25] C. Bona, T. Ledvinka, C. Palenzuela-Luque, and M. Žáček. Constraint-preserving boundary conditions in the Z4 numerical relativity formalism. *Class. Quantum Grav.*, 22(13):2615–2633, 2005.

[26] C. Bona and J. Massó. Harmonic synchronizations of spacetime. *Phys. Rev. D*, 38(8):2419–2422, 1988.

[27] C. Bona and C. Palenzuela. Dynamical shift conditions for the Z4 and BSSN formalisms. *Phys. Rev. D*, 69(104003), 2004.

[28] H. Bondi, M.G.J. van der Burg, and A.W.K Metzner. Gravitational Waves in General Relativity: VII. Waves from Axi-Symmetric Isolated Systems. *Proc. R. Soc. London A*, 269:21–52, 1962.

[29] J.H. Bramble, J.E. Pasciak, and J. Xu. The Analysis of Multigrid Algorithms for Nonsymmetric and Indefinite Problems. *Math. Comp.*, 51(184):289–414, 1988.

[30] A. Brandt. Multilevel adaptive solutions to boundary value problems. *Math. Comput.*, 31:333–390, 1977.

[31] W. Briggs, V.E. Henson, and S.F. McCormick. *A Multigrid Tutorial*. SIAM, 1999.

[32] D. Brill. On the Positive Definite Mass of the Bondi-Weber-Wheeler Time-Symmetric Gravitational Waves. *Ann. Phys.*, 7:466–483, 1959.

[33] O. Brodbeck, S. Frittelli, P. Hübner, and O. A. Reula. Einstein's equations with asymptotically stable constraint propagation. *J. Math. Phys.*, 40(2):909–923, 1999.

[34] Y. Bruhat. Théorème d'existence pour certaines systèmes d'équations aux dérivées partielles nonlinéaires. *Acta Math.*, 88:141–225, 1952.

[35] W. L. Burke. Gravitational Radiation Damping of Slowly Moving Systems Calculated Using Matched Asymptotic Expansions. *J. Math. Phys.*, 12(3):401–418, 1971.

[36] J.C. Butcher. *Numerical Methods for Ordinary Differential Equations.* Wiley, 2003.

[37] G. Calabrese, L. Lehner, and M. Tiglio. Constraint-preserving boundary conditions in numerical relativity. *Phys. Rev. D*, 65(104031), 2002.

[38] G. Calabrese, J. Pullin, O. Sarbach, M. Tiglio, and O. Reula. Well posed constraint-preserving boundary conditions for the linearized Einstein equations. *Comm. Math. Phys.*, 240:377–395, 2003.

[39] S.J. Campbell and J. Wainwright. Algebraic computing and the Newman-Penrose formalism in general relativity. *GRG*, 8:987–1001, 1977.

[40] M.W. Choptuik. Universality and scaling in gravitational collapse of a massless scalar field. *Phys. Rev. Lett.*, 70:9–12, 1993.

[41] M.W. Choptuik, E.W. Hirschmann, S.L. Liebling, and F. Pretorius. An axisymmetric gravitational collapse code. *Class. Quantum Grav.*, 20:1857–1878, 2003.

[42] M.W. Choptuik, E.W. Hirschmann, S.L. Liebling, and F. Pretorius. Critical collapse of the massless scalar field in axisymmetry. *Phys. Rev. D*, 68(044007), 2003.

[43] W. Davidson. Barotropic perfect fluid in steady cylindrically symmetric rotation. *Class. Quantum Grav.*, 14:119–127, 1997.

[44] T. De Donder. *La Gravifique Einsteinienne.* Gauthier-Villars, Paris, 1921.

[45] O. Dreyer, B. Krishnan, D. Shoemaker, and E. Schnetter. Introduction to isolated horizons in numerical relativity. *Phys. Rev. D*, 67(024018), 2003.

[46] D.M. Eardley and L. Smarr. Time functions in numerical relativity: Marginally bound dust collapse. *Phys. Rev. D*, 19:2239–2259, 1979.

[47] H.C. Elman, O.G. Ernst, and D.P. O'Leary. A Multigrid Method Enhanced by Krylov Subspace Iteration for the Discrete Helmholtz Equations. *SIAM J. Sci. Comput.*, 23(4):1291–1315, 2001.

[48] K. Eppley. Evolution of time-symmetric gravitational waves: Initial data and apparent horizons. *Phys. Rev. D*, 16(6):1909–1614, 1977.

[49] K. Eppley. Pure gravitational waves. In L. Smarr, editor, *Sources of Gravitational Radiation*, pages 275–291. Cambridge University Press, 1979.

[50] F. Estabrook, H. Wahlquist, S. Christensen, B. DeWitt, L. Smarr, and E. Tsiang. Maximally slicing a black hole. *Phys. Rev. D*, 7(10):2814–2817, 1972.

[51] C.R. Evans and J.S. Coleman. Critical Phenomena and Self-Similarity in the Gravitational Collapse of Radiation Fluid. *Phys. Rev. Lett.*, 72(12):1782–1785, 1994.

[52] L.C. Evans. *Partial Differential Equations.* American Mathematical Society, 1998.

[53] V.A. Fock. *The Theory of Space Time and Gravitation.* Pergamon, London, 1959.

[54] J.A. Font. Numerical hydrodynamics in general relativity. *Living Reviews in Relativity*, 3, May 2000.

[55] J. Frauendiener. Discretizations of axisymmetric systems. *Phys. Rev. D*, 66(104027), 2002.

[56] H. Friedrich. On the regular and the asymptotic characteristic initial value problem for Einstein's vacuum field equations. *Proc. R. Soc. London A*, 375:169, 1981.

[57] H. Friedrich. Hyperbolic reductions for Einstein's equations. *Class. Quantum Grav.*, 13:1451–1469, 1996.

[58] H. Friedrich and G. Nagy. The Initial Boundary Value Problem for Einstein's Vacuum Field Equations. *Comm. Math. Phys.*, 201:619–655, 1999.

[59] S. Frittelli and O.A. Reula. First-Order Symmetric Hyperbolic Einstein Equations with Arbitrary Fixed Gauge. *Phys. Rev. Lett.*, 76(25):4667–4670, 1996.

[60] B. Fryxell, K. Olson, P. Ricker, F.X. Timmes, M. Zingale, D.Q. Lamb, P. MacNeice, R. Rosner, Truran J.W., and H. Tufo. FLASH: An Adaptive Mesh Hydrodynamics Code for Modeling Astrophysical Thermonuclear Flashes. *Astr. J. Suppl.*, 131:273–334, 2000.

[61] D. Garfinkle. Harmonic coordinate method for simulating generic singularities. *Phys. Rev. D*, 65(044029), 2002.

[62] D. Garfinkle and G.C. Duncan. Numerical Evolution of Brill Waves. *Phys. Rev. D*, 63(044011), 2000.

[63] D. Garfinkle, E.N. Glass, and J.P. Krisch. Solution generating with perfect fluids. *Gen. Rel. Grav.*, 29(4):467–480, 1997.

[64] B.L. Gates and M.C. Dewar. *GENTRAN User's Manual – REDUCE Version*. RAND, Santa Monica and University of Bath, 1991.

[65] R. Geroch. A Method for Generating Solutions of Einstein's Equations. *J. Math. Phys.*, 12(6):918–924, 1971.

[66] D. Gilbarg and N.S. Trudinger. *Elliptic Partial Dfferential Equations of Second Order*. Springer, 1977.

[67] E. Gourgoulhon, P. Grandclement, and S. Bonazzola. Binary black holes in circular orbits. I. A global spacetime approach. *Phys. Rev. D*, 65(044020), 2002.

[68] C. Gundlach. Angular momentum at the black hole threshold. *Phys. Rev. D*, 57:7080–7083, 1998.

[69] C. Gundlach. Critical phenomena in gravitational collapse. *Living Reviews in Relativity*, 2, 1999.

[70] C. Gundlach, G. Calabrese, I. Hinder, and J. M. Martín-García. Constraint damping in the Z4 formulation and harmonic gauge. *Class. Quantum Grav.*, 22:3767–3773, 2005.

[71] C. Gundlach and J. M. Martín-García. Symmetric hyperbolic form of systems of second-order evolution equations subject to constraints. *Phys. Rev. D*, 70(044031), 2004.

[72] C. Gundlach and J. M. Martín-García. Symmetric hyperbolicity and consistent boundary conditions for second-order Einstein equations. *Phys. Rev. D*, 70(044032), 2004.

[73] B. Gustafssohn, H.-O. Kreiss, and J. Oliger. *Time dependent problems and difference methods*. Wiley, 1995.

[74] W. Hackbusch. *Multi-Grid Methods and Applications*. Computational Mathematics. Springer, 1985.

[75] S. Hahn and R. Lindquist. The two-body problem in geometrodynamics. *Ann. Phys.*, 29:304, 1964.

[76] R. Hamade and J.M. Stewart. The spherically symmetric collapse of a massless scalar field. *Class. Quantum Grav.*, 13:497–512, 1996.

[77] I. Hawke. *Computational Ultrarelativistic Hydrodynamics*. PhD thesis, University of Cambridge, 2001.

[78] I. Hawke and J.M. Stewart. The dynamics of primordial black hole formation. *Class. Quantum Grav.*, 19:3687–3707, 2002.

[79] S.W. Hawking and G.F.R. Ellis. *The Large Scale Structure of Space-time*. Cambridge University Press, 1973.

[80] A.C. Hearn. *REDUCE User's Manual 3.5*. Konrad-Zuse-Zentrum Berlin, 1993.

[81] S.D. Hern. *Numerical relativity and Inhomogeneous Cosmologies*. PhD thesis, University of Cambridge, 1999. Available on arXiv::gr-qc/0004036.

[82] M. Holst and D. Bernstein. Adaptive finite element solution of the constraint equations in relativity. *Preprint*, 2005.

[83] M. Holst, L. Lindblom, R. Owen, H. Pfeiffer, M.A. Scheel, and L.E. Kidder. Optimal constraint projection for hyperbolic evolution systems. *Phys. Rev. D*, 70(085017), 2004.

[84] P. Jordan, J. Ehlers, and W. Kundt. Exact solutions of the field equations of general relativity. *Akad. Wiss. Lit. (Mainz) Abhandl. Math.-Nat. Kl. 2*, 21, 1960. In German.

[85] T. Kaluza. On the problem of unity in physics. *Sitzungsber. Preuss. Akad. Wiss., Berlin, Math. Phys.*, K1:966, 1921. In German.

[86] E. Kasner. Geometrical theorems on Einstein's cosmological equations. *Am. J. Math.*, 43:217–221, 1921.

[87] L. E. Kidder, M. A. Scheel, and S. A. Teukolsky. Extending the lifetime of 3d black hole computations with a new hyperbolic system of evolution equations. *Phys. Rev. D*, 64(064017), 2001.

[88] L.E. Kidder, L. Lindblom, M.A. Scheel, L.T. Buchman, and H.P. Pfeiffer. Boundary conditions for the Einstein evolution system. *Phys. Rev. D*, 71(064020), 2005.

[89] O. Klein. Quantum theory and five-dimensional relativity theory. *Z. Phys.*, 37:895, 1926. In German.

[90] A. Komar. Covariant Conservation Laws in General Relativity. *Phys. Rev.*, 113(1):934–936, 1959.

[91] A.S. Kompaneets. Strong gravitational waves in vacuum. *Zh. Eksper. Teor. Fiz.*, 34:953, 1958. In Russian.

[92] D. Kramer. Cylindrically symmetric static perfect fluids. *Class. Quantum Grav.*, 5(2):393–398, 1988.

[93] H.-O. Kreiss. Initial boundary value problems for hyperbolic systems. *Commun. Pure Appl. Math.*, 23:277, 1970.

[94] H.-O. Kreiss and J. Oliger. Methods for the approximate solution of time dependent problems. Technical Report 10, Global atmospheric research programme publication series, 1973.

[95] C.B. Laney. *Computational Gasdynamics*. Cambridge University Press, 1998.

[96] L. Lehner. Numerical relativity: A review. *Class. Quantum Grav.*, 18:R25–R86, 2001. Topical Review.

[97] R. J. LeVeque. *Numerical Methods for Conservation Laws*. Birkhäuser Verlag, 1992.

[98] L. Lindblom and M. A. Scheel. Dynamical gauge conditions for the Einstein evolution equations. *Phys. Rev. D*, 67(124005), 2003.

[99] R. Löhner. An adaptive finite element scheme for transient problems in CFD. *Comp. Meth. App. Mech. Eng.*, 61:323–338, 1987.

[100] K. Maeda, M. Sasaki, T. Nakamura, and S. Miyama. A New Formulation of the Einstein Equations for Relativistic Rotating Systems. *Prog. Theor. Phys.*, 63:719–721, 1980.

[101] A. Majda and S. Osher. Initial-Boundary Value Problems for Hyperbolic Equations with Uniformly Characteristic Boundary. *Comm. Pure & Appl. Math.*, 28:607–675, 1975.

[102] C.W. Misner, K.S. Thorne, and J.A. Wheeler. *Gravitation*. Freeman, 1970.

[103] G. Nagy, O. Ortiz, and O. Reula. Strongly hyperbolic second order Einstein's evolution equations. *Phys. Rev. D*, 70(044012), 2004.

[104] T. Nakamura, K. Oohara, and Y. Kojima. General relativistic collapse of axially symmetric stars and 3d time evolution of pure gravitational waves. *Prog. Theor. Phys. Suppl.*, 90:13–109, 1987.

[105] D.W. Neilsen and M.W. Choptuik. Critical phenomena in perfect fluids. *Class. Quantum Grav.*, 17:761–782, 2000.

[106] D.W. Neilsen and M.W. Choptuik. Ultrarelativistic fluid dynamics. *Class. Quantum Grav.*, 17:733–759, 2000.

[107] J. Oliger. *Numerical Methods for Partial Differential Equations*. New York: Academic, 1978.

[108] R. Penrose and W. Rindler. *Spinors and space-time 2: Spinor and twistor methods in space-time geometry*. Cambridge University Press, 1986.

[109] W. H. Press et al. *Numerical Recipes in C++: the art of scientific computing*. Cambridge University Press, 2nd edition, 2002.

[110] F. Pretorius. *Numerical Simulations of Gravitational Collapse*. PhD thesis, University of British Columbia, 2002.

[111] F. Pretorius. Evolution of Binary Black Hole Spacetimes. *Preprint, arXiv::gr-qc*, (0507014), July 2005.

[112] F. Pretorius. Numerical relativity using a generalized harmonic decomposition. *Class. Quantum Grav.*, 22(2):425–451, 2005.

[113] F. Pretorius and M.W. Choptuik. Adaptive Mesh Refinement for Coupled Elliptic-Hyperbolic Systems. *Preprint, arXiv::gr-qc*, (0508110), August 2005.

[114] M.H. Protter and H.F. Weinberger. *Maximum principles in differential equations*. Prentice-Hall, 1967.

[115] J. Rauch. Symmetric positive systems with boundary characteristic of constant multiplicity. *Trans. Am. Math. Soc.*, 291:167–187, 1996.

[116] O. Reula. Hyperbolic Methods for Einstein's Equations. *Living Rev. Relativity*, 1(3), 1998.

[117] O. Reula and O. Sarbach. A model problem for the initial-boundary value formulation of Einstein's field equations. *Preprint, arXiv::gr-qc*, (0409027), 2004.

[118] O. Rinne. Numerical Studies of Axisymmetric Spacetimes. Smith-Knight Prize Essay, University of Cambridge, January 2004.

[119] O. Rinne and J. M. Stewart. A strongly hyperbolic and regular reduction of Einstein's equations for axisymmetric spacetimes. *Class. Quantum Grav.*, 22(6):1143–1166, 2005.

[120] R. Sachs. Gravitational Waves in General Relatvity: VIII. Waves in asymptotically flat space-time. *Proc. R. Soc. London A*, page 103, 1961.

[121] O. Sarbach and M. Tiglio. Boundary conditions for Einstein's field equations: Analytical and numerical analysis. *Preprint, arXiv::gr-qc*, (0412115), 2004. To appear in JHDE.

[122] M.A. Scheel, L.E. Kidder, L. Lindblom, H.P. Pfeiffer, and S.A. Teukolsky. Toward stable 3D evolutions of black-hole spacetimes. *Phys. Rev. D*, 66(124005), 2002.

[123] W.E. Schiesser. *The Numerical Method of Lines: Integration of Partial Differential Equations.* Academic Press, New York, 1991.

[124] P. Secchi. Well-Posedness of Characteristic Symmetric Hyperbolic Systems. *Arch. Ration. Mech. Anal.*, 134:155–197, 1996.

[125] J.R. Shewchuk. An Introduction to the Conjugate Gradient Method Without the Agonizing Pain. Unpublished draft, 1994.

[126] C.-W. Shu. Essentially non-oscillatory and weighted essentially non-oscillatory schemes for hyperbolic conservation laws. Technical Report 97-65, ICASE, 1997.

[127] C.-W. Shu and S. Osher. Efficient implementation of essentially non-oscillatory shock-capturing schemes. *J. Comp. Phys.*, 77:439–471, 1988.

[128] J.M. Stewart. *Advanced general relativity.* Cambridge University Press, 1991.

[129] J.M. Stewart. The Cauchy problem and the initial boundary value problem in numerical relativity. *Class. Quantum Grav.*, 15:2865–2889, 1998.

[130] J. Stoer and R. Bulirsch. *Introduction to Numerical Analysis.* Springer, second edition, 2002.

[131] R. Tabensky and A.H. Taub. Plane-symmetric self-gravitating fluids with pressure equal to energy density. *Comm. Math. Phys.*, 29:61–77, 1973.

[132] S.A. Teukolsky. Linearized quadrupole waves in general relativity and the motion of test particles. *Phys. Rev. D*, 26(4):745–750, 1982.

[133] S.A. Teukolsky. Stability of the iterated Crank-Nicholson method in numerical relativity. *Phys. Rev. D*, 61(087501), 2000.

[134] E.F. Toro. *Riemann Solvers and Numerical Methods for Fluid Dynamics*. Springer, 1997.

[135] E.F. Toro and V.A. Titarev. MUSTA schemes for multi-dimensional hyperbolic systems: analysis and improvements. *Isaac Newton Institute preprint*, (NI04032-NPA), 2004.

[136] E.F. Toro and V.A. Titarev. MUSTA Schemes for Systems of Conservation Laws. *Isaac Newton Institute preprint*, (NI04033-NPA), 2004.

[137] H.A. van der Vorst. BI-CGSTAB: a fast and smoothly converging variant of BI-CG for the solution of nonsymmetric linear systems. *SIAM Journal on Scientific and Statistical Computing*, 13:631–644, 1992.

[138] J.A. van Hulzen. *SCOPE 1.5 – A Source-Code Optimization PackagE for REDUCE 3.5*. University of Twente, Department of Computer Science.

[139] R.M. Wald and V. Iyer. Trapped surfaces in the Schwarzschild geometry and cosmic censorship. *Phys. Rev. D*, 44:R3719, 1991.

[140] J. Weber and J.A. Wheeler. Reality of the cylindrical gravitational waves of Einstein and Rosen. *Rev. Mod. Phys.*, 29(3):509–515, 1957.

[141] P. Wesseling. *An Introduction to Multigrid Methods*. Pure and Applied Mathematics. Wiley, 1992.

[142] J.R. Wilson. A numerical method for relativistic hydrodynamics. In L. Smarr, editor, *Sources of Gravitational Radiation*, pages 423–445. Cambridge University Press, 1979.

[143] G. Yoneda and H. Shinkai. Constraint propagation in the family of ADM systems. *Phys. Rev. D*, 63(124019), 2001.

[144] J.M. York. Kinematics and dynamics of general relativity. In L. Smarr, editor, *Sources of Gravitational Radiation*, page 83. Cambridge University Press, 1979.

[145] J.M. York. Initial data for collisions of black holes and other gravitational miscellany. In C. Evans, L. Finn, and D. Hobill, editors, *Frontiers in Numerical Relativity*, pages 89–109. Cambridge University Press, 1989.